Mapping of the human sinus node with emphasis on the expression and function of key microRNAs

A thesis submitted to the University of Manchester for the degree of Doctor of Philosophy in the Faculty of Biology, Medicine, and Health

2018

Maria Atanasova Petkova

School of Medicine

Table of contents

Word count: 71, 674

Abstract

A thesis submitted to the University of Manchester by Maria Petkova for the degree of Doctor of Philosophy entitled

Mapping of the human sinus node with emphasis on the expression and function of key microRNAs

September 2018

The sinus node (SN) is the primary pacemaker of the heart. Its unique function depends on the expression of ion channels, connexins, and Ca^{2+}-handling proteins, involved in the pacemaker mechanisms, and regulated by small non-coding RNAs (microRNAs) and transcription factors. The aims of my work were 1) to map the most abundant microRNAs in the healthy human SN in comparison with the right atrial (RA) working myocardium, 2) to study their role in the SN pacemaker activity, and 3) to map the transcription factors that potentially regulate the pacemaking mechanism of the healthy human adult SN compared to RA. To address the first aim I used tissue from six human SN/RA preparations that were characterised via histology and immunolabelling/immunoblotting for SN-specific ion channels and Tbx18. Using quantitative polymerase chain reaction (qPCR) and RealTime Statminer software, I identified 66 microRNAs that were significantly more or less expressed in the human SN compared to the RA. miR-1-3p, miR-10b-5p, miR-30c-5p, miR-133a-3p, miR-153-3p, miR-198, miR-204, miR-215-5p, miR-371-3p, miR-422a, miR-429, miR-486-3p, miR-512-5p, miR-938 and miR-1225-3p were predicted to target genes regulating the pacemaking mechanisms using Ingenuity Pathways Analysis (IPA) software. TarBase database, miRecords, TargetScan, and RNA22 online softwares were used to predict that 7 of these microRNAs are conserved in human and rat, and were injected in cultured rat SN preparations for 24 hours. Extracellular recording showed miR-486-3p and miR-429 significantly reduced the beating rate of the SN preparations. Luciferase reporter gene assay in H9C2 cells demonstrated that miR-486-3p binds to the HCN4 3'untranslated region (UTR). Immunolabelling and qPCR demonstrated that HCN4 protein expression and mRNA levels were significantly reduced in the presence of miR-486-3p in isolated rat SN preparations. miR-133a-3p transfected cardiac induced pluripotent stem cells (iPSCs) exhibited significant downregulation of HCN4 mRNA levels. Transcription factors expression in human SN vs. RA were measured via next generation sequencing (NGS), which identified 68 transcription factors significantly more expressed in the human SN, and 60 transcription factors significantly less expressed in the SN compared to the RA. IPA software narrowed down the list of cardiac specific transcription factors to Isl1, Tbx1, Shox2, Tbx3 and Tbx18, which were upregulated, and Tbx5 and Nkx2-5, which were downregulated in the human adult SN. This study demonstrated the complex regulatory machinery of the human SN, which is based on a precise balancing of microRNAs and transcription factors.

Declaration

I declare that that no portion of the work referred to in the thesis has been submitted in support of an application for another degree or qualification of this or any other university or other institute of learning.

Copyright statement

1. The author of this thesis (including any appendices and/or schedules to this thesis) owns certain copyright or related rights in it (the "Copyright") and she has given The University of Manchester certain rights to use such Copyright, including for administrative purposes.

2. Copies of this thesis, either in full or in extracts and whether in hard or electronic copy, may be made only in accordance with the Copyright, Designs and Patents Act 1988 (as amended) and regulations issued under it or, where appropriate, in accordance with licensing agreements which the University has from time to time. This page must form part of any such copies made.

3. The ownership of certain Copyright, patents, designs, trademarks and other intellectual property (the "Intellectual Property") and any reproductions of copyright works in the thesis, for example graphs and tables ("Reproductions"), which may be described in this thesis, may not be owned by the author and may be owned by third parties. Such Intellectual Property and Reproductions cannot and must not be made available for use without the prior written permission of the owner(s) of the relevant Intellectual Property and/or Reproductions.

4. Further information on the conditions under which disclosure, publication and commercialisation of this thesis, the Copyright and any Intellectual Property and/or Reproductions described in it may take place is available in the University IP Policy (see http://documents.manchester.ac.uk/DocuInfo.aspx?DocID=2442 0), in any relevant Thesis restriction declarations deposited in the University Library, The University Library's regulations (see http://www.library.manchester.ac.uk/about/regulations/) and in The University's policy on Presentation of Theses

Abbreviations list

3D	Three dimensional
A	Adenine
A-band	Anisotropic band
ANOVA	Analysis of variance
ATP	Adenosine triphosphate
ATPase	Adenylpyrophosphatease
AP	Action potential
Argo/RISC	Argonaute/RNA-induced silencing sequence
AVB	Atrioventricular bundle
AVC	Atrioventricular canal
bp	Base pairs
BSA	Bovine serum albumin
C	Cytosine
cAMP	Cyclic adenosine monophosphate
CAMTA	Calmodulin-binding transcription activator
cDNA	Complementary deoxyribonucleic acid
CDS	Coding domain sequence
Ct	Threshold cycle
CT	Computer tomography
cx	Connexin
DNA	Deoxyribonucleic acid
DMEM	Dulbecco's modified eagle's medium

ECG	Electrocardiogram
ERG	Ether-a-go-go-related gene
G	Guanine
GAPDH	Glyceraldehyde 3 3phosphate dehydrogenase
GO	Graphene oxide
HCN	Hyperpolarisation-activated cyclic nucleotide-gated cation
hESC	Human embryonic stem cells
hMSCs	Human mesenchymal stem cells
H-zone	Hello zone
$I_{Ca.L}$	L-type Ca^{2+} current
$I_{Ca.T}$	T-type Ca^{2+} current
I-band	Isotropic band
IFT	Inflow tract
IVC	Inferior vena cava
I_f	Funny current
$I_{K,1}$	Inward rectifying K^+ current
$I_{K,r}$	Rapidly activated delayed rectifier K^+ current
$I_{K,s}$	Slowly activated delayed rectifier K^+ current
$I_{K,ur}$	Ultra-rapidly activated delayed rectifier K^+ current
I_{Na+}	Na^+ current
$I_{Na,Ca}$	Na^+-Ca^{2+} exchanger current
IPA	Ingenuity pathway analysis
iPSCs	Induced pluripotent stem cells
Isl1	Insulin gene enhancer protein

K_{IR}	Inward-rectifier potassium channel
I_{to}	Transient outward current
LA	Left atrium
LIPO	Lipofectamine
LSH	Left sinus horn
LV	Left ventricle
M-band	Middle band
miR	microRNA
mRNA	Messenger ribonucleic acid
Ms	Mouse
NCX	Na^{+}-Ca^{2+} exchanger
NGS	Next generation sequencing
Nkx2-5	NK2 homeobox 5
Nppa	Natriuretic peptide
OCT	Optimal cutting compound
OFT	Outflow tract
PA	Pulmonary artery
PBS	Phosphate buffer saline
PCR	Polymerase chain reaction
Pitx2	Paired-like homeodomain transcription factor 2
PVDF	Polyvinyl difluoride
qPCR	Quantitative polymerase chain reaction
RA	Right atrium
RIN	RNA integrity number

RNA	Ribonucleic acid
RNase	Ribonuclease
RSH	Right sinus horn
RT	Reverse transcription
RyR	Ryanodine receptor
SDS-PAGE	Sodium dodecyl sulphate polyacrylamide gel electrophoresis
Shox2	Short stature homeobox2
SVC	Superior vena cava
SERCA	Sarco-endoplasmic reticulum calcium ATPase
SN/SAN	Sinus node
SR	Sarcoplasmic reticulum
SRF	Serum response factor
SSS	Sick sinus syndrome
T	Thymine
Taq	Thermus aquaticus
Tbx	T-box
TC/CT	Terminal crest
T_m	Melting temperature
TTX	Tetradotoxin
UTR	Untranslated region

Acknowledgements

I would like to thank extensively the people who contributed to the work described in this thesis.

Special mention goes to my supervisor Dr. Halina Dobrzynski not only for the tremendous academic support she has provided me with, but also for the exciting opportunities she has given me to travel around the world and communicate my work. I would like to express my gratitude to my other supervisor Dr. Delvac Oceandy who has always been truly enthusiastic about the challenges science presents us with.

I would like to acknowledge all of my work colleagues. Profound gratitude goes to Luke Stuart whose expertise in the lab and dedicated mentoring during my thesis writing has been invaluable. I also greatly appreciate Violeta Trendafilova for her faith in me, and her constant encouragement throughout the course of my studies.

I would like to acknowledge the financial support by the University of Manchester and the British Heart Foundation, which gave me the opportunity to not only carry out this work, but also to develop my skills and confidence as a professional.

Finally, but for no mean least, I send my warmest and deepest gratitude to my family, and especially Tanya, Atanas, and Petko, for the financial, mental and moral support through the seven hard years of studies overseas I have undertaken. Without them I would not be in the place I am now, and this is why I humbly dedicate this work to them.

Chapter 1

1 Introduction

1.1 General introduction

The sinus node (SN) is the major pacemaker of the heart, which initiates and propagates an action potential (AP), and thus induces every heartbeat (Figure 1.1)(Flack, 1910; Gaskell, 1883; Keith and Flack, 1907; Sanchez-Quintana et al., 2005). This structure is equipped with unique molecular, structural and functional properties, allowing fast and well-coordinated conduction of the AP through the heart.

The function of pacemaker myocytes is to generate AP, and this ability is referred to as automaticity (Mangoni and Nargeot, 2008). SN myocytes are not the only cardiac cell type capable of pacemaking activity (Joyner et al., 1998; Kirchhof et al., 1987; Moe et al., 1956); however, they are the primary pacemaker cells that overrule any other activity in the heart under physiological conditions (Joyner and Vancapelle, 1986).

Even though SN cells exhibit their own internal automaticity, their function is also influenced by external factors such as the sympathetic and parasympathetic nervous systems (Heinz et al., 1992; Urthaler et al., 1986). Burke et al., showed that the normal human sinus cycle length ranges from 918 to 971 ms and the normal heart rate is 60-80 beats per minute. Double automatic ß-adrenergic and parasympathetic blockade with propranolol and atropine decreases the cycle length significantly, leading to increased heart rate (Burke et al., 1996). These data confirm that the SN intrinsic tone is much faster than it is in physiological conditions, and thus it overrides the pacemaking activity of other

cardiomyocytes in the heart that are capable of automaticity (Heinz et al., 1992). Pathological conditions affecting the SN, such as the sick sinus syndrome (SSS), are characterised by slower intrinsic pacemaker tone produced by other pacemaker cells due to dysfunction of the SN (Heinz et al., 1992).

The automaticity of the SN is governed by a cross-talk between two major mechanisms – the membrane-voltage clock (Joung et al., 2011; Lakatta and DiFrancesco, 2009) and the Ca^{2+} clock (Bogdanov et al., 2001; Huser et al., 2000), which synergistically generate diastolic depolarisation (phase 4) of the SN AP (Figure 1.4 - 1.7). Alterations of the SN regulatory mechanisms lead to pathologies such as SSS (Atkinson et al., 2013).

Currently the only available treatment for SN dysfunctions such as SSS, characterised by intrinsic slow heart rate (bradycardia) or asystolic pauses, is implantation of electronic pacemaker devices. SSS accounts for ~ 27% of the electronic pacemaker implantation surgeries in the UK and despite their demonstrated efficacy, electronic pacemakers have been related to a number of limitations such as lead malfunction, finite battery life, and device related infections (Baddour et al., 2010; Fischer et al., 2011; Fortescue et al., 2004). For these reasons biological pacemakers, as alternative to implantable hardware, have received great scientific attention in the recent years (Cingolani et al., 2018). It has been suggested that gene therapy could be one potential mechanism in the development of biological pacemakers.

microRNAs are small non-coding molecules that regulate the expression of their target genes by inhibiting their expression. Studies of the human genome have reported the discovery of ~2000 microRNAs, some of which were demonstrated to be tissue-specific and to play key roles during embryonic development (Bartel, 2009). Extensive scientific work describes the role of microRNAs in cardiovascular physiology and pathology as well

as their use as disease biomarkers (Condorelli et al., 2014; van Rooij et al., 2008a; Wang et al., 2014b).

Transcription factors are another subtype of regulatory molecules that regulate gene expression during embryonic development and adulthood. They have been recently employed together with induced pluripotent stem cells (iPSCs) as another target in creating faithful replicas of genuine pacemaker cells through somatic cell reprograming (Bucchi et al., 2006; Hu et al., 2014; Marban and Cingolani, 2015; Potapova et al., 2004).

1.2 Anatomy of the human sinus node

The sinus node (SN) is the primary pacemaker of the heart and it owes its function to the highly specialised cells it is comprised of. The first description of its anatomy dates back to 1907 when Keith and Flack identified the SN, while studying the mole's heart (Keith and Flack, 1907). Further studies reported the presence of this structure in many other mammals including human (Keith, 1942). James et al., described for the first time the ultrastructure of the dog and human SN, and compared it to the surrounding working myocardium of the right atrial myocardium (RA) (James et al., 1966).

The SN area extends from the superior vena cava towards the inferior vena cava along the SN artery. It is located in the subepicardial intercaval region of the right atrium (RA) and it is in a close proximity to the crista terminalis (Figure 1.1, 1.2 and 1.3) (James, 1961; Matsuyama et al., 2004; Sanchez-Quintana et al., 2005). Unlike smaller mammals such as rabbit, cat, and monkey (Alings et al., 1990; Bleeker et al., 1980; Opthof et al., 1987a), the human SN location varies within the crista terminalis.

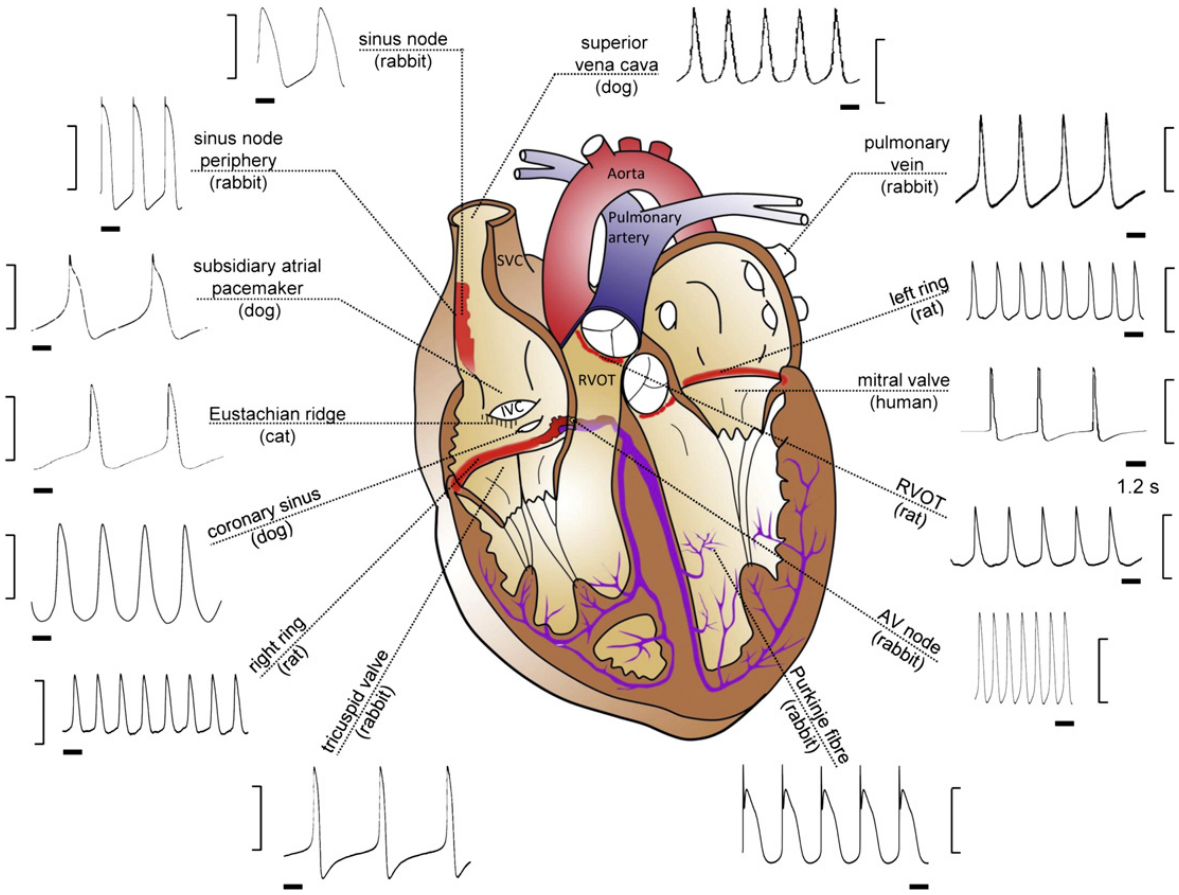

Figure 1.1. Anatomy of the cardiac conduction system and action potentials shapes from each heart area. Sinus node is located at the junction of the superior vena cava (SVC) with the right atrium and it can extend from the superior vena cava to the inferior vena cava (IVC). AP generation occurs in the SN and it is spread through the right and left atria until it reaches the atrioventricular node (AV node). The AP is delayed in the AV node in order to allow ventricular filling, which is then followed by AP propagation towards the His-Purkinje system (purple). The image depicts AP shapes from the different areas in the working myocardium and cardiac conduction system measured in rat, rabbit, cat, dog, or human. Adapted from Dobrzynski et al., 2013.

The SN structure itself comprises of three areas – head, body, and tail (Chandler et al., 2011; Opthof et al., 1987a; Sanchez-Quintana et al., 2005). The head is located at the top of the SN structure and it is situated at the junction between the superior vena cava and the right atrium. The body is continuation of the head and it spreads towards and around the SN artery (Chandler et al., 2011; Sanchez-Quintana et al., 2005). A general principle of locating the SN is to use the SN artery as a marker for its presence (Figure 1.3) (Chandler et al., 2011; James, 1961; Keith, 1942). To this end, it served as a guide when injecting microRNAs in the rat SN *ex vivo* (see Chapter 4). The SN body extends into the tail region, which is located between the terminal crest and the top of the inferior vena cava (Chandler et al., 2011; Sanchez-Quintana et al., 2005). The head and the tail region have been described to be closer to the endocardial region in comparison with the SN body, forming a crescent shaped structure (Chandler et al., 2011; Sanchez-Quintana et al., 2005).

Variability in the location of the earliest activation of pacemaker activity in the human SN has been observed in human open-heart surgeries, when the leading pacemaking site distribution would alter to various sites along the terminal crest and between the superior and inferior vena cava (Boineau et al., 1988; Chandler et al., 2011). Smaller mammals such as rabbit and dog were also shown to exhibit varying pacemaker location throughout the intercaval region (Fedorov et al., 2006; Kalman et al., 1995). Three-dimensional (3-D) anatomical reconstruction of the rabbit SN demonstrated the SN extends along about two-thirds of the intercaval region (Dobrzynski et al., 2005). Histological and immunohistochemical experiments on human tissue demonstrated the human SN dimensions are approximately 29.5 mm in length, 1.8 mm height, and 6.4 mm width (Figure 1.3) (Chandler et al., 2011). A recent 3D *ex vivo* computer model of the cardiac conduction system produced through micro-computer tomography (CT) scanning of blocks

containing human SNs, reported human SN structure dimensions of 18.8 mm in length and 43 mm width (Stephenson et al., 2017). Apart from the SN structure, another tissue that may be capable of automaticity, known as paranodal area, was identified at the inferior part of the crista terminalis (Figure 1.2, 1.3 and 1.4) (Chandler et al., 2011) and the Eustacian ridge (Morris et al., 2013; Rubenstein et al., 1987).

The SN structure has been shown to comprise of densely embedded individual myocytes distributed amongst connective and adipose tissue, collagen fibres, and fibroblasts (Figures 1.3 and 1.4) (Lowe et al., 1988). The SN area appears to be pale in comparison to the surrounding RA due to higher collagen concentrations (Figure 1.3 and 1.4). This structural variability with the RA allows it to be easily differentiated upon histological staining. Collagen content in the SN varies through the different species as it has been reported to account for 50% of the SN volume in smaller mammals such as rat, guinea pig, and cat, in comparison to 70-75% in bigger mammals such as pig and human (Figure 1.3 and 1.4) (Alings et al., 1995; Opthof et al., 1987a, b; Opthof et al., 1986). Opthof et al., suggest higher collagen content in the SN is related to more efficient structural support during contraction (Opthof et al., 1987b). Boyett et al., however, implied that is one of the mechanisms that protects the SN from the hyperpolarising resting membrane potential of the surrounding RA, and thus allows more depolarised membrane potential in the SN (Boyett et al., 2000).

There are three distinct subtypes of SN cells that are divided according to their size and electrophysiological properties into categories: 1) elongated spindle shaped cells at ~80 μm length containing one/two nuclei, 2) spindle cells at ~40 μm length containing one nuclei and 3) spider cells have irregular branched body architecture (Verheijck et al., 1998).

Electron microscopy studies demonstrated that the SN myocytes are pale and smaller, with few mitochondria and poorly organised myofilaments compared to the RA myocytes (James et al., 1966). According to their structural properties, SN myocytes have been observed to gradually transition from small, central SN myocytes to larger, peripheral SN myocytes. The peripheral SN myocytes (in small mammals) and paranodal area in human share structural properties with both SN and RA myocytes, which is the reason why it is considered as an intermediate transitional region between the nodal area and the working myocardium area (Boyett et al., 2000; Dobrzynski et al., 2013).

The SN exhibits distinct functional properties. The membrane potential of the SN is much more depolarised (-60 mV) compared to the resting potential of the surrounding RA (-80 mV) (Figure 1.5). This feature allows the spontaneous opening of the hyperpolarisation-activated cyclic nucleotide –gated channel (HCN), which upon activation induced firing of AP (Difrancesco and Tortora, 1991) (Figure 1.5 and 1.6). Hyperpolarisation of the SN membrane potential by the surrounding RA is prevented by weak electrical coupling (Boyett et al., 2000). This mechanism was supported by studies that reported SN pacemaking activity is increased by removal of the RA (Kirchhof et al., 1987; Kodama and Boyett, 1985). Moreover, computer simulation of direct coupling between SN and RA myocytes completely abolished automaticity (Joyner et al., 1998; Toyama et al., 1995). Joyner et al., produced a numerical model of the SN showing that its electrical coupling should be precisely balanced – it should be coupled sufficiently to excite the adjacent RA, but coupling should be lower than that in the RA to circumvent the hyperpolarising influence of the RA (Joyner and Vancapelle, 1986). The AP propagation from the SN towards the RA occurs through exit pathways involving peripheral SN myocytes. Dobrzynski et al., created a computer model of the SN demonstrating the impulse exit

pathway in the peripheral nodal cells express large-conductance channels, connexin43 (Cx43), responsible for electrical coupling in the working myocardium (Dobrzynski et al., 2005).

The spontaneous electrical activity in the SN can be generated in various sites (Fedorov et al., 2010). The SN leading pacemaker site is the area that is activated first usually within the SN head, but it could alter its location to either the inferior region or multifocal sites (Bleeker et al., 1980; Fedorov et al., 2010; Ramanathan et al., 2006). Pacemaking activity originating from the SN head has been demonstrated to be faster compared to inferior regions, suggesting there is hierarchy of the SN myocytes, where the conduction velocity is gradually decreased by shifting the leading pacemaker site from superior to inferior regions (Schuessler et al., 1996) (Figure 1.2). The inferior region of the SN is considered as a subsidiary or latent pacemaker, which is activated upon rapid atrial pacing, premature atrial stimulation, carotid sinus massage, or rarely occurs spontaneously (Boyett et al., 2000; Gomes and Winters, 1987). The subsidiary pacemaker site is considered as an escape mechanism with a longer cycle length than the leading pacemaker site. It has been suggested that shifting of the leading pacemaker site to inferior regions of the SN might be accountable for SSS development (Gomes and Winters, 1987).

1.3 Function of the sinus node

1.3.1 Sinus node action potential

The SN action potential (AP) differs from that in other regions of the heart (Figure 1.5 and 1.6). As shown in Figure 1.5 the AP in the RA consists of 5 phases: depolarisation (phase 0), rapid repolarisation (phase 1), plateau phase (phase 2), repolarisation (phase 3), and diastole (phase 4). In the SN there is no phase 1 (Figure 1.5 and 1.6).

The unique molecular and electrophysiological properties of the SN allow it to produce pacemaker potential, also known as diastolic depolarisation during phase 4 and propagate the AP to the RA myocardium (Dobrzynski et al., 2007; Irisawa et al., 1993; Mangoni and Nargeot, 2008). The resting membrane potential of the RA at diastole (during phase 4) is ~-80mV in comparison to the SN, where the membrane potential is more depolarised ~-60 mV (Drouin, 1997; Verkerk et al., 2007a; Verkerk et al., 2007b). A unique feature of the SN is the lack of resting membrane potential during phase 4 due to poor expression of K_{IR} channels responsible for the "inward rectifier" $I_{K,1}$ (Hibino et al., 2010) (Figure 1.6), which usually maintains the resting membrane potential in the working myocardium. For this reason the SN membrane potential is much more positive, which is a requirement for the opening of the HCN channels that conduct the pacemaking current known as I_f during phase 4. As it could be noted from their name HCN channels could be also activated by the presence of 3'-5'-cyclic adenosine monophosphate, which in turn allows the regulation of the beating rate by the autonomic nervous system (DiFrancesco, 2010; Robinson, 2003).

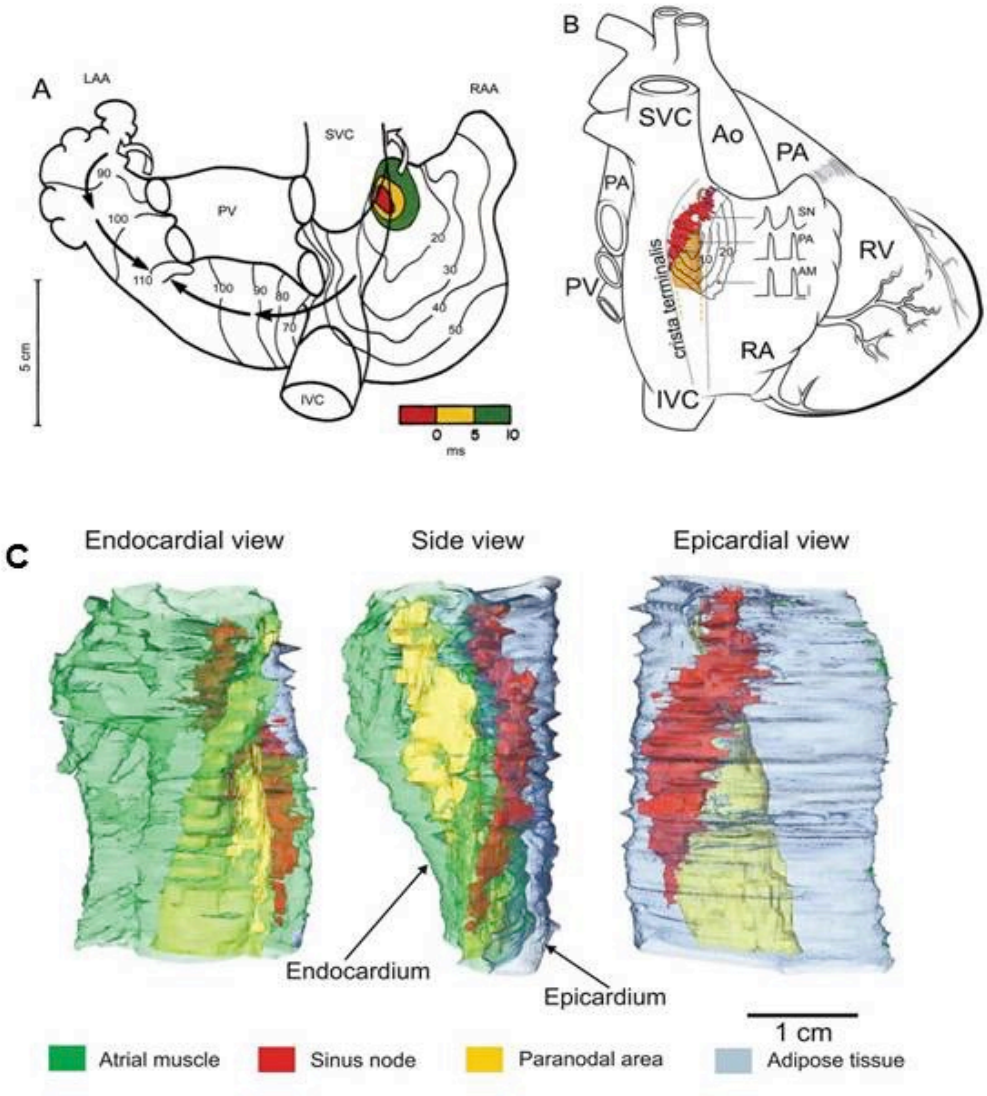

Figure 1.2. A. Dorsal view of the atria of a patient during open-heart surgery shows the leading pacemaker site (red) of the SN and the activation sequence of the atrial myocardium after AP; the activation sequence is shown as a colour scale and by the isochrones in ms. Adapted from Boineau et al., 1988. B. Model of the SN (red) and paranodal area (yellow) superimposed on a schematic diagram of the heart (dorsal view). Ao, aorta; IVC, inferior vena cava; PA, pulmonary artery; PV, pulmonary veins; RA, right atrium; RV, right ventricle; SVC, superior vena cava. C. 3D anatomical model of the human SN. Representation of endocardial and epicardial views -SN (yellow), paranodal area (green), atrial muscle (green), adipose tissue (blue); PM, pectinate muscle, TC, terminal crest. Adapted from Chandler et al., 2011.

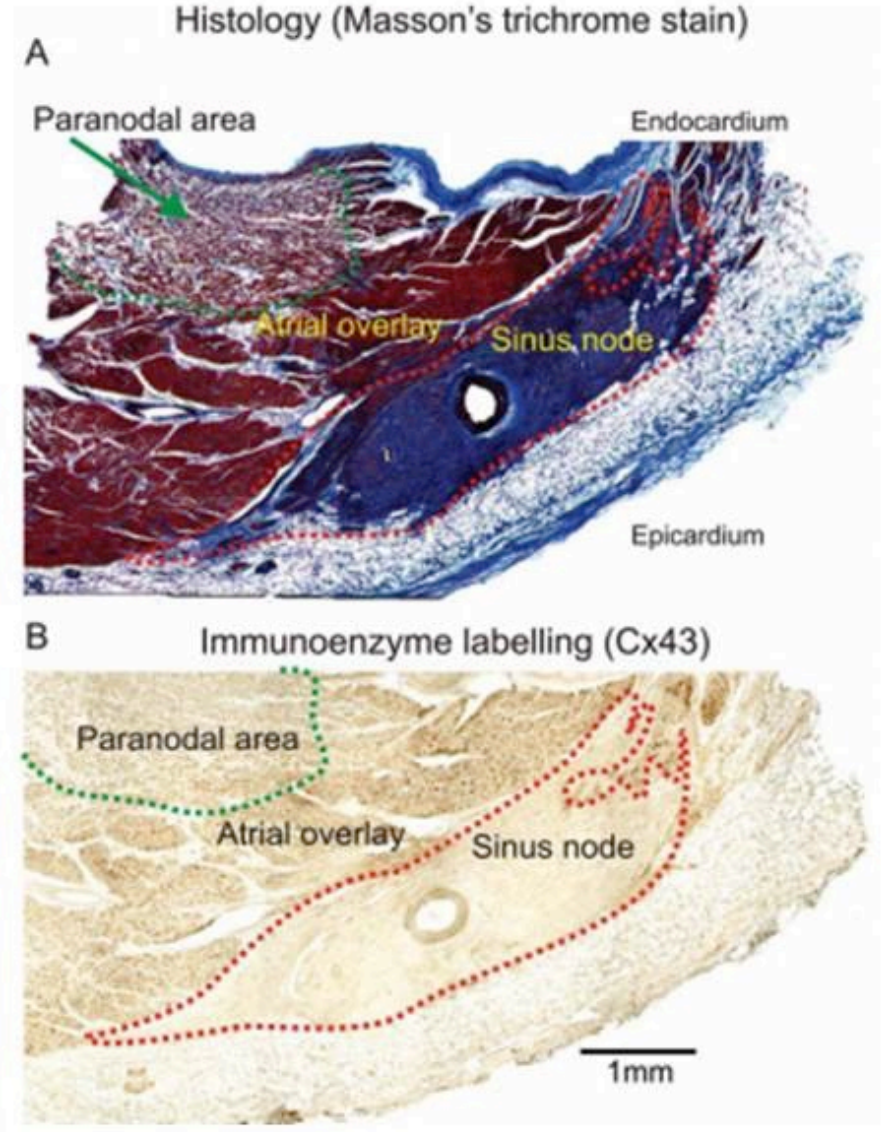

Figure 1.3. Masson's trichrome characterisation (A) and immunoenzyme labelling of Cx43 (B) of the human SN and paranodal area. A. Myocytes stained in purple, connective tissue in blue. B. Cx43 is labelling shown as small brown spots. Red dashed line denotes SN and green dashed line – paranodal area. Adapted from Chandler et al., 2011.

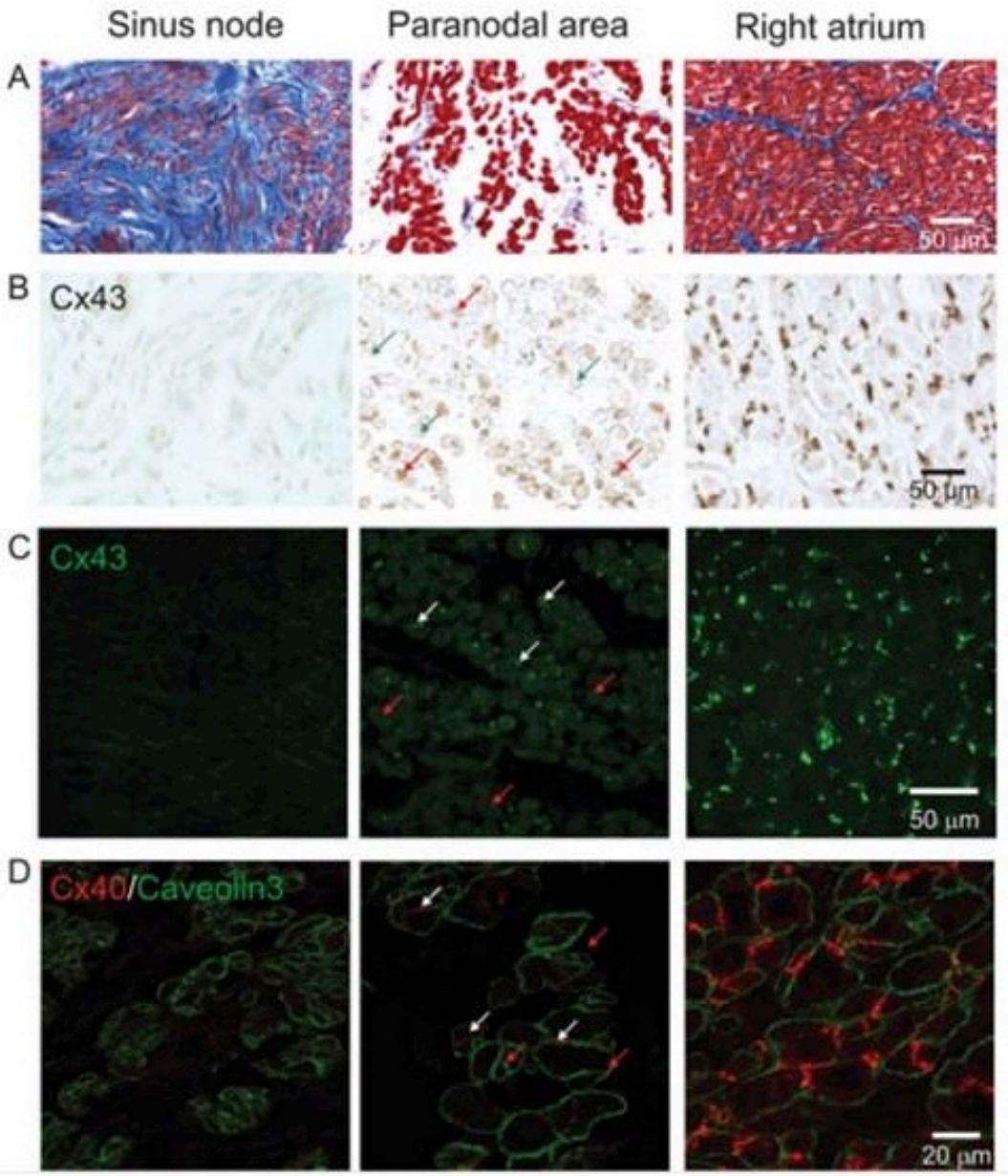

Figure 1.4. High magnification images of Masson's trichrome staining of sinus node, paranodal area, and right atrium tissue sections in A. Myocytes are red and connective tissue is blue. Cx43 immunoenzyme labelling in B. Cx43 is depicted in dark brown. Immunofluorescence labelling of Cx43 in C and Cx40 and caveolin3 in D. White arrows denote Cx43-expressing myocytes and red arrows highlight myocytes not expressing Cx43. White arrows denote Cx40 and red arrows – myocytes not expressing Cx40. Adapted from Chandler et al., 2011.

Phase 0 of the SN AP is characterised by slow (~5 V/s) upstroke produced by the opening of slow T-type, $Ca_V3.1$ ($I_{Ca,T}$) (Figure 1.5) (Leuranguer et al., 2000) and L-type, $Ca_V1.3$ ($I_{Ca,L}$) (Mangoni et al., 2003) channels and their respective currents. In contrast, the AP in the RA is characterised by fast (>100V/s) upstroke (Drouin, 1997; Verkerk et al., 2007a; Verkerk et al., 2007b) due to the cardiac Na^+ channel $Na_V1.5$, responsible for the fast I_{Na} (Irisawa et al., 1993; Mangoni and Nargeot, 2008). $I_{Ca,T}$ also takes part in the later part of phase 4 (discussed later). The SN AP lacks early phase of repolarisation (phase 1). Its plateau phase 2 is maintained by $Ca_V1.2/1.3$ channels, responsible for $I_{Ca,L}$ (Boyett et al., 1999). The role of $I_{Ca,L}$ in different areas of the SN structure has been studied by pharmacological inhibition with nifedipine in rabbit SN myocytes, which led to abolition of the SN pacemaking activity (Kodama et al., 1997). The role of $I_{Ca,T}$ role in the SN has been highly controversial as knockout mutation of the α subunit of $Ca_V3.1$ and $Ca_V3.2$ channels in mice was not related to electrocardiogram (ECG) changes (Chen et al., 2003; Mangoni et al., 2006). In contrast, Tanaka et al., reported $I_{Ca,T}$ to be responsible for the later part of the diastolic depolarisation during phase 4, where inhibition of the T-type Ca^{2+} as the phase is prolonged in the mouse and guinea pig SN due to inhibition of the current through specific T-type Ca^{2+}current using R(-)efonidipine caused phase 4 prolongation in the mouse and guinea pig SN (Tanaka et al., 2008).

The longer downward gradient and plateau phase 2 of the SN AP (Figure 1.6) has been suggested to prevent the occurrence of re-entry circuits (Boyett et al., 1999). Phase 2 is followed by repolarisation (phase 3) caused by inactivation of $Ca_V1.2$ and $Ca_V1.3$, and activation of K^+ channels responsible for $I_{to,}$ $I_{K,ur,}$ $I_{K,r,}$ *and* $I_{K,s}$ (ultra-rapid, rapid and slow delayed rectifier K^+ currents, respectively) during phase 3 (Figure 1.6) (Leuranguer et al., 2000; Ono and Ito, 1995; Verheijck et al., 1995).

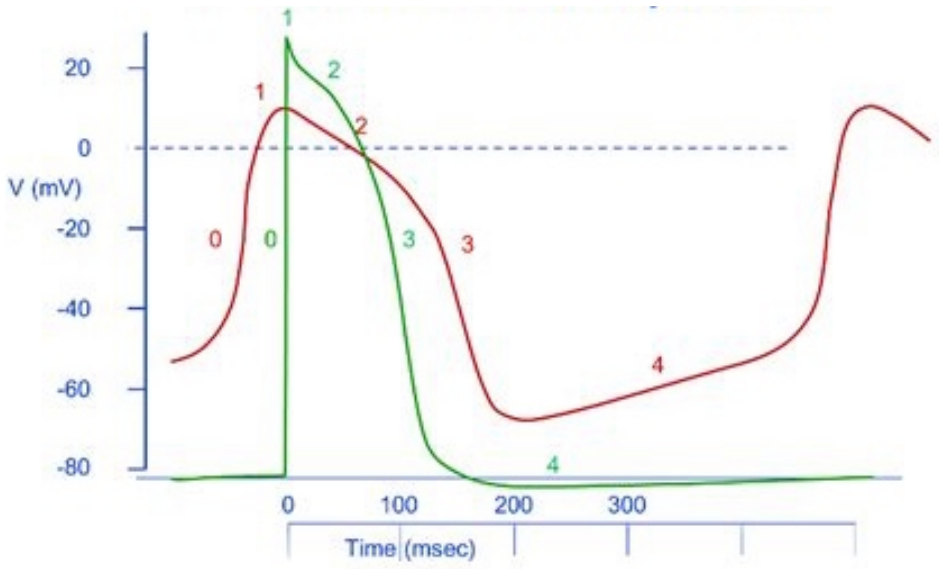

Figure 1.5. Atrial vs. sinus node action potentials (AP). Right atrial AP is denoted in green, sinus node AP in red. Numbers on the APs represent the different phases of the AP in the sinus node and the right atrium: 0 – AP upstroke, 1 – rapid repolarisation, 2 - plateau phase, 3 – repolarisation, 4 – diastole. Atrial threshold AP activation is -80 mV; SN threshold AP activation is -60 mV. 0 mV is denoted with an interrupted line. Adapted from Zipes, DP and Jalife J. Cardiac Electrophysiology; from Cell to Bedside. 5th ed. p.129.

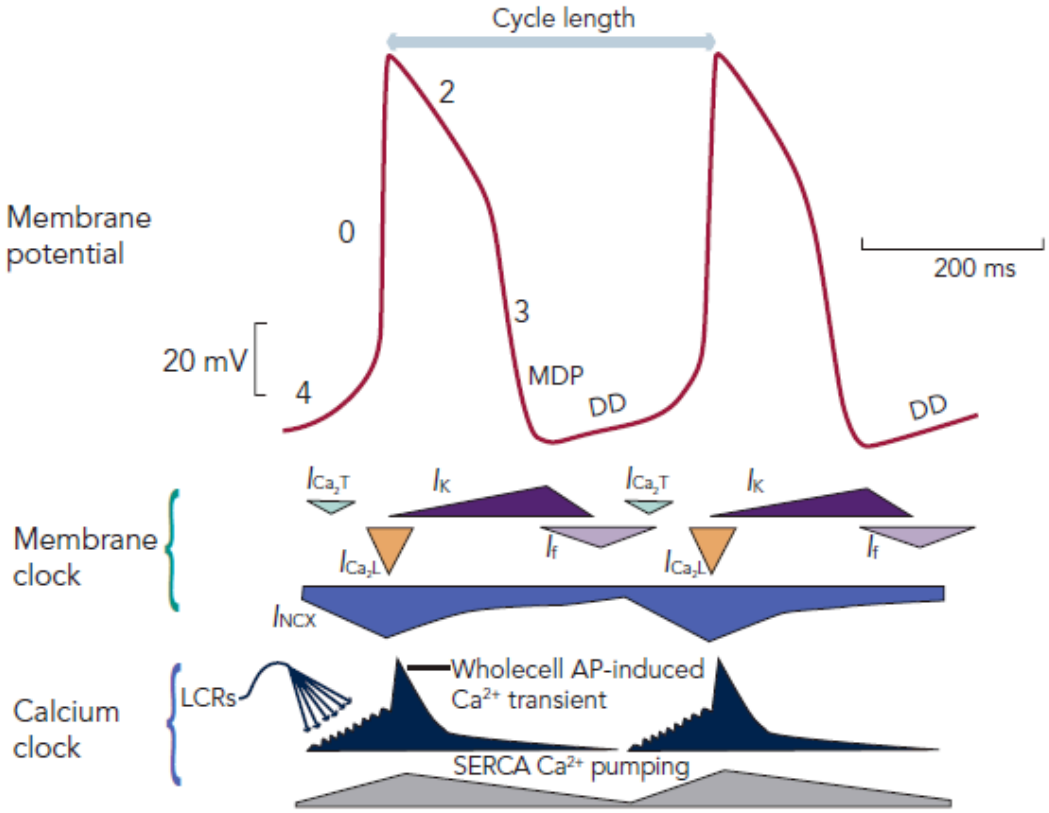

Figure 1.6. Sinus node action potential (AP) and role of membrane-voltage and Ca^{2+} clock. SN AP is denoted with a red trace. Phase 4 is the diastolic depolarisation (DD) regulated by I_f (HCN1/HCN4 channels). Phase 0 – AP upstroke regulated by slow T-type, $Ca_V3.1$ ($I_{Ca,T}$) and L-type $Ca_V1.3$ ($I_{Ca,L}$) channels. SN AP lacks early phase of repolarisation, phase 1, and exhibits longer plateau phase, phase 2 (due to $Ca_V1.2/1.3$ ($I_{Ca.L}$) in comparison with right atrium AP (Figure 1.5)). Phase 3 is regulated by transient outward K^+ current (I_{to}), $I_{K,ur}$, $I_{K,r}$ *and* $I_{K,s}$ (rapid, ultra-rapid and slow delayed rectifier K^+ currents respectively). I_{NCX} represents the current produced by NCX. SERCA – sarco-endoplasmic reticulum calcium pump. Adapted from Choudhury et al., 2015.

1.4 Clock mechanisms and sinus node automaticity

The membrane-voltage clock and the Ca^{2+} clock are the two major mechanisms that regulate the SN pacemaking activity and shape its AP (Lakatta and DiFrancesco, 2009). Figure 1.7 and 1.8 show these two mechanisms.

1.4.1 Membrane-voltage clock

1.4.1.1 The pacemaking inward "funny" current (I_f)

The membrane-voltage clock consists of the ion channels expressed at the SN cell membrane and the respective ionic currents they conduct. The AP is shaped by the conductance of positive and negative ionic currents in an inward and outward direction. The currents that cause positive polarisation of the SN intracellular membrane create diastolic depolarisation during phase 0 – I_f, $I_{Ca,L}$, and $I_{Ca,T}$ (Mangoni and Nargeot, 2008).

The major pacemaking channel is HCN4 and it is responsible for the conduction of the "funny" current (I_f), which is slowly activated by hyperpolarisation. I_f carries positively charged ions such as Na^+ ions, as well as K^+ and Li^+ to a lesser extent, resulting in the conductance of depolarising inward current (Azene et al., 2003). The positive net inward current depolarises the SN membrane potential to the activation threshold of T- and L-type Ca^{2+} channels, at which point they open and carry positively charged Ca^{2+} ions in order to induce further membrane depolarisation (Robinson et al., 2006). Pharmacological experiments in rabbit demonstrated the importance of I_f in the SN by reporting significant downregulation of the beating rate upon application of the I_f blocker Cs^+ (Denyer and Brown, 1990). Large-scale random mutagenesis studies in zebrafish associated for the first time mutations in HCN channels with decreased of heart rate in embryos and adult fish due

to inhibition of I_f conductance velocity and density, and decrease in channel expression (Baker et al., 1997; Warren et al., 2001). Ivabradine is a reversible inhibitor of I_f as it blocks HCN channels. The drug is used in the treatment of stable angina as it decreases the pacemaking activity of the SN, leading to subsequent decrease in the heart rate (Baruscotti and DiFrancesco, 2004; Bucchi et al., 2007).

Gauss et al., and Ludwig et al., were the first to clone and characterise the HCN ion channel family responsible for the conduction of I_f (Gauss et al., 1998; Ludwig et al., 1998). HCN ion channels are part of the voltage-gated K^+ channel family and are comprised of four members – HCN1-4. Mapping of the mouse and rabbit SN has shown presence of HCN1, HCN2, and HCN4 isoforms (Marionneau et al., 2005; Shi et al., 1999; Tellez et al., 2006). Ludwig et al., reported expression of only two isoforms (HCN2 and HCN4) in the human SN at mRNA level (Ludwig et al., 1999). HCN4 was demonstrated to be the predominant isoform in the human and rodent SN in comparison with atrial myocardium at protein level (Chandler et al., 2009; Dobrzynski et al., 2007; Yamamoto et al., 2006). HCN4 knockout mice exhibited 50% decrease in heart rate and recurrent sinus pauses, leading to deep bradycardia, followed by AV block (Baruscotti et al., 2011; Herrmann et al., 2007). Verkerk et al., reported the presence of the pacemaker current in the human SN (Verkerk et al., 2007b). Mutations in the human HCN4 gene were associated with sinus bradycardia, SSS, and familial SSS (Benditt et al., 1987; Milanesi, 2006; Schulze-Bahr et al., 2003; Ueda et al., 2004).

1.4.1.2 The inward Na^+ current (I_{Na})

The fast inward Na^+ current (I_{Na}) is responsible for the high velocity upstroke during depolarisation of the atrial AP, but it is absent in the SN (Kodama et al., 1997). As already mentioned the SN AP is characterised by low velocity upstroke indicating the absence of

I_{Na}. This concept was proven in rabbit central SN cells, where pacemaking activity was not affected by tetradotoxin (I_{Na} blocker) (Kodama et al., 1997). $Na_V1.5$ has been demonstrated to be the most abundantly expressed Na^+ channel isoform in the atria (Marionneau et al., 2005; Tellez et al., 2006). At both mRNA and protein levels, $Na_V1.5$ was confirmed to be more abundantly expressed in the right atrium compared to the SN (Chandler et al., 2009; Dobrzynski et al., 2007; Marionneau et al., 2005; Tellez et al., 2006). Even though $Na_V1.5$ was shown to be absent in the SN, knockout mutations of the channel in a mouse model were found to induce SN dysfunction, bradycardia, and slower SN conduction efficiency (Lei et al., 2005). Further studies in the role of I_{Na} in the SN reported the presence of two different I_{Na} components in the SN periphery – a tetradotoxin-sensitive neural component conducted by the $Na_V1.1$ channel isoform (Baruscotti et al., 1996) and a tetradotoxin-resistant component conducted by $Na_V1.5$ (Lei et al., 2005). The tetradotoxin-sensitive neural component was demonstrated to participate in the SN pacemaking activity in infant rabbits and adult mice (Baruscotti et al., 1996; Baruscotti et al., 1997; Lei et al., 2004), whereas the tetradotoxin-resistent component participated in the intranodal conduction (Lei et al., 2005).

1.4.1.3 The inward Ca^{2+} currents ($I_{Ca,L}$ and $I_{Ca,T}$)

Two separate Ca^{2+} currents have been reported to participate in and shape the SN AP - the long-lasting (approximately 300 ms) Ca^{2+} current ($I_{Ca,L}$) and the transient (approximately 30 ms) Ca^{2+} current ($I_{Ca,T}$) (Hagiwara et al., 1988; Irisawa et al., 1993). Kodama et al., showed that dihydropyridines like nifidipine abolish the spontaneous pacemaking activity of the SN (Kodama et al., 1997), proving $I_{Ca,L}$ is essential for the SN AP upstroke. Verheijck et al, reported $I_{Ca,L}$ activation threshold at -60 mV, suggesting it is contributing to the SN diastolic depolarisation (Verheijck et al., 1999). There are two channel isoforms

responsible for the conduction of $I_{Ca,L}$ - $Ca_V1.2$ and $Ca_V1.3$. Both $Ca_V1.2$ and $Ca_V1.3$ channels have been previously reported to be expressed in mouse, rabbit, and human SN (Chandler et al., 2009; Marionneau et al., 2005; Tellez et al., 2006). $Ca_V1.3$ isoform of which shown to be more abundantly expressed in the SN compared to $Ca_V1.2$, the abundance was higher in the atrial myocardium (Chandler et al., 2009; Marionneau et al., 2005; Tellez et al., 2006). $Ca_V1.3$ knockout mouse model demonstrated its contribution to the SN pacemaking activity as deletion of the $Ca_V1.3$ gene resulted in SN dysfunction, which was accompanied with bradycardia and spontaneous arrhythmias (Mangoni et al., 2003).

Application of Ni^{2+} or tetramethrin blocks $I_{Ca,T}$, but no effect over $I_{Ca,L}$ is observed (Hagiwara et al., 1988). Abolition of $I_{Ca,T}$ was shown to cause prolongation of the diastolic depolarisation duration resulting in longer cycle length (Hagiwara et al., 1988). The ion channel isoforms responsible for the conduction of the $I_{Ca,T}$ current are $Ca_V3.1$ and $Ca_V3.2$. $Ca_V3.1$ was found to be more abundantly expressed in the mouse SN compared to its surrounding atrial myocardium. The role of $Ca_V3.1$ in the mouse was shown using $Ca_V3.1$ knockout model, which exhibited bradycardia (Mangoni et al., 2006). $Ca_V3.1$ could not be detected in the rabbit (Tellez et al., 2006). Interestingly, $Ca_V3.2$ was equally detected in both mouse SN and the surrounding atrial myocardium (Marionneau et al., 2005). $Ca_V3.1$ was also shown to be more abundantly expressed in the human SN compared to RA (Chandler et al., 2009).

1.4.1.4 The outward delayed rectifier K^+ currents ($I_{K,ur}$, $I_{K,r}$ and $I_{K,s}$)

The delayed rectifier K^+ current is comprised of three different components – the ultra-rapid current ($I_{K,ur}$), the rapid current ($I_{K,r}$), and the slowly, gradually activated current ($I_{K,s}$) (Tristani-Firouzi et al., 2001). The delayed rectifier current is thought to dictate the

depolarisation phase during the cardiac AP, as well as the maximum diastolic potential, as it opposes the positive depolarising current and drives it back to resting membrane potential (Guo et al., 2011; Verheijck et al., 1995). Several studies demonstrated that pharmacological blockade of $I_{K,r}$ with a specific blocker E-4031 resulted in longer AP duration in the SN, a positive shift in the maximum diastolic potential and decreased diastolic depolarisation rate (Lei et al., 2001; Ono and Ito, 1995; Verheijck et al., 1995). The human working myocardium was reported to conduct all three components of the delayed rectifier K^+ current (Li et al., 1996).

The ion channel isoforms responsible for the conduction of $I_{K,ur}$, $I_{K,r}$, *and* $I_{K,s}$ are $K_V1.5$, $K_V11.1$ (also known as ether-a-go-go-related gene (ERG)) channel, and $K_V7.1$ (also known as K_VLQT1), respectively. All three isoforms were reported to be more abundantly expressed in the mouse and rabbit SN (Marionneau et al., 2005; Tellez et al., 2006), but only $K_V1.5$ and ERG were significantly more expressed in the human SN compared to RA (Chandler et al., 2009) at mRNA and protein levels. ERG's importance in the formation of the delayed rectifier K^+ current and the pacemaking function of the SN has been demonstrated using an ERG mutant knockout mouse model, which was reported to exhibit sinus bradycardia (Lees-Miller et al., 2003).

1.4.2 Ca^{2+} clock

Ca^{2+} plays a major role in linking the excitation of cardiomyocytes and their contraction (Joung et al., 2011). Sinus rhythm plays an essential role in spontaneous release of Ca^{2+} from the SR. High Ca^{2+} concentrations in the SR predispose to higher probability of spontaneous Ca^{2+} release and vice versa decrease in SR Ca^{2+} load decreases spontaneous Ca^{2+} release probability. The Ca^{2+} clock is referred to as the rhythmic changes of SR Ca^{2+}

release. Since SR Ca^{2+}concentrations depend on the change of the cell membrane voltage and the opening of the voltage-activated Ca^{2+}channels, the Ca^{2+}clock, and the membrane-voltage clock are interdependent (Figure 1.6). Higher Ca^{2+} levels trigger the release of Ca^{2+} from the sarcoplasmic reticulum (SR) through the ryanodine receptors (RyR) located at the SR membrane in the form of Ca^{2+} sparks (Chen et al., 2009; Cheng et al., 1996; Haga et al., 2012; Huser et al., 2000). Vinogradova et al., suggested that Ca^{2+} is released spontaneously, as voltage clamp experiments in chemically skinned SN myocytes demonstrated oscillatory spikes of Ca^{2+} (Vinogradova et al., 2005). Depletion of Ca^{2+} in the SR leads to increased Ca^{2+} influx from the extracellular space, implying that Ca^{2+} clock is essential for SN pacemaking function (Ju et al., 2007). Depolarisation of the cell membrane leads to an increased intracellular Ca^{2+} concentration, which in turn leads to further increase of intracellular Ca^{2+} from the intracellular Ca^{2+} stores located in the SR. Intracellular Ca^{2+} concentration increases from ~10^{-7} to ~10^{-6} M, which in turn activates the contractile apparatus – the sarcomere (Cheng et al., 1996; Monfredi et al., 2013). Upon gradual repolarisation of the membrane potential, the velocity of the inward Ca^{2+} currents decrease, and the high Ca^{2+} concentrations are recycled back to the SR through the sarco-endoplasmic reticulum ATPase (SERCA) or removed back to the extracellular space by the Na^{+}/ Ca^{2+} exchanger (NCX) (Figure 1.7 and 1.8) (Zipes et al., 2015).

Local higher Ca^{2+} concentrations also lead to activation of the electrogenic NCX, which works by extruding 1 Ca^{2+} ion in exchange for 3 Na^{+} ions, resulting in accumulation of net positive charge in the intracellular space (Bogdanov et al., 2001). The current produced by NCX, $I_{Na,Ca}$, depolarises further the SN cell membrane and thus it regulates the generation of the steep, exponential shape of the late diastolic depolarisation (Lakatta and DiFrancesco, 2009). This explains the involvement of NCX in the initiation of the SN

pacemaking activity. Lakatta et al., reports that the spontaneous SR Ca^{2+} release is manifested as Ca^{2+} sparks and it plays a major role in automaticity (Lakatta and DiFrancesco, 2009). The increase Ca^{2+} concentration leads to diastolic depolarisation in the SN through $I_{Na,Ca}$ conduction, which regulates synchronously both the membrane-voltage and the Ca^{2+} clock (Figure 1.6) (Bogdanov et al., 2001; Vinogradova et al., 2002; Maltsev et al., 2006). Pharmacological inhibition of $I_{Na,Ca}$ by Li^{+} was found to abolish SN pacemaking activity, proving the electrogenic current produced by NCX is essential for the SN spontaneous depolarisation (Bogdanov et al., 2001). Pharmacological blockade of RyR with ryanodine in rabbit and guinea pig has been shown to abolish Ca^{2+} release through RyR and cause decreased pacemaking rate in the SN (Bogdanov et al., 2001; Lyashkov et al., 2007; Rigg and Terrar, 1996). Furthermore, RyR2 mutation has been related to bradycardia (Postma et al., 2005), confirming RyR contributes to the spontaneous depolarisation produced by the SN.

Mammalian species have been found to express two isoforms of RyR – RyR2 and RyR3. RyR2 was reported to be significantly more expressed in the mouse, rabbit, guinea pig, and human RA in comparison with SN (Chandler et al., 2009; Marionneau et al., 2005; Musa et al., 2002; Rigg et al., 2000; Tellez et al., 2006). In contrast RyR3 was reported to be significantly more expressed in the mouse and rabbit SN in comparison with RA at mRNA level (Marionneau et al., 2005; Tellez et al., 2006). SERCA2a and NCX1were found to be more expressed in the human RA compared to SN at mRNA and protein levels (Chandler et al., 2009). They have been also found to be expressed in mouse and rabbit SN and RA (Marionneau et al., 2005; Musa et al., 2002; Tellez et al., 2006).

As already mentioned, mutations in the various components of the membrane-voltage and Ca^{2+} clock abolish SN activity (Hund and Mohler, 2008; Le Scouarnec et al., 2008).

Therefore, this strong connection between the membrane-voltage and Ca^{2+} clock (Figure 1.7 and 1.8) allows the generation of robust automated and cyclical diastolic depolarisation, which underlies efficient and spontaneous pacemaking activity in the SN (Zipes et al., 2015).

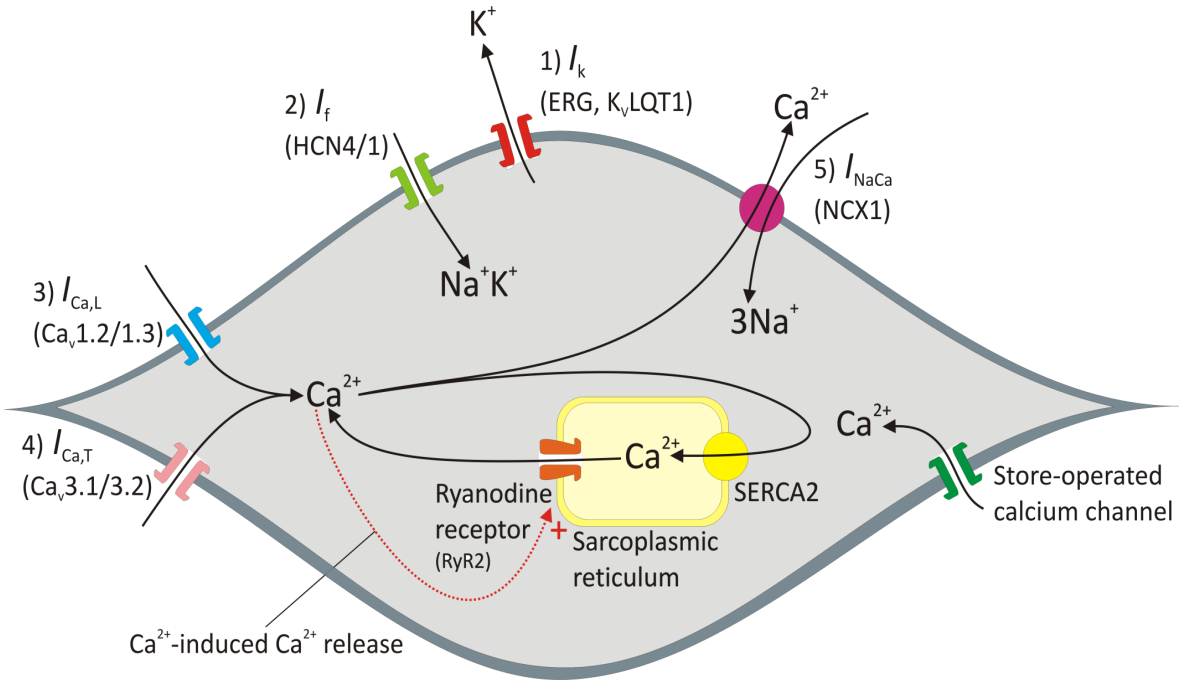

Figure 1.7. Relationship between membrane-voltage and Ca^{2+} clock. HCN1/4 and $Ca_V3.1/3.2$ synergistically generate spontaneous diastolic depolarisation, which leads to the opening of the L-type voltage gated Ca^{2+} channels $Ca_V1.2/1.3$. Higher local Ca^{2+} concentrations activate RyR2, which releases of Ca^{2+} from the intracellular stores of the sarcoplasmic reticulum (SR). Ca^{2+} is recycled back to the SR through SERCA2a, or released in the extracellular space by NCX1. Repolarisation current is produced by ERG and K_VLQT1 channels. Adapted from Monfredi et al. Pacing Clinical Electrophysiology (2010).

1.4.3 Electrical coupling in the SN

Part of the coordinated fashion of AP propagation is the electrical coupling between adjacent cardiomyocytes. Cardiomyocytes connect through intercalated discs that contain non-specific gap junctions responsible for the propagation of the electrical signal (Severs, 1995). The gap junctions are extensively expressed throughout the working myocardium (Figure 1.4) (Severs et al., 2004), but it has been generally concluded that they are absent from the SN cellular organisation (Figure 1.4) (James et al., 1966; Opthof et al., 1986). However, Lowe et al., demonstrated presence of intercalated discs between SN myocytes clusters (Lowe et al., 1988). Moreover, individual and poorly organised gap junctions were found to be randomly arranged in SN myocytes (Severs et al., 2004).

Each gap junction is comprised of hemichannels (connexons) that are located on the cell membrane of each cell they are connecting. These hemichannels consist of six transmembrane proteins (connexins). These non-selective channels allow small molecules to travel from one cell to its neighbouring one causing the propagation of the electrical signal following AP. Mathematical modelling of the SN has predicted that in order to preserve its pacemaking function SN should be poorly coupled in comparison with the RA (Joyner and Vancapelle, 1986). Well-developed electrical coupling between SN myocytes, however, would lead to abolition of SN pacemaking due to hyperpolarisation of the membrane potential caused by the surrounding atrial myocardium (Boyett et al., 2000). Gap junctions in the human SN have been reported to be sparsely distributed and smaller in diameter compared to the atrial myocardium (Boyett et al., 2006).

Connexins are a large family of proteins, each of which is characterised by specific conductance velocity, for example Cx40, Cx43, and Cx45 conductance is 153 pS, 60 pS,

and 25 pS, respectively. The myocardium has been reported to express Cx31.9, Cx37, Cx40, Cx43, and Cx46 (Chandler et al., 2009; Kanter et al., 1992; Kreuzberg et al., 2005; Vozzi et al., 1999). Cx43, a large-conductance channel, has been shown to be the most abundant one. Cx43 is absent from the SN in the human as well as other species (Davis et al., 1995). Cx40 was found to be more expressed in the human RA in comparison with the SN too (Chandler et al., 2009; Davis et al., 1995). Cx45 was found to be expressed in the human SN (Davis et al., 1995), and it was found to be equally abundant in the RA (Chandler et al., 2009). These molecular properties underlie fast conduction velocity of the AP in the working myocardium compared to the SN (Sano and Yamagishi, 1965). Poor electrical coupling in turn prevents the hyperpolarisation of the SN membrane potential by the surrounding RA (Joyner and Vancapelle, 1986). Therefore the fast conduction velocity of the RA working myocardium is attributed to the expression of Cx43, Cx40 and $Na_V1.5$ (Sano and Yamagishi, 1965). Functional experiments in rabbit confirmed the poor electrical coupling in the SN, reporting slower AP conduction velocity (0.03-0.05 m/s) compared to the atrial myocardium (~1m/s) (Boyett et al., 2000).

1.5 The transverse tubules and the sarcolemma

SN cells automaticity that causes diastolic depolarisation during phase 4 of the AP is regulated by intracellular Ca^{2+} concentrations (Maltsev et al., 2008; Wu et al., 2009). Furthermore, studies in larger animals report that SN Ca^{2+} concentrations are controlled by the interactions between the voltage-gated sarcollemal Ca^{2+} channels and the RyR2 located on the SR (Bogdanov et al., 2001; Huser et al., 2000). Despite the reports of the SR Ca^{2+} in the SN automaticity, our understanding of the SN SR Ca^{2+} release is incomplete. In our current study we hypothesised that SN cells own a “local control” mechanism to control cytosolic Ca^{2+} and thus they regulate automaticity. We were interested to investigate if t-

tubules are involved in the fast, coordinated Ca^{2+} release in the SN cells, where they could potentially enhance SN automaticity.

We owe our current knowledge of "local control" of intracellular Ca^{2+} release to ventricular cardiomyocytes. The transverse tubules (t-tubules) are membrane invaginations that penetrate deep within the cardiomyocytes. A dense SR network surrounds the t-tubules, facilitating Ca^{2+} -induced Ca^{2+} release following the initial Ca^{2+} entry through L-type Ca^{2+} channels during the action potential, and regulates the synchronous rise of intracellular Ca^{2+} through RyR2 at the junctional membrane of the SR (Brette and Orchard, 2003; Hong et al.2010). The closely positioned L-type Ca^{2+} channels and RyR2 build Ca^{2+} releasing units, which in turn initiate Ca^{2+} transients as a result of each action potential generated by the SN (Pinali et al., 2013; Wong et al., 2013). The synchrony of the SR Ca^{2+} release is owed to the widely distributed and regularly organised t-tubules that allow synchronous spread of Ca^{2+} throughout the entire cardiomyocytes. This mechanism produces rapid and synchronous Ca^{2+} cycling, since the longest distance between the cytoplasm and a neighbouring t-tubule is not more than 1 μm.

The sophisticated process of Ca^{2+}-induced Ca^{2+} release controlled by the t-tubular network and the surrounding SR is further involved in the rapid force generation and relaxation of the cardiomyocytes (Figure 1.8) (Gautel and Djinovic-Carugo, 2016). Myofibrils are the major unit of the cardiomyocyte contractile apparatus. They are tubular cross-striated structures located along the entire length of the cell (Figure 1.9) (Ehler et al., 2004). The myofibrils contain various sub-regions including the Z-lines or Z-discs (Luther, 1991; Luther et al., 2002). T-tubules occur at each Z-line, but branch further into the intracellular space forming a complex network comprised of transverse and longitudinal tubules (Soeller and Cannell, 1999). The distance between two Z-lines defines the sarcomere,

which is approximately 2 μm (Figure 1.9) (Irving et al., 2011). The sarcomere consists of thin filaments made up of actin, thick filaments made up of myosin, and titin filaments (Ehler et al., 2004; Maruyama et al., 1977). The thin actin filaments are anchored in the Z-lines, where they link to antiparallel actin and titin filaments from adjacent sarcomeres through α-actinin (Figure 1.9) (Djinovic-Carugo et al., 1999; Luther, 1991; Young et al., 1998). The thick myosin filaments are located in the centre of the sarcomere and they are interconnected within the sarcomere with other thick filaments via M-lines (Figure 1.9) (Irving et al., 2011). Titin filaments are located at the I-band region and it connects the M-lines with the Z-lines (Tokuyasu and Maher, 1987). Dystrophin plays an important structural role in interconnecting the t-tubular network, the myofibrils and the sarcomeric Z-lines (Frank et al., 1994; Klietsch et al., 1993; Rivier et al., 1999). The costameres are dystrophin-glycoprotein complexes, which are located at the intercalated discs of neighboring myocytes and provide cell-cell and cell-matrix connections (Di Mauro et al., 2009; Tokuyasu, 1989). The costameres are involved in the aligning of the Z-lines of neighboring cells via cytoskeletal actin filaments (Di Mauro et al., 2009). The organisation of the actin filament in the cardiomyocytes allows stable anchorage of the sarcomeric Z-lines during mechanical strain experienced during contraction (Vigoreaux, 1994).

Ventricular myocytes are characterised by the presence of well-organised t-tubular network, which allows rapid AP propagation as well as synchronised contraction-relaxation cycle (Figure 1.8) (Brette and Orchard, 2003; Heinzel et al., 2008; Louch et al., 2006). Formamide-induced detubulation of ventricular rat myocytes resulted in increased Ca^{2+} concentrations at the cell periphery, centre, and loss of $I_{Na,Ca}$ commensurate with inhibition of Ca^{2+} extrusion (Yang et al., 2002). T-tubular network has been reported to be absent from the atrial myocytes of smaller mammals such as mouse, rat, and rabbit

(Greiser et al., 2011; Huser et al., 1996; Woo et al., 2002). Lack of t-tubules in atrial myocytes from these species has been characterised by increased Ca^{2+} concentrations upon AP propagation in the cell periphery only (Kockskamper et al., 2001; Mackenzie et al., 2001). Studies in large mammalian species such as sheep, dog, cow, and human have demonstrated presence of extensive t-tubular network in the atrial myocytes (Boyden and Hoffman, 1981; Caldwell et al., 2014; Dibb et al., 2009; Lenaerts et al., 2009; Pardo et al., 1983; Richards et al., 2011). AP-triggered Ca^{2+} concentration increases in sheep atrial myocytes have been shown to be simultaneous in both cell periphery and cell centre (Dibb et al., 2009). Similarly, dog atrial myocytes were reported to increase their intracellular Ca^{2+} at the same time at the subsarcolemmal and the central cell regions (Wakili et al., 2010).

1.6 microRNAs in health and disease

1.6.1 Biology of microRNAs

In the past it has been thought that only 3% of the human genome is transcribed into functional proteins and the rest is "junk". Recent extensive work on non-coding molecules has begun to recognise their robust gene regulatory functions. One family of non-coding molecules are the microRNA family. MicroRNAs are ~18-24 nucleotide long single stranded RNAs, which regulate mRNA transcription into functional protein through post-transcriptional repression (Figure 1.10) (Griffiths-Jones et al., 2006). Inhibition of mRNA expression is achieved through binding of a microRNA to the 3' untranslated regions (3'UTR) of its target mRNA, although it has been reported that some microRNAs bind to coding domain sequence (CDS) of their target too (Brummer and Hausser, 2014; Pillai et al., 2004). The mRNA fate then depends on its sequence complementarity with that of the

silencing microRNA. Direct translational repression and sending of the mRNA for degradation is achieved due to perfect or near-perfect complementarity between the microRNA and its target sequence (Figure 1.10); this process is more common in plants (Lanet et al., 2009). In contrast, the mismatched target/sequence mechanism is more

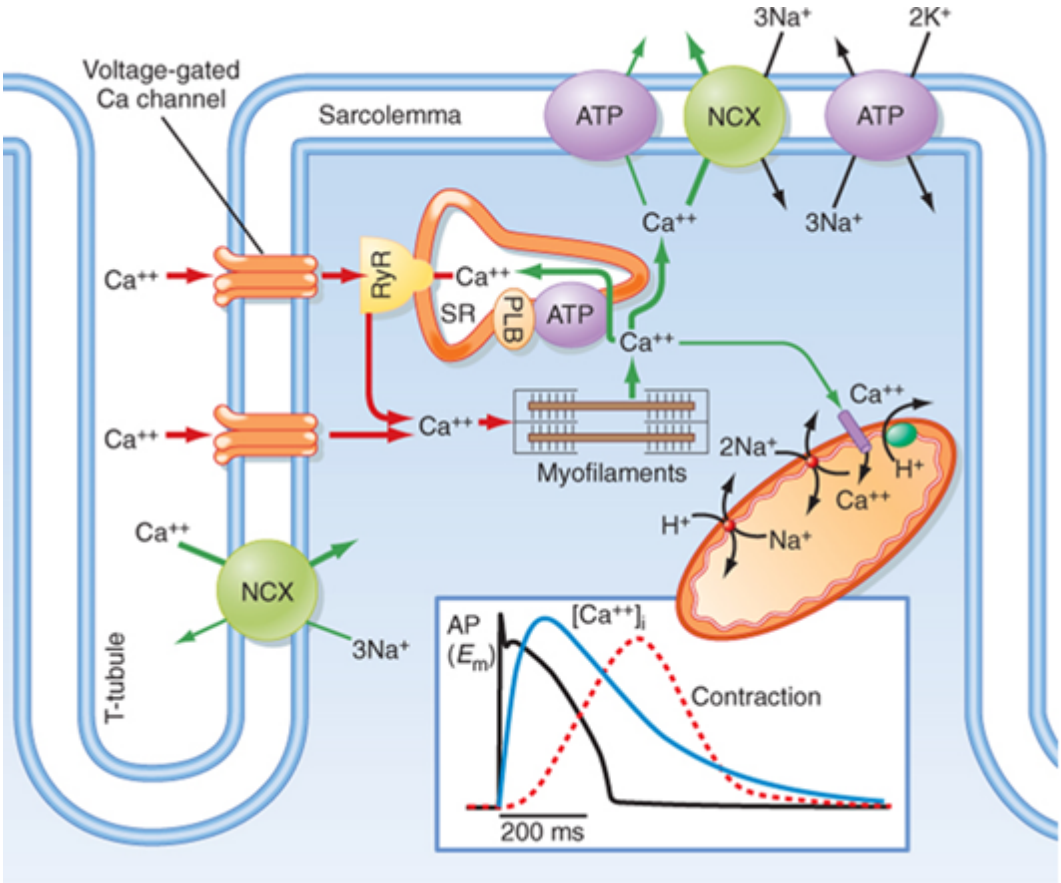

Figure 1.8. Excitation contraction coupling mechanism. Opening of L-type and T-type Ca^{2+} channels located at the membrane of the t-tubular cell membrane invaginations upon membrane depolarisation activates the opening of RyR at the sarcoplasmic reticulum membrane leading to further increase in intracellular Ca^{2+} concentrations. Ca^{2+} is a major player involved in the initiation of myofilament contraction caused by sliding of the thin actin and thick myosin filaments. Adopted from Koeppen and Stanton: Berne and Levy Physiology, 6th ed.

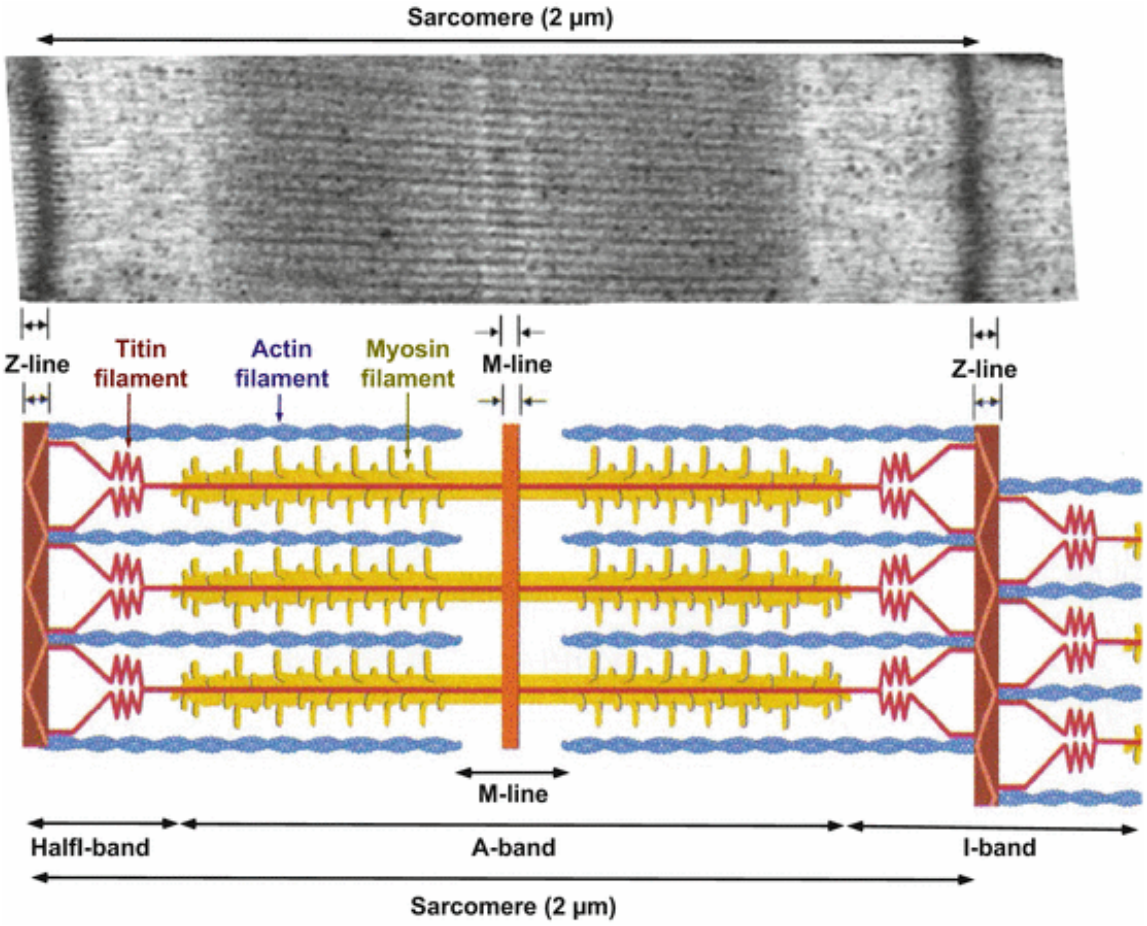

Figure 1.9. Cardiomyocyte sarcomere. Top panel represents electron microscopy image of the cardiomyocyte sarcomere. Image taken by Sh. Mahmoodzadeh 2014. Bottom panel represents a schematic diagram of the cardiomyocyte sarcomere corresponding to the sarcomere in the top panel. A-band (anisotropic band), I-band (isotropic band), H-zone (Hello zone), M-band (middle band). Adopted from Linke and Pfitzer: Physiolgie des Menschen, Ch.6, 2011.

common in mammals and it is characterised by cleaving of the mRNA sequence by a microRNA, which targets it for degradation or prevents its further translation to functional protein (Wahid et al., 2010). Translational repression of the mRNA target sequence is achieved by the matching of only 5-7 microRNA sequence bases (Lewis et al., 2005). MicroRNA expression can be tissue specific and their function in the cardiac development, adulthood, and various physiological and pathophysiological processes in the heart such as cardiac hypertrophy, fibrosis, arrhythmias, and heart failure has been recognised by large literature body (Boettger and Braun, 2012; Romaine et al., 2015).

1.6.2 microRNAs in the developing and adult heart

Multiple microRNAs have been reported to play an important role during embryonic cardiac development (Thum et al., 2007). Their critical role was assessed in mouse model studies that disrupted both global and cardioselective microRNA processing. MicroRNA depletion resulted in oedema, poor development of ventricular myocardium, and lethality (Martins et al., 2008). Large sequencing studies identified a number of microRNAs involved in the normal homeostasis of the healthy adult heart such as miR-1, miR-16, miR-27b, miR-30d, miR-126, and miR-133 (Landgraf et al., 2007; Thum et al., 2008).

1.6.3 microRNAs in cardiac hypertrophy and heart failure

Martins et al., study implies that many of the cardiac microRNAs are related to cardiac development and remodelling (Martins et al., 2008). The most abundant cardiac microRNAs – miR-1 and miR-133 – have been found to participate in skeletal muscle proliferation and differentiation (Chen et al., 2006). miR-1 knockout in mice resulted in abolition of ventricular chamber expansion during cardiac development (Zhao et al., 2007). miR-1 and miR-133 expression was demonstrated to be downregulated in mouse and

human cardiac hypertrophy (Care et al., 2007b). Scavenging of miR-133 with artificially produced antagomiR (an antisense sequence designed to bind and sequester its target microRNA) resulted in cardiac hypertrophy (Care et al., 2007b). These studies suggest that tight control over microRNA expression is essential for normal development and homeostasis.

Devaux et al., reported that circulating microRNAs such as miR-122, miR-133, miR-210, and miR-423-5p are potential prognostic indicators in the development of heart failure and acute myocardial infarction (Devaux et al., 2013).

1.6.4 microRNAs and arrhythmogenesis

Computational prediction algorithms identified $Ca_V1.2$ as a target of miR-328, suggesting the microRNA plays a role in the cardiac AP regulation. MiR-328 expression was increased 4 fold in left atrial samples in a canine model of atrial fibrillation, and also in human patients with rheumatic heart disease (Lu et al., 2010).

MiR-328 overexpressed via adenoviral transduction in canine atrium and also in a transgenic approach using a mouse model resulted in inhibition of $I_{Ca,L}$ and shorter AP duration, leading to higher atrial fibrillation susceptibility (Lu et al., 2010). To this end, knockdown of miR-328 with anti-miR-328 reversed atrial fibrillation via rescue of $Ca_V1.2$ and $I_{Ca,L}$ (Lu et al., 2010).

Increased levels of miR-423-5p were reported to directly target and inhibit HCN4 mRNA expression as well as I_f in the SN in a mouse model of training-induced bradycardia (D'Souza et al., 2017). Inhibition of miR-423-5p with antagomiR-423-5p reversed the training-induced bradycardia and rescued HCN4 expression and subsequently I_f (D'Souza et al., 2017). miR-17-92 and miR-106b-24 deficient mice were shown to exhibit atrial

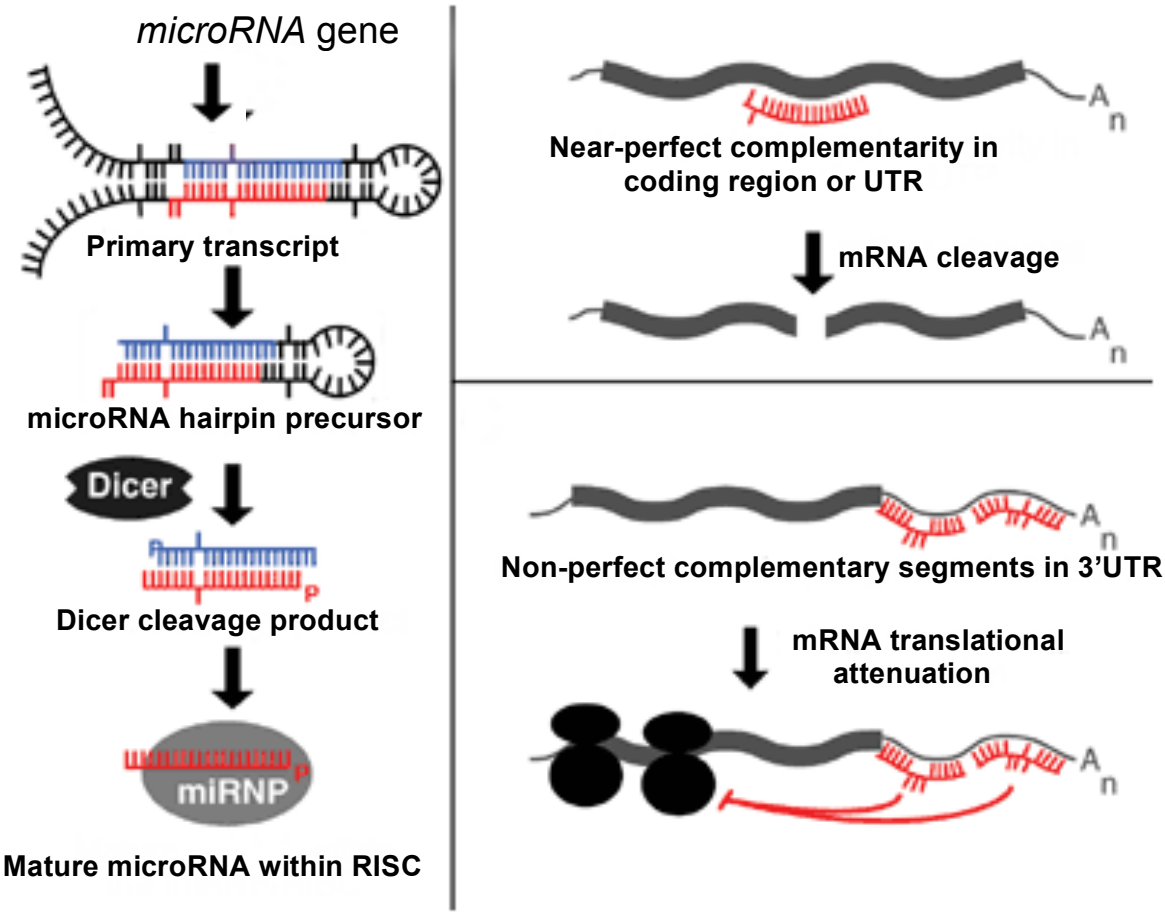

Figure 1.10. Biogenesis and functional role of microRNAs. MicroRNAs are transcribed from the microRNA gene to a primary transcript sequence. The primary transcript is further processed to a shorter pre- microRNA structure. The ribonuclease Dicer cleaves the double-stranded pre- microRNA structure into single strands. The single stranded microRNA fragments bind to the Argonaute (Argo/RISC) complex, which travels to its target mRNA and binds it. Target recognition is achieved when the nucleotides at position 2-8 at the 5'-end of the microRNA molecule, known as the seed region, achieve near-perfect or non-perfect complementarity with the recognition seed elements at the 3'untranslated region of the target mRNA. Depending on their complementarity the interaction between the microRNA and its target mRNA leads to translational attenuation or targeting of the mRNA for degradation.

fibrillation upon pacing (Wang et al., 2014a). Further abnormalities such as prolonged PR intervals were observed in mice with cardiospecific miR-17-92 inactivation, and SN dysfunction in mice with miR-17-92 inactivation and miR-106b-24 heterozygosity (Wang et al., 2014a).

MiR-1 was reported to be overexpressed by human patients with coronary artery disease (Yang et al., 2007). Introduction of miR-1 in infarcted rat hearts resulted in exacerbation of arrhythmogenesis due to slowed conduction and more depolarised membrane potential caused by Cx43 and $K_V2.1$ repression *ex vivo* (Yang et al., 2007). Arrhythmogenesis was ameliorated by miR-1 antagomiR (Yang et al., 2007). Further studies showed an inverse relationship between miR-1 and $K_{ir}2.1$, where $K_{ir}2.1$ expression was significantly upregulated in patients with atrial fibrillation, in comparison with miR-1 levels that were 86% decreased (Girmatsion et al., 2009). *Ex vivo* tachystimulation of atrial slices from human specimens exhibited an inverse relationship between $K_{ir}2.1$ protein levels miR-1 (Girmatsion et al., 2009). This study suggests $K_{ir}2.1$ is a direct target of miR-1 and dysregulation in their balance causes arrhythmias.

Matkovich et al., reported that upregulation of miR-133 is correlated to prolonged QT intervals in mouse ventricular myocytes (Matkovich et al., 2010). It was suggested that this is due to inhibition of the fast component of I_{to}. However, direct correlation between miR-133, and $K_V4.2$ and $K_V4.3$ channels was not found, suggesting that miR-133 regulates I_{to} in an indirect manner (Lagos-Quintana et al., 2002). Another study in a rat ventricular hypertrophy model reported increased HCN2 and HCN4 expression, downregulation of miR-1 and miR-133 and arrhythmogenesis and hypertrophy (Luo et al., 2008), suggesting a close regulation of HCN channels by miR-1 and miR-133.

miR-212 levels were reported to be significantly upregulated in an animal model of heart failure and in human heart failure samples (Thum et al., 2007). miR-212 was later predicted to target $K_{ir}2.1$ expression (Goldoni et al., 2012). Whole-cell patch-clamp recordings from HeLa cells overexpressing miR-212 displayed reduction of $I_{K,1}$ current density. Moreover, miR-212 levels were upregulated in patients with atrial fibrillation and mitral stenosis (Xiao et al., 2011).

Several studies reported the role of miR-1 in the regulation of cardiac electrical coupling by targeting Cx43. Cardiomyocytes from a mouse model of viral myocarditis were found to express significantly elevated levels of miR-1 commensurate with downregulated Cx43 levels (Xu et al., 2012; Yang et al., 2007). Another study in a rat model of myocardial infarction showed upregulation of miR-1 correlated to Cx43 and $K_{ir}2.1$ downregulation (Yang et al., 2007). MiR-208 was reported to regulate Cx40 expression and stress-dependent cardiac growth (Callis et al., 2009). ECG from a miR-208 knockout mouse model demonstrated significant increases in atrial fibrillation events due to prolonged PR intervals (Callis et al., 2009).

Adenoviral-mediated miR-1 forced overexpression in rat ventricular myocytes contributed to increased $I_{Ca,L}$ amplitude and higher frequency of Ca^{2+} sparks, leading to decreased Ca^{2+} concentrations in the SR (Terentyev et al., 2009). Moreover, miR-1-overexpressing cardiomyocytes generated spontaneous arrhythmogenic oscillations in the presence of isoproterenol, which stimulates β_1 receptors and thus increases cardiac contractility (Terentyev et al., 2009). This study demonstrated that miR-1 regulates excitation-contraction coupling by indirectly upregulating the activity of RyR2 and L-type Ca^{2+} channels (Terentyev et al., 2009). A study using SERCA2a adenoviral transfection as gene therapy for heart failure reported that SERCA2a forced expression rescued downregulated

miR-1 levels as well as NCX1 levels in failing cardiomyocytes (Kumarswamy et al., 2012). A luciferase activity reporter gene assay validated NCX1 as a target of rat miR-1 (Kumarswamy et al., 2012). Target identification studies revealed that miR-214 prevents apoptosis in cardiomyocytes during ischemia reperfusion injury by reducing cytosolic Ca^{2+} overload through NCX1 (Aurora et al., 2012). Another microRNA from the same family, miR-24, was found to regulate Ca^{2+} homeostasis by targeting junctophilin-2 expression (Xu et al., 2012). These data imply that many microRNAs are involved in the regulation of the Ca^{2+} homeostasis, which is important for both cell survival and excitation-contraction coupling. Summary of the microRNAs involved in arrhythmogenesis in human patients and animal models is summarised in Table 1.1.

MicroRNAs have been also studied as potential biomarkers of cardiovascular pathologies. Increased miR-1 (Cheng et al., 2010), miR-133 (Wen et al., 2014), miR-208a (Corsten et al., 2010), miR-423-5p (Thum et al., 2007) serum levels were discovered in both patients with and animal models of acute myocardial infarction (van Rooij et al., 2008b), heart failure (Thum et al., 2007), and cardiac hypertrophy (Care et al., 2007a).

microRNA	Target	Model	Paper
miR-328	$Ca_V1.2$	Dog model of atrial fibrillation; Human patients	Lu et al., 2010
miR-423-5p	HCN4	Training-induced mouse model of bradycardia	D'Souza et al., 2017
miR-17-92 miR-106b-24	Shox2 and Tbx3	Mouse model	Wang et al., 2014a
miR-1	Cx43 and $K_V2.1$; HCN2 and HCN4; Cx43; L-type Ca^{2+} channels and RyR2; SERCA2a and NCX1	Rat model and atrial fibrillation patients; Rat ventricular hypertrophy model; Mouse model of viral myocarditis; Rat ventricular myocytes; Failing cardiomyocytes	Yang et al., 2007; Girmatsion et al., 2009; Luo et al., 2008; Xu et al., 2012; Yang et al., 2007; Terentyev et al., 2009; Kumarswamy et al., 2012
miR-133	$K_V4.2$ and $K_V4.3$; HCN2 and HCN4	Mouse ventricular myocytes; Rat ventricular hypertrophy model	Matkovich et al., 2010; Lagos-Quintana et al., 2002; Luo et al., 2008;
miR-212	$K_{ir}2.1$	Human heart failure samples; HeLa cells; Atrial fibrillation and mitral stenosis patients	Thum et al., 2007; Goldoni et al., 2012; Xiao et al., 2011;
miR-208	Cx40	miR-208 knockout mouse model	Callis et al., 2009
miR-214	NCX1	Cardiomyocytes during ischemia reperfusion	Aurora et al., 2012
miR-24	Junctophilin-2	Rat ventricular cardiomyocytes	Xu et al., 2012

Table 1.1. Summary of microRNAs targeting ion channels, Ca^{2+}-handling proteins, connexins and transcription factors associated with arrhythmogenesis in human patients and animal models.

1.7 Transcription factors and the sinus node

Transcription factors are proteins that regulate the transcription of specific genes by binding to their DNA target sequences (Latchman, 1997; Mitchell and Tjian, 1989). Unlike microRNAs, which are also regulatory non-coding molecules, transcription factors can regulate their target genes positively or negatively depending on their tissue availability (Latchman, 1997). They have been found to have extensive role not only in embryogenesis, but in adulthood too (Sun et al., 2008; Sun et al., 2007). Tightly regulated expression and tissue specificity, important for normal homeostasis, make transcription factors a potential therapeutic target. The transcription factor gene network in the SN is divided into two major branches – T-box (Tbx) factors – Tbx1, Tbx3, Tbx5, and Tbx18, and the homeodomain factors – Shox2, Nkx2-5, and Isl1 (Figure 1.12) (Greulich et al., 2011; Harvey et al., 2002; He et al., 2011).

The early stages of cardiac development in the embryo are characterised by development of a linear heart tube built from primitive myocytes exhibiting automaticity (Figure 1.11) (van Weerd and Christoffels, 2016). The proliferation and maturation of these early myocytes is controlled by a tight gene regulatory programme, which distinguishes the working myocardium from the cardiac conduction system through tissue specific expression of Cx40, Cx43, and $Na_V1.5$ (Figure 1.12) (Moorman and Christoffels, 2003). In turn, the chamber-specific gene programme initiating the proliferation of the working myocardium is actively repressed in the sinus venosus, which gives rise to the SN at later stages (Figure 1.11). Mouse cardiac embryonic development studies reveal that the initial heart tube expressed Nkx2-5. Nkx2-5 is a major transcription factor in the developing and adult working myocardium, atrioventricular node and atrioventricular bundle (Figure 1.12) (Moskowitz et al., 2007). It directly or indirectly reinforces Cx40, Cx43, and $Na_V1.5$

expression, and abolishes Tbx3 and HCN4 expression (Figure 1.12) (Espinoza-Lewis et al., 2009; Ye et al., 2015). Further development of the sinus venosus in the early heart tube was shown express Tbx18, but Nkx2-5 was absent. Furthermore, mouse embryos lacking the Tbx18 gene fail to develop the SN head and exhibit malformations of the sinus venosus structure. Tbx18 appears to be essential in the morphological formation of the SN, but Tbx18 knockout mutant mice display normal pacemaking activity, suggesting its expression is dispensable for the SN functional maturation (Ionta et al., 2015). In contrast, another study reported that viral transfection with Tbx18 enhances the SN gene programme in quiescent cardiomyocytes (Kapoor et al., 2013). Both studies, however, agree that Tbx18 is capable of inhibiting the working myocardium gene programme.

Nkx2-5 works in coordinated fashion with Tbx5 during cardiac and ventricular conduction system development (Figure 1.12) (Bruneau et al., 2001; Moskowitz et al., 2007; Pashmforoush et al., 2004). They have been shown to physically interact and potentially co-activate target genes depending on their tissue availability (Bruneau et al., 2001; Hiroi et al., 2001). Tbx5/Nkx2-5 knockout mouse embryos were reported to exhibit impaired myocardial differentiation (Luna-Zurita et al., 2016).

Nkx2-5 role in the adult heart was demonstrated in studies of cardiac hypertrophy, where expression levels were increased upon pressure overload and stress stimulation. In a feline model of right-ventricular pressure overload and phenylephrine- and isoproterenol-induced cardiac hypertrophy also exhibited increased Nkx2-5 levels (Saadane et al., 1999; Thompson et al., 1998). Moreover, Nkx2-5 is involved in cardiac hypertrophy through indirect regulation of other transcription factors such as GATA4, SRF, and CAMTA (Chen and Schwartz, 1996; Durocher et al., 1997; Shiojima et al., 1999; Song et al., 2006). Nkx2-5 was also reported to play a role as a survival factor, as Nkx2-5 knockout mice exhibited

cardiac dysfunction and cardiomyocyte apoptosis (Toko et al., 2002). Furthermore, doxorubicin-induced cardiomyocyte apoptosis was much more pronounced in Nkx2-5 knockout mice compared to control, suggesting Nkx2-5 has a cardioprotective function (Toko et al., 2002). In contrast, Kasahara et al., reported that Nkx2-5 forced expression in mouse heart resulted in organ failure and cardiac conduction alterations, suggesting Nkx2-5 levels are under tight regulation, because imbalanced expression leads to pathological conditions (Kasahara et al., 2003).

Malformations in the morphogenesis of the cardiac outflow tract have been related to alterations of Tbx1 expression (Xu et al., 2004; Zhang et al., 2006). Tbx1 involvement in the SN was demonstrated in Tbx1 knockout mice, where the elevated cell proliferation in the cardiac outflow tract, from which the SN originates, was noted (Xu et al., 2004).

Tbx3 is a major regulatory transcription factor involved in the generation, maturation, and functional maintenance of the SN (Figure 1.12) (Hoogaars et al., 2007b). In the SN during embryogenesis, it supresses the chamber-specific gene expression programme involved in the working myocardium maturation (Hoogaars et al., 2007b). Tbx3 forced expression in foetal atria was demonstrated to induce downregulation of atrial specific genes such as Cx40 and Nppa (natriuretic peptide) and upregulation of characteristic SN genes such as HCN1, HCN2, HCN4, $Ca_V1.3$, and Cx30.2, leading to ectopic pacemaking activity (Figure 1.12) (Hoogaars et al., 2007b). Tbx3 was also found to play an important role in the adult heart too, as Tbx3 overexpression in the atria inhibited the working myocardium gene programme, but it did not induce SN gene programme expression as it did in mouse foetuses (Bakker et al., 2012), suggesting the ability of Tbx3 to initiate SN programme genes is lost during maturation.

Shox (short stature homeobox) genes are a family of transcription factors regulating cell fate, cycle, and growth. Developing hearts of human embryos were shown to express Shox2 (Figure 1.12) (Blaschke et al., 1998; Clement-Jones et al., 2000; Rao et al., 1997), which is another transcription inhibitor of the chamber-specific gene programme of the working myocardium. Shox2 represses Nkx2-5 and activates the insulin gene enhancer protein (Isl1) (Figure 1.12) (Hoffmann et al., 2013; Tessadori et al., 2012; Vedantham et al., 2015), and thus indirectly initiates the SN development gene programme (Blaschke et al., 2007). The function of Shox2 was demonstrated with studies examining the effect of Shox2 loss-of-function mutation, which resulted in hypoblastic SN development (Blaschke et al., 2007). Shox2 forced expression in embryonic stem cells, however, initiated automaticity (Ionta et al., 2015). Isl1, as already mentioned, works in accordance with Shox2 (Hoffmann et al., 2013). RNA sequencing revealed that Isl1 is expressed in developing pacemaker cells (Vedantham et al., 2015). Isl1 participates in the mechanism of SN precursor cell proliferation and differentiation, and its targeted repression causes Tbx3 and Shox2 gene downregulation and lethality in embryos (Dorn et al., 2015; Liang et al., 2015).

A recent study from D'Souza et al., depicted the close relationship between transcription factors and microRNAs in the regulation of SN function. Upregulation of Nkx2-5 in the SN of a mouse model of training-induced bradycardia caused upregulation of miR-423-5p levels, which resulted in decreased HCN4 levels and subsequent downregulation of I_f (D'Souza et al., 2017). The paired-like homeodomain transcription factor 2 homeobox gene (Pitx2) is a transcription factor involved in early embryogenesis when it represses the SN gene programme and inhibits automaticity in the working myocardium (Figure 1.12) (Nadadur et al., 2016; Wang et al., 2014a). Moreover, Pitx2 role in the SN was shown to

be important in arrhythmogenesis through microRNA regulation (Wang et al., 2014a). Pitx2 was also found to enhance miR-17-92 and miR-106b-25 expression. miR-17-92 and miR-106b-25 downregulation was shown to causes pacing-induced atrial fibrillation, prolonged PR intervals and SN dysfunction (Wang et al., 2014a). miR-17-92 and miR-106b-25 were also shown to repress Shox2 and Tbx3, which are a part of the SN gene programme and a requirement for its development (Wang et al., 2014a).

The ability of transcription factors to reinforce or suppress gene programmes from the early stages of embryogenesis to the late tissue maturation underlie their potential functional role in transforming working myocardium cells into pacemaker-like cells and vice versa. This property has been widely studied in the development of biological pacemakers, which will be further discussed in the Biological pacemakers sections of the general introduction.

1.8 Clinical relevance

Sick sinus syndrome (SSS) is characterised by dysfunction of the SN and inability to perform its main function as a pacemaker, characterised by irregular AP generation and/or disruptions of the mechanism controlling the propagation of the AP towards the rest of the cardiac conduction system and the working myocardium. SSS encompasses a range of heart rate abnormalities such as sinus bradycardia, sinus arrest, SN exit block, slower intrinsic heart rate and longer SN recovery periods, which account for up to 50% of electronic pacemaker implantations around the world (Benditt et al., 1987; Mond and Proclemer, 2011; Rubenstein et al., 1972). The primary cause of SSS, however, is aging, illustrated by the inverse relationship between age and SSS morbidity in those over the age of 65 years (Benditt et al., 1987; Haqqani and Kalman, 2007).

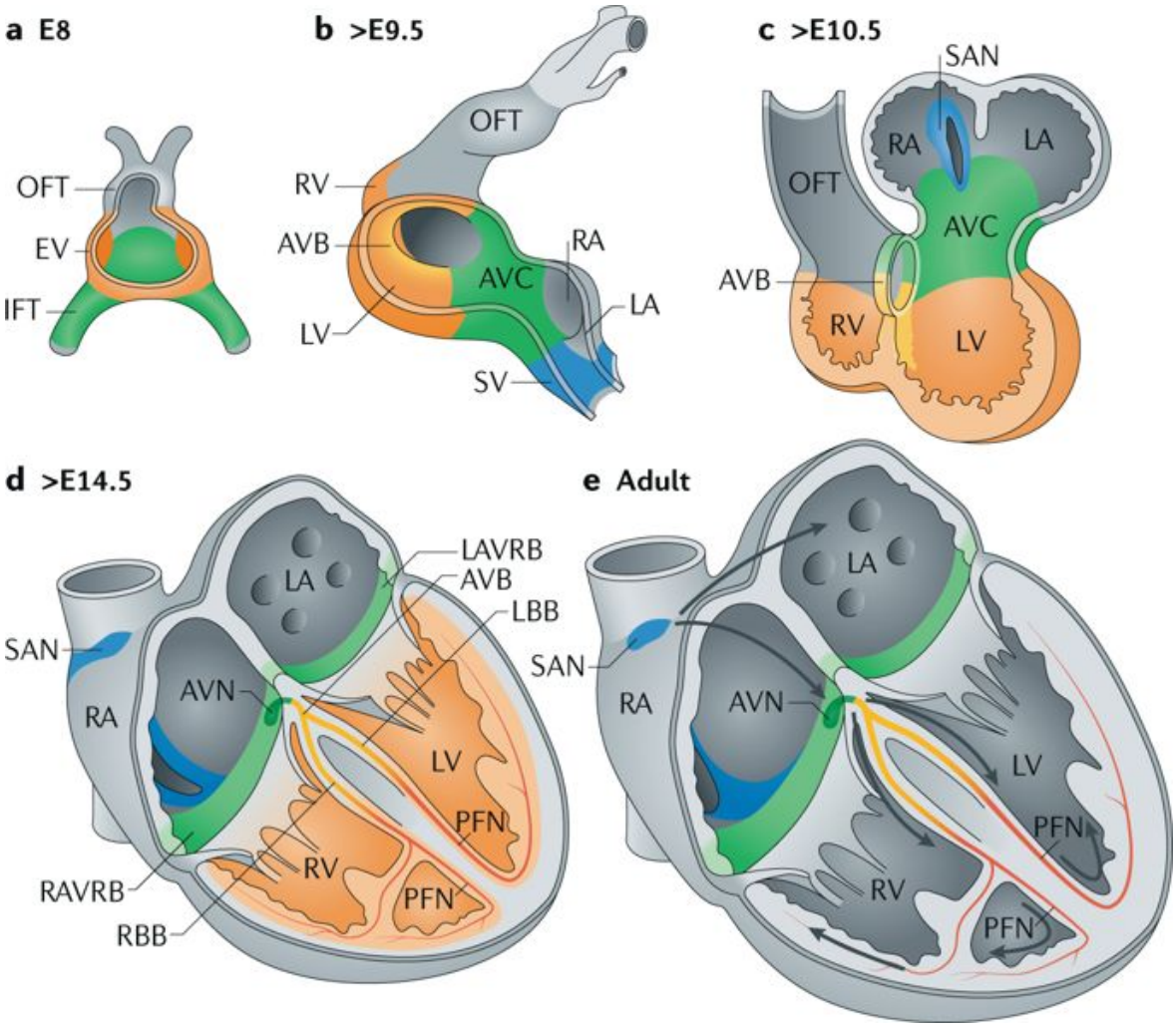

Figure 1.11. Cardiac development in mammals. A. Cardiac embryonic development at day 8; IFT (inflow tract); OFT (outflow tract); EV (embryonic ventricle). B. Cardiac embryonic developments after day 9.5; AVC (atrioventricular canal); RV and LV (right and left ventricle); RA and LA (right and left atrium); AVB (atrioventricular bundle).C. Sinus node (SAN) development starts after day 10.5 and it is depicted in blue. It is generated from the right sinus horn. D. Cardiac development after day 14.5. E. Adult developed heart. Adopted from van Eif et al., 2018.

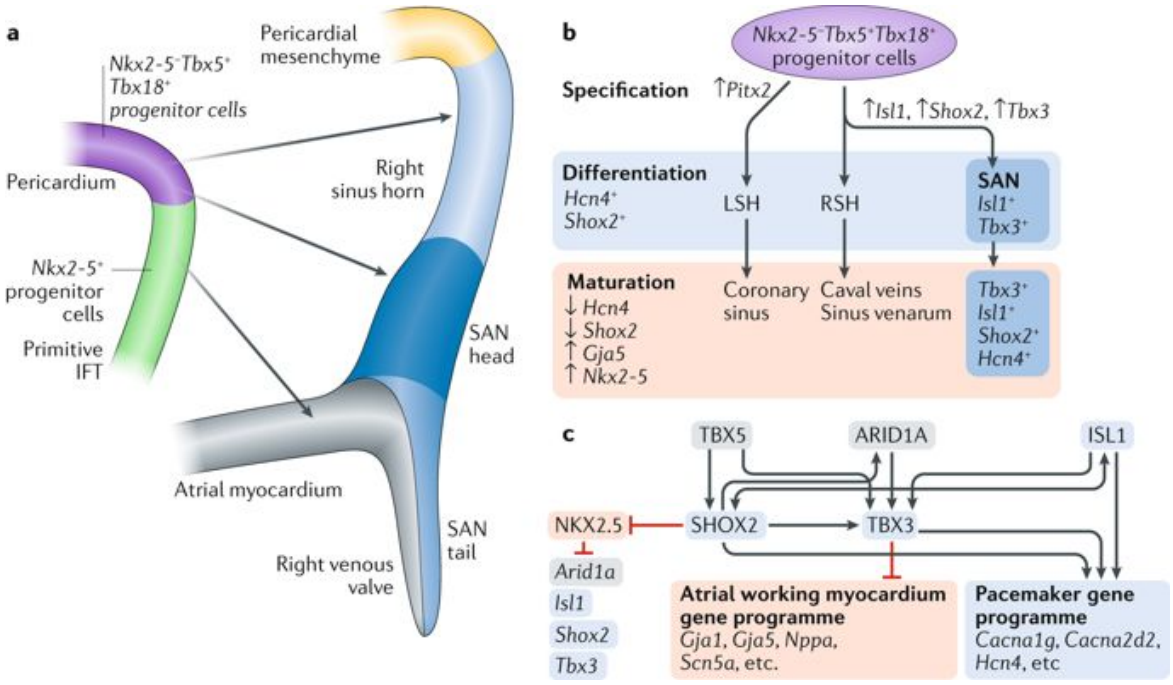

Figure 1.12. Transcription factors in the development of the sinus node. A. The sinus node develops from the embryonic sinus horn under the influence of Tbx18, in contrast to the working myocardium, where the gene programme is controlled by Nkx2-5. B. Pitx2, Isl1, Shox2 and Tbx3 are major regulators of the development of the right and left sinus horns (RSH and LSH), which eventually mature to Caval veins, sinus venarum and Coronary sinus respectively. C. Transcription positive and negative loops that enhance or suppress the sinus node and the atrial working myocardium gene programmes. Nkx2-5 enhances Cx40 (Gja5), Cx43 (Gja1), $Na_V1.5$, and Nppa expression in the working myocardiumby inhibiting Shox2, Tbx3, and Isl1, while their function is to enhance $Ca_V3.1$ and HCN4 sinus node specific genes expression. Adapted from van Eif et al., 2018.

SSS has been also associated with familial inherited mutations in genes coding for major ion channels expressed in the heart such as 1) $K_{ir}2.1$, which results in $I_{K,1}$ inhibition and development of Andersen syndrome (Andelfinger et al., 2002); 2) HCN4, which results in inhibition of the pacemaker current I_f and development of sinus bradycardia (Milanesi, 2006); 3) $Na_V1.5$, which results in the development of arrhythmogenesis and potential heart block (Grant et al., 2002).

Many SSS cases have been associated with fibrosis and SN atrophy, although others showed that the disorder can be related to normal heart morphology, and cases where patients with severe heart fibrosis exhibited no alterations in their SN rhythm have been documented (Evans and Shaw, 1977; Thery et al., 1977). Age-dependent remodelling of the extracellular matrix genes such as collagen1 and 3 were observed in the SN of obese rats (Yanni et al., 2010). This animal model was also exhibiting slower intrinsic heart rate and decreased levels of $Na_V1.5$ protein expression, consistent with SN dysfunction (Yanni et al., 2010). The present data cannot draw a clear relationship between fibrosis and SSS, but it suggests that SN morphological alterations could be a potential cause.

Aging has been correlated with deterioration in the SN function (Alings and Bouman, 1993). Ageing in the SN has been linked to slower intrinsic heart rate and longer SN conduction periods (Alings and Bouman, 1993). Age related morphological and functional alterations of the SN have been studied in the rat, rabbit, cat, and guinea pig (Alings et al., 1995; Anyukhovsky et al., 2005; Jones et al., 2004; Tellez et al., 2011; Yanni et al., 2010) and human (Matsuyama et al., 2004). Deterioration of the aging SN has been associated with alterations of ion channels expression, connexins, and morphological remodelling (Dobrzynski et al., 2007). Electrical remodelling due to ageing in the atrial myocardium, as well as the SN, has been also correlated with impaired cardiac function (Dibb et al., 2009;

Tellez et al., 2006). A variety of ion channel knockout mouse models for $Na_V1.5$, HCN4, Cx40, $Ca_V1.3$, and $Ca_V3.1$ demonstrated SSS features and bradycardia development (Dobrzynski et al., 2007; Hao et al., 2011). Aged rats were reported to exhibit $Na_V1.5$, HCN1, HCN2, HCN4, and RyR2 downregulation, as well as longer AP duration, slower intrinsic heart rate, and shifting of the pacemaker site from the SN head to the SN tail, indicative of SN dysfunction (Huang et al., 2007; Tellez et al., 2011; Yanni et al., 2010). A study in aging guinea pigs demonstrated conduction slowing due to Cx43 depletion from the periphery of the SN. This would potentially reduce the electrical coupling in the intermediate area between the centre of the SN and the surrounding atrial myocardium and could explain the age-related prolongation of the SN conduction period (Jones et al., 2004). Ion channel remodelling, morphological alterations, and changes in the electrical coupling and AP properties imply that SSS is not related to one single cause, but it could be multifactorial mechanism.

In many occasions, SSS develops alongside other cardiac disorders, and the ion channel and morphological remodelling linked to them, such as in atrial fibrillation (Yeh et al., 2009), heart failure (Zicha et al., 2005), infarction (Yanni et al., 2011), and pulmonary hypertension (Yanni et al., 2010). More research in the recent years focuses on the extremely high incidence of resting bradycardia in endurance athletes. In many occasions bradycardia is considered an adaptation process in athletes unless it develops further into a pathological condition, requiring surgical implantation of electronic pacemakers (Boyett et al., 2013). An athletically trained rat model was reported to express significantly lower SN $Ca_V3.1$, RyR2, and NCX1 mRNA levels compared to sedentary rats (Monfredi et al., 2011). Further analysis of training-induced bradycardia demonstrated reduction of HCN4 and Tbx3 expression and overexpression of Nkx2-5, miR-423-5p, and miR-1 levels in the

mouse and rat SN (D'Souza et al., 2014; D'Souza et al., 2017). Knockdown of miR-423-5p with antagomiR rescued HCN4 levels and restored its corresponding current, I_f (D'Souza et al., 2017). Nkx2-5 was shown to drive miR-423-5p expression (D'Souza et al., 2017), suggesting higher miR-423-5p levels in the sedentary mouse atrial myocardium prevent the expression of HCN4 and potential ectopic automaticity. This study showed for the first time the involvement of microRNAs in the modulation of the cardiac conduction system.

1.9 Biological pacemakers

At present, electronic pacemaker implantation is the only available treatment for SN dysfunctions. Electronic pacemakers are devices that modulate the heart rhythm. However, they are not a cure, and they are limited by a number of drawbacks such as poorly regulated rate adaptation to the physiological demands, due to shortcoming in the sensing and stimulating leads, a need for regular replacement of the batteries due to short longevity (Biffi et al., 2010) and infections at the site of the implantation (de Bakker and Zaza, 2007) (Mond and Freitag, 2014). Research has focused on developing a biological alternative to the electronic pacemaker or the so-called "biological pacemaker". The aim of biological pacemakers would be to provide a cure for SN dysfunctions that would generate spontaneous rate within the physiological range, and would not require maintenance, or regular treatments, or cause further pathologies related to arrhythmias, neoplasia, or infection due to rejection (Cohen et al., 2005).

1.9.1 Gene–based approach

The first attempt in developing a biological pacemaker through DNA delivery introduced β_2-adrenergic receptor cDNA in a mouse and pig right atria (Edelberg et al., 1998; Edelberg et al., 2001). Although this approach did not manage to generate a true biological

pacemaker, the experiment led to increased diastolic depolarisation, followed by higher heart rate in both models potentially due to increase intracellular cAMP levels (Edelberg et al., 1998; Edelberg et al., 2001). Not long after that another approach managed to create the first *de novo* biological pacemaker, which aimed to decrease ventricular automaticity through knockout of its main hyperpolarising current $I_{K,1}$ conducted through $K_{ir}2.1$ (Miake et al., 2002). The number of functional $K_{ir}2.1$ channels was decreased by delivery of dominant negative $K_{ir}2.1$ isoform, which resulted in translation of dysfunctional $K_{ir}2.1$ protein due to substitution of essential amino acids in its structure. The introduction of the mutant transcript was performed via adenoviral transfection in the left ventricle of a guinea pig, resulting in substantial $K_{ir}2.1$ attenuation. Ventricular cardiomyocytes exhibited depolarisation of the resting membrane potential to -60 mV and spontaneous automaticity in response to β-adrenergic stimulation (Miake et al., 2002). This study implies that ventricular myocardium is capable of pacemaking activity, but this is attenuated by the hyperpolarising $I_{K,1}$ current in order to prevent ectopic automaticity. This approach managed to unleash pacemaking activity by manipulating a single current, without trying to create a replica of the SN, as the ventricular myocytes generating the AP remained structurally and genetically unchanged.

Another approach focused on the reinforced expression of the pacemaking current I_f. Er et al., showed that knockout of HCN channel function through dominant negative HCN2 subunit expression in neonatal cardiomyocytes led to abolition of pacemaking (Er et al., 2003). Overexpression of HCN2 was conducted through adenoviral delivery in canine left atrial appendage and it resulted in spontaneous rhythm originating from the left atria upon SN rhythm attenuation by vagal stimulation (Qu et al., 2003). Following studies by the same group demonstrated that adenoviral transfection with HCN2 transcript in the left

bundle branch generated spontaneous ventricular rhythm (Plotnikov et al., 2004). Morris et al., overexpressed HCN2 via adenovirus-mediated gene transfer in organ-cultured rat SN preparations, leading to an increased pacemaker rate (Morris et al., 2013). These independent studies provided evidence that ion channel remodelling leading to suppression of $I_{K,1}$ or overexpression of I_f in normal working myocardium creates a potential for pacemaker generation.

1.9.2 Cell-based approach

The cell-based approach in biological pacemaker generation is aiming to introduce a cluster of spontaneously beating cells in the heart, which would initiate physiological, well-coordinated pacemaking activity (Cho and Marban, 2010; Rosen et al., 2004).

Human embryonic stem cells (hESCs) readily differentiate into pacemaker cardiomyocytes (Xu et al., 2002). Transplantation of hESC-derived cardiomyocytes in the left ventricle of guinea pig hearts generated well-coordinated pacemaking activity, which successfully spread depolarising membrane potential across the surrounding myocardium (Xue et al., 2005). A pig model of complete heart block injected with hESC-derived cardiomyocytes integrated, electrically coupled with the surrounding myocardium through Cx43 formation, and generated spontaneous pacemaking activity from the site of hESC injection at a rate of 59 beats/minute (Kehat et al., 2004).

As the hESCs approach is not readily available and it requires immunosuppression to prevent rejection, induced pluripotent stem cells (iPSCs) approach has been employed into the development of biological pacemakers. iPSC-induced cardiomyocytes were introduced into dog hearts causing spontaneous pacemaking in only 50% of the animals exhibiting 40-50 beats per minute (Protze et al., 2017). Keratinocytes-induced iPSC cardiomyocytes

were injected into the left ventricles of dogs with atrioventricular block and 14 weeks later iPSCs were found to lack pluripotency markers, exhibited cardiac-specific markers and demonstrated I_f-induced pacemaking activity (Chauveau et al., 2017). A major drawback of iPSCs from embryoid bodies is that the cells are a mixed population with varying phenotype at different stages of maturity. These issues could lead to variability of cellular function, and could impose a risk from migration and differentiation into variable cell types (Medvedev et al., 2010). A possible solution of this problem could be the use of human mesenchymal stem cells (hMSCs) that already express HCN channels. A canine model with complete atrioventricular block was injected with HCN2 expressing hMSCs, which induced ventricular automaticity at rates of 50-60 beats/minutes without immunological rejection (Plotnikov et al., 2007). This approach avoids some major drawbacks such as the use of viral vectors to incorporate the gene of interest and immunosuppressing treatment due to immunological rejection reactions to the introduction of unrecognised material.

1.9.3 Somatic cells reprogramming approach

Modulation of transcription factors expression in somatic cells has been employed in the reprogramming of differentiated mature cardiomyocytes into SN-like cells that could produce a functional replica of the SN structure. Boink et al., reported that single neonatal cardiomyocytes generated faster spontaneous beating rate as well as decreased diastolic potential and attenuation of $I_{K,1}$ and I_{Na} currents (Boink et al., 2008). Kapoor et al., demonstrated similar results in Tbx18 overexpressing neonatal cardiomyocytes, which showed morphological and molecular changes such as a decreased cell size, downregulation of Cx43 expression and upegulation of HCN4 expression and cAMP levels, typical for SN cardiomyocytes nature (Kapoor et al., 2011). An *in vivo* study by the

same group showed Tbx18-induced reprogramming in the guinea pig heart apex produced spontaneous automaticity by affecting both membrane-voltage and Ca^{2+} clock (Kapoor et al., 2013). The guinea pig heart block model created a biological pacemaker rhythm, which was sensitive to autonomic stimulation (Kapoor et al., 2013). These proof-of-concept studies provided a substantial amount of evidence that Tbx18 overexpression induces somatic cells reprogramming both *in vivo* and *in vitro*. In order to further validate this reprogramming method, Hu et al., injected adenoviral vectors containing Tbx18 into the His-bundle region in a swine model of complete heart block (Hu et al., 2014). The animals exhibited pacemaking activity from the site of injection, enhanced autonomic response and improved exercise capacity (Hu et al., 2014). The cardiomyocytes gene expression was also altered towards SN-like phenotype, for instance $K_{ir}2.1$ transcript levels were downregulated, whereas HCN4 transcript levels were upregulated (Hu et al., 2014). This reprogramming- based approach, which works by altering differentiated cardiomyocytes in SN-like myocytes, might be more relevant in terms of physiology as it changes the whole cell phenotype and not only different parts of the membrane-voltage or Ca^{2+} clock mechanisms.

Although, nothing is known yet about microRNAs role in reprogramming somatic cells in SN-like cells, their role in cardiomyocytes differentiation has been studied. Knockout of miR-1 has been correlated to various defects concerning cardiogenesis and cardiac conduction (Zhao et al., 2007). Forced overexpression of miR-1 in mouse and human embryonic stem cells has been shown to produce significant upregulation of Nkx2-5 (Ivey et al., 2008; Wilson et al., 2010). Introduction of mouse embryonic stem cells overexpressing miR-1 at the border zone of myocardial infarction was shown to exhibit cardioprotective properties and decreased apoptosis levels (Glass and Singla, 2011). In

contrast, miR-133 was shown to attenuate cardiomyocyte differentiation as its overexpression in mouse and human embryonic stem cells supressed expression of cardiac lineage markers, but in its absence cardiomyocytes differentiated partly (Chen et al., 2006; Liu et al., 2008a).

MicroRNAs were also found to have a role in cardiomyocyte genetic remodelling. A combination of miR-1, miR-133, miR-208, and miR-499 were found to reprogramme fibroblasts into cardiomyocytes *in vitro* and *in vivo* through administration of microRNAs in ischemic mouse myocardium (Jayawardena et al., 2012). Although microRNA expression and function in the human SN is not known yet, these molecules capable of gene regulation and remodelling could be of a potential interest as a gene therapy technology.

1.10 Hypothesis and aims

We hypothesised that the complex mechanism of the SN automaticity is regulated by microRNAs and transcription factors that control the expression profile of membrane-voltage and Ca^{2+} clocks genes. These modulatory molecules could be potentially used in gene expression remodelling for the development of biological pacemakers as a treatment for SN dysfunctions.

The first aim of my study was to investigate the expression profile of the most abundant microRNAs in the healthy human SN in comparison with the RA. To characterise the human tissue I used histology, immunolabelling, and immunoblotting to look into the membrane-voltage and Ca^{2+} clock expression profile. Tissue samples were then used for qPCR reactions that investigated the expression of 754 most abundant microRNAs in the human.

The second aim of my work was to study the functional roles of 7 key microRNAs targeting important pacemaker channels, Ca^{2+}-handling proteins and connexins. IPA software was used to match those microRNAs that target these genes based on mRNA data from Chandler et al., 2009 study. Rat SN preparations were injected and iPSCs were transfected with microRNAs of interest, luciferase reporter gene assays were used to investigate the binding of microRNAs to their target genes, qPCR and/or immunolabelling was used to analyse any target gene expression changes at mRNA/protein levels.

The third aim was to determine if t-tubules are present in the human SN as well as RA in order to characterise human SN myocytes structure. Extensive immunolabelling and staining experiments studied the striated expression pattern of proteins involved in the contractile apparatus and Ca^{2+}-handling proteins in both tissue types.

The fourth aim was to map the transcription factors involved in the regulatory machinery of the healthy adult SN compared to RA. Next generation sequencing compared the expression profile of transcription factors mRNA in the SN vs. RA.

Chapter 2

2 Materials and methods

2.1 Human specimens and animals information

Human sinus node (SN) with surrounding right atrium (RA) tissue blocks were obtained from Prince Charles Hospital, Brisbane, Australia and the National Institute of Legal Medicine, Bucharest, Romania by Prof. Peter Molenaar and Dr. Filip Perde. The tissue was obtained from either unused transplant or post-mortem hearts under local ethics approval of Prince Charles Hospital, the National Institute of Legal Medicine. Specimen information and patient profiles are provided in Chapter 3, Data supplement, Table S1. Upon dissection the SN/RA preparations were frozen, kept at -80^{o}C, shipped to Manchester on dry ice and stored under the Human Tissue Act. A photo of a typical human SN/RA preparation used in the study is shown in Figure 2.1.

A total of 64 young adult (≈42 days old) male Wistar-Hanover rats (Charles River UK Ltd, Kent, UK, 250 ± 15 g, $p<0.05$) were used in accordance with the Animal (Scientific Procedures) Act 1982. Institutional approval was received from The University of Manchester Animal Welfare and Ethical Review Board. Animals were housed in a temperature of 20-23^{o}C and humidity of ≈50% on a 12-hour light/12-hour dark schedule. Rats were housed in cages containing 4 rats each, with food (5L79, PMI Nutrition International) and sterile water provided *ad libitum*. Animal details are reported in accordance with ARRIVE (Animal Research: Reporting of *in vivo* Experiments) guidelines.

The rats were humanely euthanised via carbon dioxide inhalation and cervical dislocation. The animals' chests were opened and their hearts were dissected out for SN preparations. The *ex vivo* SN preparations were transfected with microRNAs of interest, their beating rate was monitored via Powerlab and LabChart v7 software (ADInstruments, Oxford, UK) for a period of 24 hours, after which SN preparations were flash frozen in liquid nitrogen for cryosectioning or RNA extraction.

2.2 Human and rat sinus node preparations cryosectioning

Human frozen SN preparations and the surrounding RA (Figure 2.1) were sectioned using a cryostat (Zeiss Microm HM500) at temperatures ranging between -10 and -20°C. The sections thickness was 30 μm and they were sectioned perpendicular to the crista terminalis (Figure 2.1). A typical SN/RA preparation is shown in Chapter 4, Figure 1.

Rat frozen SN preparations were serially sectioned at 10 μm, using a cryostat (Leica CM1900) at temperatures ranging between -10 and -20°C. Each section was mounted onto SuperFrost Plus glass slides (Thermo Fisher Scientific) and stored at -80^{o}C.

2.3 Histology

Histological staining was used to locate the SN region in each tissue section. Masson's trichrome staining was used for histology experiments. Masson's trichrome is a preferred staining method for SN identification, because the SN is embedded into significant amounts of connective tissue (which stains blue). A typical human SN tissue section stained with Masson's trichrome is shown in Chapter 1, Figure 1.3, Figure 1.4 and Chapter 3, Figure 1. A detailed protocol description for Masson's trichrome staining is contained in Chapter 3, Data supplement. Masson's trichrome staining protocol stained the cell nuclei

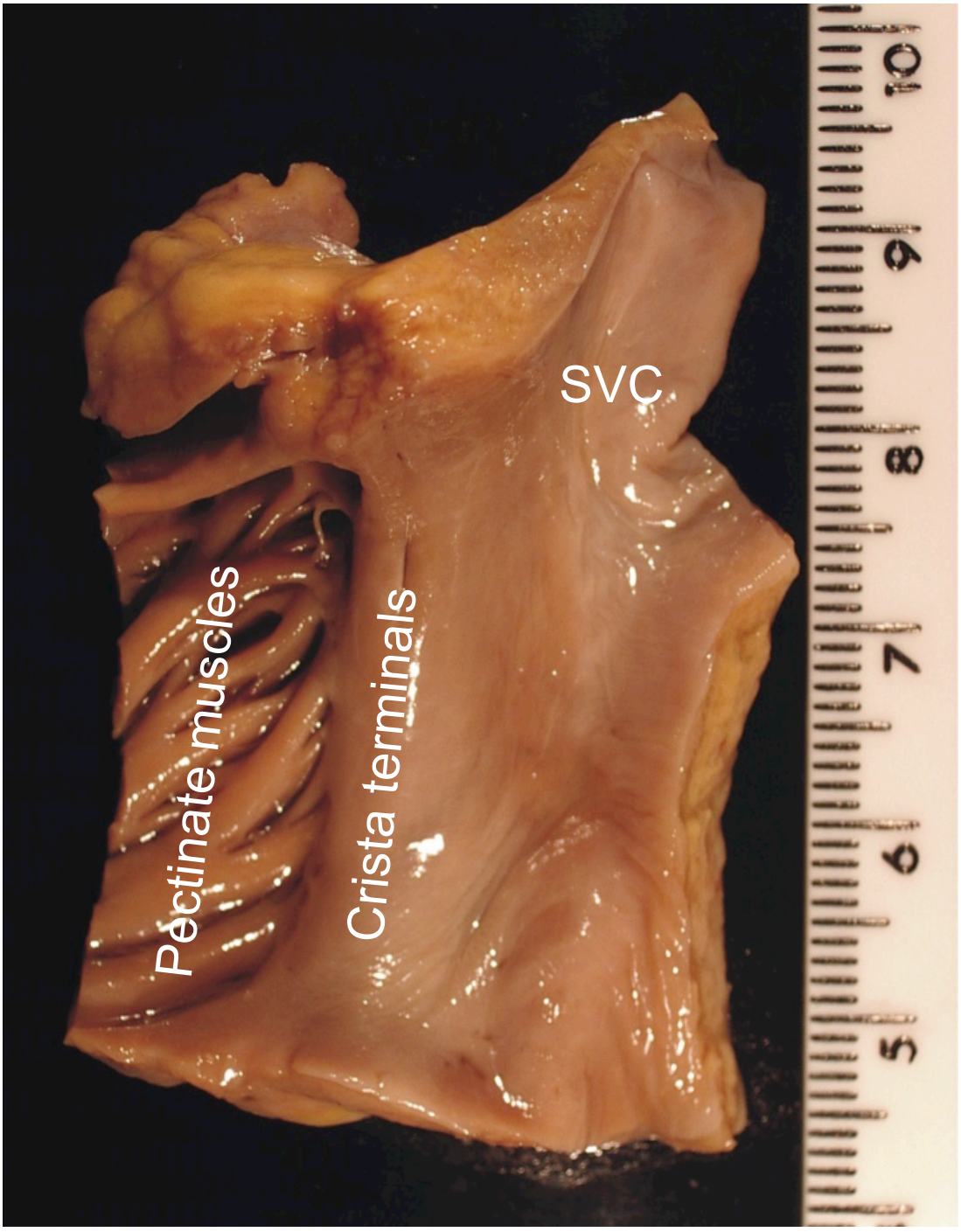

Figure 2.1. Endocardial view of a human sinus node preparation. Tissue sections were cut at perpendicular plane to the cristae terminalis and the superior vena cava (SVC). Image is adapted from Chandler., 2009.

dark blue, myocytes purple, and connective tissue blue. Tissue sections were then kept at room temperature for subsequent imaging using a light microscope (Zeiss LSM5) and Axiocam camera (Zeiss), and images were collected with Axiovision software (Zeiss).

2.4 Immunofluorescence

2.4.1 Principles of immunohistochemistry

Immunohistochemistry/ immunolabelling is a technique used to detect and localise protein antigens in tissue sections via binding of complementary antibodies. Primary antibodies recognise antigens according to their epitopes and bind them. Secondary antibodies raised against specific primary antibodies allow their detection. The secondary antibodies are conjugated to fluorochromes that fluoresce at specific wavelengths when excited at a certain wavelength. Confocal microscopes are used to visualise the secondary antibodies through laser excitation (Figure 2.2). Immunohistochemistry was used to both study the expression profile of proteins in human SN preparations and to quantify the fluorescent signal produced by the fluorochromes.

2.4.2 Immunohistochemistry/immunolabelling protocol

The primary antibodies used in the study are listed in Chapter 3, Data supplement, Table S2 and Chapter 5, Table 5.1; secondary antibodies are listed in Chapter 5, Table 5.2. The specificity of the antibodies listed has been previously tested by our laboratory (Chandler et al., 2009; Dobrzynski et al., 2005; Lyashkov et al., 2007; Musa et al., 2002; Yanni et al., 2011; Yanni et al., 2010). The detailed immunohistochemical protocol used in the study is described in Chapter 3, Data supplement and Chapter 5, section Materials and methods. Upon labelling tissue sections were visualised using a Zeiss LSM5 confocal laser scanning

microscope (Carl Zeiss Microscopy) and Pascal software (Zeiss Microscopy). Background readings of control sections treated with primary or secondary antibody only were negligible.

2.5 Single cells isolation

Male Wistar-Hanover rats (230-250 g) and male C57BL/6 mice were sacrificed by CO2 inhalation and cervical dislocation in accordance with the Home Office procedures. The animals' chests were opened; their hearts were dissected out and placed at 37^{o}C in Tyrode's solution. A detailed description of SN dissections and single cells isolations are contained in Chapter 5, section Material and methods. Cell isolations were performed by Dr. Yanwen Wang and Dr. Louise Miller, University of Manchester.

2.6 Immunocytochemistry

The detailed immunocytochemistry protocol is described in Chapter 5, section Material and methods. Upon labelling tissue sections, they were visualised using a Zeiss LSM5 confocal laser scanning microscope (Carl Zeiss Microscopy) and Pascal software (Zeiss Microscopy).

2.7 Microscopy

2.7.1 Light microscopy

The major feature of the light microscope is that it uses visible light. Each light microscope contains a condenser, which contains a combination of magnifying lenses. When light is emitted from the light source in the microscope over the tissue section, the condenser focuses it onto the region of interest. This region is magnified and examined via the

objective lens. A Zeiss LSM5 light microscope was used to visualise histologically stained sections. Image collection was then performed via Axiocam camera (Zeiss) and Axiovision software (Zeiss).

2.7.2 Confocal laser scanning microscopy

Confocal microscopy is an optical imaging technique (Figure 2.1). Its visualising ability is based on the property of the sections stained with fluorochromes to emit fluorescence when excited. A laser beam is emitted from the light source through a pinhole located on the confocal plane with a detector. The laser beam is then focused by the objective lens on a specific point of the fluorescent specimen, which is referred to as a scanning point. The point that has been illuminated by the laser then emits fluorescent light and it also reflects some of the laser light onto the objective lens. This light is then reflected onto the dichromatic mirror, which in turns directs it through the confocal pinhole onto the photodetector. The photodetector then transforms the received light signal into an electronic one.

Confocal microscopy can be advantageous compared to the conventional fluorescent microscopy because:

1) When the scanning point is illuminated by the laser, the fluorescent molecules are excited and they emit light in all directions. The pinhole apparatus, however, rejects any out-of-focus light and thus prevents image background noise and increases image resolution;
2) Decrease of background light allows significant improvement of the noise-to-signal ratio.

Immunofluorescent tissue sections and single cells in this work were imaged using confocal microscopy. The secondary antibodies conjugated to either FITC or Cy3 fluorochromes are described in Chapter 4, Data supplement and Chapter 5, Table 5.2. Tissue sections and single cells were visualised and images were taken using Zeiss LSM5 confocal microscope (Carl Zeiss Microscopy) and Pascal software (Zeiss Microscopy).

2.8 Signal intensity and cell diameter measurements

HCN4 expression in rat SN preparations injected with miR-486-3p or control was visualised using confocal microscopy and signal intensity was measured using Volocity 4 image analysis software (PerkinElmer, Waltham, MA). The background signal in each image was determined using control images with no primary antibody added and it was omitted when quantifying signal intensity. The average intensity measurement were then taken and compared between the two groups. The same confocal parameters were used when capturing the images.

Cell diameter of human SN and RA myocytes was measured in human SN sections. In order to measure cell diameter, primary antibody against caveolin3, labelling the myocytes cell membrane, was used. Measurements were then performed using LSM images browser software (Zeiss).

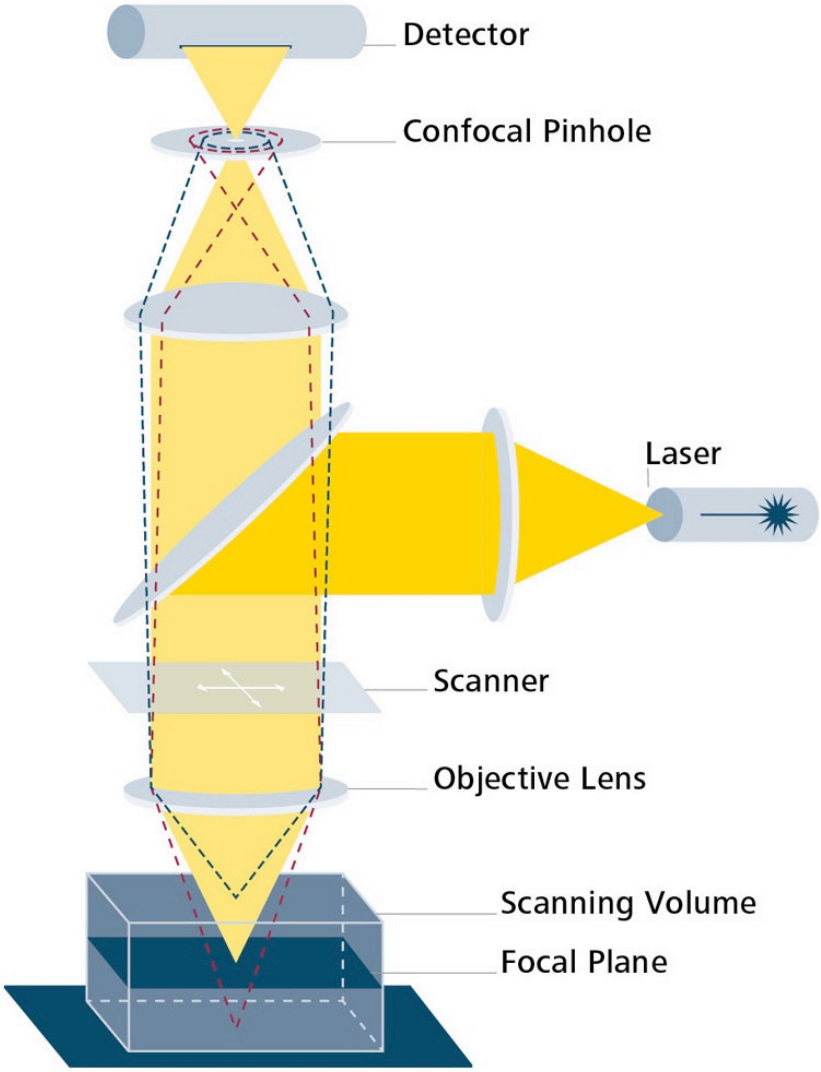

Figure 2.2. Confocal laser scanning microscopy. The objective lens focuses a light ray produced by a light source onto a fluorescent specimen. The objective lens and the detecting apparatus then collect the emitted fluorescence by the specimen. The confocal pinhole both converts the light signal into electronic and blocks the background noise. Image is adapted from Zeiss LSM 800, www.zeiss.com/microscopy/us/products/confocal-microscopes/lsm-800-for-materials.html.

2.9 Immunoblotting

Immunoblotting is a widely used analytical method for detecting and quantifying proteins of interest in a given sample based on their ability to bind to primary antibodies. The method is comprised of two major processes – SDS-polyacrylamide gel electrophoresis (SDS-PAGE) and protein blotting.

SDS-PAGE is used to separate the proteins in a given sample according to their electrophoretic mobility, which is defined by proteins charge, size, and structure. SDS gels separate proteins mainly according to their molecular weight. SDS is an anionic detergent used to denaturate proteins to their primary structure and linearise them by breaking their hydrogen bonds and destroying the secondary and tertiary protein structures. Mercaptoethanol, for instance, is a reducing agent used in the protein samples mixture to break strong disulphide bonds of cysteine residues. Upon voltage application, the negatively charged molecules of the proteins move towards the positive electrode; proteins with smaller molecular weight migrate faster than the ones with higher molecular weight. The separated proteins from the gel are then transferred to a polyvinyl difluoride (PVDF) membrane via electrophoresis. The unreacted protein sites on the membrane then need to be blocked in order to prevent non-specific binding of the primary antibody to other protein antigens. In our study we used bovine serum albumin (BSA), which was found to be appropriate as it does not replace the proteins on the PVDF membrane, it does not bind to the epitope of the target protein, and it does not produce any cross-talk with primary or secondary antibodies. Similarly to what we carried out in immunolabelling experiments the PVDF membrane was incubated with a specific primary antibody for the protein of interest, which was then exposed to a secondary antibody raised against the species the primary antibody had been raised in. Unlike immunolabelling, the secondary antibody is

conjugated to an enzyme. When a chromogenic substrate is introduced to the secondary antibody, a colour reaction is produced allowing the protein of interest to be visualised, quantified and characterised amongst a mixture of other proteins. A detailed description of the protocol for immunoblotting is provided in Chapter 3, Data supplement. A list of specimens information and the primary antibodies used is provided in Chapter 3, Data supplement, Table S1 and S2, respectively. The protein abundance was analysed according to the chemiluminescent intensity of the signal and was quantified (Image lab Bio-Rad) by normalising it to the corresponding intensity of the house keeping endogenous protein β-actin.

2.10 Quantitative polymerase chain reaction (qPCR)

Quantitative polymerase chain reaction (qPCR) is a method used to study mRNA expression levels of a gene of interest in a given sample. The qPCR method is appropriate to analyse and compare the small differences in the abundance of a gene transcript as it is highly sensitive and requires only a small amount of RNA input for examination. Moreover, the qPCR method is not hampered by the presence of extraneous material such as DNA or ethanol contamination (Saiki et al., 1988). What makes it a good quantitative method is the fact that a fluorescent system allows the amplification of the cDNA to be recorded in real time while the PCR reaction is carried out.

2.10.1 Total RNA extraction for mRNA, microRNA, and NGS studies

For our purposes, RNA was extracted in two different ways depending on the tissue type and the aim of the subsequent experiments.

1) The human tissue samples were first characterised by histological, immunolabelling and immunoblotting techniques. Upon confirmation of the SN and RA areas of the preparations, total RNA was isolated from small biopsies taken around the SN artery for each preparation. Samples were then flash frozen in liquid nitrogen and kept at -80^{o}C. Total RNA, for microRNA studies, was extracted using mirVana miRNA Isolation Kit (Applied Biosystems). The SN and RA tissue biopsies were homogenised using an Ika T10 homogeniser (Ika Werke) for 1 minute. 10 volumes of Lysis/binding buffer were added to and mixed with each sample. 1.25 volumes of 100% ethanol were added to the samples and they were then centrifuged at 10, 000 rpm for 25 seconds. The spin column filter was then washed with 700 µl miRNA wash solution followed by two more consequtive washes with 500 µl wash solution 2/3. The total RNA was eluted into 100 µl nuclease-free H_2O. The samples then underwent enrichment procedure for small RNAs, which started with addition of 1/3 volumes of 100% ethanol to the samples. This was followed by centrifugation of the mixture at 10, 000 rpm for 25 seconds. The filtrate was mixed with 2/3 volumes of 100% ethanol and centrifuged at 10, 000 rpm for 25 seconds. The filtrate was discarded as the RNA was accumulated in the spin column filter. 700 µl miRNA wash solution was added followed by another two washes with 500 µl 2/3 wash solution. The final total RNA was then eluted with 100 µl nuclease-free H_2O. RNA quality (260/280), quantity, and RNA integrity number (RIN) were assessed using an Agilent 2100 Bioanalyzer.
2) Total RNA from rat SN preparations, as well as cardiac induced pluripotent stem cells (iPSCs), was extracted using an RNeasy Micro Kit (Qiagen). Approximately 1 mm x 1 mm biopsies from the rat SN preparations were collected around the SN artery bifurcation. iPSCs were dissociated from their wells using TrypLE Express

(Thermo Fisher Scientific) via incubation for 5 minutes at 37°C. DMEM/F12 (Sigma-Aldrich) was added to stop the dissociation process and cells were centrifuged at 300 rpm for 5 minutes. The samples were then resuspended into 350 µl RLT buffer (Qiagen) containing 10 µl β-mercaptoethanol, flash frozen in liquid nitrogen and kept at -80°C.

The rat SN biopsies and isolated iPSCs were then homogenised using an Ika T10 homogeniser (Ika Werke) for 1 minute. RNase free H_2O was then added to the samples. Proteinase K (Qiagen) was also added in order to break any connective tissue between the cells. The sample mixture was incubated on a heater at 55^{o}C for 15-20 minutes in order to activate the β-mercaptoethanol used to reduce the protein disulphide bonds and lyse the cells in order to make sure all available RNA is extracted from the sample. The samples were then centrifuged at 13, 000 rpm for 5 minutes. The samples' supernatant was then mixed with 150µl 100% ethanol and centrifuged through Qiagen columns at 10, 000 rpm. RW1 Qiagen buffer was mixed with the samples and centrifuged through the spin columns at 10, 000 rpm for 25 seconds. The flow-through was removed as the RNA was accumulated at the spin columns membrane. RDD/DNase mix was applied to the spin columns and they were incubated at room temperature for 20 minutes. This step allowed the digestion of genomic DNA in the samples. RW1 buffer was added to the spin columns again and the samples were centrifuged through the spin columns at 10, 000 rpm for 25 seconds again. RPE buffer was then added and the columns were spun at 10, 000 rpm for 25 seconds. Upon addition of 500 µl 80% ethanol to the samples, the columns were centrifuged at 10, 000 rpm for 2 minutes and again at 13, 000 rpm for 5 minutes to remove any additional ethanol contamination. RNase

free H_2O was then added to the membrane of the spin columns containing the total RNA in order to elute the RNA samples.

2.10.2 RNA quality and quantity assessment

RNA concentration needs to be quantified in order to make sure that in the following reverse transcription protocol we use equal amounts of total RNA to generate a true reflection of the mRNA levels in the initial samples. RNA quality is also checked in order to make sure there are no genomic DNA or ethanol contaminations, which could affect our qPCR results. These two measurements were carried out via Agilent 2100 Bioanalyzer for RIN numbers (see Chapter 3, Data supplement, Table S1) and Nano Drop 1000 spectrophotometer (NanoDrop Technologies) for 260/280 and 260/230 values.

2.10.3 Reverse transcription of total RNA to cDNA

Reverse transcritpion of total RNA to cDNA was carried out in two different ways depending if total RNA was converted in cDNA to study microRNA expression or mRNA expression:

1) Total RNA conversion into microRNA cDNA of the human samples for microRNA analysis of human SN vs. RA is described in detail in Chapter 3, Data supplement. qPCR was performed using TaqMan Array Human MicroRNA A+B Cards Set v3.0 (Thermo Fischer Scientific). The cards A + B contained 384 TaqMan MicroRNA Assay each, giving a total of 754 human microRNAs.
2) Total RNA was converted to microRNA cDNA using qScript microRNA cDNA Synthesis kit (Quanta BioScience). Poly(A) tailing buffer (5x) (2µl), RNase free H_2O, 1 µl Poly(A) polymerase and total RNA were mixed to make up 10 µl 200 ng/µl total RNA concentration. The first step of the cDNA conversion was

produced by incubation of the samples for 60 minutes at 37^{o}C and 5 minutes at 70^{o}C in qPCR Veriti 96 well thermal cycler (Life Technologies). The second step involved mixing the already produced 10 µl sample with 9 µl microRNA cDNA reaction mix and qScript reverse transcriptase to a final volume of 20 µl. The samples were then incubated in qPCR Veriti 96 well thermal cycler for 20 minutes at 42^{o}C and 5 minutes at 85^{o}C. The cDNA was then stored at -20^{o}C.

3) Total RNA was converted to mRNA cDNA using a High Capacity RNA-to-cDNA kit (Applied Biosystems). 10 µl 2x RT buffer, 1 µl 20x enzyme mix, RNase free H_2O, and total RNA sample were mixed to make up 200 ng/µl total RNA concentration. The mixture was then incubated for 60 minutes at 37^{o}C and 5 minutes at 95^{o}C in qPCR Veriti 96 well thermal cycler (Life Technologies). The cDNA was then stored at -20^{o}C.

2.10.4 Real time quantitative PCR

The PCR method involves a series of temperature changes that initiate different processes during the PCR amplification. The first stage allows the denaturation of the DNA double chain. The second stage allows annealing of the primers to their complementary nucleotide. The third stage performs extension of the primers with DNA polymerase. Every heat cycle is characterised with exponential doubling the amount of target DNA amplified with every following cycle. The exponential amplification results in accumulation of PCR product, which reaches a plateau level when more primer-target sequence is accumulated than the amount of the DNA polymerase can act upon. This saturation is characterised with linear rather than exponential accumulation of PCR product on the PCR amplification curve (Saiki et al., 1988).

Quantification of the accumulating PCR product is possible as the fluorescence emitted during the reaction is proportional to the DNA amplified during each heat cycle (Figure 2.3). In our current work we used either TaqMan (Thermo Fischer Scientific) or SYBR-green (Applied Biosystems). SYBR-green is a fluorescent cyanine dye used as a nucleic acid stain. It binds to single or double stranded DNA and produces a DNA-dye-complex, which absorbs blue light at 497 nm and emits green light at 520 nm. The DNA amplification product binds to SYBR-green and thus the fluorescent signal increases exponentially too (Figure 2.3). The first detectable increase in fluorescent signal above background and beyond the amplification threshold is used as in indicator of the initial target DNA present in the sample and thus it can be quantified and compared to the amount of DNA in other samples.

Thermus aquaticus (Taq) DNA polymerase is a thermostable enzyme. Taq DNA polymerase has a 5' to 3' exonuclease activity and during PCR reaction it could cleave a specific PCR product (Arya et al., 2005). This property is used to detect DNA amplification as Taq DNA polymerase cleaves the PCR product into smaller fragments that can be detected unlike intact DNA. Fragmentation of the PCR product occurs only if the target DNA is amplified. PCR product fragments are quantified via thin-layer chromatography in order to distinguish between DNA fragments from intact DNA molecules (Arya et al., 2005).

The qPCR protocols, as well as information about the primers and the housekeeper genes used, are contained in Chapter 4, Data supplement, quantitative PCR for miR-486-3p expression section and Quantitative PCR for HCN4, $Ca_V1.3$ and $Ca_V3.1$ mRNA expression section for rat SN reparations injected with miR-486-3p vs. control. The same information

for iPSCs could be found in Chapter 7, Material and methods section, iPSCs qPCR for miR-133a-3p and miR-486-3p expression and iPSCs qPCR for HCN4 expression.

The PCR protocols for experiments determining microRNA and mRNA expression in a given sample vary as the different primer sequences anneal to their target sequences at different rates and different cycle temperatures. The specificity of the PCR product is determined via a dissociation curve, which represents the denaturation properties of the double-stranded DNA at the PCR heating cycles (Figure 2.3). The melting temperature of the DNA of interest is defined as the temperature at which 50% of the DNA sequence is dissociated (T_m). In order to check if only one specific PCR product of the primer is amplified, a dissociation curve is produced at the end of each PCR reaction when all the DNA product can be denaturated (Figure 2.3). DNA different from the target seuqence will denaturate at different times and different melting temperature due to varying properties. The midpoint of the sigmoid melting curve peak showing SYBR-green fluorescence is the melting temperature (Figure 2.3). The presence of low melting temperature is an indication of primer-dimer formation.

2.10.5 qPCR quantification

The relative PCR abundance was first normalised to the abundance of an endogenous control – a housekeeper gene. The housekeepers used for microRNA abundance in the human SN and RA samples were RNU44, RNU48, and U6 snRNA (Qiagen); for the rat SN and iPSCs samples – RNU1A1 for microRNA expression and 18S/GAPDH (Qiagen) for mRNA expression. The equation used for calculation of the results was $\Delta Ct_{(Target)}$ - $\Delta Ct_{(Housekeeper)}$, where Ct is the threshold value. The qPCR results were plotted as a fold

change $2^{-\Delta Ct}$ and/or relative abundance. Statistical analysis was performed using GraphPad Prism 7 and/or RealTime StatMiner softwares.

In order to identify the gene targets of the significantly more/less expressed microRNAs in the human SN/RA, we married these data with the mRNA expression data of cardiac specific ion channels, Ca^{2+} -handling proteins, and connexins from a previously published study (Chandler et al., 2009) using Ingenuity Pathway Analysis (IPA; Ingenuity Systems). The software made predictions of microRNA-mRNA interactions on the basis of their sequence compatibility. TarBase database, miRecords (http://mirecords.biolead.org/), TargetScan (http://www.targetscan.org/) and rna22 (https://cm.jefferson.edu/rna22/) were used to confirm IPA predictions and assess if rat and human microRNAs are conserved.

2.11 Next generation sequencing

NGS is a high-throughput DNA sequencing method. In a single run it is able to generate hundreds of millions gigabase of nucleotide data. The basic principle of the NGS technology is that DNA polymerase drives the binding of fluorescently labelled deoxyribonucleotide triphosphates to the DNA template strand during the cycles of DNA amplification. Fluorophore excitation determines the nucleotides in the DNA sequence during each cycle. The main advantage, however, is that instead of sequencing a single DNA fragment, NGS sequences millions of DNA fragments simultaneously for multiple samples. NGS accuracy of the results is achieved through multiple sequencing of the same DNA fragment leading to a generation of a consensus sequence. NGS is carried out according to four general steps:

1) Library preparation involves random fragmentation of the cDNA samples to create smaller sequence strands. The smaller fragments are then ligated to

adapters (short, synthetic DNA sequences) using DNA ligase. Ligation occurs between the 3'-OH and the 5'-P end of the cDNA fragment. The adapters function is to enable the cDNA fragments to bind to a complimentary sequence. Upon ligation to adapters the cDNA-fragmented sequences are PCR amplified and gel purified. cDNA amplification allows accurate detection due to stronger signal produced by the higher cDNA abundance (Figure 2.4).

2) Cluster generation requires incorporation of the cDNA library into optical flow-cells where single-stranded cDNA fragments are captured through their adapters.
3) Further bridge amplification of the cDNA fragments through repeated 76 cycles generates distinct, clonal clusters of localised strands.
4) Sequencing involves the use of proprietary designed reversible nucleotide terminators, which detect single bases in the cDNA template strands. This method provides highly accurate base-to-base sequencing, which excludes context-specific errors.

Our study focused on identifying transcription factors expression in the human SN vs. RA. Total RNA was extracted from frozen human SN and RA samples according to the miRVana RNA extraction protocol described above. NGS was carried out in the Genomic Technology Core Facility, University of Manchester. The specific protocol of NGS used in our study, its analysis, and specimens information are described in a detail in Chapter 6, Methods section and Table 6.1.

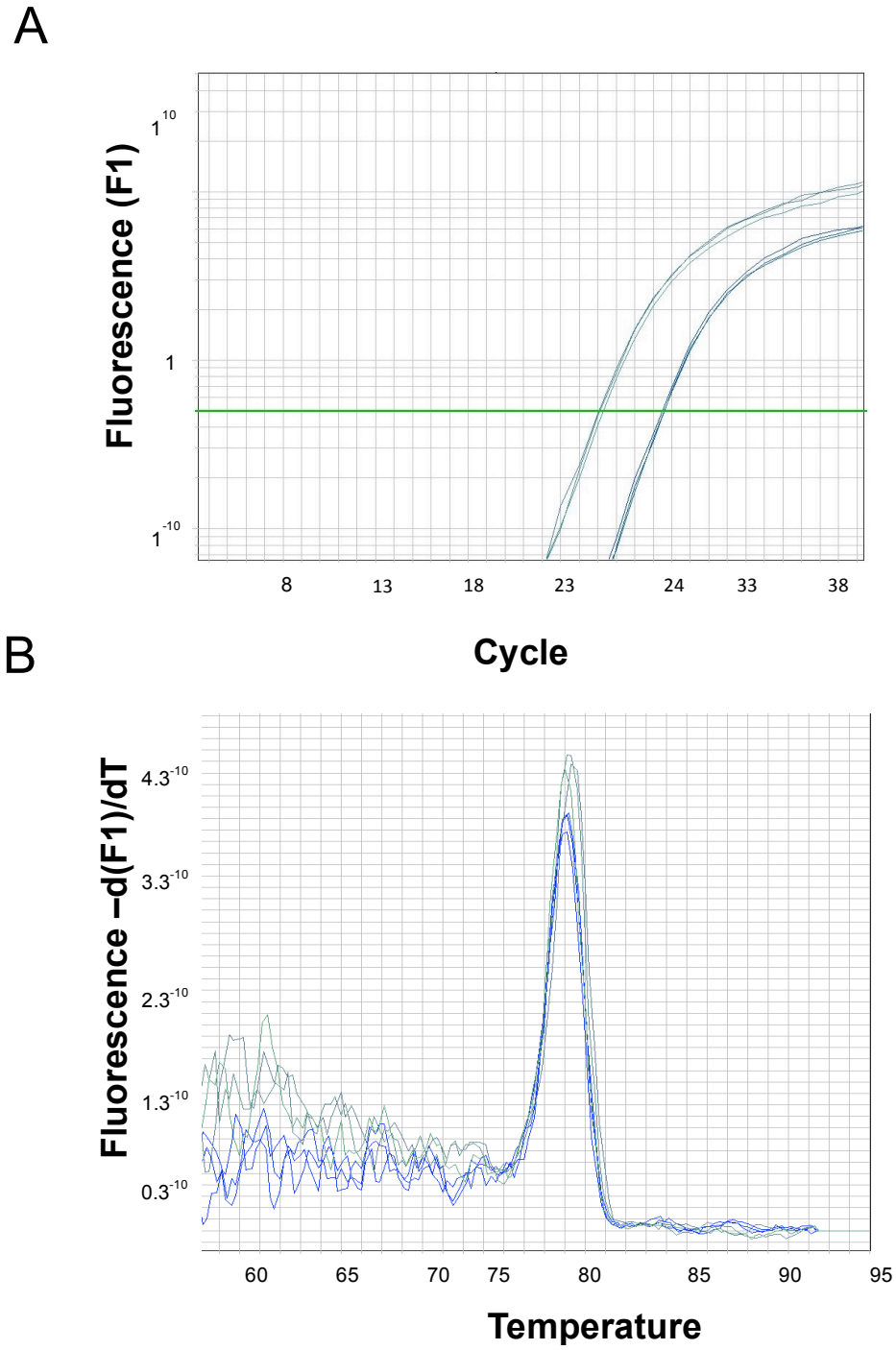

Figure 2.3. Quantitative PCR reaction specificity. A. Amplification plot of HCN4 mRNA expression in iPSCs transfected with miR-133a-3p (blue) and control (green) detected through the change of SYBR-green fluorescence. Green line indicated the amplification threshold. Ct value is the cycle number at which the fluorescent curve crosses the threshold. B. Dissociation curve of the replicates in panel A. The peak of the curve represents the melting temperature (Tm) of the samples. DNA denaturation is directly proportional to temperature increase.

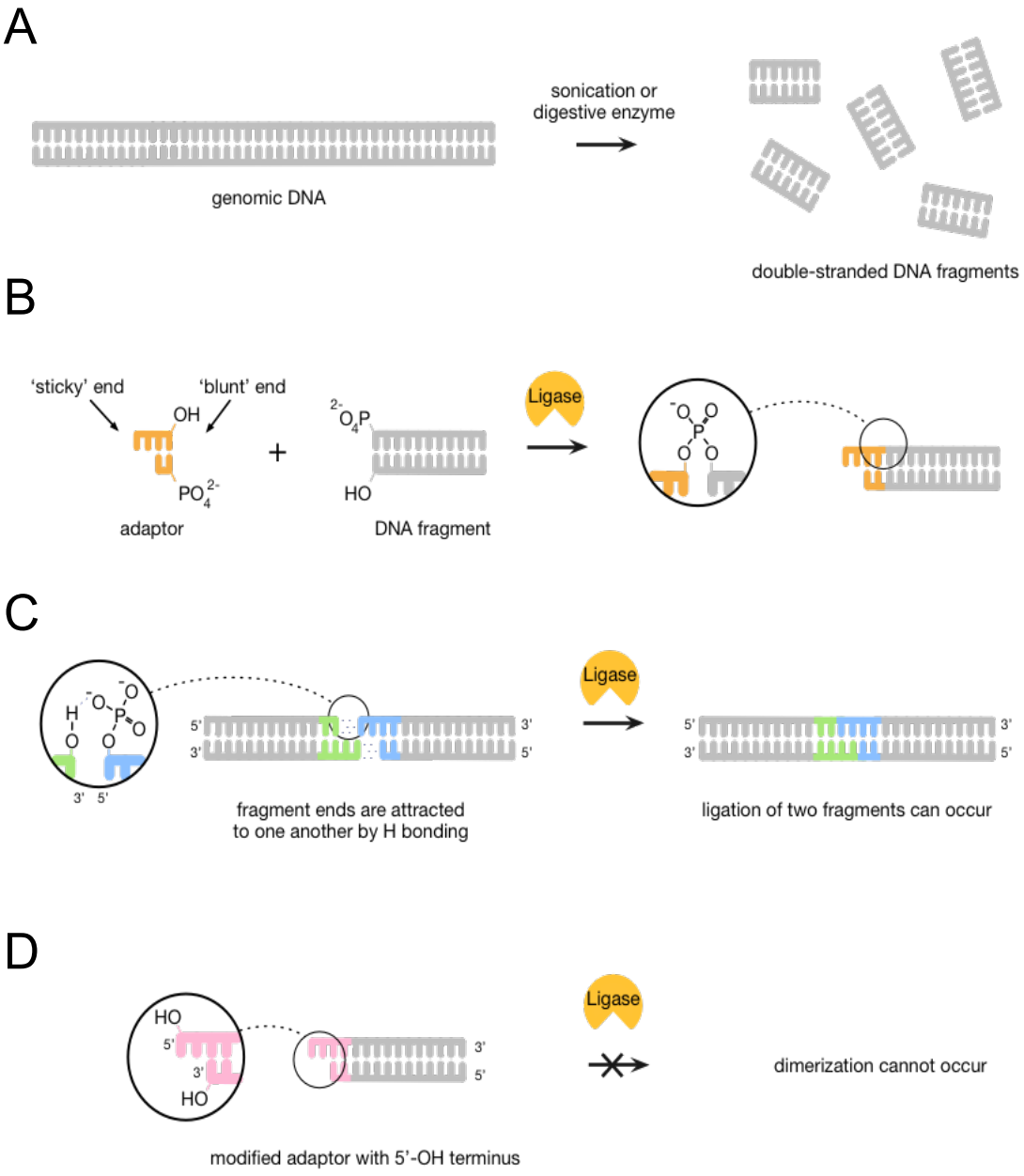

Figure 2.4. Library preparation during next generation sequencing. A. cDNA random fragmentation through sonication or enzyme digestion. B. smaller cDNA fragments are ligated with adapter molecules via 5'-OH sticky fragments ends. C. library cDNA fragments could be ligated through H bonding between 5'-OH sticky ends. D. 3'-OH blunt non-cohesive ends preventing dimer formation. Image is adapted from Atdbio next generation sequencing protocol; https://www.atdbio.com/content/58/Next-generation-sequencing.

2.12 Extracellular potential recording of cultured rat sinus node preparations

A detailed description of rat SN preparation disection and culturing over a 24-hour period, as well as extracellular potential recordings and measurements, is contained in Chapter 4, Data supplement, Materials and methods section. The transfection reagent used for introduction of microRNAs in the SN preparations was lipofectamine RNAmix (Life Technologies). Lipofectamine was also used for transfection of H9C2 cells with miR-486-3p, miR-429 and HCN4, $Ca_V1.3$, and Tbx18 plasmids, Chapter 4; and iPSCs transfection with miR-133a-3p, Chapter 7.

2.13 Lipofectamine as a transfection reagent

Lipofectamine is used for transfections of cells with nucleic acids. In physiological conditions, the negatively charged cell membrane repels the free-floating nucleic acids in the extracellular space, which are also negatively charged. The electrostatic repulsion is overcome by lipofectamine – a cationic compound, which forms possitively charged liposomes carrying nucleic acid molecules across the cell membrane. The positively charged lipid head group consists of one or more positive nitrogen atoms, which in turn interact with the negatively charged sugar-phosphate backbone of the nucleic molecules. The head groups of the lipids form the surface of the liposome, which fuses with the negatively charged cell membrane and thus introduces the nucleic acids to the intracellular space. Lipofectamine was also shown to be successful in transferring DNA from the extracellular space through the nucleous membrane, where it could reach the transcriptional machinery and achieve expression of the transgene (Ohki et al., 2001).

An important factor for the success of lipofectamine transfections in cell culture is the cell density. Higher seeding cell densities could cause inhibition of cell division, growth, and metabolism. In contrast, lower seeding densities could cause cell culture recovery from the effects of the nucleic acids introduced to the media. It has been considered that the best cell density for transfection should be 90-95% in order to avoid inhibition of cell growth and subsequent variability (Romoren et al., 2004).

Lipofectamine has also been a reagent used widely in the transfection various mammalian cells with short interfering RNAs as well as for luciferase reporter gene assays (Gitlin et al., 2002; Yu et al., 2002; Zou et al., 2003).

In our study we used lipofectamine for the transfection of rat SN preparations with a number of microRNAs (see Chapter 4), H9C2 cells with plasmid of interest, and microRNAs in order to assess the bidning of microRNAs to their predicted targets (see Chapter 4) as well as transfection of iPSCs with miR-133a-3p (see Chapter 7).

2.14 Graphene oxide as a transfection reagent

Graphene is essentially a sheet of carbon atoms (Choi et al., 2010). Graphene oxide (GO) is a highly oxidised isoform of graphene, forming a two-dimentional nanomaterial (Compton and Nguyen, 2010; Park and Ruoff, 2009). Oxidation of graphene has been shown to improve graphene solubility and electrical properties (Veca et al., 2009). The functional groups of the GO chemical structure allow it to conjugate with various molecules such as DNA and drug ligands, and it acts as a delivery system (Liu et al., 2008b; Wu et al., 2017). GO has shown a number of desirable properties as a transfection reagent, inclueding biocompatibility, large surface area, and low toxicity when deliverying

plasmid DNA into HeLa cells (Bao et al., 2011), suggesting GO has a great potential as a gene delivery system.

Other studies have reported GO works synergistically in gene transfection experiments together with polyethylenimine. GO is a negatively charged reagent, which binds to the positively charged polyethylenimine through electrostatic interactions, and forms a stable complex with high cationic density allowing loading of nucleic acid molecules. In contrast to polyethylenimine alone, the polyethylenimine-GO comples exhibit significantly lower cytotoxicity and higher transfection efficacy (Feng et al., 2011; Kim et al., 2011; Wu et al., 2017; Yan et al., 2013).

GO was used in our study as a marker for the area of the injection in rat SN preparations, to show microRNAs were successfully injected at the SN artery bifurcation region (see Chapter 4). It was also used in iPSCs in order to assess its transfection efficacy and to identify if it has a potentially toxic effect (see Chapter 7). GO labels the tissue through electrostatic interactions with it. The positive charge of the GO sheets allows them to attach to the tissue and be absorbed by it due to the negative charge of the cell membrane. Labelling with GO is physically assessed through imaging with light microscope (Zeiss LSM5) and Axiocam camera (Zeiss) and collected with Axiovision software (Zeiss) for rat SN preparations, and EVOS digital inverted microscope (Life Technologies) for iPSCs.

2.15 Luciferase reporter gene assay

The luciferases are derived from from firefly (*Photinus pyralis*), and are bioluminescent substances that emit fluorescent light when energy is released upon the interaction of the luciferase enzyme with the luminescent substrate luciferine. Nearly all the energy produced during the chemical reaction is converted into fluorescent light.This efficiency makes the

assay sensitive to small changes in the corresponding protein expression levels (McElroy and Rainwater, 1948; Tauriainen et al., 1999).

The luciferase reporter gene assay is widely used to determine target genes expression in cell culture (Figure 2.5). The luciferase gene is usually cloned downstream of a target DNA sequence into an expression vector, which is then introduced into the cell line. Upon transfection with the vector that contains the luciferase gene (for example, a microRNA binding site) of the target gene upstream of the luciferase gene, cells are incubated and left to grow for 24 hours. They are then collected, lysed, and luciferine enzyme is added. Luciferine interacts with all the proteins released from the cell culture including the luciferase protein. Their reaction is detected and quantified with luminometer (Figure 2.5). Since the target gene has been fused with the luciferase reporter gene, luciferase activity is directly proportional to the target gene expression (Lin et al., 2008).

Luciferase reporter gene assay has been used to study the effect of RNA interference molecules such as microRNAs that inhibit protein expressionby post-transcriptional repression. Sequential measurement of luciferase reporter gene activity, as well as renilla reporter gene (*Renilla reniformis*), is used for normalistion of the results produced by the luciferase reporter gene.

In the current study, the luciferase reporter gene assay was performed in H9C2 cells transfected with PEZX-MT06 luciferase expression vector for luciferase and renilla reporter genes, as well as HCN4, $Ca_V1.3$, or Tbx18 3'UTR fragments, which contained microRNA binding sites (GeneCopoeia). H9C2 rat derived cardiomyocytes were also co-transfected with either miR-486-3p or miR-429 (Life Technologies) in order to study their inhibitory effect on the target genes protein expression. A detailed description of the cell

culture, transfection with luciferase transfection reagent, and luciferase reporter gene assay method is described in Chapter 4, Data supplement section.

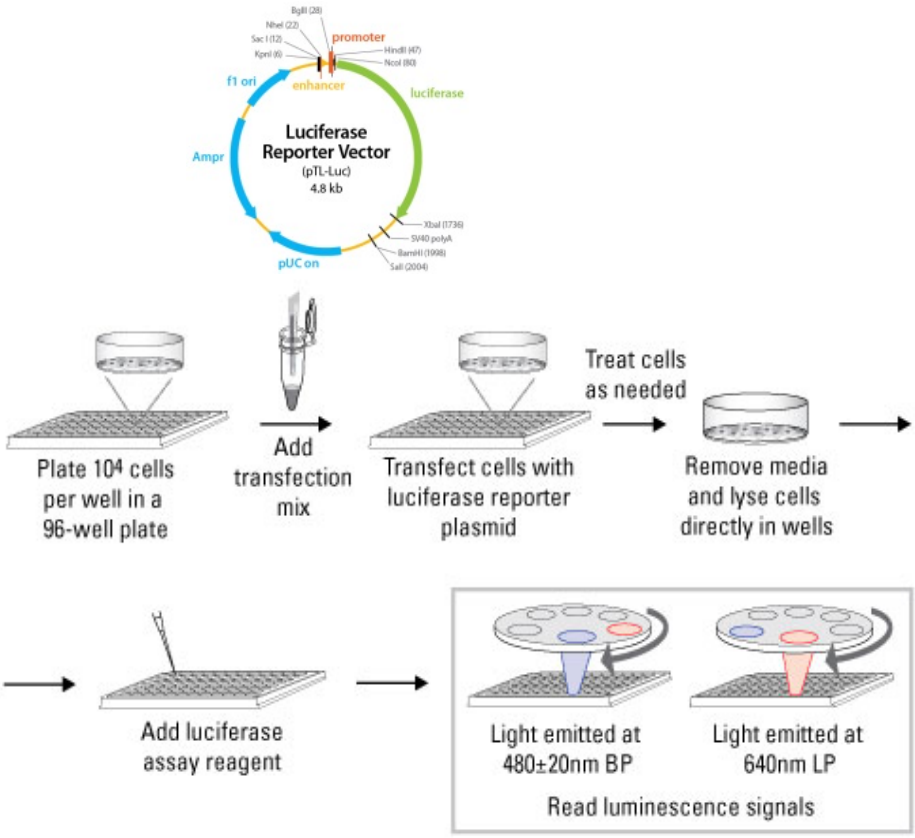

Figure 2.5. Luciferase reporter gene assay principles. Promoter response element of interest is cloned upstream of the luciferase gene. Upon transfection, successful translation of the protein of interest results in directly proportional increase of fluorescence levels to protein expression. Addition of the luminescent substrate, luciferin, allows protein quantification using luminometer. Image adapted from BioTek; https://www.biotek.com/resources/application-notes/.

2.16 Human cardiac induced pluripotent stem cells

Adult somatic cells that could be reprogrammed into iPSCs generate a unique system that could be used to investigate specific physiological and pathopysiological molecular processes. Our study examined the effect of miR-133a-3p on the beating rate of cardiac iPSCs and investigated if endogenous HCN4 levels were affected by miR-133-3p forced overexpression (Chapter 7).

Cells were derived from human donor dermal skin fibroblasts (Yoon et al., 2014). They were cultured and characterised as previosuly described (Chiang et al., 2011; Juopperi et al., 2012). Upon collection of skin biopsies, iPSCs were derived through retroviral transduction with four transcription factors – Oct3/4, Sox2, c-MYC, and Klf4. The newly derived iPSCs were maintained on mouse embryonic fibroblasts in hESM medium. In order to characterise the cells pluripotent markers levels such as Nanog, Oct4, Sox2, SSEA3, SSEA4, TRA-1-60, their expression was measured by immunohistochemistry as previously described (Chiang et al., 2011). *In vivo* characterisation involved immunohistochemical experiments with antibodies for α-fetoprotein, nestin, and α-smooth muscle actin. Final *in vitro* assessment involved subcutaneous injection of confluent iPSCs in female NOD.CB17-*Prkdc*^{scid}*/J* mice. Histological staining for haematoxylin assessed the morphology of the tumors formed after 12 weeks post-injection (Juopperi et al., 2012).

Cell differentiation was performed by Dr. Anna Liakhovitskaia according to a previously described method (Burridge et al., 2014). The cells were maintained on matrigel-coated plates in mTESR1 medium (Stem Cell Techologies), 10 mkM Y-27632 was added for 1 hour before and for 24 hours after passaging. Detailed method of cell differentiation,

culturing, maintainance, transfection, and beating rate recording is contained in Chapter 7, Materials and methods section.

2.17 Statistical analysis

The software used for the statistical analysis was GraphPad Prism 6 or 7 (Prism). Normal distribution between groups was determined using Shapiro-Wilk normality test and Kolmogorov-Smirnov test. Experiments comparing the results of two independent groups with parametric distribution used two-tailed unpaired student's t-test. If results were nonparametrically distributed, they were tested with Mann-Whitney test. Comparison between multiple groups that were normally distributed was performed via one-way ANOVA, while non-normally distributed data was analysed using Kruskal-Willis test. Significant difference of data was considered when $p<0.05$. Figures depict data mean±standard error of the mean (SEM). * depict $p<0.05$, ** $p<0.005$, *** $p<0.05$. Statistical analysis of microRNA data in human SN vs. RA and NGS is described in detail in Chapter 3, Data supplement and Chapter 6, Materials and methods sections, respectively.

Histological, immunohistochemical, and western blot experiemnts in chapter 3 were performed on tissue from 4 human secimens in order to characterise the tissue and observe the expression of major pacemakeing mechanisn proteins. Quantitative PCR analysis of human microRNA expression was compared between 7 SN and 7 RA. Further functional analysis of 7 human microRNAs in chapter 4 was assessed through injection of 4 rat SN preparations vs. 4 controls injected with scrambled microRNA. Luciferase reported gene experiments for miR-486-3p and HCN4, as well as $Ca_V1.3$, and miR-429 and Tbx18 were were measured through 4 different conditions. Each condiction was measured in 4 repeats

(wells) in 3 individual batches of cells (cell plates). mRNA expression of miR-486-3p, as well as HCN4, $Ca_V1.3$, and $Ca_v3.1$ was measured in 4 rat SN preparations compared to controls injected with scrambled microRNA. HCN4 and caveloin3 protein levels were measured in 5 rat SN preparations compared to control. Chapter 5 immunohistochemical expression of various membrane and Ca^{2+} clock mechanism proteins was measured in 6 human SN and RA sections. Single cell experiments from rat and mouse were performed in n=5 cells for each cell type in each condition. Chapter 6 represents the expression of a number of TFs in 3 healthy human SN and RA. Chapter 7 reports the mRNA expression of miR-133a-3p in 3 heart failure and 5 healthy human hearts. Further functional miR-133a-3p function and qPCR analysis is performed in iPSCs treated with miR-133a-3p (n=5 wells), negative control (n=6 wells), and scrambled microRNA (n=4 wells).

Chapter 3

3 Identification of key small non-coding microRNAs controlling the pacemaker mechanisms in the human sinus node

3.1 Other authors contribution to the paper

The vast majority of the experimental work for this study was performed by myself, I also created and wrote the paper. I greatly appreciate and acknowledge the input from the following authors:

- Joseph Yanni carried out human SN/RA microRNA expression experiment
- Vadim Fedorov and Ning Li carried out microRNA expression experiment in samples from heart failure patients
- Alicia D'Souza aided me in data analysis and experiment design
- Yu Zhang carried out western blot experiments
- Andrew Atkinson aided me with confocal microscopy and technical support
- Balint Borbas and Connor Geraghty were undergraduate students who aided me with part of the experimental work and analysis under my supervision
- Fatemeh Jafarzadeh aided me with analysis of the human microRNA data
- Luke Stuart provided critical and valuable comments on my manuscript
- Delvac Oceandy had a supervisory role and aided in experiment design
- Filip Perde and peter Molenaar provided the human SN specimens
- Halina Dobrzynski had a major supervisory role and aided me with the experimental work and provided critical and valuable comments on my manuscript

3.2 Paper

Identification of key small non-coding microRNAs controlling the pacemaker mechanisms in the human sinus node

Short title: microRNA, pacemaker mechanisms, human sinus node

M. Petkova (MRes)[1], J. Yanni (PhD)[1], N. Li (PhD)[2], A. D'Souza (PhD)[1], Y. Zhang (PhD)[1], A. Atkinson (MSc)[1], B. Borbas[1], F. Jafarzadeh (Mres)[1], C. Geraghty (BSc)[1], L. Stuart (Mres)[1], D. Oceandy (PhD)[1], F. Perde (PhD)[3], P. Molenaar (PhD)[4, 5], V.V. Fedorov (PhD)[2], H. Dobrzynski (PhD)[1]

[1]Cardiovascular Sciences, University of Manchester, Faculty of Biology, Medicine and Health Manchester, UK

[2]Physiology and Cell Biology Department, The Ohio State University Wexner Medical Center, Columbus, USA

[3]National Institute of Legal Medicine, Bucharest, Romania

[4] Queensland University of Technology and [5]Cardio-Vascular Molecular & Therapeutics Translational Research Group, The Prince Charles Hospital, Brisbane, Australia

Corresponding Author:

E-mail address: halina.dobrzynski@manchester.ac.uk

Address: CTF Building, 46 Grafton Street, Manchester M13 9NT

Tel: +441612751182, Fax: +441612751183

Total word count: 6610

Abstract

Background –The sinoatrial/sinus node (SN) is the primary pacemaker of the heart. It initiates and propagates the electrical signal and thus regulates the heart rate. Its function depends on the expression of ion channels, connexins, and Ca^{2+}-handling proteins involved in pacemaker mechanisms, regulated by small non-coding RNAs called microRNAs. The aim of this study was to compare the expression profile of the most abundant microRNAs in the human SN with right atrial (RA) muscle.

Methods – Seven human SN and RA muscle samples were obtained from unused donor or post-mortem hearts. The SN tissue was characterised by histology, immunolabelling/immunoblotting techniques using antibodies to ion channels responsible for pacemaking: HCN4 (a major isoform of funny channels), $Ca_V1.3$, $Ca_V3.1$ (isoforms of L-type and T-type Ca^{2+} channels, respectively), and Tbx18 (a transcription factor required for development of pacemaker cells). Total RNA was isolated from specimens and qPCR (using TaqMan array human microRNAs cards) was performed for 754 most abundant microRNAs. The data were analysed using RealTime Statminer and Ingenuity Pathway Analysis (IPA).

Results – The SN was embedded in a network of connective tissue and contained smaller and poorly organised cells. Immunolabelling and/or immunoblotting showed that HCN4, $Ca_V1.3$, $Ca_V3.1$, and Tbx18 are more abundant in the SN vs. RA muscle. Using qPCR analysis we observed 48 and 18 microRNAs significantly less and more expressed in the SN vs. RA muscle, respectively ($p<0.05$, Student's t-test). Out of these key 66 microRNAs, those that are of potential interest for regulating the heart rate by targeting molecules involved in pacemaker mechanisms are: miR-1-3p, miR-10b-5p, miR-30c-5p,

miR-133a-3p, miR-153-3p, miR-198, miR-204, miR-215-5p, miR-371-3p, miR-422a, miR-429, miR-486-3p, miR-512-5p, miR-938, and miR-1225-3p.

Conclusions – This is the first study that shows the human SN has a unique microRNA expression pattern that likely contributes to its molecular profile and electrical activity. Targeting specific microRNAs such as miR-133a-3p and miR-486-3p that regulate HCN4 expression could lead to potential therapies for sick sinus syndrome.

Key words: sinus node, pacemaker mechanisms, membrane and Ca^{2+} clocks, microRNAs

Introduction

The sinus node (SN) is the primary pacemaker of the heart, located at the junction of the superior vena cava with the right atrium. It is an extensive structure and its anatomy has recently been shown in 3D within the whole *ex vivo* human heart by Stephanson et al.,[1]. The SN myocytes are characterised by the expression of specific ion channels and Ca^{2+} handling proteins (described in human by Chandler et al., 2009) responsible for two main pacemaking mechanisms – the so-called membrane voltage and Ca^{2+} clocks [2, 3]. These two mechanisms generate pacemaker potential during phase 4 of the nodal action potential (AP). Hyperpolarisation-activated cyclic nucleotide-gated (HCN1 and 4) channels, activated by 3'-5'-cyclic adenosine monophosphate (cAMP), are responsible for the funny current, I_f, during phase 4, and the initiation of the AP [4]. During phase 4, the SN lacks resting membrane potential due to the poor expression of $K_{ir}2.1$, the inward rectifier K^+ channel responsible for $I_{K,1}$. Unlike the working myocardium, the SN AP shape is characterised by a slow upstroke during phase 0, because the upstroke is generated by slow Ca^{2+} channels, $Ca_V3.1$ (responsible for $I_{Ca,T}$), and $Ca_V1.3$ (responsible for $I_{Ca,L}$) rather than

$Na_V1.5$ responsible for the fast I_{Na}, characteristic for the atrial and ventricular myocardium [5, 6]. $Ca_V3.1$ also contributes to the later part of phase 4. Unlike the AP of the surrounding atrial muscle, the AP of the SN lacks early phase of repolarisation, phase 1, and exhibits longer plateau, phase 2, due to mainly higher expression of $Ca_V1.3$ (rather than $Ca_V1.2$) [7]. The repolarisation of the SN AP (phase 3) results from the inactivation of the Ca^{2+} channels, and the activation of various K^+ channels: $K_V1.4$ (responsible for transient outward K^+ current, I_{to}), $K_v1.5$, hERG and K_vLQT (ultra-rapid, rapid and slow delayed rectifier K^+ currents, $I_{K,ur}$, $I_{K,r}$, and $I_{K,s}$, respectively) [8].

The Ca^{2+} clock plays a role in the pacemaking activity of the SN synergistically with the membrane voltage clock. Ca^{2+} is released from the SR through the opening of ryanodine receptors type 2 (RyR2) in the form of spontaneous "sparks" or local Ca^{2+} release [9]. The local Ca^{2+} release contributes to an increase in intracellular Ca^{2+} concentration during phase 4 of the AP. This leads to the activation of the cell membrane electrogenic Na^+-Ca^{2+} exchanger (NCX1). These Ca^{2+} proteins were shown to be expressed in the human SN [7].

Cardiac cells are electrically coupled via connexins. The two main high-conductance connexnis, Cx40 and Cx43 are poorly expressed in the SN compared to the atrial muscle [7], confirming the poor electrical coupling in the SN. Cx45 (the low-conductance connexin), however, is equally expressed in the SN and atrial muscle, suggesting that it provides low level of electrical coupling of the nodal cells [10].

About 2,000 microRNAs have been discovered in the human genome, and many of them are tissue-specific [11]. They are approximately 18-24 nucleotide single stranded RNAs that inhibit the expression of specific mRNA targets through binding to the 3' untranslated region (3'UTR) of their target mRNAs. A number of cardiac specific microRNAs have been shown to regulate critical cardiac developmental processes as well as various

pathophysiological mechanisms such as in cardiac hypertrophy, fibrosis, arrhythmias, and heart failure [12, 13]. Extensive amounts of data accumulated in recent years demonstrate their important role in the physiology and pathophysiology of cardiovascular disorders as well as their potential role as biomarkers of some diseases [14-16].

Although microRNAs are increasingly being recognised as major modulators of the cardiac function [17-19] their role in controlling the expression of key genes responsible for the SN pacemaker and conduction mechanisms has not been explored. Therefore, the aim of this work was determine the microRNAs expression profile of the healthy human SN in comparison to its surrounding atrial tissue.

Material and Methods

The human specimens used in this study are described in detail within the Supplemental data file and Table S1. They were obtained, dissected and frozen by co-authors in Australia (PM) and Romania (FP) under their local ethical approval procedures (Ethics approval number EC2565, The Prince Charles Hospital Human Research Ethics Committee). No informed consent was required.

The techniques used were: histology, immunohistochemistry, immunoblotting, RNA isolation, reverse transcription, preamplification and qPCR for microRNAs and bioinformatics. These techniques are in details described in Supplemental data.

Table S2 provides details of the antibodies used in this study.

Results

The location of the SN and the surrounding atrial myocardium was investigated on histological sections stained with Masson's trichrome (Figure 1 A). The SN area was

identified by the presence of the SN artery and a large amount of connective tissue (stained in blue, Figure 1 A). Higher magnification images show the morphological differences between the nodal tissue and atrial myocardium – as the SN is characterised by the presence of small, sparse cells (stained purple, Figure 1 B) embedded in the network of connective tissue. The atrial tissue is recognised by the presence of the cardiomyocytes, where they exceed the size of those observed in the SN, and less connective tissue is present, Figure 1 C, F. The cell size of the SN and RA was compared through immunohistological experiment using caveolin3 as membrane-labelling marker, Figure 1 D, E, F. Caveolin3 staining allowed the cell membrane to be distinguished from the surrounding connective tissue, and the cell diameter was measured showing that the RA myocytes (20 ± 0.62 μm) are significantly bigger than the SN myocytes (6.6 ± 0.31 μm) ($p<0.005$), Figure 1 D, E, F.

Figures 2 and 3 show the expression of key proteins involved the SN and its surrounding atrial tissue function.

Cx43, which is a large conduction connexin and is involved in the electrical coupling of the heart cells, is known to be predominantly absent in the SN, and highly abundant in the RA in small and bigger mammals, which was also the case in the human sections observed in this study shown in Figure 2 A, B. Therefore, Cx43 is usually used in our laboratory as a negative marker of the SN. Cx43 abundance in the SN and RA was measured in four human specimens by immunoblotting confirming the significantly higher Cx43 protein content in the RA (0.2 ± 0.05 r.a.) compared to the SN (0.02 ± 0.002 r.a. $p\leq0.05$, Figure 3A, where r.a. stands for relative abundance).

The SN is the primary pacemaker of the heart due to the high expression of HCN4, responsible for the hyperpolarisation-activated “funny” current, I_f. Its higher expression in

the SN in comparison to the RA is a prerequisite of its use as a positive marker of the primary pacemaker cells. Figure 2 shows that HCN4 is abundantly expressed in the SN compared to the RA (Figure 2 C, D). Immunoblotting experiments confirmed the significantly higher abundance of HCN4 in the SN (0.15 ± 0.01 r.a.) vs. the RA 0.09 ±0.02 r.a.; $p \leq 0.05$ (Figure 3D).

The HCN4-initiated action potential depolarises the cell membrane and leads to the opening of voltage-gated Ca^{2+} channels $Ca_V1.3$ (responsible for $I_{Ca,L}$), involved in the upstroke of the action potential and $Ca_V3.1$ (responsible for $I_{Ca,T}$), important for the later phase of the diastolic depolarisation. Figure 2 shows that the human SN sections express higher fluorescence levels of both these channels compared to the RA (Figure 2 E, F, G, H). Both of these Ca^{2+} channels were shown to be more expressed in the SN (Figure 3 E, F). $Ca_V1.3$ in the SN was 2.11 ± 0.1 r. a. vs. RA 1.55 ± 0.15; $p \leq 0.05$ (Figure 3 E). $Ca_V3.1$ in the SN was 1.38 ± 0.7 r. a vs. RA 1.06 ± 0.15; $p \leq 0.05$ (Figure 3 F).

$Na_V1.5$, which is a major action potential upstroke channel in the atrial and ventricular myocardium, is producing the inward I_{Na}. Previous studies report that $Na_V1.5$ is predominantly absent in the SN area. $Na_V1.5$ expression in this study was confirmed by immunoblotting to be significantly less abundant in the SN 1.7 ± 0.09 r. a. compared to the RA 1.9 ± 0.09 r. a.; $p \leq 0.05$ (Figure 3B).

Tbx18 is a transcription factor, which during embryonic development is involved in the formation of the SN [20]. Figure 3C shows that Tbx18 is significantly more abundant in the SN area 4.24 ± 0.4 r. a. compared to the RA 2.9 ± 0.25 r.a.; $p \leq 0.05$.

Ca^{2+}-handling proteins play a significant role in the pacemaker mechanisms. NCX1 is the major Na^+/Ca^{2+}-exchanger in the heart and is shown to be more significantly expressed in

the RA 0.42 ± 0.07 r. a. compared to the SN 0.12 ±0.02 r.a.; $p \leq 0.05$ (Figure 3 G) in our human samples. The sarcoplasmic reticulum Ca^{2+} pump, SERCA2a, was confirmed to be significantly more abundant in the RA 1.89 ± 0.03 compared to the SN 1.02 ±0.2 r.a. $p \leq 0.05$ (Figure 3 H).

In order to map the expression profile of microRNAs in the SN and RA, biopsies from 7 human hearts (Table 1 S) were isolated and the expression of 754 most abundant human microRNAs was studied using TaqMan Gene Expression Assay. The RNA quality and quantity is shown in Table 1 S. Our results showed that out of 754 most abundant microRNAs, 48 were less abundant in the SN (Figure 4 B) (Table S3, $p \leq 0.05$). Of the 18 microRNAs that were more abundant in the SN, 7 were predicted by Ingenuity Pathway Analysis software to target ion channels, connexin and Ca^{2+}-handling proteins involved in the regulation of the membrane and Ca^{2+} clocks (IPA, Qiagen, Table 1, Figure 5). Predictions were based on microRNA to mRNA sequence binding probability in combination with microRNA data from this study and previous mRNA data from Chandler et al., 2009. The microRNAs were predicted to target mRNAs that were expressed at lower levels in the SN compared to the RA (Chandler et al., 2009; Table 1). miR-10b-5p was found to target Cx40; miR-153 was predicted to target $Ca_V1.2$, RyR2, and $Na_V1.5$; miR-198 was predicted to target $Ca_V1.2$, RyR2, and ERG; miR-204 was targeting $Ca_V1.2$; miR-215 was predicted to target $K_V1.4$; miR-512-5p was predicted to target Cx43 and miR-1225-3p was predicted to target $Na_V1.5$.

Of the 48 microRNAs expressed at higher levels in the RA than SN, 8 were found to be targeting genes that were expressed at lower levels in the RA compared to the SN (Figure 6, Table 1, Chandler et al., 2009). miR-1-3p was predicted to target HCN1, HCN4, and Tbx3 (a transcription factor responsible for the embryonic development of the SN); miR-

30c was predicted to target HCN1 and $Ca_V1.3$; miR-133a was predicted to target HCN4; miR-371-3p was predicted to target $Ca_V1.3$ and Cx45; miR-422a was predicted to target Tbx3; miR-429 was predicted to target Tbx18; miR-486-3p was predicted to target $Ca_V1.3$, HCN1 and HCN4; and miR-938 was predicted to target $Ca_V1.3$.

Table 1 summarises those microRNAs that are differentially expressed in the SN vs. RA and their predicted targets. TargetScan Human and/or TarBase software was used for source of prediction of target mRNA. Rna22 software was used to find out the number of binding sites.

Figure 7 shows simplified gene regulatory feedback loop mechanisms. In the SN high expression of Tbx3 and Tbx18 enhance expression of pacemaker channels (HCN1, HCN4, $Ca_V1.3$, and $Ca_V3.1$) and enhance expression of microRNAs (153-3p, 204-5p, 1225-5p, 512-5p, 2015-5p, and 10b-5p). In the RA, higher expression of Nkx2-5 enhances the expression of gap junction channels (Cx40, Cx43), ion channels ($Na_V1.5$, $Ca_V1.2$, $K_V1.4$), and ryanodine receptor (RyR2), in red as well as microRNAs (422a, 429 and 486-3p). In the SN, higher expression of miRs-153-3p, 204-5p, 1225-5p, 512-5p, 2015-5p, and 10b-5p inhibit expression of Nkx2-5, Cx40, Cx43, $Na_V1.5$, $Ca_V1.2$, $K_V1.4$, and RyR2. In the RA, higher expression of miRs-422a, 429, and 486-3p inhibit expression of HCN1, HCN4, $Ca_V1.3$, and $Ca_V3.1$ and inhibit expression of Tbx3 and Tbx18. Therefore, positive and negative loop mechanisms are created.

Discussion

This study for the first time shows a distinct expression pattern of microRNAs in the human SN vs. RA that are predicted to affect the expression of target molecules responsible for pacemaker mechanisms.

The current study reports 8 microRNAs expressed at higher levels in the RA compared to the SN that are predicted to inhibit molecules that are important for peacemaking (Table 1): miR-1-3p, miR-30c-5p, miR-133a-3p, miR-371-3p, miR-422a, miR-429, miR-486-3p, and miR-938.

miR-486-3p was previously shown to be involved in the regulation of muscle growth and homeostasis, and its expression is regulated by a few transcription factors such as SRF, MRTF-A, and MyoD [21]. miR-486 expression was found to be inhibited in Duchenne's muscular dystrophy [22] and in denervation-induced muscle atrophy [21, 22], confirming its role in muscle growth and homeostasis. miR-486-3p was shown to play a major role in a signalling pathway, where it inhibits phosphatase and tensin homolog (PTEN) and Foxola, and thus increase PI3kinase/AKT activity in muscle cells [21], and overexpression of miR-486-3p leads to muscle hypertrophy [21]. PI3 kinase in turn is known to stimulate skeletal muscle hypertrophy and atrophy [23]. It has been shown that left ventricular hypertrophy often occurs before acute myocardial infarction [24], and a recent study reported increased expression of miR-486-3p in the serum of patients with acute myocardial infarction [25]. Pharmacological block of PI3 kinase was reported to initiate infarct resorption and inhibit cardiac remodelling, caused by myocardial infarction in mice [26]. Another group also reported that miR-486-3p expression is upregulated in cats suffering from hypertrophic cardiomyopathy, when compared to healthy cats [27].

In our current study we predicted that the higher expression of miR-486-3p in the RA inhibits key pacemaker channels (HCN4, Cav1.3, and Cav3.1 – Table 1). Our recent study shows that this microRNA is upregulated in the SN in a mouse model of athletic training [28]. We have also showed, in the same study, that miR-486-3p binds to HCN4 using a luciferase reporter assay. Based on these data, miR-486-3p is probably inhibiting the

expression of HCN4 in the human RA (Table 1). In addition, our unpublished data showed that miR-486-3p injected into the *ex vivo* rat SN preparations causes significant reduction of the beating rate as well as downregulation of HCN4 at mRNA and protein level, but no change in expression Cav1.3 and Cav3.1.

miR-133 and miR-1 have also been previously shown to regulate ion channels. A study in a rat model of ventricular hypertrophy reported increased HCN4 expression, which was related to downregulation of miR-1 and miR-133, leading to arrhythmogenesis and hypertrophy [17], suggesting the close relation and modulation of HCN channels in the heart by miR-1 and miR-133. This supports our study that higher expression of both of these microRNAs in the RA (together with miR-486-3p) inhibits the expression of HCN4 (Table 1). Interestingly our preliminary data on 3 healthy and 3 heart failure SNs using qPCR show that miR-1-3p and miR-133a-3p are upregulated in the SN in heart failure giving further evidence that they are important molecules involved in the pacemaker mechanisms.

miR-30c was found to be highly expressed in the heart [29] and has an extensive role in cardiac hypertrophy, induced by a signalling pathway activated by Cdc42 and Pak1 [30]. Overexpression and inhibition of miR-30c in cardiomyocytes showed that there is an inverse relationship between miR-30c and Cdc42 and Pak1 activity, and thus it endogenously prevents cardiac hypertrophy [30]. In our study miR-30c was predicted to inhibit key pacemaker ion channels, which is why it could be expressed less in the RA (Table 1).

Not much is known about miR-422a and miR-429 in the heart. It has been shown that miR-422a is highly expressed in atherosclerotic lesion plaques in human carotid arteries' monocytes [31]. A study on miR-429 implicated its role in the development of cardiometabolic disease due to variations in nutrition during pregnancy [32] and has a pro-

inflammatory and hypertrophic effect in diabetic mice [33]. Our study predicts that miR-422a is inhibiting Tbx3 and miR-429 is inhibiting Tbx18 in the RA (Table 1). These two transcription factors are highly expressed in the SN (Table 1).

Two studies that examined microRNAs as biomarkers for various cardiovascular disorders reported an upregulation of miR-371-3p in a group of patients suffering from chronic congestive heart failure [34]. In our study, this microRNA was predicted to inhibit $Ca_V1.3$ and Cx45 in the RA (Table 1).

Nothing is yet reported about miR-938 and its function in the cardiovascular system. It has been observed, however, that this microRNA promotes colorectal cell proliferation [35], and it is also associated with gastric [36] and pancreatic cancer susceptibility [37]. In our study miR-938 was predicted to inhibit $Ca_V1.3$ (Table 1).

Our study reports 7 microRNAs expressed at higher levels in the SN compared to RA that are predicted to bind to molecules that are expressed at lower levels in the SN (Table 1): miR-10b-5p, miR-153-3p, miR-198, miR-204-5p, miR-215-5p, miR-512-5p, and miR-1225-3p.

miR-10 expression was reported to be significantly downregulated in human heart failure samples [38]. There are no other reports about its function in the heart; however one study described miR-10 contribution to regulation of inflammatory processes in the atherosusceptible endothelial cells. A decreased expression of miR-10 was related to an increased expression of Homeobox A1, and it is known to regulate NF-kB signalling in in these cells [39]. Our study predicted that this microRNA inhibits the expression of Cx40 in the SN (Table 1) and could explain slower electrical coupling of the nodal cells.

A recent study reported that miR-153 is involved in oxidative stress induced-apoptosis in the heart [40]. Its expression was found to be significantly increased upon H_2O_2 application, and the inhibition of the endogenous miR-153 produced an anti-apoptotic effect, but stimulated autophagy during oxidative stress, leading to the conclusion that miR-153 is involved in the survival mechanism of cardiomyocytes during oxidative stress through the modulation of apoptosis and autophagy. In our study this microRNA was predicted to inhibit $Ca_V1.2$ and $Na_V1.5$ (Table 1) in the SN explaining the slower AP upstroke in the SN.

miR-198 expression was found to be increased together with two other microRNAs; miR-134 and miR-370 in patients with unstable angina pectoris in comparison with patients with stable angina pectoris, suggesting that it might be useful as a biomarker for patients who are at risk of myocardial infarction [41]. Our study showed that miR-198 is inhibits ERG in the SN and can also explain a longer AP duration (Table 1).

miR-204 is well-known for its role as an inhibitor of osteoblastogenesis, and it was recently found to inhibit smooth muscle cell calcification *in vitro* and *in vivo* through targeting the Runx2 gene in mouse smooth muscle cells cultured in calcifying media [42]. Overexpression of miR-204 inhibited vitamin D3-induced vascular calcification within 3 days of treatment [43]. In our study this microRNA was predicted to inhibit $Ca_V1.2$ (Table 1).

miR-215 was found to be upregulated and involved in a network of microRNAs regulating the mechanism of inflammation in patients who had atrial fibrillation [44]. In our study this microRNA was predicted to inhibit $K_v1.4$ in the SN (Table 1) contributing to a longer AP duration.

miR-512 function in the cardiovascular system is not yet known, however, several studies report its function in the mechanism of apoptosis used for the treatment of breast cancer cells [45], lung cancer cells [45] and suppression of tumour growth by inhibiting the activity of hTERT carcinoma *in vitro* and *in vivo* cells [46]. In our study this microRNA was predicted to inhibit Cx43 (Table 1) and could explain slower electrical coupling of the nodal cells.

Finally, plasma miR-1225 has been found to be significantly higher in patients with an acute coronary syndrome such as acute myocardial infarction and unstable angina, suggesting its role in the heart physiology and pathophysiology [47]. In our study this microRNA was shown to inhibit $Na_V1.5$ (Table 1).

Translational application and future direction

This is the first study to show the microRNA expression profile in healthy SN and RA. In the future, using luciferase assay we will functionally validate loop mechanisms (namely if the selected microRNAs are controlled by transcription factors and if microRNAs bind to their predicated targets, summarised in Figure 7). In the future we will also explore disease-induced changes in microRNA expression and the resulting proteins remodelling in the human SN. Understanding the expression profile and function of these microRNAs in healthy and diseased human SN may lead to potential novel strategies for developing biological pacemakers and treatments of SN dysfunction. Reinforced overexpression or complete abolition of the expression of certain genes form the genome could lead to detrimental consequences. For this reason post-translational silencing of mRNA expression through microRNA regulation could allow fine-tuning of the relationship between mRNAs, microRNAs, and other transcription regulators such as some transcription factors.

Conclusion

The SN is the primary pacemaker of the heart and it has a unique expression pattern of microRNAs that control its unique expression of the proteins (via inhibition of mRNAs) involved in the pacemaker activity responsible for the heat beat. Therefore, microRNAs are potential therapeutic targets in diseases and abnormalities related to abnormal cardiac conduction system activity.

Acknowledgments

None.

Source of funding

This work was supported by the British Heart Foundation (grant numbers RG/11/18/29257 and new grant number to add, HD) and NIH R01 HL115580 and HL135109 (VVF).

Disclosures

None.

Affiliations

University of Manchester, Manchester, UK (M.P., J.Y., A.D., Y.Z., A.A., B.B., F.J., L.S., D.O., H.D.); Ohio State University, Columbus, USA (N.L., V.F.); National Institute of Legal Medicine, Bucharest, Romania (F.P.); Queensland University of Technology, Brisbane, Australia (P.M.).

References

1. Stephenson RS, Atkinson A, Kottas P, Perde F, Jafarzadeh F, Bateman M, Iaizzo PA, Zhao JC, Zhang HG, Anderson RH, Jarvis JC and Dobrzynski H. High resolution 3-Dimensional imaging of the human cardiac conduction system from microanatomy to mathematical modeling. *Scientific Reports*. 2017;7.

2. Lakatta EG and DiFrancesco D. What keeps us ticking: a funny current, a calcium clock, or both? *Journal of Molecular and Cellular Cardiology*. 2009;47:157-170.

3. Joung B, Chen PS and Lin SF. The role of the calcium and the voltage clocks in sinoatrial node dysfunction. *Yonsei Medical Journal*. 2011;52:211-219.

4. DiFrancesco D. The role of the funny current in pacemaker activity. *Circulation Research*. 2010;106:434-446.

5. Irisawa H, Brown HF and Giles W. Cardiac pacemaking in the sinoatrial node. *Physiological Reviews*. 1993;73:197-227.

6. Mangoni ME and Nargeot J. Genesis and regulation of the heart automaticity. *Physiological Reviews*. 2008;88:919-982.

7. Chandler NJ, Greener ID, Tellez JO, Inada S, Musa H, Molenaar P, DiFrancesco D, Baruscotti M, Longhi R, Anderson RH, Billeter R, Sharma V, Sigg DC, Boyett MR and Dobrzynski H. Molecular architecture of the human sinus node insights into the function of the cardiac pacemaker. *Circulation*. 2009;119:1562-1575.

8. Ono K and Ito H. Role of rapidly activating delayed rectifier K^+ current in sinoatrial node pacemaker activity. *American Journal of Physiology-Heart and Circulatory Physiology*. 1995;269:453-462.

9. Cheng HP, Fill M, Valdivia H and Lederer WJ. Models of Ca^{2+} release channel adaptation. *Science*. 1995;267:2009-2010.

10. Dobrzynski H, Li J, Tellez J, Greener ID, Nikolski VP, Wright SE, Parson SH, Jones SA, Lancaster MK, Yamamoto M, Honjo H, Takagishi Y, Kodama I, Efimov IR, Billeter R and Boyett MR. Computer three-dimensional reconstruction of the sinoatrial node. *Circulation*. 2005;111:846-854.

11. Bartel DP. MicroRNAs: Target recognition and regulatory functions. *Cell*. 2009;136:215-233.

12. Boettger T and Braun T. A new level of complexity the role of microRNAs in cardiovascular development. *Circulation Research*. 2012;110:1000-1013.

13. Romaine SPR, Tomaszewski M, Condorelli G and Samani NJ. MicroRNAs in cardiovascular disease: an introduction for clinicians. *Heart*. 2015;101:921-928.

14. Condorelli G, Latronico MVG and Cavarretta E. MicroRNAs in cardiovascular diseases current knowledge and the road ahead. *Journal of the American College of Cardiology*. 2014;63:2177-2187.

15. van Rooij E, Sutherland LB, Thatcher JE, DiMaio JM, Naseem RH, Marshall WS, Hill JA and Olson EN. Dysregulation of microRNAs after myocardial infarction reveals a role of miR-29 in cardiac fibrosis. *Proceedings of the National Academy of Sciences of the United States of America*. 2008;105:13027-13032.

16. Thum T, Galuppo P, Kneitz S, Fiedler J, Wolf C, Van Laake L, Mummery CL, Engelhardt S, Ertl G and Bauersachs J. MicroRNAs in the human heart: a clue to fetal gene reprogramming in heart failure. *European Heart Journal*. 2007;28:258-267.

17. Luo X, Lin H, Pan Z, Xiao J, Zhang Y, Lu Y, Yang B and Wang Z. Down-regulation of miR-1/miR-133 contributes to re-expression of pacemaker channel genes HCN2 and HCN4 in hypertrophic heart. *Journal of Biological Chemistry*. 2008;283:20045-20052.

18. Xiao J, Yang B, Lin H, Lu Y, Luo X and Wang Z. Novel approaches for gene-specific interference via manipulating actions of microRNAs: Examination on the pacemaker channel genes HCN2 and HCN4 (Retraction of 212, pg 285, 2007). *Journal of Cellular Physiology*. 2012;227:285-292.

19. Kim GH. MicroRNA regulation of cardiac conduction and arrhythmias. *Translational Research*. 2013;161:381-392.

20. Wiese C, Grieskamp T, Airik R, Mommersteeg MTM, Gardiwal A, de Gier-de Vries C, Schuster-Gossler K, Moorman AFM, Kispert A and Christoffels VM. Formation of the sinus node head and differentiation of sinus node myocardium are independently regulated by Tbx18 and Tbx3. *Circulation Research*. 2009;104:388-397.

21. Small EM, O'Rourke JR, Moresi V, Sutherland LB, McAnally J, Gerard RD, Richardson JA and Olson EN. Regulation of PI3-kinase/Akt signaling by muscle-enriched microRNA-486. *Proceedings of the National Academy of Sciences of the United States of America*. 2010;107:4218-4223.

22. Alexander MS, Casar JC, Motohashi N, Myers JA, Eisenberg I, Gonzalez RT, Estrella EA, Kang PB, Kawahara G and Kunkel LM. Regulation of DMD pathology by an ankyrin-encoded miRNA. *Skeletal Muscle*. 2011;1-27.

23. Glass DJ. PI3 kinase regulation of skeletal muscle hypertrophy and atrophy. *Phosphoinositide 3-Kinase in Health and Disease, Vol 1*. 2010;346:267-278.

24. Larsson CA, Daka B, Gullberg B, Rastam L and Lindblad U. Clusters of AMI risk factors and their association with left ventricular hypertrophy: A population-based study within the Skaraborg project, Sweden. *International Journal of Cardiology*. 2013;168:5416-5421.

25. Hsu A, Chen SJ, Chang YS, Chen HC and Chu PH. Systemic approach to identify serum microRNAs as potential biomarkers for acute myocardial infarction. *Biomed Research International*. 2014.

26. Seropian IM, Abbate A, Toldo S, Harrington J, Smithson L, Ockaili R, Mezzaroma E, Damilano F, Hirsch E and Van Tassell BW. Pharmacologic inhibition of phosphoinositide 3-kinase gamma (PI3K gamma) promotes infarct resorption and prevents adverse cardiac remodeling after myocardial infarction in mice. *Journal of Cardiovascular Pharmacology*. 2010;56:651-658.

27. Weber K, Rostert N, Bauersachs S and Wess G. Serum microRNA profiles in cats with hypertrophic cardiomyopathy. *Molecular and Cellular Biochemistry*. 2015;402:171-180.

28. D'Souza A, Pearman CM, Wang YW, Nakao S, Logantha S, Cox C, Bennett H, Zhang Y, Johnsen AB, Linscheid N, Poulsen PC, Elliott J, Coulson J, McPhee J, Robertson A, Martins PAD, Kitmitto A, Wisloff U, Cartwright EJ, Monfredi O, Lundby A, Dobrzynski H, Oceandy D, Morris GM and Boyett MR. Targeting miR-423-5p reverses exercise training-induced HCN4 channel remodeling and sinus bradycardia. *Circulation Research*. 2017;121:1058-1568.

29. Zhang CX, Cheng YH, Yang J, Dean DB, Liu XJ and Chen H. microRNAs are aberrantly expressed in hypertrophic heart: do they play a role in cardiac hypertrophy? *Faseb Journal*. 2007;21:129-129.

30. Raut SK, Kumar A, Singh GB, Nahar U, Sharma V, Mittal A, Sharma R and Khullar M. MiR-30c mediates upregulation of Cdc42 and Pak1 in diabetic cardiomyopathy. *Cardiovascular Therapeutics*. 2015;33:89-97.

31. Bidzhekov K, Gan L, Denecke B, Rostalsky A, Hristov M, Koeppel TA, Zernecke A and Weber C. microRNA expression signatures and parallels between monocyte subsets and atherosclerotic plaque in humans. *Thrombosis and Haemostasis*. 2012;107:619-625.

32. Casas-Agustench P, Iglesias-Gutierrez E and Davalos A. Mother's nutritional miRNA legacy: nutrition during pregnancy and its possible implications to develop cardiometabolic disease in later life. *Pharmacological Research*. 2015;100:322-334.

33. Reddy MA, Jin W, Villeneuve L, Wang M, Lanting L, Todorov I, Kato M and Natarajan R. Pro-inflammatory role of microRNA-200 in vascular smooth muscle cells from diabetic mice. *Arteriosclerosis Thrombosis and Vascular Biology*. 2012;32:721-446.

34. Cakmak HA, Barman HA, Coskunpinar E, Oltulu YM, Ikitimur B, Can G, Ozcan S and Vural VA. The diagnostic importance of microRNAs in congestive heart failure. *Journal of the American College of Cardiology*. 2013;62:17-18.

35. Li CF, Li YC, Jin JP, Yan ZK and Li DD. miR-938 promotes colorectal cancer cell proliferation via targeting tumor suppressor PHLPP2. *European Journal of Pharmacology*. 2017;807:168-173.

36. Wu YH, Jia ZF, Cao DH, Wang C, Wu X, You LL, Wen SM, Pan YC, Cao XY and Jiang J. Predictive value of miR-219-1, miR-938, miR-34b/c, and miR-218 polymorphisms for gastric cancer susceptibility and prognosis. *Disease Markers*. 2017.

37. Cao Z, Feng MY, Yang G and Zhang TP. Plasma miRNAs effectively distinguish patients with pancreatic cancer from controls: a multicenter study. *Journal of the American College of Surgeons*. 2017;225:1173-1179.

38. Divakaran V and Mann DL. The emerging role of microRNAs in cardiac remodeling and heart failure. *Circulation Research*. 2008;103:1072-1083.

39. Fang Y, Shi CZ, Manduchi E, Civelek M and Davies PF. MicroRNA-10a regulation of proinflammatory phenotype in athero-susceptible endothelium *in vivo* and *in vitro*. *Proceedings of the National Academy of Sciences of the United States of America*. 2010;107:13450-13455.

40. Zou YH, Liu WT, Zhang JX and Xiang DC. miR-153 regulates apoptosis and autophagy of cardiomyocytes by targeting Mcl-1. *Molecular Medicine Reports*. 2016;14:1033-1039.

41. Hoekstra M, van der Lans CAC, Halvorsen B, Gullestad L, Kuiper J, Aukrust P, van Berkel TJC and Biessen EAL. The peripheral blood mononuclear cell microRNA signature of coronary artery disease. *Biochemical and Biophysical Research Communications*. 2010;394:792-797.

42. Huang J, Zhao L, Xing LP and Chen D. MicroRNA-204 Regulates Runx2 protein expression and mesenchymal progenitor cell differentiation. *Stem Cells*. 2010;28:357-364.

43. Cui RR, Li SJ, Liu LJ, Yi L, Liang QH, Zhu X, Liu GY, Liu Y, Wu SS, Liao XB, Yuan LQ, Mao DA and Liao EY. MicroRNA-204 regulates vascular smooth

muscle cell calcification in vitro and in vivo. *Cardiovascular Research*. 2012;96:320-329.

44. Zhang H, Liu LM, Hu JG and Song L. MicroRNA regulatory network revealing the mechanism of inflammation in atrial fibrillation. *Medical Science Monitor*. 2015;21:3505-3513.

45. Dinami R, Buemi V, Sestito R, Zappone A, Ciani Y, Mano M, Petti E, Sacconi A, Blandino G, Giacca M, Piazza S, Benetti R and Schoeftner S. Epigenetic silencing of miR-296 and miR-512 ensures hTERT dependent apoptosis protection and telomere maintenance in basal-type breast cancer cells. *Oncotarget*. 2017;8:95674-95691.

46. Li J, Lei H, Xu Y and Tao ZZ. miR-512-5p suppresses tumor growth by targeting htert in telomerase positive head and neck squamous cell carcinoma in vitro and in vivo. *Plos One*. 2015;10.

47. Li XD, Yang YJ, Wang LY, Qiao SB, Lu XF, Wu YJ, Xu B, Li HF and Gu DF. Plasma miR-122 and miR-3149 potentially novel biomarkers for acute coronary syndrome. *Plos One*. 2015;10.

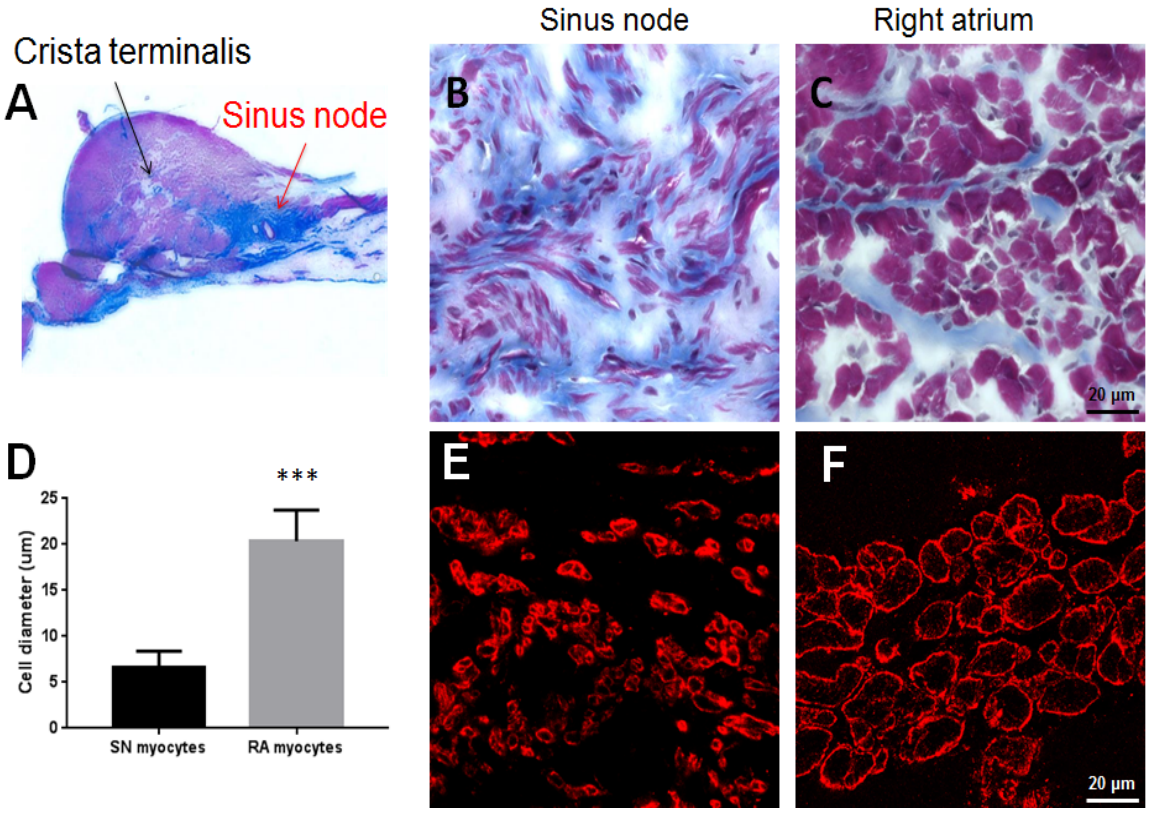

Figure 1. Morphology of the human SN in comparison to the RA. Tissue sections were stained with Masson's trichrome to differentiate between myocytes (in purple) and connective tissue (in blue). A. Representative image of tissue section (at low magnification) though the SN and the surrounding RA myocardium. B and C. Representative higher magnification images of the SN and RA. D, cell diameter measured using AxioVision software (n=36 SN and n=30 RA myocytes); $p<0.005$, student's t-test (GraphPad Prism software); error bars are presented as standard error. E and F. Representative images showing expression of caveolin3 protein (red signal) in tissue sections adjacent to those in B and C. Similar observation was obtained from n = 4 SN and 4 RA.

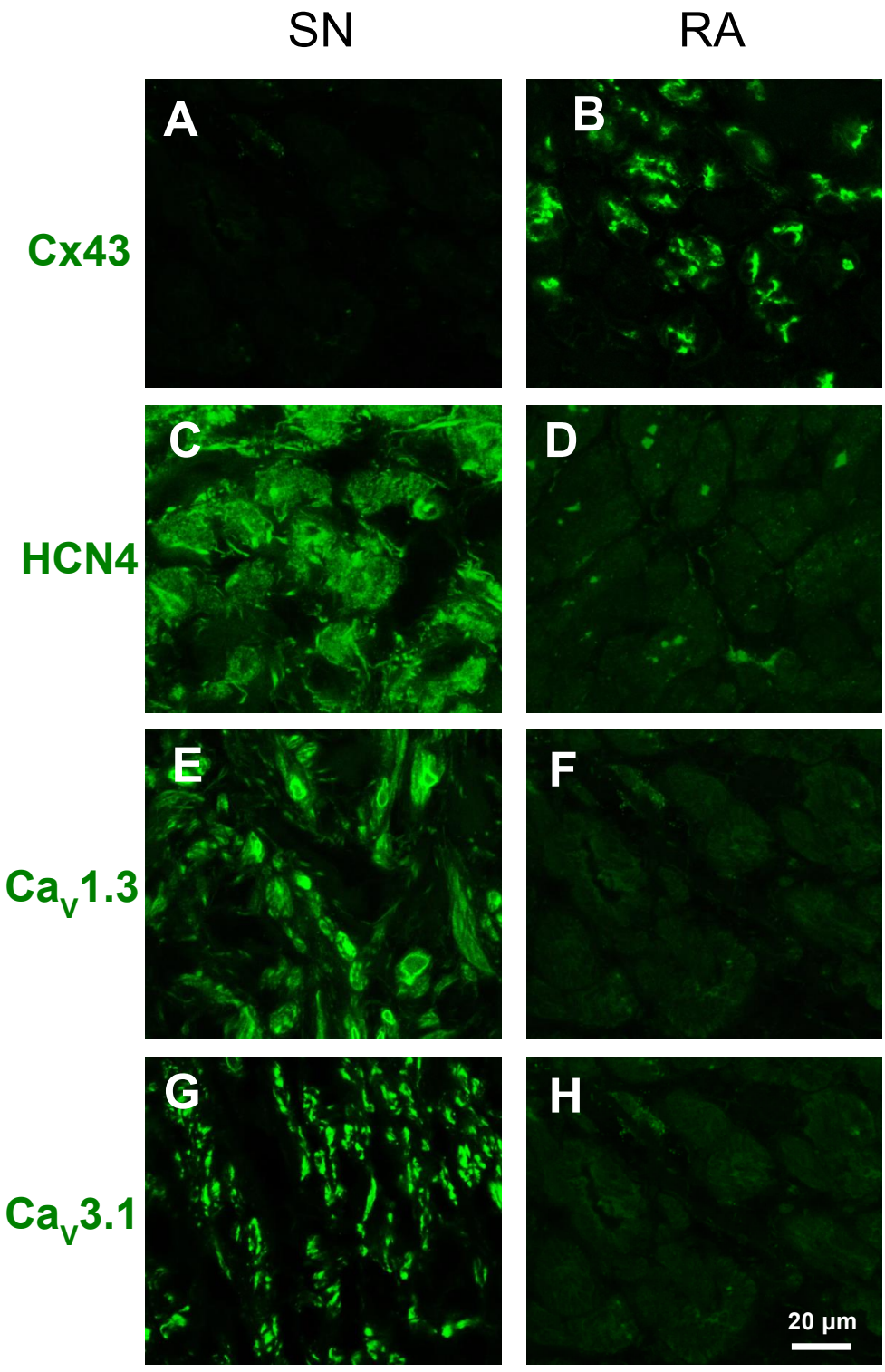

Figure 2. Representative immunoconfocal images of key proteins expression in the SN compared to the RA. A and B Cx43 expression (green signal). C and D HCN4 expression (green signal). E and F $Ca_V1.3$ expression (green signal). G and H $Ca_V3.1$ expression (green signal). Similar observation was obtained from n = 4 SN and 4 RA.

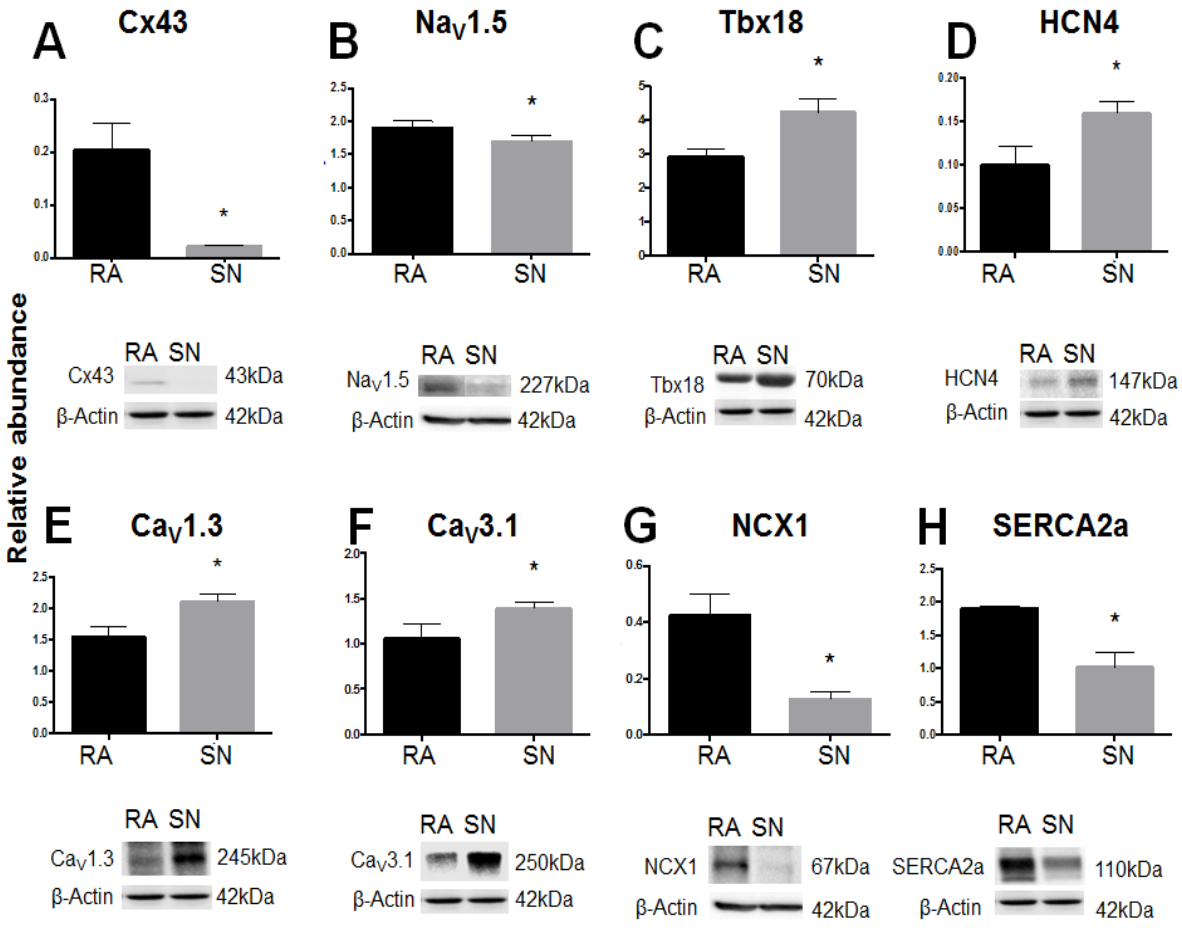

Figure 3. Key proteins expression in the SN compared to RA. Western blot was performed using biopsies from n=4 human SN and n=4 RA. A. Cx43 expression. B. $Na_V1.5$ expression. C. Tbx18 expression. D. HCN4 expression. E. $Ca_V1.3$ expression. F. $Ca_V3.1$ expression. G. NCX1 expression. H. SERCA2a expression. Membranes were stained with primary antibodies (Table S2). Representative bands for each protein are shown under each graph to visualise the difference in the expression of the proteins in the SN and RA. Signal intensity of each protein investigated was quantified using Image lab Bio-Rad software against the expression of β-Actin. Data was analysed and plotted using GraphPad Prism 7. Student's t-test was used for statistical calculations, error bars are presented as standard error, $p<0.05$.

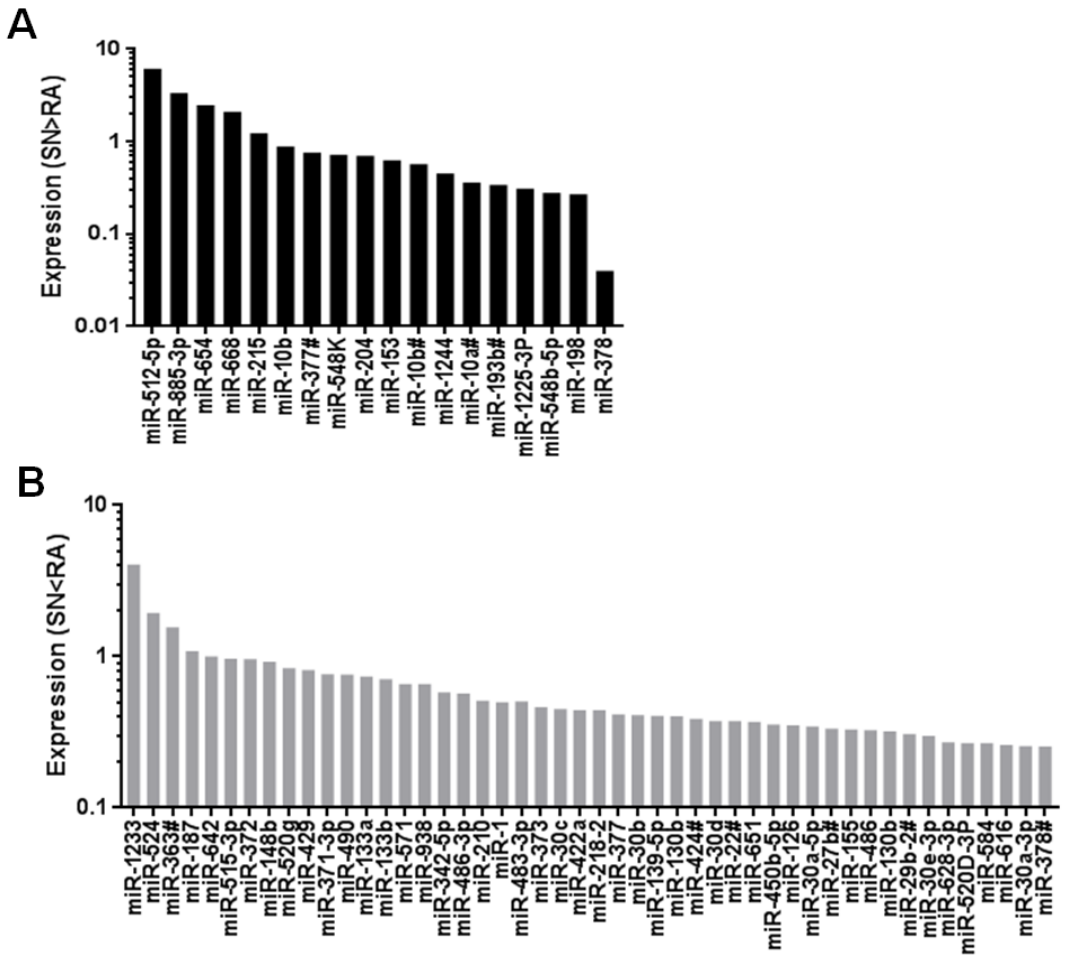

Figure 4. MicroRNAs significantly less or more expressed in the SN in comparison to RA. A. 18 microRNAs that are significantly higher in the human SN compared to RA. B. 48 microRNAs that are significantly lower in the human SN compared to RA, n=7 SN and n=7 RA. RQ manager (Applied Biosystems) and RealTime StatMiner were used to calculate the expression level of microRNAs against RNU44, U6 snRNA and RNU48 housekeepers. The statistical significance was confirmed using Benjamini-Hochberg statistical test, and plots were created using GraphPad Prism 7, $p<0.05$.

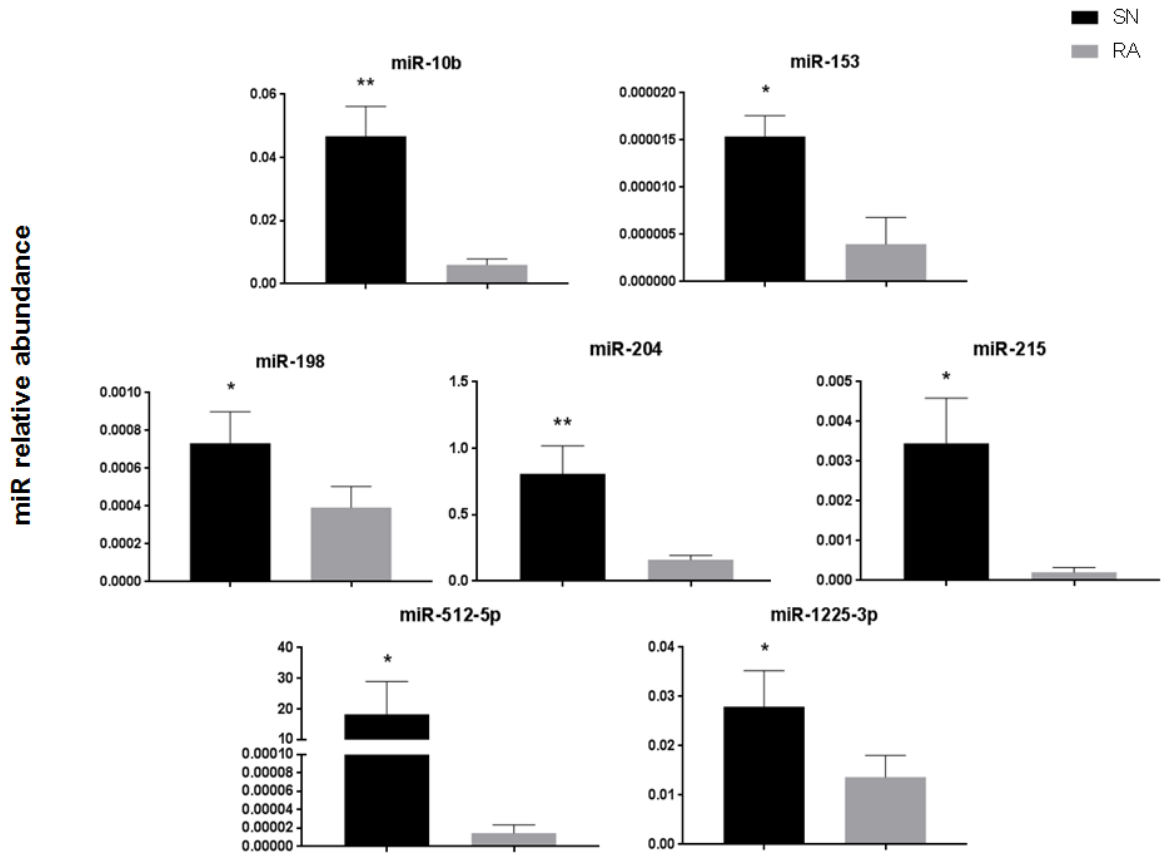

Figure 5. Selected microRNAs from Figure 4 that are enriched in the SN in comparison to the RA, and are predicted to inhibit the expression of physiologically relevant pacemaker gene targets summarised in Table 1. Data is presented as relative abundance of the microRNAs against housekeepers and error bars represent standard error. Data was calculated using RealTime StatMiner and paired student's t-test was used for statistical analysis, n=7 SA and n=7 RA, $p<0.05$.

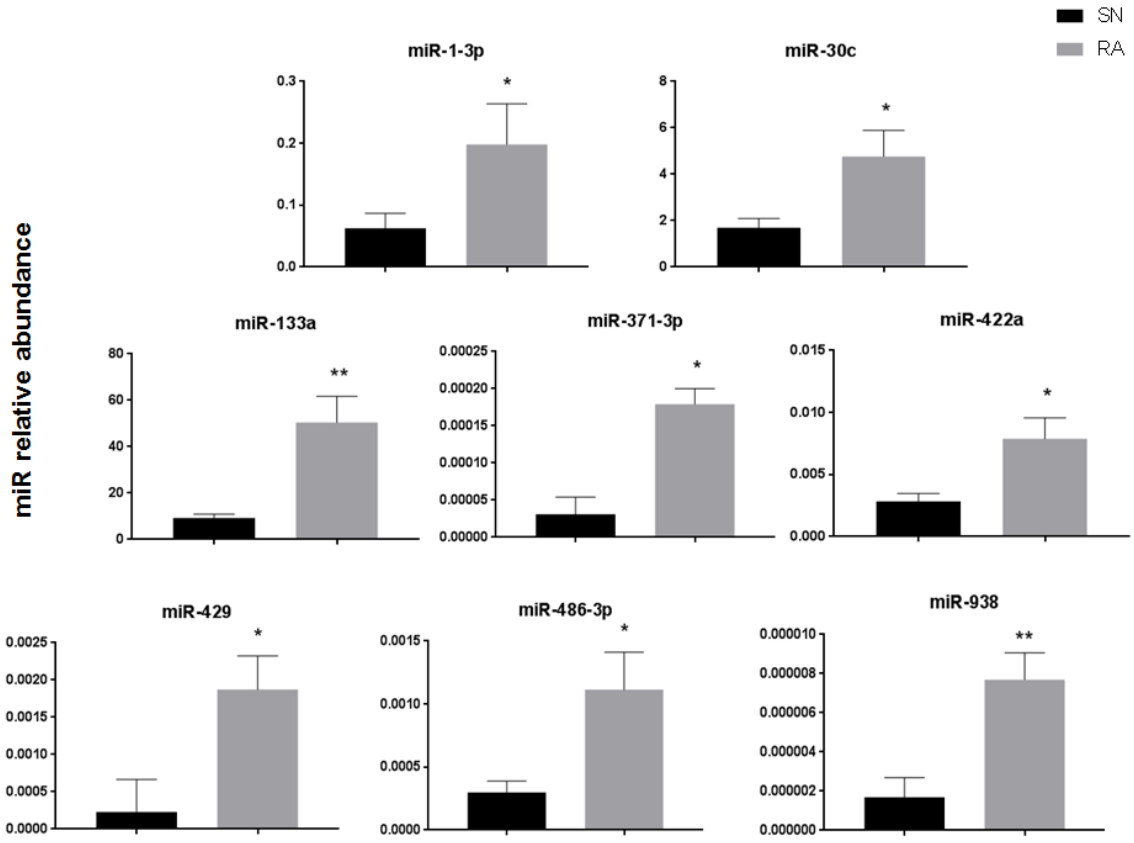

Figure 6. MicroRNAs less expressed in the SN compared to the RA that are predicted to inhibit the expression of physiologically relevant pacemaker gene targets summarised in Table 1. Data is presented as relative abundance of the microRNAs against housekeepers and error bars represent standard error. Data was calculated via RealTime StatMiner and paired student's t-test was used for statistical analysis, n=7 SN and n=7 RA, $p<0.05$.

miR expression in SN vs RA	Protein name of predicted target important in pacemaking mechanisms	Gene name of predicted target	Protein tissue expression based on current and Chandler et al., 2009 studies SNvsRA	Total no of binding sites for each micrRNA on predicted target P<0.05 and P>0.05
hsa-miR-1-3p	TBX3	TBX3	↑	1
	HCN1	HCN1	↑	1
	HCN4	HCN4	↑	1
hsa-miR-10b-5p	Cx40	GJA5	↓	1
hsa-miR-30c-5p	$Ca_V1.3$	CACNA1D	↑	1
	HCN1	HCN1	↑	1
	HCN4	HCN4	↑	1
hsa-miR-133a-3p	HCN4	HCN4	↑	5
hsa-miR-153-3p	$Ca_V1.2$	CACNA1C	↓	1
	RYR2	RYR2	↓	2
	$Na_V1.5$	SCN5A	↓	1
hsa-miR-198	$Ca_V1.2$	CACNA1C	↓	2
	ERG	KCNH2	↓	7
	RYR2	RYR2	↓	1
hsa-miR-204-5p	$Ca_V1.2$	CACNA1C	↓	1
has-miR-215-5p	$K_V1.4$	KCNA4	↓	1
hsa-miR-371-3p	$Ca_V1.3$	CACNA1D	↑	1
	Cx45	GJC1	↑	5
hsa-miR-422a	TBX3	TBX3	↑	1
hsa-miR-429	TBX18	TBX18	↑	1
hsa-miR-486-3p	$Ca_V1.3$	CACNA1D	↑	6
	$Ca_V3.1$	CACNA1G	↑	1
	HCN4	HCN4	↑	7
	HCN1	HCN1	↑	6
hsa-miR-512-5p	Cx43	GJA1	↓	1
hsa-miR-938	$Ca_V1.3$	CACNA1D	↑	9
hsa-miR-1225-3p	$Na_V1.5$	SCN5A	↓	2

Table 1. Summary of the microRNA expression data of this study combined with mRNA data from Chandler et al., 2009 and prediction of interactions. In blue are those that are less expressed in the SN compared to RA. In red are those that are more expressed in the SN compared to RA. TargetScan Human and/or TarBase software was used for source of prediction of target mRNA. RNA22v2 software was used to predict the number of binding sites.

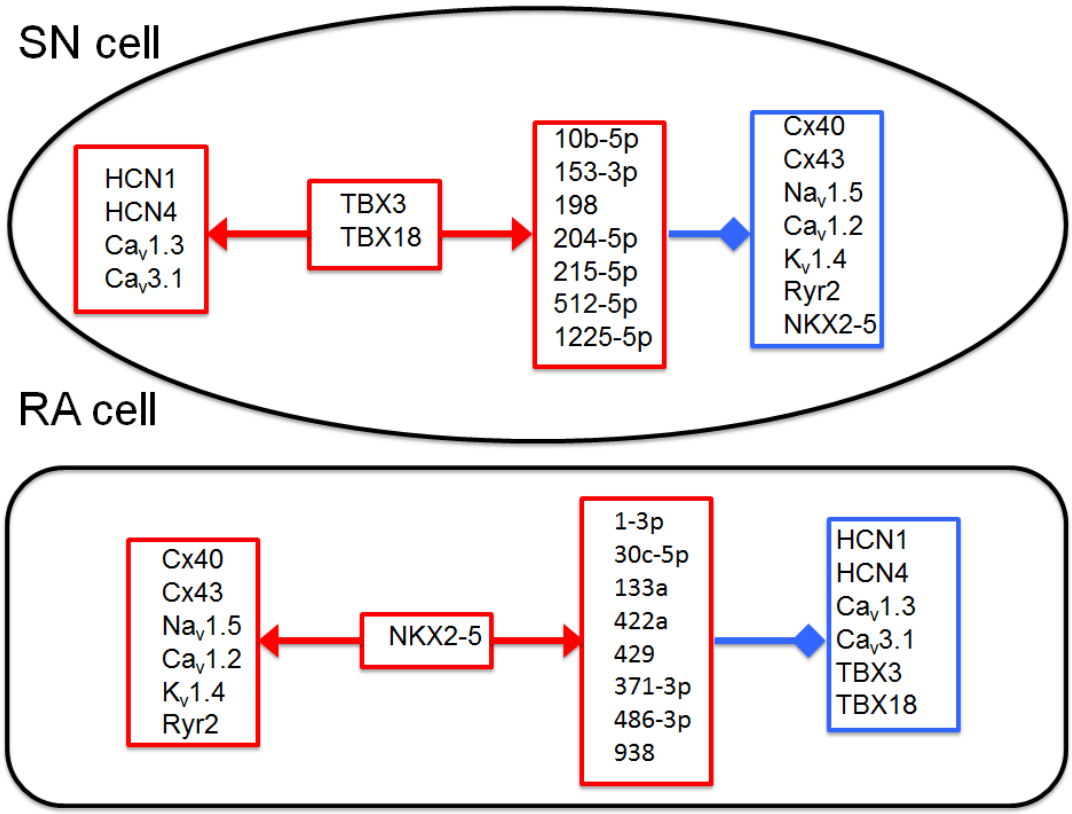

Figure 8. Proposed simplified gene regulatory feedback loop mechanisms based on the current study and Chandler et al., 2009. In the sinus node (SN) high expression of Tbx3 and Tbx18 (transcription factors, TFs - in red) enhances expression of pacemaker channels HCN1, HCN4, $Ca_V1.3$, and $Ca_V3.1$ – in red, and enhances expression of miRs-153-3p, 204-5p, 1225-5p, 512-5p, 2015-5p, and 10b-5p - in red. In the RA, higher expression of TFs Nkx2-5 – in red enhances the expression of gap junction channels Cx40 and Cx43, ion channels $Na_V1.5$, $Ca_V1.2$, $K_V1.4$, and RyR2, in red as well as miRs-422a, 429, and 486-3p – in red. In the SN, higher expression of miRs-153-3p, 204-5p, 1225-5p, 512-5p, 215-5p, and 10b-5p (in red) inhibits expression of Nkx2-5, Cx40, Cx43, $Na_V1.5$, $Ca_V1.2$, $K_V1.4$, and RyR2 (in blue). In the RA, higher expression of miRs-422a, 429, and 486-3p (in red) inhibits the expression of HCN1, HCN4, $Ca_V1.3$, and $Ca_V3.1$ and inhibits the expression of Tbx3 and Tbx18 (in blue). Therefore, positive and negative loop mechanisms are created.

3.3 Data supplement

DATA SUPPLEMENT

Identification of key small non-coding microRNA controlling the pacemaker mechanisms in the human sinus node

M. Petkova, J. Yanni, N. Li, F. A. D'Souza, Y. Zhang, A. Atkinson, B. Borbas, F. Jafarzadeh, C. Geraghty, L. Stuart, D. Oceandy, F. Perde, P. Molenaar, V. Fedorov, H. Dobrzynski

Methods

Details of human specimens

Nine human sinus node (SN) with surrounding right atrium (RA) tissue blocks were obtained, dissected and frozen by collaborators in Australia (PM) and Romania (FP) under their local ethical approval procedures as previously described by (Chandler et al., 2011; Chandler et al., 2009; Perde et al., 2016; Stephenson et al., 2017). Specimens were shipped to HD's laboratory on dry ice and were stored at -80^{o}C under the Human Tissue Act. Detailed information about the gender, age, and cause of death of people the specimens were obtained from can be found in Table S1. These specimens were used for techniques described below.

Histology

Histology was carried out on 10-30 μm thin tissue sections, which were cut from a part of each specimen listed in Table S1 using a Zeiss cryostat. Sections were mounted onto

SuperFrost Plus glass slides (VWR) and kept at and the remaining tissue blocks to be used for other experiments described below were also kept at -80^{o}C. Masson's trichrome staining was performed in order to identify the location of the SN within each specimen and to characterise the morphology of the SN and the surrounding atrial muscle as previously described by (Chandler et al., 2009; Stephenson et al., 2017).

Masson's trichrome staining was performed by fixing the sections overnight at room temperature in Bouin's solution ((1.2% (w/v) aqueous picric acid, 40% (w/v) formalin, formaldehyde and glacial acetic acid (Sigma)). Sections were rehydrated in 70% alcohol for 10 minutes and stained with Celestine blue for 5 minutes and washed in tap water for 10 minutes. They were next stained with Cole's alum haematoxylin for 10 minutes and washed for 15 minutes in tap water. Staining continued with acid fuschin for 5 minutes, followed by washing for 30 minutes in tap water. Sections were then stained with phospholimbic acid for 5 minutes, drained and then placed in methyl green for 1 minute and washed for 20 minutes in tap water. Sections were dehydrated by emersion in graded series of alcohol as follows: 70% alcohol (1 minute), 90% alcohol (1 minute), 100% alcohol (2 minutes), and 100% alcohol (2 minutes). Finally, sections were placed in two histoclear solutions for 5 minutes and mounted with DPX (Thermo Fischer) and covered with glass coverslips. Histological sections were visualised with a light microscope (Zeiss LSM5) and Axiocam camera (Zeiss) and collected with Axiovision software (Zeiss).

Immunohistochemistry

Immunohistochemistry experiments were performed on sections neighbouring those used for histological verification of the microanatomy of each preparations described above. (Chandler et al., 2009) described this technique previously. Tissue sections were fixed in 10% neutral buffer formalin (Sigma) for 30 minutes and washed three times for 10 minutes

in 0.01 M phosphate buffered saline (PBS, Sigma). Tissue sections were then treated with 0.1% Triton X-100 for 30 minutes, washed 3 times for 10 minutes in PBS and then blocked with 1% bovine serum albumin (BSA, Sigma) in PBS for 1 hour at room temperature. Sections were then incubated overnight at room temperature with primary antibodies. The antibodies used in immunohistochemical experiments are listed in Table S2 and were diluted in 1% BSA in PBS. The following day, secondary antibodies conjugated to fluorescence markers were applied to tissue sections for 2 hours at room temperature; they were diluted 1:100 in 1% BSA in PBS. Sections were washed three times in PBS after incubation with the primary and secondary antibodies. Finally, sections were mounted with glass coverslips and mounting medium Vectashield (Vector laboratories) and sealed with nail varnish. Immunofluorescence was detected by confocal microscopy (Zeiss LSM5, Carl Zeiss Microscopy) and images were taken with Pascal software (Zeiss Microscopy).

Western blot

After identification of the location of the SN in each human tissue block by histology and immunohistochemistry, lysate was obtained by homogenising snap frozen small biopsies from the SN and RA (as described by (Li et al., 2015)) from four human subjects (Table S1). Western blot technique used in this study was recently described by (D'Souza et al., 2017). The samples were prepared by using MP FastPrep-24 5^{G} and 2 ml tubes containing FastPrep metal bead lysing matrix (1.4 mm) in 200 µl RIPA buffer (Sigma). The samples were centrifuged at 4°C for 5 minutes at 3000 rpm. The supernatant formed at the top was discarded. Total protein concentration in each sample was measured by using Bradford protein assay against a bovine serum albumin (BSA 0-0.05 mg/ml) standard curve. Laemmli buffer (25% SDS-sample buffer – 100 mM Tris-HCl, pH 6.8, 25% (v/v) glycerol, 10% (v/v) SDS, 10% (v/v) β-mercaptoethanol, 0.1% (w/v) bromophenol blue) was added

to the samples to a final protein concentration of 1 μg/μl and the aliquots were stored at -80°C.

Prior to loading the samples on the gel, they were heated to 90°C for 5 minutes in order to completely denaturate the protein content. Samples were loaded onto a 6-9% stain-free SDS-polyacrylamide gel (Bio-Rad) with Precision Plus (Bio-Rad) protein standards and run at 90 mV for 2 hours in SDS running buffer (25 mM Tris, 192 mM glycine, 0.1% SDS). Stain-free gels were imaged by ChemiDoc MP system and transferred to PVDF (polyvinyl difluoride) membranes via Trans-Blot Turbo transfer system (Bio-Rad) at 1.3 A constant and 25 V for 30 minutes in semi-dry transfer buffer at room temperature. Prior to protein transfer PVDF membranes were activated in 100% ethanol.

PVDF membranes were washed with TBST (0.1% (v/v) Tween 20 in PBS) for 5 minutes and blocked in 3% (w/v) BSA in TBST at room temperature for 1 hour with gentle rocking. Membranes were then incubated with the primary antibodies (Table S2) overnight at 4°C with gentle rocking. Membranes were then washed 3 times for 10 minutes in TBST and incubated in HRP-conjugated secondary antibody (1:1000) for 2 hours at room temperature with gentle rocking. Membranes were then washed 3 times for 10 minutes in TBST to remove excessive amounts of non-specific secondary antibody binding. Membranes were then visualised with Clarity Western ECL chemiluminescent reagent (Bio-Rad) and Bio-Rad ChemiDoc MP system. The chemiluminescent intensity of the signal was quantified (Image lab Bio-Rad) by normalising it to the corresponding intensity of β-actin and statistical analysis between SN and RA samples was calculated according to student's t-test and $p<0.05$ values were assumed as significant.

RNA isolation

After identification of the location of the SN in each human tissue block by histology, immunohistochemistry, and western blotting described above, total RNA was isolated from small biopsies taken around the sinus node artery for each sinus node and the right atrial pectinate muscle (located further away from then SN) and were flash frozen in liquid nitrogen using mirVana miRNA Isolation Kit (Applied Biosystems) with phenol (Life Technologies) according to the manufacturer's instructions and as described recently by (D'Souza et al., 2017). The tissue biopsies from the SN and RA were homogenised with Ika T10 homogeniser (Ika Werke) for 1 minute. RNA was treated with DNase (Ambion). RNA purity (260/280), concentration, and RNA integrity number (RIN) were measured using Agilent 2100 Bioanalyzer. Quality and quantity of RNA extracted from each specimen can be found in Table S1.

Reverse transcription to cDNA, preamplification and qPCR for microRNAs

254 ng RNA from each sample were reverse-transcribed to cDNA with SuperScript® VILO cDNA Synthesis Kit (ThermoFischer Scientific) in 20 µl reaction mixture. The cDNA samples were run on qPCR Veriti 96 well thermal cycler (Life Technologies) in accordance with the manufacturer's recommended protocol.

185 ng RNA from each sample were reverse-transcribed using TaqMan® microRNA Reverse Transcription Kit (Cat. N°4366597). The product of this reaction (2.5 µl) was preamplified with Megaplex PreAmp Primers. The primers were divided into pool A and B, each pool containing 380 stem-looped reverse transcription primers and TaqMan PreAmp Master Mix (Applied Biosystems) in a 25 µl PCR reaction. The preamplification cycles were run as follows: 95°C (10 minutes), 55°C (2 minutes), and 75°C (2 minutes)

followed by 12 cycles of 95°C (15 seconds) and 60° (4 minutes) each. The cDNA products for each sample were diluted to 100 µl with 0.1x TE (pH = 8.0). 10 µl of the diluted cDNA were analysed on a TaqMan® Array Card run on a 7900HT Fast Real-Time PCR System. qPCR was performed using TaqMan Array Human MicroRNA A+B Cards Set v3.0 (ThermoFischer Scientific). The cards A+B contained 384 TaqMan MicroRNA Assay each, giving a total of 754 human microRNAs. Each card contained three TaqMan MicroRNA Assay endogenous controls (U6 snRNA, RNU44, and RNU48). The acquired data were analysed using RQ Manager (Applied Biosystems) and RealTime StatMiner (Integromics). RQ Manager was used to obtain the average threshold cycle (Ct) values. Ct values were calculated via an automatic baseline setting and a threshold of 0.2. Ct values <36 were considered under the detection level of the assay, therefore microRNAs with a Ct value ≥36 were considered as significantly expressed.

RealTime StatMiner was used to analyse the data further. Data were calculated $2^{-\Delta Ct}$, where ΔCt is $\Delta Ct_{(Target)}$-$\Delta Ct_{(Housekeeper)}$. GeNorm stability score method assessed the suitability of the housekeepers for the analysis of cards A and B on the basis of similar expression in SN and RA. Both cards were analysed by the formula $E^{-\Delta Ct}$. Based on the GeNorm score results, housekeepers RNU44 and RNU48 were selected to analyse card A, whilst card B used RNU44 and U6 snRNA. Card A was analysed via housekeepers RNU44 and RNU48, whereas card B – RNU44 and U6 snRNA as RealTime StatMiner software calculates if the expression level of the housekeeper genes amongst the samples is similar and decides on the best housekeepers for the samples. Statistical analysis of the expression levels was performed using Benjamini-Hochberg test and $p<0.05$ values were assumed as significant; graphs were plotted using GraphPad Prism 7. 66 statistically significant microRNAs were identified to be differentially expressed in the SN vs. RA, and are listed in Table S3 and

plotted in Figure 3.

Bioinformatics

66 microRNAs listed in Table 1 were then married with the mRNA data for the SN and RA from Chandler et al., 2009 and the analysis of these data sets was performed with Ingenuity Pathway Analysis (IPA; Ingenuity Systems) to identify which out of 66 of these microRNAs target those mRNA molecules that are involved in pacemaker mechanisms; the so called the membrane clock (targeting ion channels) and Ca^{2+} clock (targeting Ca^{2+} handling proteins) as well as gap junctional channels (connexins; responsible for electrical coupling between heart cells). IPA was used to visualise microRNA-mRNA interactions and relationships. IPA uses data from TarBase database, miRecords (http://mirecords.biolead.org/), TargetScan (http://www.targetscan.org/), and rna22 (https://cm.jefferson.edu/rna22/) were used in order to predict if any of these 66 microRNAs of interest are targeting mRNAs on the basis of conserved 8mer (≥0.8 conserved branch length) and 7mer sites that match the seed region of each microRNA. With the help of bioinformatics, 15 microRNAs were identified to target mRNAs that are key molecules to be involved in the pacemaker mechanisms and the summary of these data are shown in Table 1 and Figures 4-6.

Specimen number	Age of patient	Gender	Cause of death	RNA Amount (ng/µl) SN/RA	RNA Quality (RIN number) SN/RA
1	29	M	Road accident	100.60/231.90	6.1/7.6
2	22	F	Road accident	30.98/301.40	8.0/7.7
3	66	M	Suicide	47.48/285.70	5.2/4.7
4	19	M	Suicide	114.11/389.00	6.4/7.2
5	60	M	Sudden death	25.4/123.25	7.2/6.5
6	54	M	Intracranial haemorrhage	164.67/400.00	8.3/8.8
7	42	M	Subarrachnoid haemorrhage	173.65/423.00	8.5/9.1

Table S1. Specimens' information. Patients 1, 2 and 4 (as result of road traffic accident) died due to polytrauma, 3 died of asphyxia.

Primary antibody	Company	Cat. #	Source	Dilution
Cx43	Millipore	MAB3068	Mono- Ms	1:200 (WB) 1:50 (IF)
$Na_v1.5$	Alomone Lab	ASC-005	Poly-Rbt	1:50 (WB)
Tbx18	Sigma	HPA029014	Poly-Rbt	1:50 (WB)
HCN4	Alomone Lab	APC-052	Poly-Rbt	1:50 (WB, IF)
$Ca_v1.3$	Alomone Lab	ACC-005	Poly-Rbt	1:50 (WB, IF)
$Ca_v3.1$	Alomone Lab	ACC-021	Poly-Rbt	1:50 (WB, IF)
SERCA2a	Thermo Fisher	MA3-910	Poly-Rbt	1:100 (WB, IF)
NCX1	Thermo Fisher	C2C12	Mono- Ms	1:50 (WB, IF)
Cavolin3	Transduction	610421	Poly-Ms	1:200 (WB) 1:50 (IF)
β-Actin	Sigma	A5441	Mono-Ms	1:200 (WB)

Table S2. Summary of antibodies for immunofluorescence experiments on gap junctions, ion channels, Ca^{2+}-handling proteins, transcription factors and structural proteins using formalin fixed fresh frozen tissue sections.

miR	SN mean	SN SEM	RA mean	RA SEM	Fold change	Log fold change	P value
hsa-miR-1-3p	6.00E-02	3.00E-02	2.00E-01	8.00E-02	-1.40E-01	-5.00E-01	3.00E-02
hsa-miR-10a-5p	**1.00E-04**	**2.00E-05**	**3.00E-05**	**1.00E-05**	**3.50E-05**	**3.60E-01**	**5.00E-02**
hsa-miR-10b-5p	**5.00E-02**	**2.00E-03**	**1.00E-02**	**1.00E-03**	**4.00E-02**	**8.90E-01**	**1.00E-03**
hsa-miR-10b-3p	**1.00E-02**	**1.00E-02**	**2.00E-03**	**2.00E-03**	**5.34E-03**	**5.70E-01**	**1.00E-02**
hsa-miR-126-3p	3.41E+00	8.90E-01	7.65E+00	1.31E+00	-4.24E+00	-3.50E-01	4.00E-02
hsa-miR-130b-3p	2.00E-03	1.00E-03	1.00E-02	1.00E-03	-3.00E-03	-4.00E-01	5.00E-02
hsa-miR-130b-5p	3.00E-03	4.00E-04	1.00E-02	1.00E-03	-3.00E-03	-3.20E-01	2.00E-02
hsa-miR-133a-3p	9.25E+00	1.77E+00	5.05E+01	1.13E+01	-4.12E+01	-7.40E-01	1.00E-03
hsa-miR-133b	3.00E-02	8.00E-03	1.62E-01	6.20E-02	-1.30E-01	-7.10E-01	5.36E-02
hsa-miR-139-5p	1.70E-01	3.00E-02	4.40E-01	6.00E-02	-2.70E-01	-4.10E-01	9.00E-03
hsa-miR-148b-3p	3.00E-03	1.00E-03	2.00E-02	1.00E-02	-2.00E-02	-8.90E-01	4.00E-02
hsa-miR-153-3p	**2.00E-05**	**1.00E-05**	**4.00E-06**	**3.00E-06**	**1.00E-05**	**5.90E-01**	**5.00E-02**
hsa-miR-155-5p	2.00E-02	1.00E-02	4.00E-02	6.00E-03	-2.00E-02	-3.10E-01	5.00E-02
hsa-miR-187-3p	3.00E-03	1.00E-03	4.00E-02	1.00E-02	-4.00E-02	-1.09E+00	1.00E-03
hsa-miR-193b-3p	**2.00E-03**	**4.00E-04**	**1.00E-03**	**2.00E-04**	**1.00E-03**	**3.40E-01**	**2.00E-02**
hsa-miR-198	**1.00E-03**	**3.00E-04**	**4.00E-04**	**3.00E-04**	**3.00E-04**	**2.70E-01**	**4.00E-02**
hsa-miR-204-5p	**8.10E-01**	**2.10E-01**	**1.60E-01**	**3.00E-02**	**6.50E-01**	**7.00E-01**	**2.00E-03**
hsa-miR-210-3p	4.00E-02	1.00E-02	1.30E-01	3.00E-02	-9.00E-02	-5.10E-01	1.00E-02
hsa-miR-215-5p	**3.00E-03**	**1.00E-03**	**2.00E-04**	**1.00E-04**	**3.00E-03**	**1.23E+00**	**1.00E-03**
hsa-miR-218-5p	2.00E-04	4.00E-05	1.00E-03	2.00E-04	-4.00E-04	-4.40E-01	5.00E-02
hsa-miR-22-3p	1.00E-02	3.00E-03	2.00E-02	2.00E-03	-1.00E-02	-3.70E-01	5.00E-03
hsa-miR-27b-3p	1.00E-02	1.00E-03	1.00E-02	1.00E-03	-6.00E-03	-3.30E-01	6.00E-03
hsa-miR-29b-3p	1.00E-03	3.00E-04	2.00E-03	2.00E-04	-8.00E-04	-3.10E-01	3.00E-02
hsa-miR-30a-3p	2.90E-01	6.00E-02	5.20E-01	7.00E-02	-2.30E-01	-2.60E-01	3.00E-02
hsa-miR-30a-5p	2.40E-01	6.00E-02	5.40E-01	7.00E-02	-3.00E-01	-3.50E-01	2.00E-02
hsa-miR-30b-5p	9.10E-01	2.30E-01	2.35E+00	5.30E-01	-1.43E+00	-4.10E-01	3.00E-02
hsa-miR-30c-5p	1.69E+00	4.30E-01	4.76E+00	1.14E+00	-3.07E+00	-4.50E-01	4.00E-02
hsa-miR-30d-5p	8.00E-02	2.00E-02	1.90E-01	3.00E-02	-1.10E-01	-3.80E-01	1.00E-02
hsa-miR-30e-3p	2.60E-01	6.00E-02	5.20E-01	7.00E-02	-2.60E-01	-3.00E-01	2.00E-02
hsa-miR-342-5p	4.00E-04	2.00E-04	2.00E-03	1.00E-03	-1.00E-03	-5.80E-01	2.00E-02
hsa-miR-363-5p	3.00E-07	1.00E-07	1.00E-05	7.00E-06	-1.00E-05	-1.56E+00	4.00E-02
hsa-miR-371-3p	3.00E-05	1.00E-05	2.00E-04	8.00E-05	-1.00E-04	-7.60E-01	4.00E-02
hsa-miR-372-3p	1.00E-03	3.00E-04	1.00E-02	3.00E-03	-5.00E-03	-9.60E-01	2.00E-02
hsa-miR-373-3p	3.00E-05	2.00E-05	1.00E-04	2.00E-05	-1.00E-04	-4.60E-01	3.00E-03
hsa-miR-377-3p	**6.90E-01**	**1.00E-05**	**1.47E+00**	**4.00E-06**	**-7.80E-01**	**-3.30E-01**	**4.00E-02**
hsa-miR-377-5p	3.00E-05	5.20E-01	5.00E-06	5.40E-01	2.00E-05	7.60E-01	4.00E-02
hsa-miR-378a-3p	3.00E-02	1.00E-02	6.00E-02	1.00E-02	-3.00E-02	-3.40E-01	2.00E-02
hsa-miR-378a-5p	**4.00E-04**	**1.00E-04**	**1.00E-03**	**1.00E-04**	**-3.00E-04**	**-2.60E-01**	**5.00E-02**
hsa-miR-422a	3.00E-03	1.00E-03	1.00E-02	2.00E-03	-5.00E-03	-4.40E-01	2.00E-02
hsa-miR-424-5p	1.00E-03	3.00E-04	3.00E-03	1.00E-03	-2.00E-03	-3.90E-01	3.00E-02
hsa-miR-429	2.00E-04	2.00E-04	2.00E-03	1.00E-03	-2.00E-03	-9.10E-01	4.00E-02

The table continues on the next page.

miR	SN mean	SN SEM	RA mean	RA SEM	Fold change	Log fold change	P value
hsa-miR-450b-5p	1.00E-04	1.00E-04	3.00E-04	1.00E-04	-1.00E-04	-3.60E-01	4.00E-02
hsa-miR-483-3p	1.40E-02	4.00E-03	5.00E-02	1.00E-02	-3.00E-02	-5.10E-01	4.00E-03
hsa-miR-486	6.00E-03	2.00E-03	1.00E-02	2.00E-03	-7.00E-03	-3.30E-01	5.00E-02
hsa-miR-486-3p	3.00E-04	1.00E-04	1.00E-03	3.00E-04	-8.00E-04	-5.70E-01	1.00E-02
hsa-miR-490-3p	9.00E-04	2.00E-04	1.00E-02	1.00E-03	-4.00E-03	-7.60E-01	4.00E-02
hsa-miR-512-5p	**1.83E+01**	**1.16E+01**	**1.00E-05**	**9.00E-06**	**1.83E+01**	**6.10E+00**	**3.00E-02**
hsa-miR-515-3p	3.00E-07	1.00E-07	3.00E-06	2.00E-06	-3.00E-06	-9.70E-01	4.00E-02
hsa-miR-520d-3p	9.00E-05	4.00E-05	2.00E-04	3.00E-05	-8.00E-05	-2.70E-01	5.00E-02
hsa-miR-520g-3p	6.00E-06	1.00E-05	0.00E+00	2.00E-05	-3.00E-05	-8.40E-01	5.00E-02
hsa-miR-524-3p	5.00E-06	2.00E-06	4.00E-04	2.00E-04	-4.00E-04	-1.95E+00	4.00E-02
hsa-miR-548b-5p	**1.00E-04**	**1.00E-04**	**1.00E-04**	**6.00E-05**	**6.00E-05**	**2.80E-01**	**4.00E-02**
hsa-miR-548k	**2.00E-06**	**1.00E-06**	**0.00E+00**	**8.00E-08**	**2.00E-06**	**7.20E-01**	**5.00E-02**
hsa-miR-571	8.00E-05	2.00E-05	4.00E-04	2.00E-04	-3.00E-04	-6.60E-01	3.00E-02
hsa-miR-584-5p	6.00E-04	1.00E-04	1.00E-03	1.00E-04	-5.00E-04	-2.70E-01	4.00E-02
hsa-miR-616-5p	2.00E-04	4.00E-05	3.00E-04	4.00E-05	-1.00E-04	-2.60E-01	4.00E-02
hsa-miR-628-3p	3.00E-03	1.00E-03	5.00E-03	1.00E-03	-2.00E-03	-2.70E-01	4.00E-02
hsa-miR-642a-5p	3.00E-03	1.00E-03	3.00E-02	1.00E-02	-2.00E-02	-1.00E+00	4.00E-04
hsa-miR-651-5p	2.00E-05	1.00E-05	4.00E-05	9.00E-06	-2.00E-05	-3.70E-01	4.00E-02
hsa-miR-654-5p	**1.00E-04**	**1.00E-04**	**4.00E-07**	**6.00E-08**	**1.00E-04**	**2.48E+00**	**3.00E-02**
hsa-miR-668-3p	**5.00E-05**	**2.00E-05**	**4.00E-07**	**8.00E-08**	**5.00E-05**	**2.11E+00**	**3.00E-02**
hsa-miR-885-3p	**1.00E-03**	**1.00E-03**	**4.00E-07**	**7.00E-08**	**1.00E-03**	**3.45E+00**	**2.00E-02**
hsa-miR-938	2.00E-06	1.00E-06	1.00E-05	1.00E-06	-1.00E-05	-6.60E-01	3.00E-03
hsa-miR-1225-3p	**3.00E-02**	**1.00E-02**	**1.00E-02**	**1.00E-02**	**1.00E-02**	**3.10E-01**	**3.00E-02**
hsa-miR-1233-3p	5.00E-04	5.00E-04	5.38E+00	4.35E+00	-5.38E+00	-4.05E+00	3.00E-02
hsa-miR-1244-3p	**3.00E-04**	**1.00E-04**	**1.00E-04**	**4.00E-05**	**2.09E-04**	**4.50E-01**	**1.00E-02**

Table S3. Significantly **up** or down-regulated microRNAs in the SN. Table includes names of the microRNAs, microRNA relative expression level in the SN and RA ± standard error (SEM), fold change ($2^{-\Delta Ct}$), log fold change ($\Delta Ct_{(Target)} - \Delta Ct_{(Housekeeper)}$) and p values, calculated via RealTime StatMiner.

References

1. Chandler NJ, Greener ID, Tellez JO, Inada S, Musa H, Molenaar P, DiFrancesco D, Baruscotti M, Longhi R, Anderson RH, Billeter R, Sharma V, Sigg DC, Boyett MR and Dobrzynski H. Molecular architecture of the human sinus node insights into the function of the cardiac pacemaker. *Circulation*. 2009;119:1562-1575.

2. Chandler N, Aslanidi OV, Buckley D, Inada S, Birchall S, Atkinson A, Kirk D, Monfredi O, Molenaar P, Anderson R, Sharma V, Sigg D, Zhang H, Boyett M and Dobrzynski H. Computer three-dimensional anatomical reconstruction of the human sinus node and a novel paranodal area. *Anatomical Record-Advances in Integrative Anatomy and Evolutionary Biology*. 2011;294:970-979.

3. Perde FV, Atkinson A, Yanni J, Dermengiu D and Dobrzynski H. Morphological characteristics of the sinus node on postmortem tissue. *Folia Morphologica*. 2016;75:216-223.

4. Stephenson RS, Atkinson A, Kottas P, Perde F, Jafarzadeh F, Bateman M, Iaizzo PA, Zhao JC, Zhang HG, Anderson RH, Jarvis JC and Dobrzynski H. High resolution 3-Dimensional imaging of the human cardiac conduction system from microanatomy to mathematical modeling. *Scientific Reports*. 2017;7.

5. Li N, Csepe TA, Hansen BJ, Dobrzynski H, Higgins RSD, Kilic A, Mohler PJ, Janssen PML, Rosen MR, Biesiadecki BJ and Fedorov VV. Molecular mapping of sinoatrial node hcn channel expression in the human heart. *Circulation-Arrhythmia and Electrophysiology*. 2015;8:1219-1227.

6. D'Souza A, Pearman CM, Wang YW, Nakao S, Logantha S, Cox C, Bennett H, Zhang Y, Johnsen AB, Linscheid N, Poulsen PC, Elliott J, Coulson J, McPhee J, Robertson A, Martins PAD, Kitmitto A, Wisloff U, Cartwright EJ, Monfredi O, Lundby A, Dobrzynski H, Oceandy D, Morris GM and Boyett MR. Targeting miR-423-5p reverses exercise training-induced HCN4 channel remodeling and sinus bradycardia. *Circulation Research*. 2017;121:1058-1568.

Chapter 4

4 miR-486-3p regulates pacemaker activity in the human heart via the funny, HCN4, channel

4.1 Other authors contribution to the paper

The vast majority of the experimental work for this study was performed by myself, I also created and wrote the paper. I greatly appreciate and acknowledge the input from the following authors:

- Joseph Yanni carried out human SN/RA microRNA expression experiment
- Alicia D'Souza aided me in data analysis and experiment design
- Andrew Atkinson aided me with confocal microscopy and technical support
- Balint Borbas and Connor Geraghty were undergraduate students who aided me with part of the experimental work and analysis under my supervision
- Luke Stuart provided critical and valuable comments on my manuscript
- Delvac Oceandy had a supervisory role and aided in experiment design
- Halina Dobrzynski had a major supervisory role and aided me with the experimental work and provided critical and valuable comments on my manuscript

4.2 Paper

miR-486-3p regulates pacemaker activity in the human heart via the funny, HCN4, channel

Short title: miR-486-3p, pacemaker mechanism, human sinus node

Maria Petkova, MRes[*], Joseph Yanni, PhD[*], Alicia D'Souza, PhD[*], Andrew Atkinson, MSc[*], Balint Borbas[*], Connor Geraghty, BSc[*], Luke Stuart (Mres)[*], Delvac Oceandy (PhD)[*], Halina Dobrzynski (PhD)[*]

[*]Cardiovascular Sciences, University of Manchester, Faculty of Biology, Medicine and Health Manchester, UK

Source of funding

This work was supported by the British Heart Foundation (grant numbers RG/11/18/29257)

Disclosures

None.

Corresponding Author:

E-mail address: halina.dobrzynski@manchester.ac.uk

Address: CTF Building, 46 Grafton Street, Manchester M13 9NT

Tel: +441612751182, Fax: +441612751183

Total word count: 4956

Abstract

Background: The primary pacemaker of the heart, the sinus node (SN) initiates and propagates action potentials in the heart. MicroRNAs are small non-coding RNA molecules, which regulate the expression of functional proteins such as ion channels.

Objective: The aim of this study was to determine the functional role of 7 microRNAs that were predicted to regulate ion channels and Ca^{2+}-handling proteins responsible for pacemaking.

Methods: Computational predictions highlighted 7 microRNAs that bind to target mRNAs of interest through conserved complimentary base pairing. Male rat SN preparations were injected with each microRNA (miR-1-3p, miR-30c-5p, miR-133a-3p, miR-153-3p, miR-371-3p, miR-429, and miR-486-3p) and cultured for 24 hours while their beating rate was recorded (n=64). Further functional experiments to validate miR-486-3p and miR-429 binding and inhibition of HCN4, $Ca_V1.3$, and $Ca_V3.1$, and Tbx18, respectively, were performed as both microRNAs reduced the beating rate of rat SN preparations over 24-hour period. A luciferase reporter assay in H9C2 cells was used to validate miR-429 and miR-486-3p complimentary binding to target mRNAs (n=3 assays). Quantitative PCR (qPCR), as well as immunohistochemistry analysis, was used to confirm post-transcriptional repression of target mRNA/ protein expression (eg. HCN4) in miR-486-3p-transfected rat SN preparations vs. control (n=8).

Results: TarBase, miRecords, TargetScan, and RNA22 were used to predict 9,13,and 10 binding sites of miR-486-3p to HCN4, $Ca_V1.3$, and $Ca_V3.1$, respectively, and no binding sites of miR0429 to Tbx18. Since Rat SN preparations exhibited downregulation of the beating rate after 13-24 hours following transfection with miR-429 and miR-486-3p, and

20-23 hours following transfection with miR-153-3p, $p \leq 0.05$. Interaction between miR-486-3p and HCN4 was confirmed by significant reduction in HCN4 3'-untranslated region luciferase reporter activity following cotrasnfection with miR-486-3p, $p \leq 0.05$. qPCR and immunohistochemical analysis confirmed that HCN4 is downregulated at mRNA and protein level in miR-486-3p transfected rat SN preparations vs. control.

Conclusion: miR-486-3p is an important regulator of the key pacemaker ion channel HCN4 and may be of interest as potential therapeutic target.

Key words human sinus node, microRNAs, pacemaking, membrane-voltage and Ca^{2+} clock, miR-486-3p, HCN4

List of abbreviations: sinus node (SN), right atrium (RA), 3'-untranslated region (3'UTR), connexin40 (Cx40), connexin43 (Cx43), connexin45 (Cx45), T-box factors 3 (Tbx3), T-box factors 18 (Tbx18), hyperpolarisation-activated cyclic nucleotide-gated channel 4 (HCN4), ryanodine receptor 2 (RyR2), Quantitative PCR (qPCR), graphene oxide (GO), microRNA (miR).

Introduction

The heart contains specialised cardiac cells that have the ability to spontaneously generate electrical impulses [1], and this unique feature is called automaticity. The electrical impulse travels along the cardiac conduction system, and the primary pacemaking structure of this system is the sinoatrial node (SN). The automatic electrical activity of the SN is strictly regulated by the crosstalk between the membrane-voltage clock mechanism, comprising of ion channels that cause membrane excitability, and the Ca^{2+} clock that determines intracellular Ca^{2+} levels [2].

The differential expression of ion channels and Ca^{2+}-handling proteins, as well as the varying morphological and functional characteristics of the SN vs. right atrium (RA)[3], allows effective propagation of the electrical signal from the nodal tissue towards the working myocardium. The action potential generation in the SN is produced by activation of I_f, mainly due to HCN4 opening during phase 4, which is followed by slow upstroke due to the opening of $Ca_V1.3$ ($I_{Ca,L}$) and $Ca_V3.1$($I_{Ca,T}$) channels during phase 0 [4,5]. The Ca^{2+} clock is involved in the pacemaking activity of the SN synergistically with the membrane-voltage clock. Ca^{2+} influx through causes Ca^{2+} release from the major intracellular Ca^{2+} store, the sarcoplasmic reticulum, through ryanodine receptor 2 (RyR2) opening, which further depolarises SN membrane potential [6]. Local higher Ca^{2+} concentrations also lead to activation of the electrogenic NCX, which works by extruding 1 Ca^{2+} ion in exchange for 3 Na^+ ions, resulting in accumulation of net positive charge in the intracellular space [1,2]. The current produced by NCX, $I_{Na,Ca}$, depolarises further the SN cell membrane and thus it regulates the generation of the steep, exponential shape of the late diastolic depolarisation [1,2].

Electrical signal conduction in cardiac tissue depends on the electrical coupling between cardiomyocytes by gap junction channels known as connexins. Poor electrical coupling in the SN is attributable to poor expression of fast conductance connexins such as connexin40 (Cx40) and connexin43 (Cx43), but high expression of the slow conductance connexin isoform - connexin45 (Cx45)[7].

SN formation, development, proliferation, and survival during embryogenesis and adulthood are controlled by transcription factors. T-box (Tbx) factors 3 and 18 are transcription factors important for the formation of the SN structure and activation of the SN gene programme [8].

MicroRNAs are small non-coding molecules that take part in regulation of functional proteins such as those responsible for pacemaking[9]. Substantial scientific literature focuses on the involvement of numerous microRNAs in the physiological as well as pathophysiological processes in the heart. D'Souza et al., reported upregulation of miR-423-5p and miR-486-3p in the SN of athletically trained mice, which exhibit HCN4 channel downregulation and subsequent bradycardia[9]. We have identified 7 microRNAs to be involved in the regulation of key molecules responsible for normal functioning of the human SN and RA (Table 1). The aim of the current study was to 1) determine if these key 7 microRNAs have binding sites for their predicted targets, and if they are conserved in human and rat, and 2) if the microRNAs have any functional effect on *ex vivo* rat SN preparations and the predicted target expression levels.

Methods

MicroRNA sequence comparison, as well as total number of microRNA binding sites on predicted target gene mRNA, was assessed via miRBase biological database (Faculty of Life Sciences, University of Manchester, Table 1 and 2).

A detailed description of the materials and methods used can be found in the Supplement file. In brief, male Wistar-Hannover rats 230-250 g (n =64) were terminated in accordance with the UK Animal (Scientific Procedures) Act 1986 with ethical approval from the University of Manchester. Spontaneous electrical activity of microRNA-injected SN preparations vs. control was measured by PowerLab 4/35, 4-channel recorder (ADInstruments, Oxford, UK) over a 24-hour period as previously described [10].

A luciferase reporter gene assay was used to confirm the targeted binding of human miR-486-3p to human HCN4 and $Ca_V1.3$ as well as miR-429 to Tbx18 3'-untranslated region

(UTR) constructs. 3'UTR mRNA sequences are primarily targeted by microRNAs through imprecise complementary base pairing[11].

Quantitative PCR (qPCR) analysis measured the expression of miR-486-3p, HCN4, $Ca_V1.3$ and $Ca_V3.1$ in *ex vivo* rat SN after miR-486-3p injection and 24h incubation vs. control, to confirm miR-486-3p successful transfection and assess microRNA effect on its predicted target mRNAs.

Immunohistochemistry was carried out on 10 μm tissue sections to assess the effect of miR-486-3p on HCN4 protein expression in rat SN vs. RA. The integrity of the cell membrane in rat SN and RA sections was confirmed by caveolin3 immunofluorescent labelling. Imuunohistochemical experiments were performed in accordance with established laboratory methods [12].

Statistical analysis was performed using Prism 7 (GraphPad software, La Jolla, CA). Two-group experiments were compared using student's t test. Three and more-group experiments were compared using One-way ANOVA; graphs represent mean ± standard error of the mean values. P values ≤0.05 were considered as statistically significant.

Results

Our study focused on 7 microRNAs involved in the regulation of key functional genes in the SN vs. RA (Table 1). These microRNAs were predicted using Ingenuity Pathway Software (IPA, Ingenuity systems, Redwood city, CA) to bind to and inhibit the expression of major ion channels, Ca^{2+}-handling proteins, and connexins, involved in SN pacemaking mechanisms [13,14] (Table 1). Table 1 further summarises the predicted binding sites of the human microRNAs to their rat mRNA counterpart. A computational search was performed using TarBase database, miRecords (http://mirecords.biolead.org/), TargetScan,

(http://www.targetscan.org/) and RNA22 (https://cm.jefferson.edu/rna22/) in order to determine if microRNAs bind to their predicted mRNA targets through complementary base pairing. Human miR-133a-3p, miR-371-3p, miR-486-3p, and miR-153-3p were predicted to have at least 1 binding site for all or some of their predicted target rat mRNAs (Table 1). Notably, human miR-486-3p was predicted to target rat HCN4 at 9 sites, $Ca_V1.3$ at 13 sites, and $Ca_V3.1$ at 10 sites, suggesting there is a high probability of binding to any of these ion channels. miR-1-3-p, miR-30c-5p, and miR-429 were found to contain no binding sites for their predicted target molecules. miRBase software was used to compare the sequences of these 7 microRNAs in human and rat, and found that all of them are conserved across these two species (Table 2).

Figure 1A shows a typical *ex vivo* rat SN preparation, which was injected with those microRNAs (listed in Table 1 and 2) at the area of the SN artery bifurcation, used as a visual marker for the SN. miR-1-3p and miR-30c-5p were used as negative controls since they were predicted to contain no binding sites for their targets (Table 2). In order to show the area of the injection, a representative SN preparation was injected with 2 µl graphene oxide (GO) around the SN artery bifurcation.

miR-1-3p, miR-30c-5p, miR-133a-3p, and miR-371-3p were found to exhibit no significant effect over the beating rate produced by *ex vivo* rat SN preparations over a 24-hour period (Figure 2 A, B, C and E). miR-1-3p and miR-30c-5p were used as negative control as no effect on the beating rate of SN preparations injected with these microRNAs was expected due to lack of binding sites at their predicted target sequences (Table 2). miR-371-3p exhibited a trend towards reduction of the beating rate after 20 hours following transfection, suggesting longer incubation time is needed. miR-153-3p, however,

showed significant reduction of the beating rate between 20 and 23 hours after transfection, followed by recovering of the beating rate to control levels (Figure 2D).

miR-429 transfection of *ex vivo* rat SN preparations showed a steady and maintained reduction of the beating rate 13 hours after injections in comparison with scrambled miR (Figure 3A). Further verification of miR-429 and Tbx18 3'UTR binding through luciferase analysis (Table 2 and Figure 3B), showed no downregulation of Tbx18 compared to H9C2 cells transfected with Tbx18 and scrambled miR, miR-429 only, or a negative control (culture media only) (Figure 3 B). Results suggest that miR-429 does not bind to Tbx18 mRNA as predicted, and potentially produces its effect, observed in Figure 3 A, through interactions with other targets such as $Na_V1.5$ and $Ca_V1.2$ (data not shown).

miR-486-3p significantly reduced the beating rate of *ex vivo* rat SN preparations 15 hours after transfection and maintained this change over the end of the 24-hour period compared to control (Figure 4 A). To verify whether HCN4 is a genuine target for miR-486-3p, we transfected H9C2 cells with vectors containing HCN4 3'UTR and a luciferase reporter gene. miR-486-3p significantly suppressed HCN4-mediated luciferase activity (Figure 4B) in comparison with cells transfected with HCN4 and scrambled miR, miR-486-3p only, or negative control (culture media only). In contrast, no downregulation of $Ca_V1.3$ (Figure 4C) was observed. We looked into the effect of miR-486-3p on $Ca_V1.3$, as $Ca_V1.3$ was predicted to have 13 binding sites for miR-486-3p (Table 1). These data imply that the miR-486-3p inhibiting effect of *ex vivo* rat SN beating rate is due to post-transcriptional repression via the HCN4 3'UTR, which results in inhibition of mRNA translation into protein, but not due to binding to $Ca_V1.3$.

To establish if the effect of miR-486-3p on the *ex vivo* rat SN preparations was due to post-transcriptional repression of HCN4, qPCR analysis revealed upregulation of miR-486-3p

in the transfected samples compared to control (Figure 5 A), and downregulation of HCN4 mRNA expression levels (Figure 5 B). No difference was observed in $Ca_V1.3$ and $Ca_V3.1$ (predicted target molecules for miR-486-3p, Table 1) mRNA expression (Figure 5 C and D), confirming that miR-486-3p does not exert its effect through binding to them, but through binding to HCN4 mRNA.

Finally, in order to determine whether HCN4 protein expression was also affected by miR-486-3p in *ex vivo* rat SN preparations, we performed immunohistochemical analysis. Results revealed decreases in HCN4 signal intensity profile in miR-486-3p transfected SNs compared to scrambled miR transfections (Figure 6A, B and E). Caveolin3, which labels cardiomyocytes cell membrane, demonstrated that the SN and RA cells membranes were preserved over the 24-hour incubation period (Figure 6 C and D), suggesting that HCN4 downregulation is genuine in miR-486-3p-treated tissue.

Discussion

The current study focused on 7 microRNAs predicted to affect distinct ion channels regulating the membrane-voltage clock, Ca^{2+}-handling proteins, and transcription factors. We focused on these microRNAs because six of them are less expressed in the human SN vs. RA (miR-1-3p, miR-30c-5p, miR-133a-3p, miR-371-3p, miR-429, and miR-486-3p) and miR-153-3p is more expressed in the human SN vs. RA (Table 1).

This study presents evidence that miR-486-3p inhibits HCN4 at mRNA and protein level, which explains why the beating rate of *ex vivo* rat SN preparations was reduced. Our data imply that miR-486-3p maintains low HCN4 levels of expression in the RA and prevents pacemaking activity. Our previous work demonstrated that downregulation of SN HCN4 levels and subsequent reduction of I_f in athletically trained mice, exhibiting bradycardia, is

attributed to miR-486-3p as well as miR-423-5p upregulation and specific binding to mouse HCN4 3'UTR [9]. This was the first report to show microRNAs regulate the cardiac pacemaking mechanism.

McGahon et al., also showed that the human miR-486-3p sequence is conserved in other species such as rat, providing evidence that the rat heart is a useful model for miR-486-3p function validation (Table 1) [15]. McGahon et al., also reported that miR-486-3p was more highly expressed in the rat endocardium compared to the epicardium, where it was predicted to target NCX1 expression, which was itself found to be negatively correlated to the microRNA levels [15]. It was also suggested that miR-486-3p targets IRX5 transcription factor in the working myocardium, which in turn negatively regulates $K_V4.2$ channels. $K_V4.2$ channel conducts I_{to}, cardiac transient potassium current, which repolarises phase 1 of the myocardial action potential [15]. miR-486-3p antagonizes the effect of IRX5 and thus potentially leads to upregulation of $K_V4.2$ expression in the mouse ventricle [16,17], which again suggests that miR-486-3p has an important role in the working myocardium.

In the current study we focus more specifically on the effect of miR-429 on Tbx18, as Tbx18 has been previously shown to promote the expression of HCN4 and regulate SN formation [8]. Rat Tbx18 mRNA was found to express no binding sites for human miR-429 (Table 2). Furthermore, luciferase reporter assay activity was not decreased by miR-429 in H9C2 cells expressing human Tbx18, confirming that the microRNA does not bind to its predicted target. Paradoxically, however, miR-429 was found to inhibit *ex vivo* rat SN beating rate. This change is potentially attributable to miR-429 post-translational repression of other targets, such as $Na_V1.5$ and $Ca_V1.2$ channels (predominantly expressed in the working myocardium) that we predicted (data not shown). D'Souza et al., carried out global microRNA expression profiling of the cardiac tissue of sedentary and exercise

trained heart failure rat model and reported upregulation of miR-429 [18]. Another study attributed apoptosis in human cardiomyocytes under hypoxic conditions, mimicking myocardial ischemia, to upregulation of miR-429. miR-429 was correlated to downregulation of Notch1 (an inhibitor of apoptosis), suggesting that miR-429 downregulation could be cardioprotective [19].

Although, we predicted 4 binding sites within rat HCN4 for miR-133a-3p (Table 1), no functional effect over SN beating rate was observed. Similarly, rat HCN1, HCN4, and Tbx3, which were predicted to be targeted by miR-1-3p, had no binding sites for it, and subsequently no functional changes in the beating rates were observed (Table 1).

We previously showed miR-1 upregulation in the SN of trained mouse and rat models [9] as well as specific binding of miR-1 to mouse HCN4 3'UTR, and reduction of HCN4 luciferase activity in H9C2 cells[18]. Another study showed downregulation of miR-1 and miR-133 in a rat model of ventricular hypertrophy was associated with upregulation of HCN4 expression, resulting in arrhythmogenesis and hypertrophy [20]. miR-1 and miR-133 are two of the most abundant microRNAs in the heart, where they are involved in both myocardial lineage differentiation and regulation of muscles gene expression [21,22], and their dysregulation is observed in heart failure and hypertrophy [23,24]. miR-133 downregulation was directly correlated to nicotine-induced profibrotic response in canine atrium, suggesting miR-133 inhibits collagen production by the atrial fibroblasts [25]. Rau et al., reported that Cx43 and $Ca_V1.2$, important for the working myocardium action potential generation and propagation, are also targeted by miR-1 [26]. miR-1 was also found to downregulate Cx43 and $K_{ir}2.1$expression in a rodent model of viral myocarditis and myocardial infarction [27]. Similarly to miR-486, miR-1-2 was demonstrated to target Irx5 and thus indirectly increase $K_V4.2$, a major repolarising factor in the ventricular wall,

resulting in dysfunctions in the ventricular repolarisation and subsequent arrhythmias [22]. The current data on miR-1 and miR-133 effects on the heart imply their complex role in cardiac conduction, repolarisation, automaticity, and fibrosis. To this end, our understanding of their effect in the SN is rather preliminary.

Although we predicted miR-30-5p is targeting HCN1, HCN4, and $Ca_V1.3$ (Table 1), no downregulation of rat SN beating rate was observed (Figure 2 B), due to absence of binding sites on any of the targets for the microRNA (Table 1). miR-30c was previously attributed to altering the balance between proliferation, apoptosis, and differentiation, resulting in embryonic cardiac malfunctions [28]. It was also found to participate in other types of cell death processes like autophagy, which is enhanced in diabetic cardiomyopathy via repression of BECN1 [29]. Dowenregulation of the miR-30 family was found to be cardioprotective against hypoxic cardiac injury in a myocardial infarction mouse model, due to increased hydrogen sulfide, H_2S, production [30]. miR-30c was also found to repress signalling pathways involved in cardiac hypertrophy by cardiac fibroblast proliferation, differentiation, migration, and collagen production by targeting TGFbRII [31,32] as well as attenuating it through inhibition of Cdc42 and Pak1 in a rat model of diabetic cardiomyopathy [33].

We predicted that miR-371-3p targets $Ca_V1.3$ and Cx43, however, no binding sites in the respective rat mRNA sequences were found, which subsequently led to no change in the beating rate of *ex vivo* rat SN preparations. Only one previous study has reported about upregulation of miR-371-3p as a biomarker of congenital heart failure in patients, using a microarray method [34].

miR-153-3p, unlike the other 6 microRNAs we focused on, was more expressed in human SN vs. RA, and it was predicted to target $Ca_V1.2$, $Na_V1.5$, and RyR2. We predicted that rat

$Ca_V1.2$ and RyR2 mRNA sequence contained 1 binding site for miR-153-3p each. Interestingly, we observed downregulation of the beating rate after 20 hours following transfection, which persisted for only 3 hours. A relatively recent study reported indirect regulation of $Na_V1.5$ by miR-153, where $Na_V1.5$ 3'UTR complex was upregulated in fibroblasts transfected with miR-153 [35]. miR-153 was also found to exhibit pro-apoptotic effects in the heart [36]. Functional experiments demonstrated miR-153 overexpression upon increase in reactive oxygen species such as H_2O_2. Reduction of miR-153 levels, however, prevented induction of apoptosis, but stimulated cell autophagy, implying miR-153 regulated cardiomyocyte cell survival during oxidative stress [36].

Conclusion

Our data reveal that the SN and the surrounding working myocardium are regulated by microRNAs. For the first time, we demonstrated that miR-486-3p directly regulates the expression of the major pacemkaing channel, HCN4, in the human heart by post-transcriptional repression, and thus potentially affects its heart rate. Alterations of the endogenous expression of HCN4 in various parts of the heart could be targeted by modulating the expression of miR-486-3p and potential other microRNAs, involved in the regulation of the molecular architecture of the heart.

Acknowledgements

None.

References

1. Mangoni ME, Nargeot J. Genesis and regulation of the heart automaticity. *Physiological Reviews.* 2008;88(3):919-982.

2. Lakatta EG, DiFrancesco D. What keeps us ticking: a funny current, a calcium clock, or both? *Journal of Molecular and Cellular Cardiology.* 2009;47(2):157-170.

3. Dobrzynski H, Boyett MR, Anderson RH. New insights into pacemaker activity – Promoting understanding of sick sinus syndrome. *Circulation.* 2007;115(14):1921-1932.

4. Mangoni ME, Couette B, Bourinet E, et al. Functional role of L-type $Ca_V1.3$ Ca^{2+} channels in cardiac pacemaker activity. *Proceedings of the National Academy of Sciences of the United States of America.* 2003;100(9):5543-5548.

5. Leuranguer V, Monteil A, Bourinet E, Dayanithi G, Nargeot J. T-type calcium currents in rat cardiomyocytes during postnatal development: contribution to hormone secretion. *American Journal of Physiology-Heart and Circulatory Physiology.* 2000;279(5):2540-2548.

6. Cheng H, Lederer MR, Xiao RP, et al. Excitation-contraction coupling in heart: New insights from Ca^{2+} sparks. *Cell Calcium.* 1996;20(2):129-140.

7. Davis LM, Rodefeld ME, Green K, Beyer EC, Saffitz JE. Gap junction protein phenotypes of the human heart and conduction system. *Journal of Cardiovascular Electrophysiology.* 1995;6(10):813-822.

8. Wiese C, Grieskamp T, Airik R, et al. Formation of the Sinus Node Head and Differentiation of Sinus Node Myocardium Are Independently Regulated by Tbx18 and Tbx3. *Circulation Research.* 2009;104(3):388-397.

9. D'Souza A, Pearman CM, Wang YW, et al. Targeting miR-423-5p Reverses Exercise Training-Induced HCN4 Channel Remodeling and Sinus Bradycardia. *Circulation Research.* 2017;121(9):1058-1065.

10. Morris GM, D'Souza A, Dobrzynski H, et al. Characterization of a right atrial subsidiary pacemaker and acceleration of the pacing rate by HCN over-expression. *Cardiovascular Research.* 2013;100(1):160-169.

11. Filipowicz W, Bhattacharyya SN, Sonenberg N. Mechanisms of post-transcriptional regulation by microRNAs: are the answers in sight? *Nature Reviews Genetics.* 2008;9(2):102-114.

12. Saeed Y, Temple IP, Borbas Z, et al. Structural and functional remodeling of the atrioventricular node with aging in rats: The role of hyperpolarization-activated cyclic nucleotide-gated and ryanodine 2 channels. *Heart Rhythm.* 2018;15(5):752-760.

13. Tellez JO, Maczewski M, Yanni J, et al. Ageing-dependent remodelling of ion channel and Ca^{2+} clock genes underlying sino-atrial node pacemaking. *Experimental Physiology.* 2011;96(11):1163-1178.

14. Yanni J, Tellez JO, Maczewski M, et al. Changes in Ion Channel Gene Expression Underlying Heart Failure-Induced Sinoatrial Node Dysfunction. *Circulation-Heart Failure.* 2011;4(4):496-454.

15. McGahon MK, Yarham JM, Daly A, et al. Distinctive profile of isomir expression and novel micrornas in rat heart left ventricle. *Plos One.* 2013;8(6).

16. Costantini DL, Arruda EP, Agarwal P, et al. The homeodomain transcription factor lrx5 establishes the mouse cardiac ventricular repolarization gradient. *Cell.* 2005;123(2):347-358.

17. He W, Jia Y, Takimoto K. Interaction between transcription factors Iroquois proteins 4 and 5 controls cardiac potassium channel Kv4.2 gene transcription. *Cardiovascular Research.* 2009;81(1):64-71.

18. Souza RWA, Fernandez GJ, Cunha JPQ, et al. Regulation of cardiac microRNAs induced by aerobic exercise training during heart failure. *American Journal of Physiology-Heart and Circulatory Physiology.* 2015;309(10):H1629-H1641.

19. Xu H, Jin L, Chen Y, Li JZ. Downregulation of microRNA-429 protects cardiomyocytes against hypoxia-induced apoptosis by increasing Notch1 expression. *International Journal of Molecular Medicine.* 2016;37(6):1677-1685.

20. Luo X, Lin H, Pan Z, et al. Down-regulation of miR-1/miR-133 contributes to re-expression of pacemaker channel genes HCN2 and HCN4 in hypertrophic heart. *Journal of Biological Chemistry.* 2008;283(29):20045-20052.

21. Liu N, Bezprozvannaya S, Williams AH, et al. microRNA-133a regulates cardiomyocyte proliferation and suppresses smooth muscle gene expression in the heart. *Genes & Development.* 2008;22(23):3242-3254.

22. Zhao Y, Ransom JF, Li A, et al. Dysregulation of cardiogenesis, cardiac conduction, and cell cycle in mice lacking miRNA-1-2. *Cell.* 2007;129(2):303-317.

23. van Rooij E, Marshall WS, Olson EN. Toward microRNA-based therapeutics for heart disease the sense in antisense. *Circulation Research.* 2008;103(9):919-928.

24. van Rooij E, Sutherland LB, Liu N, et al. A signature pattern of stress-responsive microRNAs that can evoke cardiac hypertrophy and heart failure. *Proceedings of the National Academy of Sciences of the United States of America.* 2006;103(48):18255-18260.

25. Shan HL, Zhang Y, Lu YJ, et al. Downregulation of miR-133 and miR-590 contributes to nicotine-induced atrial remodelling in canines. *Cardiovascular Research.* 2009;83(3):465-472.

26. Rau F, Freyermuth F, Fugier C, et al. Misregulation of miR-1 processing is associated with heart defects in myotonic dystrophy. *Nature Structural & Molecular Biology.* 2011;18(7):840-U120.

27. Yang BF, Lin HX, Xiao JN, et al. The muscle-specific microRNA miR-1 regulates cardiac arrhythmogenic potential by targeting GJA1 and KCNJ2. *Nature Medicine.* 2007;13(4):486-491.

28. Liu XH, Li MM, Peng YZ, et al. miR-30c regulates proliferation, apoptosis and differentiation via the Shh signaling pathway in P19 cells. *Experimental and Molecular Medicine.* 2016;48.

29. Chen C, Yang SL, Li HP, et al. Mir-30c is involved in diabetic cardiomyopathy through regulation of cardiac autophagy via BECN1. *Molecular Therapy-Nucleic Acids.* 2017;7:127-139.

30. Shen YQ, Shen ZQ, Miao L, et al. miRNA-30 family inhibition protects against cardiac ischemic injury by regulating cystathionine-gamma-lyase expression. *Antioxidants & Redox Signaling.* 2015;22(3):224-240.

31. Xu J, Wu HQ, Chen SW, et al. MicroRNA-30c suppresses the pro-fibrogenic effects of cardiac fibroblasts induced by TGF-beta 1 and prevents atrial fibrosis by targeting TGF beta RII. *Journal of Cellular and Molecular Medicine.* 2018;22(6):3045-3057.

32. Abonnenc M, Nabeebaccus AA, Mayr U, et al. extracellular matrix secretion by cardiac fibroblasts role of microRNA-29b and microRNA-30c. *Circulation Research.* 2013;113(10):1138-1147.

33. Raut SK, Kumar A, Singh GB, et al. miR-30c mediates upregulation of Cdc42 and Pak1 in diabetic cardiomyopathy. *Cardiovascular Therapeutics.* 2015;33(3):89-97.

34. Cakmak HA, Coskunpinar E, Ikitimur B, et al. The prognostic value of circulating microRNAs in heart failure: preliminary results from a genome-wide expression study. *Journal of Cardiovascular Medicine.* 2015;16(6):431-437.

35. Daimi H, Lozano-Velasco E, Khelil AH, et al. Regulation of SCN5A by microRNAs: miR-219 modulates SCN5A transcript expression and the effects of flecainide intoxication in mice. *Heart Rhythm.* 2015;12(6):1333-1342.

36. Zou YH, Liu WT, Zhang JX, Xiang DC. miR-153 regulates apoptosis and autophagy of cardiomyocytes by targeting Mcl-1. *Molecular Medicine Reports.* 2016;14(1):1033-1039.

37. Chandler NJ, Greener ID, Tellez JO, et al. Molecular architecture of the human sinus node insights into the function of the cardiac pacemaker. *Circulation.* 2009;119(12):1562-1575.

microRNA expression in SN vs. RA	Gene name of predicted target	mRNA tissue expression based on Yanni et al., and Tellez et al.,	Total № of binding sites for each human microRNA on predicted rat mRNA target
miR-1-3p	HCN1	↑	-
	HCN4	↑	-
	Tbx3	↑	-
miR-30c-5p	HCN1	↑	-
	HCN4	↑	-
	$Ca_V1.3$	↑	-
miR-133a-3p	HCN4	↑	4
miR-153-3p	$Ca_V1.2$	↓	1
	$Na_V1.5$	↓	-
	RyR2	↓	1
miR-371-3p	$Ca_V1.3$	↑	1
	Cx43	↑	-
miR-429	Tbx18	↑	-
miR-486-3p	HCN4	↑	9
	$Ca_V1.3$	↑	13
	$Ca_V3.1$	↑	10

Table 1. Summary of microRNA expression in SN vs. RA, predicted mRNA targets from Yanni et al., Tellez et al, and Chandler et al., [13,14,37] prediction of interaction. Blue indicates significantly lower expression in the SN vs. RA. Red indicates significantly higher expression in the SN vs. RA. Analysis was performed using TarBase, miRecords, TargetScan, and RNA22.

microRNA	Species	Aligned sequence
miR-1-3p	human	UGGAAUGUAAAGAAGUAUGUAU
	rat	UGGAAUGUAAAGAAGUGUGUAU
miR-30c-5p	human	UGUAAACAUCCUACACUCUCAGC
	rat	UGUAAACAUCCUACACUCUCAGC
miR-133a-3p	human	UUUGGUCCCCUUCAACCAGCUG
	rat	UUUGGUCCCCUUCAACCAGCUG
miR-153-3p	human	UUGCAUAGUCACAAAAGUGAUC
	rat	UUGCAUAGUCACAAAAGUGAUC
miR-371-3p	human	AAGUGCCGCCAUCUUUUGAGUGU
	rat	AAGUGCCGCCAUGUUUUGAGUGU
miR-429	human	UAAUACUGUCUGGUAAAACCGU
	rat	UAAUACUGUCUGGUAAUGCCGU
miR-486-3p	human	CGGGGCAGCUCAGUACAGGAU
	rat	CGGGGCAGCUCAGUACAGGAU

Table 2. Sequences of miR-1-3p, miR-30c-5p, miR-133a-3p, miR-153-3p, miR-371-3p, miR-429, and miR-486-3p in human and rat. Data compared in miRBase.org and McGahon et al., 2013.

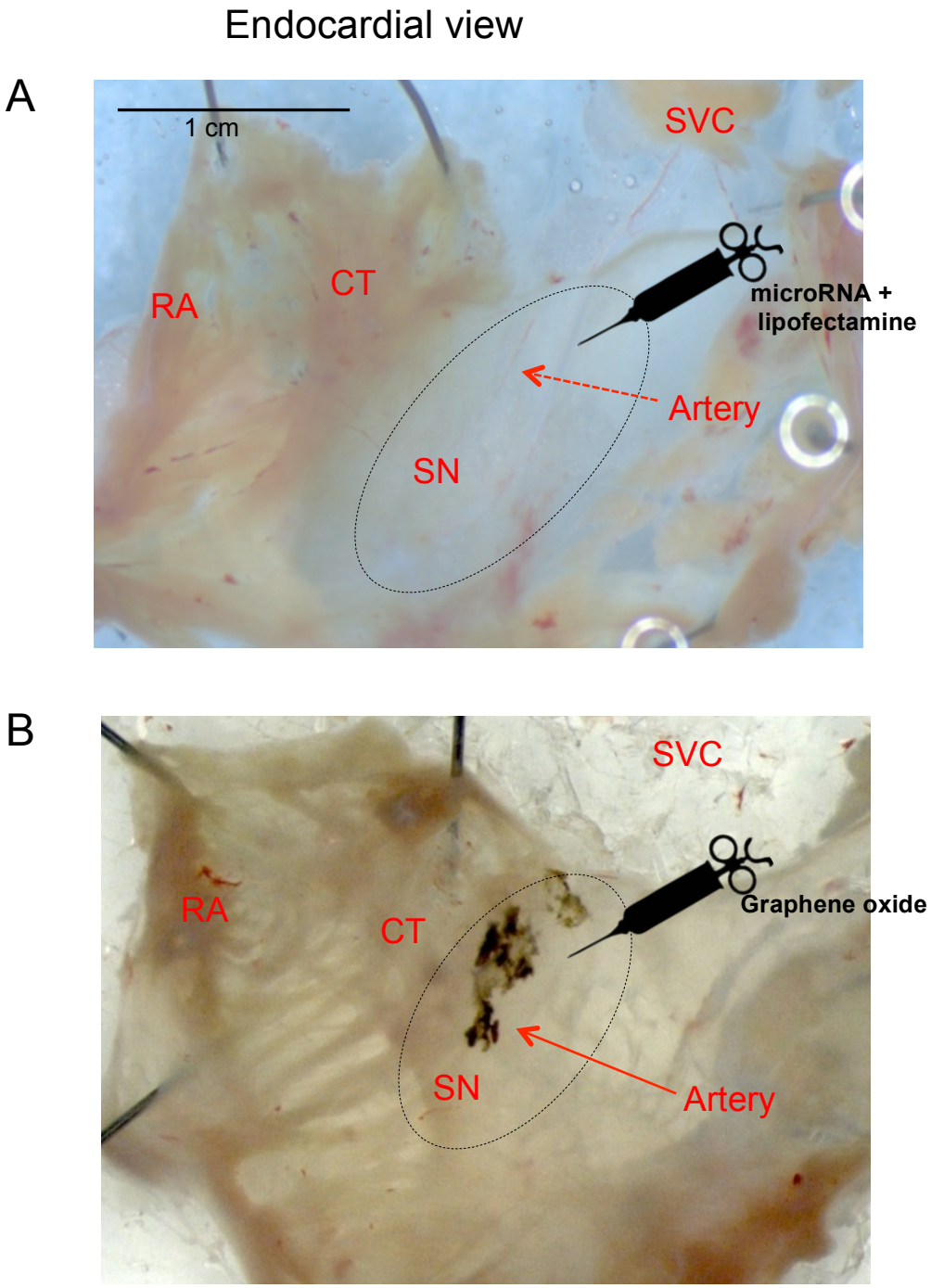

Figure 1. Endocardial view of rat SN preparation. Low magnification images were taken by AxioVison software. SAN – sinus node artery, CT – cristae terminalis, SVC – superior vena cava. A. 2 µl microRNA and lipofectamine and B. 2 µl graphene oxide in transfection medium were injected at the bifurcation of the sinus node artery.

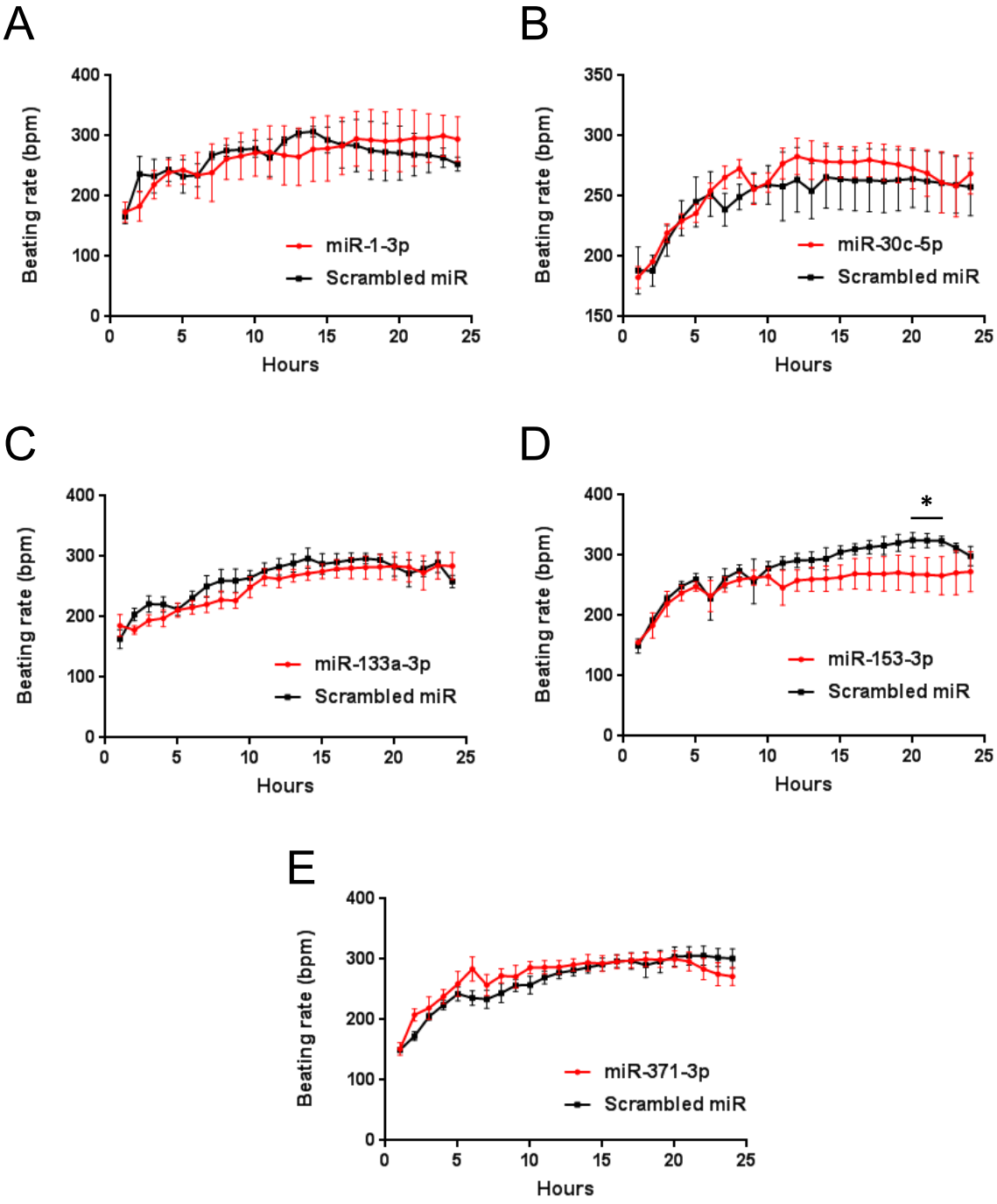

Figure 2. Extracellular membrane recording of *ex vivo* rat SN preparation mean beating rate of microRNA transfection vs. control (scrambled miR). Data was analysed using student's t-test (GraphPad Prism 7), * indicates p≤0.05. Graphs represent mean ± standard error of the mean (SEM), n=4. Preparations were injected with microRNAs as follows A. miR-1-3p, B. miR-30c-5p, C. miR-133a-3p, D. miR-153-3p and E. miR-371-3p.

A

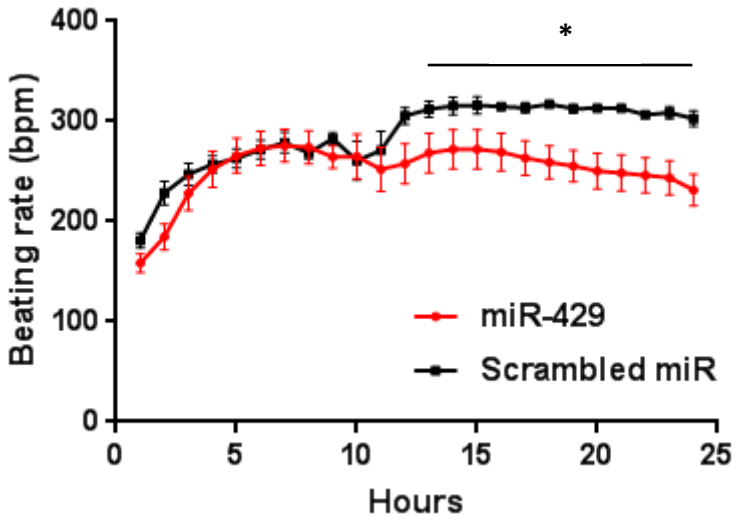

B

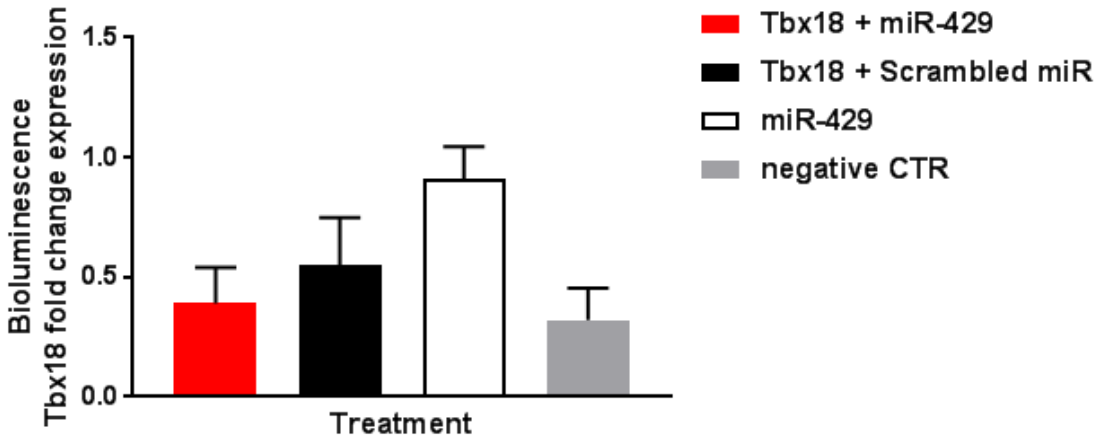

Figure 3. A. Extracellular membrane recording of *ex vivo* rat SN preparation mean beating rate of miR-429 transfection vs. control (scrambled miR). Data was analysed using student's t-test (GraphPad Prism 7), * indicates p≤0.05. Graphs represent mean ± standard error of the mean (SEM), n=4. B. Luciferase reporter gene assay showing Tbx18 3'UTR is not post-transcriptionally repressed by miR-429. Luciferase activity is shown 24 hours after co-transfection of H9C2 cells with Tbx18 3'UTR and control (scrambled miR), miR-429 only, or negative control (culture media only). Data was analysed using One-Way ANOVA (GraphPad Prism 7), p≥0.05. Graphs represent mean ± SEM, n = 3 batches of cells with 4 replicates.

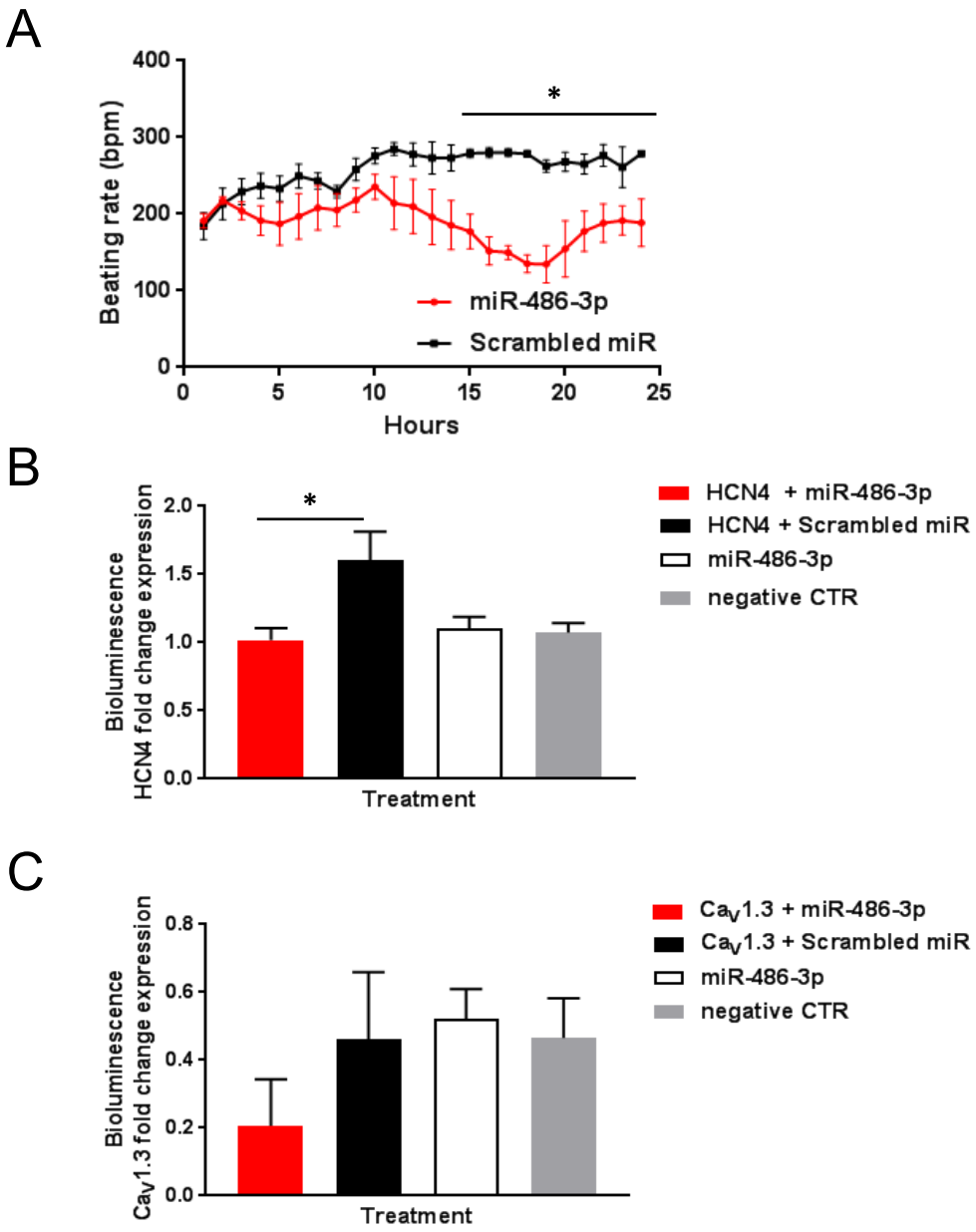

Figure 4. A. Extracellular membrane recording of *ex vivo* rat SN preparation mean beating rate of miR-486-3p transfection vs. control (scrambled miR). Data was analysed using student's t-test (GraphPad Prism 7), * indicates p≤0.05. Graphs represent mean ± standard error of the mean (SEM), n=9. Luciferase reporter gene assay showing B. HCN4 3'UTR or C. $Ca_V1.3$ 3'UTR is post-transcriptionally repressed by miR-486-3p. Luciferase activity is shown 24 hours after co-transfection of H9C2 cells with HCN4/$Ca_V1.3$ 3'UTR and control (scrambled miR), miR-486-3p only, or negative control (culture media only). Data was analysed using One-Way ANOVA (GraphPad Prism 7) B. * indicates p≤0.05 and C. p≥0.05. Graphs represent mean ± SEM, n = 3 batches of cells with 4 replicates.

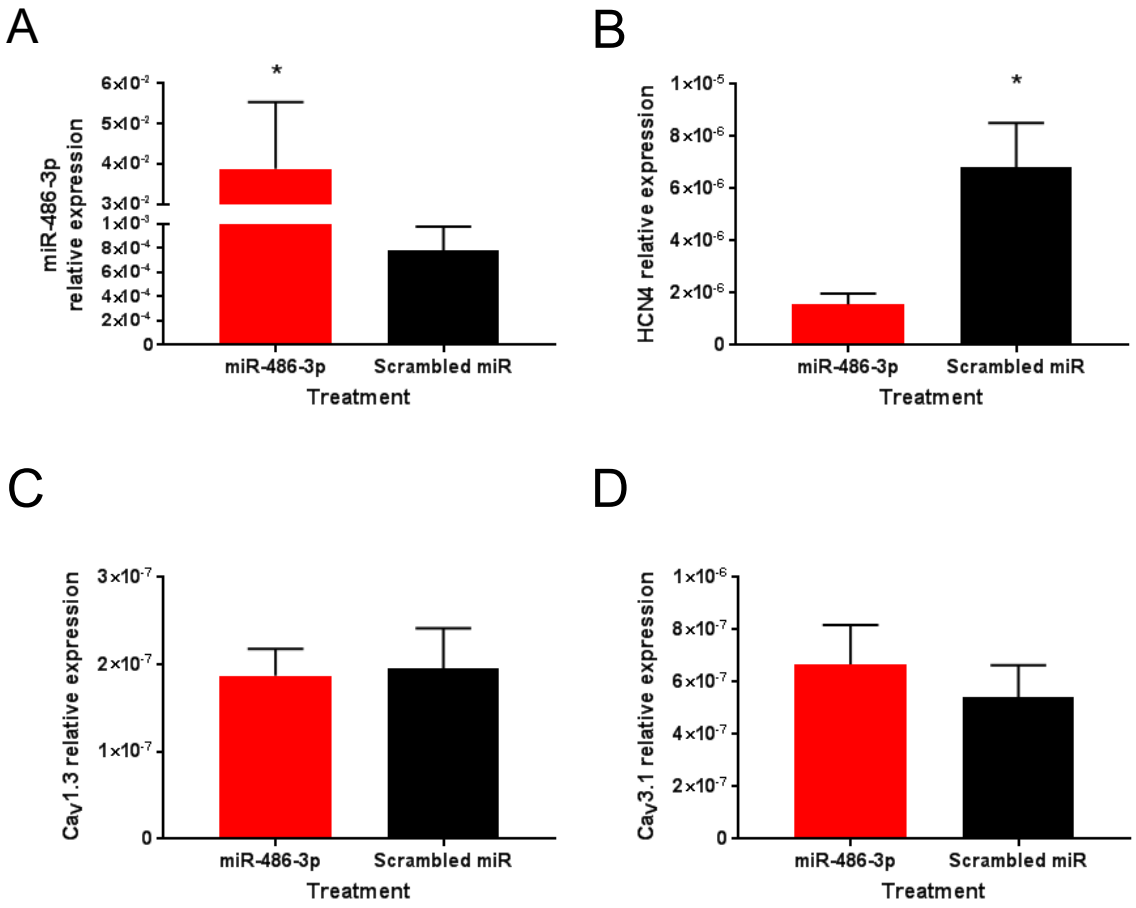

Figure 5. Expression of A. miR-486-3p mRNA (measured by qPCR) in rat sinus node preparation after 24-hour period of transfection**.** Data are normalised to RNU1A1 housekeeper gene. B. HCN4 mRNA C. $Ca_V1.3$ mRNA and D. $Ca_V3.1$ mRNA mRNA (measured by qPCR in rat sinus node preparation after 24-hour period of miR-486-3p transfection. Data are normalised to 18S housekeeper expression. Data was analysed using student's t-test (GraphPad Prism 7), * indicates $p \leq 0.05$. Graphs represent mean ± standard error of the mean (SEM), n=4.

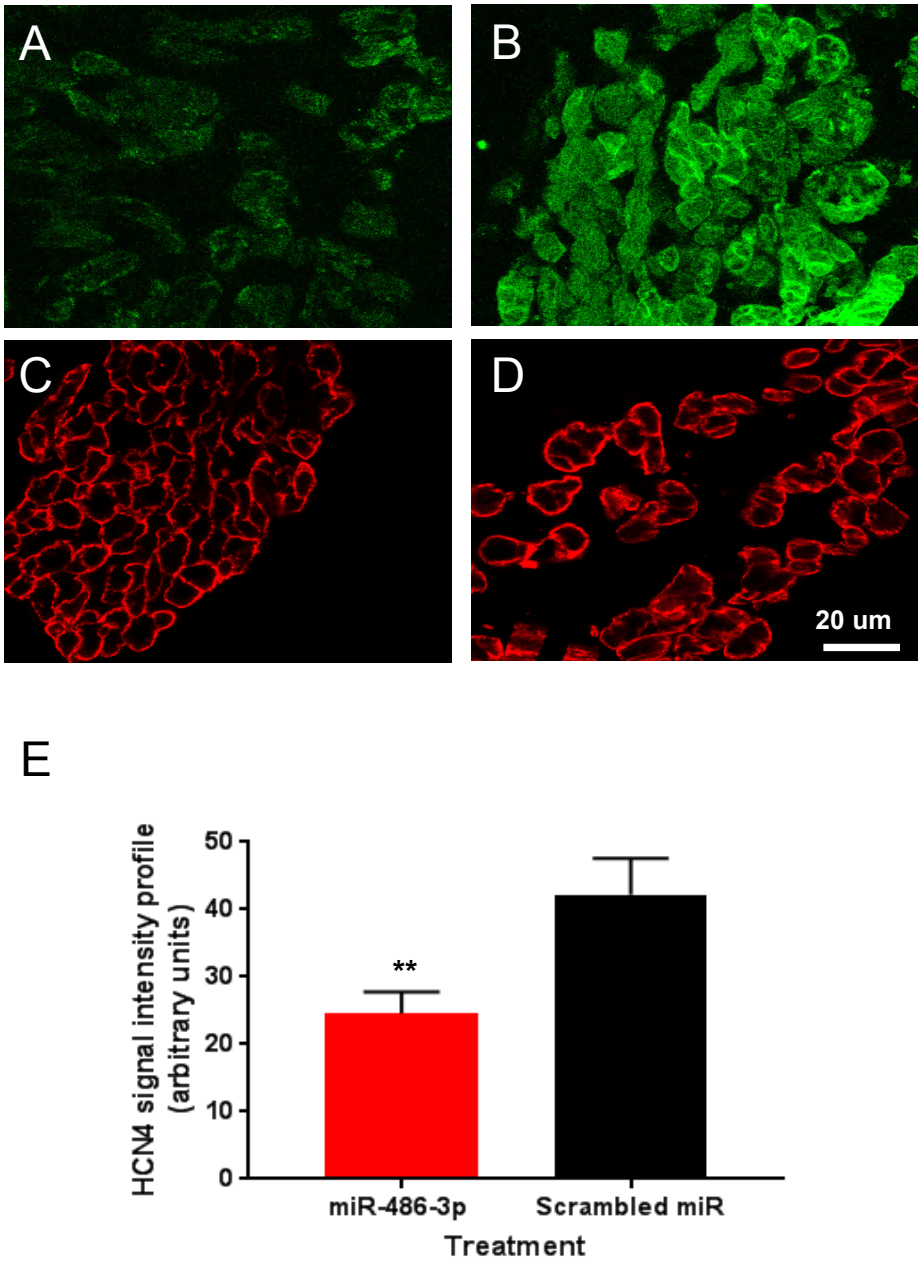

Figure 6. HCN4 (FITC-conjugated) and caveolin3 (Cy3-conjugated) expression in *ex vivo* rat sinus node preparation transfected with A and C miR-486-3p and B and D control (scrambled miR). Images were taken from the sinus node region of the preparations and immunofluorescent signal was detected with confocal microscope (Zeiss LSM5, Carl Zeiss Microscopy). Images were taken with Pascal software (Zeiss Microscopy). HCN4 signal profile was measured using Volocity 4 image analysis software. Data was analysed using student's t-test (GraphPad Prism 7), ** indicates $p \leq 0.005$. Graphs represent mean ± standard error of the mean (SEM), n=5.

4.3 Data supplement

Material and methods

Bioinformatics

We looked into the expression of the most abundant microRNAs in the human SN and RA (Table 1). Ingenuity Pathway Analysis (IPA; Ingenuity Systems, Qiagen Bioinformatics, Redwood city, CA) determined microRNAs targeting those mRNAs molecules that are involved in the pacemaker mechanisms of the SN. Table 1 compared 7 of these human microRNA sequences to their respective rat sequences to verify they are conserved amongst the species. Verification was performed using miRBase website (Faculty of Life Sciences, University of Manchester). TarBase database, miRecords (http://mirecords.biolead.org/), TargetScan (http://www.targetscan.org/) [1], and RNA22 (https://cm.jefferson.edu/rna22/) [2] were used to predict the number of binding sites that occur between the 7 human microRNA sequences and their target rat mRNAs, as functional validation was performed in rat tissue (Table 2).

Animals

Male Wistar-Hanover rats (Charles River UK Ltd, Kent, UK, 230-250 g) were terminated in accordance with the Animal (Scientific Procedures) Act 1982 and the ethical standards of the University of Manchester. In total 64 rats were used in this study.

Dissection solution

Dissections were performed in standard physiological solution i.e. Tyrode's solution, containing NaCl 120 mM, CaCl 1.2 mM, KCl 4mM, $MgS0_4.7H_20$ 1.3 mM, $NaH_2P0_4.2H_2O$

1.2 mM, $NaHC0_3$ 25.2 mM, glucose 5.8 mM. The solution was prepared on the day of the experiment, bubbled with 95% O_2/5% CO_2, and maintained at 37^0C.

Sinus node preparations

The rats were humanely euthanised via carbon dioxide inhalation and cervical dislocation. Preparations were dissected out as previously described [3]. The animal's chest was opened; its heart was dissected out and placed in 37^0C Tyrode's solution. Lungs, trachea, thyroid gland, and additional connective tissue were excised. The dissection of the sinus node preparation was performed according to the following protocol: the apex of the heart was excised; the right side of the heart was unfurled by producing a transverse incision from the inferior most point of the right ventricle, through the tricuspid valve, reaching the upper end of the superior vena cava. The surrounding fat and connective tissue, together with the left atrium and ventricles were removed, leaving the RA, containing the SN and the superior vena cava. The SN preparation was then stretched and pinned down in a silicone-covered glass dish with dissection pins. About 2 µl transfection mixture, containing 6 µl 1 x Opti-MEM, reduced serum medium (Life Technologies, Warrington, UK), 1.5 µl Lipofectamine RNAmix (Life Technologies, Warrington, UK), and 2.5 µl microRNA was injected with a 10 µl NanoFil syringe (World Precision Instruments, Hitching, UK). miR-1-3p (MC10617), miR-30c-5p (MC11060), miR-133a-3p (MC10413), miR-371-3p (MC12262), miR-153-3p (MC10122), miR-429 (MC10221), and miR-486-3p (MC12986) were purchased from Life Technologies, Warrington, UK. Injection was aimed at the bifurcation of the SN artery, where the SN region is expected to lie. Control preparations were transfected with Cy3-labelled Pre-miR negative control (Thermo Fisher Scientific, Altrincham, UK). The dissection medium was changed to Opti-MEM medium, containing 5% foetal bovine serum (Life Technologies, Warrington, UK). Preparations were

incubated at 37°C/5% CO_2. The culture medium was changed eight hours after injection to Advanced DMEM/F-12 medium (Life Technologies, Warrington, UK), containing 10% feotal bovine serum and penicillin, and 1% penicillin-streptomycin (Sigma-Aldrich, Dorset, UK).

Extracellular potential recording

To ensure that the SN and RA tissue was driving the atrial muscle, extracellular potentials were recorded from the right atrial appendage using two 0.15 mm diameter stainless steel electrodes (ADInstruments, Oxford, UK) insulated with silicone to within 3-4 mm of the tips as previously described [3]. The electrodes were pinned in the RA. In addition, the culture medium surrounding the preparation was grounded with a 0.15 mm wire earth electrode. The electrodes were connected to a PowerLab 4/35, 4-channel recorder (ADInstruments, Oxford, UK). Extracellular potentials were continuously recorded using Powerlab and LabChart v7 software (ADInstruments, Oxford, UK). The average beating rate of the SN preparation was calculated via the detection of a deflection greater than two standard deviations as a paced beat. The SN preparation was kept and spontaneous electrical activity was measured for 24 hours. The tissue was then collected for further experiments.

Plasmids

Human HCN4 (NCBI Reference Sequence: NM_005477.2; HmiT088528-MT06), $Ca_V1.3$ (NCBI Reference Sequence: NM_000720.2; HmiT054373-MT06), or Tbx18 (NCBI Reference Sequence: NM_001080508.1; HmiT022062-MT06) 3'UTR-containing plasmids were purchased from GeneCopoeia, Rockville, MD. The pEZX-MT06 luciferase microRNA expression vector contained reporter genes for luciferase and Renilla luciferase.

The amplification of the plasmids was performed as follows: *E.coli* cells (DH5α, Sigma-Aldrich, Dorset, UK) were transformed with the plasmids. A single bacterial colony transfected with the plasmid was incubated in 2 ml LB medium, containing 100 μg/ml ampicillin overnight at 37°C, shaking at150 rpm. Plasmid DNA was purified from the transduced *E.coli* using Purelink Plasmid Kit (Thermo Fisher Scientific, Altrincham, UK) according to manufacturer's protocol. Restriction digest, to confirm the presence of the correct ligation of the microRNA 3'UTR inserts in the pEZX-MT06 vector, was then carried out. 1μg of each plasmid was incubated with restriction endonuclease enzymes EcoRV and HindIII (New England Biolabs, Ipswich, Massachusetts, USA) overnight at 37°C. DNA gel electrophoresis was then performed to confirm the presence of the expected DNA fragments.

Cell culture, transfection, and luciferase reporter gene assay

Rat cardiac H9C2 cells (ATCC, Middlesex, UK) were maintained in Dulbecco's modified Eagle's medium (DMEM; Invitrogen, UK), containing 10% foetal bovine serum, and 1% penicillin-streptomycin. H9C2 cells were seeded at a density of 5 x 10^5 cells per well in 24-well plates 24 hours prior to the transfection experiment. Cells were transfected with 500 ng HCN4, $Ca_V1.3$, or Tbx18 3'UTR plasmids and 1 μg miR-486-3p or miR-429, scrambled miR, or culture media only. Transfection agent used was Lipofectamine 2000 (Invitrogen, UK) in accordance with the manufacturer's instructions. The DNA-Lipofectamine transfection complex was incubated for 20 minutes at room temperature and then transferred at 37°C and 5% CO_2 for a 24-hour period, followed by washing with phosphate buffer saline and lysis via passive lysis buffer (Promega, Southampton, UK) on a rocker for 20 minutes.

Luciferase reporter gene activity, which is directly proportional to mRNA expression of

the target gene, was assessed using luciferase assay system (Promega, Southampton, UK). Luminometer (Berthold Technologies Lumat LB 9507, Bad Wildbad, Germany) was used to measure the bioluminescent activity in 10 μl cell lysate. Each measurement was supplemented with 50 μl assay reagent injection, followed by 2 seconds of pre-reading delay and 7 seconds reading period. Each assay was performed in quadruplicates and repeated three independent times. The luciferase assay activity was normalised to Renilla (Promega, Southampton, UK) activity, and expressed as a ratio. The procedure protocol used was previously described [4].

Total RNA extraction

After 24–hour incubation of rat SN preparations, the tissue was washed with Tyrode's solution and a ~1 mm x 1 mm biopsy was collected from the SN around the SN artery bifurcation, and a separate biopsy from the pectinate muscles of the RA. The tissue samples were flash frozen in liquid nitrogen and stored at -80°C. Total RNA was extracted using Rneasy Micro Kit (Qiagen, Manchester, UK) according to the manufacturer's instructions. RNA quality and quantity was determined using a NanoDrop ND-1000 spectrophotometer (NanoDrop Technologies, Wilmington, DE, USA). The procedure protocol used was previously described [4].

Quantitative PCR for miR-486-3p expression

MicroRNA cDNA was synthesised from total RNA, using qScript microRNA cDNA Synthesis kit (Quanta BioScience, VWR International Ltd, Leicestershire, UK) according to manufacterer's instructions. miR-486-3p primer was purchased from Exiqon, Vedbaek, Denmark. qPCR was carried out using ABI Prism 7900 HT Sequence Detection System (Applied Biosystems/Life Technologies Corporation, Carlsbad, CA, USA). The reaction

mixture contained 1 µl cDNA, 1 µl primer assay, 5 µl SYBR Green Master Mix (Applied Biosystems, Carlsbad, CA), and Dnase-free water. All samples were run in triplicates. The reaction conditions were: 95°C for 10 minutes, 40 cycles of 95°C for 10 seconds and 60°C for 1 minute. The melting curve conditions were 95°C for 15 seconds, 60°C for 15 seconds and 95°C for 15 seconds. MicroRNA expression was calculated by the $2^{-\Delta Ct}$, where ΔCt is $\Delta Ct_{(Target)}$-$\Delta Ct_{(Housekeeper)}$ method and normalised to the expression of RNU1A1 (Qiagen, Manchester, UK).

Quantitative PCR for HCN4, $Ca_V1.3$, and $Ca_V3.1$ mRNA expression

Messenger RNA (mRNA) cDNA was synthesised from total RNA, using Rneasy Micro Kit for mRNA cDNA (Qiagen, Manchester, UK) according to manufacterer's instructions. HCN4, $Ca_V1.3$, and $Ca_V3.1$ were purchased from Qiagen, Manchester, UK. The reaction conditions were as follows: 50°C for 2 minutes, 95°C for 10 minutes, 40 cycles of 95°C for 15 seconds, 60°C for 1 minute. The melting curve conditions were the same as described above. mRNA expression was calculated as described above and normalised to the expression of GAPDH (Qiagen, Manchester, UK).

Immunohistochemistry

Following miR-486-3p injection in rat SN preparations experiments, 4 microRNA- and 4 scrambled miR-injected preparations were flash frozen in OCT (BDH, UK) with isopentane (Sigma-Aldrich, Dorset, UK) and stored at 80 °C. The SN preparations were then serially sectioned at 10 µm, using a cryostat (Meyer Instruments, Houston, TX) at temperatures ranging between -10 and -20°C. SN preparation sections were mounted onto SuperFrost Plus glass slides (Thermo Fisher Scientific, Altrincham, UK) and stored at -80 °C.

Briefly, the sections were fixed in 10% neutral buffer formalin (Sigma-Aldrich, Dorset, UK) for 30 minutes and washed with 0.01 M phosphate buffer solution (PBS; Sigma-Aldrich, Dorset, UK) three times at 10-minute intervals. The tissue was permeabilized in 0.1% Triton X-100 in PBS for 30 minutes, and washing with PBS was repeated. Blocking of the non-specific protein sites was carried out using 1% bovine serum albumin in PBS for 1 h at room temperature. The tissue sections were then incubated overnight at 4 °C with a primary antibody for rabbit HCN4 (AGP-004; Alomone Labs, Jerusalem, Israel) or mouse caveolin3 (610421; BD Transduction Laboratories, USA) at a concentration 1:100 in 1% BSA. On the following day, tissue sections were washed in PBS three times at 10 minute-intervals. They were then incubated for 2 hours at room temperature with secondary antibodies, respectively: Anti-rabbit (Goat) FITC (fluorescein isothiocyanate)-conjugated (Life Technologies, Warrington, UK), or anti-mouse (donkey) Cy3 (indocarbocyaninne)-conjugated (Millipore, Burlington, MA). They were diluted 1:1000 in 1%BSA. The tissue sections were then washed final three times at 10-minute intervals and mounted with anti-fade Vectashield H-1000 (Vector Laboratories, Peterborough, UK), glass coverslips and sealed with nail varnish. The procedure protocol used was previously described [5].

Immunofluorescent signal was detected with a confocal microscope (Zeiss LSM5, Carl Zeiss Microscopy) and images were taken with Pascal software (Zeiss Microscopy). HCN4 was used as a positive marker of the SN area, and it was used in order to identify the SN. HCN4 signal profile of SN from miR-486-3p or scrambled miR (control) transfected *ex vivo* rat SN preparations was determined using Volocity 4 image analysis software (PerkinElmer, Waltham, MA) after background correction. Background signal level was determined by measuring the signal intensity of the control experiment where application

of primary antibody was omitted. The average intensity measurements were then taken and compared between the two groups.

Statistical analysis

Prism 7 (GraphPad software, La Jolla, CA) was used to perform the statistical analysis and plot the results of the study. Two-groups experiments were compared using student's t-test. If data were not normally distributed, the Mann-Whitney test was used. Three and more-group experiments were compared using One-way ANOVA. Figures represent mean ± standard error of the mean (SEM) values. P values ≤0.05 were considered as statistically significant.

References

1. Agarwal V, Bell GW, Nam JW, Bartel DP. Predicting effective microRNA target sites in mammalian mRNAs. *Elife.* 2015;4.

2. Miranda KC, Huynh T, Tay Y, et al. A pattern-based method for the identification of microRNA binding sites and their corresponding heteroduplexes. *Cell.* 2006;126(6):1203-1217.

3. Morris GM, D'Souza A, Dobrzynski H, et al. Characterization of a right atrial subsidiary pacemaker and acceleration of the pacing rate by HCN over-expression. *Cardiovascular Research.* 2013;100(1):160-169.

4. D'Souza A, Pearman CM, Wang YW, et al. Targeting miR-423-5p reverses exercise training-induced HCN4 channel remodeling and sinus bradycardia. *Circulation Research.* 2017;121(9):1058-67.

5. Chandler NJ, Greener ID, Tellez JO, et al. molecular architecture of the human sinus node insights into the function of the cardiac pacemaker. *Circulation.* 2009;119(12):1562-1575.

Chapter 5

5 Do human heart pacemaker cells have t-tubules?

5.1 Other authors contribution to the paper

The vast majority of the experimental work for this study was performed by myself, I also created and wrote the paper. I greatly appreciate and acknowledge the input from the following authors:

- Yanwen Wang and Louise Miller carried out single cell isolation
- Andrew Atkinson aided me with confocal microscopy and technical support
- Luke Stuart provided critical and valuable comments on my manuscript
- Balint Borbas was an undergraduate student who aided me with part of the experimental work and analysis under my supervision
- Filip Perde and peter Molenaar provided the human SN specimens
- Halina Dobrzynski had a major supervisory role and aided me with the experimental work and provided critical and valuable comments on my manuscript

5.2 Paper

Do human heart pacemaker cell have t-tubules?

Maria A. Petkova[1], Yanwen Wang[1], Andrew J. Atkinson[1], Luke E. Stuart[1], Louise Miller[1], Balint Borbas[1], Filip Perde[2], Peter Molenaar[3, 4], Halina Dobrzynski[1]

[1]Cardiovascular Sciences, University of Manchester, Faculty of Biology, Medicine and Health Manchester, UK

[2]National Institute of Legal Medicine, Bucharest, Romania

[3]Queensland University of Technology and [4]Cardio-Vascular Molecular & Therapeutics Translational Research Group, The Prince Charles Hospital, Brisbane, Australia

Corresponding Author:

e-mail address: halina.dobrzynski@manchester.ac.uk

Address: CTF Building, 46 Grafton Street, Manchester M13 9NT

Tel: +441612751182, Fax: +441612751183

Abstract

Every heartbeat is generated by spontaneously depolarising specialised nodal cells that make up the sinus node (SN). The SN unique properties depend on two complex mechanisms - the membrane-voltage and the Ca^{2+} clocks, regulated by strictly defined expression of ion channels, connexins, and Ca^{2+}-handling proteins. In the working myocardium, these proteins are accumulated in specialised membrane structures– the transverse tubules (t-tubules). It is well known that small mammals do not exhibit t-tubules in their atrium, but such structures are observed in the atria of bigger mammals such as sheep. No information on t-tubules in the human SN is present yet. The aim of our study was to determine if t-tubules are present in the human SN as well as surrounding atrial myocardium. Expression of dystrophin, Na^{+}-Ca^{2+} exchanger (NCX1), sarcoplasmic-endoplasmic reticulum calcium adenosine triphosphatase (SERCA2a), α-actinin, and ryanodine receptor 2 (RyR2) were investigated. Staining with wheat germ agglutinin (WGA, specific marker of t-tubules) demonstrated that human RA cells contain t-tubules, but these structures are very sparse in the SN. Experiments in single nodal cells from rat and mouse showed no expression of a t-tubular network, but striated expression pattern of RyR2 was obtained similar to the human sections, suggesting its manner of organisation is dependent on α-actinin colocalisation.

Key words: sinus node, right atrium, pacemaker mechanisms, membrane and Ca^{2+} clocks, NCX1, SERCA2a, α-actinin, RyR2, t-tubules

Introduction

The cardiac heartbeat is initiated in a specialised nodal structure, known as the sinus node (SN) (1-3). This structure is characterised by specific molecular and functional properties that distinguish it from the surrounding right atrial (RA) myocardium. Automaticity is most prominent property of the SN. It is characterised by the ability of the SN to spontaneously generate electrical impulses, which are detected as a diastolic depolarisations during the SN action potential (4).

The human SN structure is located subepicardially within the posterior wall of the right atrium, and it extends from the superior vena cava towards the inferior vena cava along the sinus node artery (3). Chandler et al., performed histological and immunohistochemical experiments on *ex vivo* human hearts, and demonstrated that SN parameters are characterised with 29.5 mm length, 1.8 mm height, and 6.4 mm width (5). Recent 3D computer modelling *ex vivo* studies of the human heart showed this structure has similar dimensions to what has been already reported by Chandler et al., (6).

Compared to the working myocardium, SN cells are sparse, and are densely embedded into fibrous connective tissue (3, 5). SN cells exhibit smaller diameter, with few mitochondria and poorly organised myofilaments compared to the surrounding RA (7).

The specialised function of the SN cells is to generate action potentials, and it is regulated by two interconnected mechanisms – the membrane voltage and the Ca^{2+} clocks (8, 9). The membrane voltage clock comprises of SN cell membrane voltage-gated ion channels, which upon activation during diastolic depolarisation, generate inward positive ionic currents, which further depolarise the SN cells membrane and cause action potential

generation. The major currents produced during diastolic depolarisation are I_f, $I_{Ca,L}$, $I_{Ca,T}$ (4, 10).

The Ca^{2+} clock, on the other hand, regulates the Ca^{2+} cycling in the SN. I_f –induced membrane depolarisation causes L-type Ca^{2+} channels opening and conduction of a large scale positively charged Ca^{2+} inward current (11). Higher intracellular Ca^{2+} concentrations activate ryanodine receptor 2 (RyR2) located at the sarcoplasmic reticulum (SR) membrane, resulting in Ca^{2+} influx from the SR towards the cytosol and myofilament contraction – Ca^{2+}-induced Ca^{2+} release (9, 11). High cytosolic Ca^{2+} concentrations activate the cell membrane electrogenic Na^{+}-Ca^{2+} exchanger (NCX1), which extrudes 1 calcium ions in exchange for 3 sodium ions, causing accumulation of net positive charge inside the cells (12). Higher Ca^{2+} concentration is also recycled back to the SR through the sarcoplasmic-endoplasmic reticulum calcium adenosine triphosphatase (SERCA) at the SR membrane (13). Thus, Ca^{2+} handling by the SR plays a major role in SN automaticity by modulating $I_{Ca,L}$, I_f, and NCX1 (12, 14-17). Lyashkov et al., reported robust expression of RyR2, NCX1, and SERCA2a in rabbit SN cells, where their disabling caused abolition of spontaneous beating, leading to the conclusion that SN automaticity is directly dependent on efficient intracellular Ca^{2+} handling, which initiates the SN impulse (18).

In order to overcome the hyperpolarisation effect of the surrounding RA and produce an electrical impulse, the small SN structure has developed a weak electrical coupling mechanism (19). The SN was reported to express significantly lower connexin43 (Cx43) levels in comparison with the working myocardium, where it plays a role of a large conductance channel and provides strong coupling between myocytes (20, 21). This mechanism guarantees the SN depolarising membrane potential would not be suppressed by the more negative resting membrane potential characteristic for the RA.

Transverse tubules (t-tubules) are membrane structures that act as a signalling hub, which regulates the excitation-contraction mechanism in the cardiomyocytes by synchronous rise of systolic Ca^{2+} (22). They are highly branched invaginations of the cardiomyocytes membrane, which form a complex network with transverse and longitudinal elements, and are located around the myofilaments where they are attached to the sarcomeric Z-discs (23, 24). T-tubules' most prominent function is the excitation-contraction coupling they produce through their high concentration of L-type calcium channels at their membrane (25). A dense SR network surrounds the t-tubules, facilitating Ca^{2+} -induced Ca^{2+} release following the initial Ca^{2+} entry through L-type Ca^{2+} channels during the action potential, and regulates the synchronous rise of intracellular Ca^{2+} through RyR2 at the junctional membrane of the SR (26, 27). The closely positioned L-type Ca^{2+} channels and RyR2 build Ca^{2+} releasing units, which in turn initiate Ca^{2+} transients as a result of each action potential generated by the SN (25, 28).

Alpha actinin (α-actinin) is a major component and a marker of the Z-discs that define the boundaries of the sarcomere, and anchors the thin actin filaments (29). A-actinin is a member of the dystrophin proteins superfamily, and its major role in the Z-discs is to cross-link thin actin filaments and titin from neighbouring sarcomeres (30, 31). Apart from its structural role in the Z-discs, α-actinin has an important functional role in the cardiomyocytes, where it colocalises with RyR2 clusters and thus allows Ca^{2+} sparks at close proximity to the Z-discs (32).

Dystrophin is a membrane protein, which apart from its structural role, serves a functional role by localising nitric-oxide synthase to the sarcolemma (33). Dystrophin also colocalises with the t-tubules (34-36), myofibrils, and Z-discs of cardiomyocytes, and downregulation

of myofibrillar dystrophin in the heart leads to cardiac insufficiency, suggesting it has a unique role at the sarcomere (37).

To our current knowledge, unlike ventricular cardiomyocytes, atrial cardiomyocytes in small mammals such as mouse, rat, and rabbit lack a t-tubular network (38-41). Larger mammalian species such as sheep, pig, and human, however, were found to express t-tubules in their atrial myocytes (42-45). Nothing is known yet about the presence of t-tubules in the human SN. To this end, the aim of the current study was to determine the t-tubular structures in the human SN and its surrounding RA by mainly examining Ca^{2+} clock proteins. We hypothesise that the organisation of the Ca^{2+} clock proteins in the SN does not depend on the t-tubular organisation, rather than the optimal Ca^{2+} clock mechanism, which controls action potential initiation.

Materials and methods

Details of human specimens

Tissue samples were obtained from six unused human donor hearts from male and female specimens, aged between 19 and 60 years old. Cause of death was road accident, suicide, intracranial, or subarachnoid haemorrhage. The SN and surrounding RA tissues were dissected out, frozen in isopentane and kept at -80^{o}C as previously described by (5, 6, 21, 46) in accordance with the Australian and Romanian local ethical approval procedures. The samples were sent to the University of Manchester on dry ice and kept at -80^{o}C at Dr. Halina Dobrzynski's laboratory in accordance with the Human Tissue Act. These samples were used for immunohistochemical experiments.

Cryosectioning of human SN and surrounding RA

The human tissue specimens, containing SN and the surrounding RA, were fixed to a cryostat disc with OCT and serially sectioned with cryostat (Zeiss Microm HM500) at temperatures ranging between -10 and -20^{o}C. Tissue samples were sectioned at a thickness of 30 μm at transverse plane orientation to the superior vena cava, and each section contained the SN and surrounding RA. Sections were mounted onto SuperFrost Plus (Thermo Fisher Scientific) glass slides and stored at -80^{o}C.

Immunohistochemistry

Sections were fixed in 10% neutral buffer formalin (Sigma) for 30 minutes and washed 3 times for 10 minutes each wash in 0.01 M phosphate buffer saline (PBS, Sigma), containing 0.138 M NaCl, 0.027 M KCl at pH 7.4. Sections were then placed in 0.1% Triton X-100 (Sigma) for 30 minutes in order to permeabilze the cells and allow the primary and secondary antibodies to bind to and label their respective antigen sites. Permeabilization allows all the reagents to reach and bind their epitopes. Tissue sections were blocked in 1% bovine serum albumin (BSA, Sigma) in PBS for 1 hour at room temperature in order to prevent antibody binding to non-specific sites, and thus decrease background signal. Primary antibodies listed in Table 1 were diluted in 1% BSA. Sections were incubated with primary antibodies overnight at room temperature. Single and double labelling with primary antibodies and/or WGA or phalloidin dye were used in the study in order to characterise the tissue. The following day, secondary antibodies listed in Table 2 were applied on the tissue sections. Secondary antibodies were also diluted in 1% BSA. They were site-specific for the species in which the primary antibodies were raised, and they were conjugated to fluorochromes. The fluorochromes used are described in Table 1. Incubation period with secondary antibodies was 2 hours at room temperature. More than 1

type of flurochromes was used in order to allow double-labelling on the same tissue section. Double labelling was achieved by the use of two different antibodies raised in different animal species, and the use of different fluorochrome-conjugated secondary antibodies targeting the primary antibodies they are specific to. Sections were then mounted with mounting medium Vectashield (Vector laboratories) with/without propidium iodide, covered with glass coverslips and sealed with nail varnish. Immunofluorescence was detected by Zeiss LSM5 confocal microscope (Carl Zeiss Microscopy). Images were taken with Pascal software (Zeiss Microscopy).

Single cells isolation

Four male Wistar-Hanover rats and four C57 male mice were sacrificed by cervical dislocation in accordance with the Home Office procedures. SN cells from rat as well as cells from left, right ventricles, and ventricular septum from rat, and SN cells from mouse were dissected into single cells by mechanical and enzymatic procedures. Tissue samples measuring 1 mm x 2 mm were dissected out and divided into strips, which were further cut into smaller rectangular pieces. The tissue pieces were enzymatically dissociated into single cells using a solution containing collagenase IV (224 U ml^{-1}, Worthington), elastase (1.42 U ml^{-1}, Sigma-Aldrich), and protease (0.45 U ml^{-1}, Sigma-Aldrich) (41, 47).

Immunocytochemistry

50 µl isolated cells in Tyrode's physiological solution were plated on Superfrost plus slides and contained via encircling with a hydrophobic PAP pen, and left for 30 minutes to allow them to attach to the base of the slides. The single cells plated onto glass slides were then horizontally positioned in an incubating tray and fixed in 2% neutral buffer formalin for 10 minutes. Cell membrane permeablization was performed using 0.1% Triton X-100

(Sigma) for 10 minutes. Primary antibody incubation was carried out overnight at 4^{o}C. The rest of the immunocytochemistry steps were the same as the steps performed in the immunohistochemistry protocol described above. The washing steps were performed very gently in order to preserve as many single cells as possible. Overnight incubation with primary antibodies and WGA dye was done at 4^{o}C.

Results

The SN region was differentiated from the RA region in accordance with well-established methods in our laboratory – via Masson's trichrome histological staining for cardiomyocytes and connective tissue, and immunolabelling for connexin43 as a negative marker for the SN (data not shown) (5, 21).

Figure 1 depicts labelling with antibody to dystrophin in SN and RA human transverse sections. Both SN and RA cells exhibit a thin and continuous layer of immunostaining at their cell membranes. A few RA cells also exhibit short intracellular invaginations of the cell membrane that could be observed at higher magnification in Figure 1 D, in contrast with Figure 1 C, where no invaginations in the SN cells are observed. These cell membrane invaginations correspond to t-tubules.

Figures 2 and 3 show the fluorescent signal produced by WGA (stained in green) in transversely sectioned human SN and RA, respectively. WGA labels the cardiomyocyte membrane and its intracellular invaginations (t-tubules), and it is non-specifically accumulated in the extracellular space around the cells. Apart from the membrane fluorescent signal, intracellular striated expression pattern is observed in the human RA (indicated with white asterisks), suggesting that WGA is also staining the t-tubular network of the working myocardium cells. Few such invaginations are observed in the SN, and

many more are present in the RA sections. WGA allows differentiation of the cardiomyocytes from the high levels of surrounding connective tissue, which is typical for human cardiac tissue sections.

Figure 4 depicts labelling to antibody for the SR Ca^{2+} release channel, RyR2, throughout longitudinal SN and RA sections. Both tissue types exhibit intracellular striated labelling throughout the cytosol (Figure 4 A, B). Figure 4 D shows a higher magnification image of a RA tissue section exhibiting RyR2 striated punctate labelling adjacent to the outer cell membrane as well as to the intracellular striations. Figure 4 C shows a high magnification image of the SN, which is characterised by intracellular striated expression pattern, but no outer cell membrane RyR2 labelling. The intracellular striated RyR2 labelling is separated from the outer cell membrane RyR2 labelling by a gap.

Figures 5 A and B represent staining of SN and RA longitudinal tissue sections to antibody labelling RyR2 and WGA dye, revealing no co-localisation of RyR2 and t-tubules in either tissue types, suggesting the intracellular striated expression pattern of RyR2 does not correspond to the t-tubular structural organisation in the cell.

RA and SN longitudinal tissue sections labelled for antibody to SR Ca^{2+} pump, SERCA2a, revealed robust uniform intracellular striated labelling, which corresponds to extensive highly developed SR network, located adjacent to the Z-discs (Figure 6 A, B). Higher magnification image of the SN sections (Figure 6C) depicts some SERCA2a labelling adjacent to the outer cell membrane too, in contrast with RA, where only intracellular labelling was observed (Figure 6D).

Figures 7 A and B show NCX1 labelling in SN and RA transverse tissue sections. High magnification image of the SN (Figure 7C) depicts NCX1 expression at the outer cell

membrane of SN cells, as well as some intracellular punctate labelling, which is related to few, sparse t-tubular invaginations. In contrast with the SN, Figure 7 D presents NCX1 punctuate, interrupted outer cell membrane labelling of the RA, which characterises more robustly developed t-tubular intracellular invaginations of the cell membrane in comparison with the SN (Figure 7C).

Figures 8 and 9 demonstrate antibody labelling to α-actinin (a sarcomeric Z-discs marker) of SN and RA longitudinal sections conjugated to Cy3 and FITC fluorochromes, respectively. Both SN and RA exhibit well-organised intracellular transverse striations along the Z-discs of the sarcolemma. A-actinin expression pattern appears to be similar to RyR2 labelling at the junctional and corbular SR.

In order to study the organisation of the t-tubular network in the human SN and RA, and to determine if its pattern depends on RyR2, Z-discs or SR organisation, we stained human SN longitudinal sections with α-actinin and WGA. A-actinin showed no overlapping with WGA signal (Figure 10 A). Similarly, no overlap of α-actinin and WGA signal was demonstrated in RA (Figure 10 B). The absence of overlapping fluorescent signal of α-actinin and WGA indicates that Z-discs and t-tubules are not colocalised in human SN and RA tissue. Z-discs labelled with α-actinin do not colocalise with WGA-stained t-tubules, leading to the conclusion that t-tubular organisation in human SN and RA is independent from sarcomeric Z-disc distribution.

Consecutive labelling to α-actinin and RyR2 antibodies of human SN and RA (Figure 11 A and B) longitudinal sections allowed us to observe the relationship between Z-discs and the SR Ca^{2+} release channel, RyR2. Complete overlap of the red and green fluorescent signals in both SN and RA (Figure 11 C and D) was exhibited as strong yellow fluorescence demonstrating colocalisation and close proximity of the Z-discs of the sarcomere and

RyR2 within the SR membrane. These data show that the robust RyR2 intracellular striated expression pattern in both SN and RA is independent from t-tubular organisation, since very few t-tubules are present in the SN (Figure 2), and no colocalisation of WGA and RyR2 (Figure 5) or α-actinin (Figure 10) is observed.

Figure 12 depicts phalloidin staining of actin filaments, located between Z-discs within myofibrils at the cardiac sarcomere in human SN and RA longitudinal sections. Both SN and RA sections exhibit intracellular alternating thin and wide striated patterns of staining.

T-tubular expression in small mammal single cardiomocytes was also studied. In order to confirm and identify the expression pattern and colocalisation of t-tubules and RyR2, we labelled rat SN and ventricular myocytes and mouse SN myocytes with RyR2 and WGA dye. WGA fluorescent signal from rat SN myocytes was observed only at the plasmalemma and the nuclear membrane, and no membrane invaginations were present, suggesting the absence of any t-tubular network (Figure 13 A and 14 A). However, the ventricular myocytes labelled with WGA showed strong signal from the plasmalemma and nuclear membrane, and a substantial t-tubular network. T-tubules were observed in all ventricular myocytes and a representative image is included (Figure 13 B). Figures13 C and D show the intracellular striated expression pattern of RyR2 in rat myocytes – regular and well-organised striations in the ventricular myocytes, and irregular and closely apposed striations in the SN cells, accompanied with uninterrupted labelling around the outer cell membrane, separated with a gap from the intracellular striated labelling (Figure 14 B). Similarly to the rat SN cell, mouse SN cells showed a striated expression pattern of RyR2, and no t-tubular signal from WGA (Figure 13 E and 14 C), suggesting t-tubules are absent in small rodent SN cells. These data imply that RyR2 organisation in small mammals and humans is unrelated to the t-tubular network in SN myocytes. Figure 14 D

shows a wide, striated pattern of phalloidin-stained actin, thin filaments in mouse single SN cells under high magnification. Figure 14 E depicts SERCA2a labelling of single mouse SN cell, which exhibits intracellular striated labelling, as well as a ring of labelling at the outer cell membrane, corresponding to the SR network adjacent to Z-discs at the sarcolemma.

Discussion

The major finding of our study is that the human SN exhibits few sporadic t-tubules (Figure 3), whereas the RA demonstrated a more abundant and better-organised t-tubular network (Figure 2) as previously described (42-44). Single SN myocytes from mouse and rat were shown to express no t-tubules, due to the absence of a striated pattern of labelling with WGA (Figure 13 A, E and 14 A, C).

T-tubules have been studied in cardiomyocytes isolated from multiple animal species such as mouse, rat, and rabbit as well as larger mammals – dog, sheep, pig, and human. Across these species, it is well accepted that t-tubules form an extensive and well-organised network in the ventricular myocytes (22, 49, 50). Studies in smaller mammals such as mouse, rat, cat, and rabbit reported absence of t-tubular network in the atria (51-54). In contrast, atrial myocytes from larger mammals and humans were found to express a scarce and irregular t-tubular network compared to the ventricular myocytes (42-44, 55). These results therefore raised the question as to whether t-tubules are present in the human SN myocytes, and if that is conserved among smaller mammals like mouse and rat.

Previous electron microscopy studies reported that t-tubules are not present in rat and hamster SN myocytes, but SR structures were observed, despite the fact that they were not as abundant as in atrial myocytes (56, 57). The expression pattern of WGA in rat and

mouse SN myocytes that we observed showed that there is no t-tubular network, as only membrane fluorescence was observed. Human RA myocytes showed WGA-labelled invaginations to confirm t-tubules are present in the working myocardium.

Human SN and RA membrane labelling with dystrophin showed t-tubular structures in the RA, but not in the SN. Dystrophin is a cytoplasmic structural protein, which connects dystroglycan complexes in the extracellular matrix to the intracellular apparatus, in order to stabilise the plasma membrane during sarcomeric contraction (48). Dystrophin was found to localise at the sarcolemma and the t-tubules where it regulates structural support during contraction (34). Furthermore, an immunolabelling study revealed that dystrophin colocalises more specifically at the Z-discs of the cardiac muscle (37), where it plays a functional role by localising nitric-oxide synthase to the sarcolemma (33). Confirming the functional role of dystrophin in the cardiac muscle, a study reported specific loss of myofibrillar dystrophin during cardiac insufficiency in cardiomyopathic hamster CHF 147 (37). Our study revealed that a limited number of t-tubules are present in the human SN as no invaginations were observed in dystrophin-labelled tissue sections, but some were observed in the RA (Figure 1).

The second important finding we observed was the striated expression pattern of RyR2 is owed to the colocalisation with the α-actinin filaments at the Z-discs of the sarcolemma, but not the t-tubular network. Hiess et al., investigated the distribution of RyR2 in living and fixed ventricular cardiomyocytes from a GFP-tagged knock-in mouse model and reported complete colocalisation of RyR2 with Z-discs (labelled with α-actinin antibody) where Ca^{2+} sparks exclusively originate from (32). Similarly, a 3-D distribution study in single rat ventricular myocytes and human ventricular tissue sections showed RyR2 localisation in close proximity with the sarcomere (58). Jayasinghe et al, reported RyR2

location within 250 nm of the local plane containing Z-discs in rat, rabbit, and human ventricular myocytes, and suggested that RyR2 organisation may be involved in regulation of sarcomere activation through local Ca^{2+} waves propagation (59).

RyR2, SERCA2a, and NCX1 expression were observed in both SN and RA (Figure 4, 6 and 7). Similar expression of NCX1 and RyR2 has been demonstrated in small mammal SN cells, where these Ca^{2+}-handling proteins have been shown to participate in impulse generation (60). NCX1 is activated in response to the increased intracellular Ca^{2+} concentrations, and produces the principal Ca^{2+} extrusion mechanism that initiates outward Ca^{2+} current and thus repolarises the membrane potential (61, 62). Lyashkov et al., looked into the expression of RyR2, NCX1, and SERCA2a in rabbit SN myocytes and reported complete colocalisation of NCX1 and RyR2, suggesting that the spontaneous beating of SN cells is largely affected by the Ca^{2+} cycling process (18). In contrast, Scriven et al., reported that colocalisation of NCX1 and RyR2 is not noticeable in rat myocytes (25), whereas another group showed that both proteins are similarly distributed (63). Apart from Ca^{2+} extrusion, NCX1 was also found to synergistically enhance the voltage sensitive Ca^{2+} channels activation during excitation-contraction coupling (64-66). Depending on its location, NCX1 could also exert another function – regulation of Ca^{2+} transient by regulating sarcoplasmic reticulum Ca^{2+} load (67).

The rat and mouse SN myocytes, as well as the human SN sections, exhibited organised, well-defined, striated RyR2 expression pattern. Interestingly, RyR2 fluorescence near the outer cell membrane was also observed in all species, confirming RyR2 is colocalised with the junctional and corbular SR as previously described (41, 68, 69). Junctional SR has been also reported to colocalise with transverse Z-discs in order to traffic cardiac calsequestrin (a Ca^{2+}-binding protein which buffers Ca^{2+} in the SR) from the rough endoplasmic

reticulum to the junctional SR (70). Electron microscopy studies in finch and hummingbird hearts confirm colocalisation of junctional and corbular SR with Z-discs (71). Our previously published data showed RyR2 colocalises with SERCA2a (41) and its striated expression pattern depends on SR organisation (18, 41). It has been previously shown that there are numerous couplings between the t-tubular system and RyR2, located on the SR, in rat ventricular and atrial myocardium (56). Another study reported a strong relationship between the Ca^{2+} transient and the Z-discs (that are built from actinin filaments), by showing that the breakdown of Z-discs during apoptosis causes loss of sarcomeric protein immunoreactivity (Maruyama et al., 2006). These studies and the finding that RyR2 completely colocalises the Z-discs of the sarcomere, suggest there is a close structural and functional relationship between RyR2, sarcomere Z-discs and junctional and corbular SR striated expression pattern in the heart.

WGA labelling of rat ventricular myocytes confirmed the presence of a well-organised t-tubular network. A similar technique has been used in various other species such as dog, sheep, cow, horse, and human to confirm the presence and the organisation of the t-tubular network in their ventricular tissue (44, 72). Phalloidin-staining of human SN and RA sections (Figure 12), as well as mouse SN single cells (Figure 14 D), demonstrated alternating wide bands correspond to the I-band interrupted by slightly darker zone, which is likely to be the Z-disc, and narrow, thin bands corresponding to the M-line of the cardiac sarcomere (73).

In a conclusion, we show there are a few t-tubules in the human SN unlike in the rodent heart. Interestingly, the striated expression pattern of RyR2 and its colocalisation with α-actinin (Z-discs marker) showed that RyR2 clusters in the Z-disc zone where Ca^{2+} sparks originate from. These results suggest that the organisation of the Ca^{2+}-handling proteins

and the RyR2 clustering around the Z-lines allows more efficient Ca^{2+} signalling and closer proximity to the junctional and corbular SR network and it allows fast, well-coordinated impulse generation, followed by repolarisation of the pacemaking SN cells.

Acknowledgments

None.

Competing Interests

The authors declared no potential conflict of interest with respect to the research, authorship, and/or publication of this article.

Author Contributions

MP performed the majority of the data collection and analysis, data acquisition, performed immunohistochemistry, immunocytochemistry and other lab bench work, and was the primary writer of the manuscript. HD was central in the experimental designs and was the primary editor of the manuscript. YW and LM performed mouse and rat sinus node and right atrium isolation and single cells isolation. AA performed data analysis. LS participated in manuscript editing. BB participated in immunohistochemistry experiments. FP and PM donated the unwanted donor human tissue heart specimens used for the human tissue experiments.

Funding

This work was supported by the British Heart Foundation (grant numbers RG/11/18/29257).

Literature cited

1. Keith A, Flack M. The form and nature of the muscular connections between the primary divisions of the vertebrate hearT. Journal of Anatomy and Physiology. 1907;41(3):172-89. PubMed PMID: WOS:000207232300002.

2. Flack M. An investigation of the sino-auricular node of the mammalian heart. Journal of Physiology-London. 1910;41(1/2):64-77. PubMed PMID: WOS:000201372400004.

3. Sanchez-Quintana D, Cabrera JA, Farre J, Climent V, Anderson RH, Ho SY. Sinus node revisited in the era of electroanatomical mapping and catheter ablation. Heart. 2005;91(2):189-94. Doi: 10.1136/hrt.2003.031542. PubMed PMID: WOS:000226413800015.

4. Mangoni ME, Nargeot J. Genesis and regulation of the heart automaticity. Physiological Reviews. 2008;88(3):919-82. Doi: 10.1152/physrev.00018.2007. PubMed PMID: WOS:000257594000003.

5. Chandler N, Aslanidi OV, Buckley D, Inada S, Birchall S, Atkinson A, et al. computer three-dimensional anatomical reconstruction of the human sinus node and a novel paranodal area. Anatomical record-advances in integrative anatomy and evolutionary biology. 2011;294(6):970-9. Doi: 10.1002/ar.21379. PubMed PMID: WOS:000291439000008.

6. Stephenson RS, Atkinson A, Kottas P, Perde F, Jafarzadeh F, Bateman M, et al. High resolution 3-Dimensional imaging of the human cardiac conduction system from microanatomy to mathematical modeling. Scientific Reports. 2017;7. Doi: 10.1038/s41598-017-07694-8. PubMed PMID: WOS:000406889500017.

7. James TN, Sherf L, Fine G, Morales AR. Comparative ultrastructure of sinus node in man and dog. Circulation. 1966;34(1):139-147. PubMed PMID: WOS:A19667938500021.

8. Lakatta EG, DiFrancesco D. What keeps us ticking: a funny current, a calcium clock, or both? Journal of Molecular and Cellular Cardiology. 2009;47(2):157-70. Doi: 10.1016/j.yjmcc.2009.03.022. PubMed PMID: WOS:000268041800001.

9. Monfredi O, Maltsev VA, Lakatta EG. Modern Concepts Concerning the Origin of the Heartbeat. Physiology. 2013;28(2):74-92. Doi: 10.1152/physiol.00054.2012. PubMed PMID: WOS:000315675900004.

10. Park DS, Fishman GI. The Cardiac Conduction System. Circulation. 2011;123(8):904-15. Doi: 10.1161/circulationaha.110.942284. PubMed PMID: WOS:000287801300017.

11. Cheng H, Lederer MR, Xiao RP, Gomez AM, Zhou YY, Ziman B, et al. Excitation-contraction coupling in heart: New insights from Ca^{2+} sparks. Cell Calcium. 1996;20(2):129-40. Doi: 10.1016/s0143-4160(96)90102-5. PubMed PMID: WOS:A1996VH52900005.

12. Bogdanov KY, Vinogradova TM, Lakatta EG. Sinoatrial nodal cell ryanodine receptor and Na^{+}-Ca^{2+} exchanger – Molecular partners in pacemaker regulation. Circulation Research. 2001;88(12):1254-8. Doi: 10.1161/hh1201.092095. PubMed PMID: WOS:000169541600008.

13. Zipes DP, Jalife J, Petrone G, Punjabi P. Cardiac Electrophysiology: From Cell to Bedside, 6^{th} edition. Perfusion-Uk. 2015;30(5):431-2. Doi: 10.1177/0267659115581145. PubMed PMID: WOS:000356011400014.

14. Hata T, Noda T, Nishimura M, Watanabe Y. The role of Ca^{2+} release from sarcoplasmic reticulum in the regulation of sinoatrial node automaticity. Heart and Vessels. 1996;11(5):234-41. Doi: 10.1007/bf01746203. PubMed PMID: WOS:A1996WQ24500003.

15. Rigg L, Terrar DA. Possible role of calcium release from the sarcoplasmic reticulum in pacemaking in guinea-pig sino-atrial node. Experimental Physiology. 1996;81(5):877-80. Doi: 10.1113/expphysiol.1996.sp003983. PubMed PMID: WOS:A1996VK34300013.

16. Li J, Qu JH, Nathan RD. Ionic basis of ryanodine's negative chronotropic effect on pacemaker cells isolated from the sinoatrial node. American Journal of Physiology-Heart and Circulatory Physiology. 1997;273(5):H2481-H9. PubMed PMID: WOS:A1997YF55300049.

17. Satoh H. Electrophysiological actions of ryanodine on single rabbit sinoatrial nodal cells. General Pharmacology. 1997;28(1):31-8. Doi: 10.1016/s0306-3623(96)00182-6. PubMed PMID: WOS:A1997VZ13000006.

18. Lyashkov AE, Juhaszova M, Dobrzynski H, Vinogradova TM, Maltsev VA, Juhasz O, et al. Calcium cycling protein density and functional importance to automaticity of isolated sinoatrial nodal cells are independent of cell size. Circulation Research. 2007;100(12):1723-31. Doi: 10.1161/circresaha.107.153676. PubMed PMID: WOS:000247530800008.

19. Boyett MR, Honjo H, Kodama I. The sinoatrial node, a heterogeneous pacemaker structure. Cardiovascular Research. 2000;47(4):658-87. Doi: 10.1016/s0008-6363(00)00135-8. PubMed PMID: WOS:000089441200006.

20. Coppen SR, Severs NJ, Gourdie RG. Connexin45 (alpha 6) expression delineates an extended conduction system in the embryonic and mature rodent heart. Developmental Genetics. 1999;24(1-2):82-90. Doi: 10.1002/(sici)1520-6408(1999)24:1/2<82::aid-dvg9>3.0.co;2-1. PubMed PMID: WOS:000078806300009.

21. Chandler NJ, Greener ID, Tellez JO, Inada S, Musa H, Molenaar P, et al. Molecular Architecture of the Human Sinus Node Insights Into the Function of the Cardiac Pacemaker. Circulation. 2009;119(12):1562-75. Doi: 10.1161/circulationaha.108.804369. PubMed PMID: WOS:000264709400003.

22. Brette F, Orchard C. T-tubule function in mammalian cardiac myocytes. Circulation Research. 2003;92(11):1182-92. Doi: 10.1161/01.res.0000074908.17214.fd. PubMed PMID: WOS:000183460200004.

23. Orchard CH, Pasek M, Brette F. The role of mammalian cardiac t-tubules in excitation-contraction coupling: experimental and computational approaches.

Experimental Physiology. 2009;94(5):509-19. Doi: 10.1113/expphysiol.2008.043984. PubMed PMID: WOS:000265186600005.

24. Soeller C, Cannell MB. Examination of the transverse tubular system in living cardiac rat myocytes by 2-photon microscopy and digital image-processing techniques. Circulation Research. 1999;84(3):266-75. PubMed PMID: WOS:000078683700003.

25. Scriven DRL, Dan P, Moore EDW. Distribution of proteins implicated in excitation-contraction coupling in rat ventricular myocytes. Biophysical Journal. 2000;79(5):2682-91. Doi: 10.1016/s0006-3495(00)76506-4. PubMed PMID: WOS:000165104500038.

26. Wong J, Baddeley D, Bushong EA, Yu ZY, Ellisman MH, Hoshijima M, et al. nanoscale distribution of ryanodine receptors and caveolin-3 in mouse ventricular myocytes: dilation of t-tubules near junctions. Biophysical Journal. 2013;104(11):L22-L4. Doi: 10.1016/j.bpj.2013.02.059. PubMed PMID: WOS:000320423700002.

27. Pinali C, Bennett H, Davenport JB, Trafford AW, Kitmitto A. Three-dimensional reconstruction of cardiac sarcoplasmic reticulum reveals a continuous network linking transverse-tubules this organization is perturbed in heart failure. Circulation Research. 2013;113(11):1219-U98. Doi: 10.1161/circresaha.113.301348. PubMed PMID: WOS:000330353100009.

28. Baddeley D, Jayasinghe ID, Lam L, Rossberger S, Cannell MB, Soeller C. Optical single-channel resolution imaging of the ryanodine receptor distribution in rat cardiac myocytes. Proceedings of the National Academy of Sciences of the United States of America. 2009;106(52):22275-80. Doi: 10.1073/pnas.0908971106. PubMed PMID: WOS:000273178700044.

29. Knoll R, Hoshijima M, Chien KR. Z-line proteins: implications for additional functions. European Heart Journal Supplements. 2002;4(I):I13-I7. Doi: 10.1016/s1520-765x(02)90105-7. PubMed PMID: WOS:000179798000004.

30. Djinovic-Carugo K, Young P, Gautel M, Saraste M. Structure of the alpha-actinin rod: Molecular basis for cross-linking of actin filaments. Cell. 1999;98(4):537-46. Doi: 10.1016/s0092-8674(00)81981-9. PubMed PMID: WOS:000082174900013.

31. Young P, Ferguson C, Banuelos S, Gautel M. Molecular structure of the sarcomeric Z-disk: two types of titin interactions lead to an asymmetrical sorting of alpha-actinin. Embo Journal. 1998;17(6):1614-24. Doi: 10.1093/emboj/17.6.1614. PubMed PMID: WOS:000072693700007.

32. Hiess F, Vallmitjana A, Wang RW, Cheng HQ, ter Keurs H, Chen J, et al. Distribution and function of cardiac ryanodine receptor clusters in live ventricular myocytes. Journal of Biological Chemistry. 2015;290(33):20477-87. Doi: 10.1074/jbc.M115.650531. PubMed PMID: WOS:000359608900045.

33. Brenman JE, Chao DS, Xia HH, Aldape K, Bredt DS. Nitric-oxide synthase complexed with dystrophin and absent from skeletal-muscle sarcolemma in duchenne muscular-dystrophy. Cell. 1995;82(5):743-52. Doi: 10.1016/0092-8674(95)90471-9. PubMed PMID: WOS:A1995RU75500009.

34. Klietsch R, Ervasti JM, Arnold W, Campbell KP, Jorgensen AO. Dystrophin-glycoprotein complex and laminin colocalize to the sarcolemma and transverse tubules of cardiac-muscle. Circulation Research. 1993;72(2):349-60. PubMed PMID: WOS:A1993KG81300012.

35. Rivier F, Robert A, Royuela M, Hugon G, Bonet-Kerrache A, Mornet D. Utrophin and dystrophin-associated glycoproteins in normal and dystrophin deficient cardiac muscle. Journal of Muscle Research and Cell Motility. 1999;20(3):305-14. Doi: 10.1023/a:1005426920070. PubMed PMID: WOS:000082560400006.

36. Frank JS, Mottino G, Chen F, Peri V, Holland P, Tuana BS. Subcellular-distribution of dystrophin in isolated adult and neonatal cardiac myocytes. American Journal of Physiology-Cell Physiology. 1994;267(6):C1707-C16. PubMed PMID: WOS:A1994PY11900023.

37. Meng HP, Leddy JJ, Frank J, Holland P, Tuana BS. The association of cardiac dystrophin with myofibrils/Z-disc regions in cardiac muscle suggests a novel role in

the contractile apparatus. Journal of Biological Chemistry. 1996;271(21):12364-71. Doi: 10.1074/jbc.271.21.12364. PubMed PMID: WOS:A1996UL66000041.

38. Huser J, Lipsius SL, Blatter LA. Calcium gradients during excitation-contraction coupling in cat atrial myocytes. Journal of Physiology-London. 1996;494(3):641-51. PubMed PMID: WOS:A1996VE39500003.

39. Greiser M, Lederer WJ, Schotten U. Alterations of atrial Ca^{2+} handling as cause and consequence of atrial fibrillation. Cardiovascular Research. 2011;89(4):722-33. Doi: 10.1093/cvr/cvq389. PubMed PMID: WOS:000287487400005.

40. Woo SH, Cleemann L, Morad M. Ca^{2+} current-gated focal and local Ca^{2+} release in rat atrial myocytes: evidence from rapid 2-D confocal imaging. Journal of Physiology-London. 2002;543(2):439-53. Doi: 10.1113/physiol2002024190. PubMed PMID: WOS:000178186200005.

41. Musa H, Lei M, Honjo H, Jones SA, Dobrzynski H, Lancaster MK, et al. Heterogeneous expression of Ca^{2+} handling proteins in rabbit sinoatrial node. Journal of Histochemistry & Cytochemistry. 2002;50(3):311-24. PubMed PMID: WOS:000174061000003.

42. Lenaerts I, Bito V, Heinzel FR, Driesen RB, Holemans P, D'Hooge J, et al. Ultrastructural and functional remodeling of the coupling between Ca^{2+} influx and sarcoplasmic reticulum Ca^{2+} release in right atrial myocytes from experimental persistent atrial fibrillation. Circulation Research. 2009;105(9):876-U111. Doi: 10.1161/circresaha.109.206276. PubMed PMID: WOS:000271032300007.

43. Dibb KM, Clarke JD, Horn MA, Richards MA, Graham HK, Eisner DA, et al. Characterization of an extensive transverse tubular network in sheep atrial myocytes and its depletion in heart failure. Circulation-Heart Failure. 2009;2(5):482-9. Doi: 10.1161/circheartfailure.109.852228. PubMed PMID: WOS:000269827500014.

44. Richards MA, Clarke JD, Saravanan P, Voigt N, Dobrev D, Eisner DA, et al. Transverse tubules are a common feature in large mammalian atrial myocytes including human. American Journal of Physiology-Heart and Circulatory

Physiology. 2011;301(5):H1996-H2005. Doi: 10.1152/ajpheart.00284.2011. PubMed PMID: WOS:000296716900027.

45. Caldwell JL, Smith CER, Taylor RF, Kitmitto A, Eisner DA, Dibb KM, et al. Dependence of Cardiac Transverse Tubules on the BAR Domain Protein Amphiphysin II (BIN-1). Circulation Research. 2014;115(12):986-U157. Doi: 10.1161/circresaha.116.303448. PubMed PMID: WOS:000346024800037.

46. Perde FV, Atkinson A, Yanni J, Dermengiu D, Dobrzynski H. Morphological characteristics of the sinus node on postmortem tissue. Folia Morphologica. 2016;75(2):216-23. Doi: 10.5603/FM.a2015.0087. PubMed PMID: WOS:000378127700011.

47. D'Souza A, Pearman CM, Wang YW, Nakao S, Logantha S, Cox C, et al. Targeting miR-423-5p reverses exercise training-induced HCN4 channel remodeling and sinus bradycardia. Circulation Research. 2017;121(9):1058-1072. Doi: 10.1161/circresaha.117.311607. PubMed PMID: WOS:000412809000010.

48. Rybakova IN, Patel JR, Ervasti JM. The dystrophin complex forms a mechanically strong link between the sarcolemma and costameric actin. Journal of Cell Biology. 2000;150(5):1209-14. Doi: 10.1083/jcb.150.5.1209. PubMed PMID: WOS:000089305500023.

49. Heinzel FR, Bito V, Biesmans L, Wu M, Detre E, von Wegner F, et al. Remodeling of T-tubules and reduced synchrony of Ca^{2+} release in myocytes from chronically ischemic myocardium. Circulation Research. 2008;102(3):338-46. Doi: 10.1161/circresaha.107.160085. PubMed PMID: WOS:000253194600013.

50. Louch WE, Mork HK, Sexton J, Stromme TA, Laake P, Sjaastad I, et al. T-tubule disorganization and reduced synchrony of Ca^{2+} release in murine cardiomyocytes following myocardial infarction. Journal of Physiology-London. 2006;574(2):519-33. Doi: 10.1113/jphysiol.2006.107227. PubMed PMID: WOS:000239688500016.

51. Forbes MS, Hawkey LA, Sperelakis N. The transverse-axial tubular system (tats) of mouse myocardium – its morphology in the developing and adult animal. American

Journal of Anatomy. 1984;170(2):143-62. Doi: 10.1002/aja.1001700203. PubMed PMID: WOS:A1984SX47000002.

52. Huser J, Blatter LA, Lipsius SL. Intracellular Ca^{2+} release contributes to automaticity in cat atrial pacemaker cells. Journal of Physiology-London. 2000;524(2):415-22. Doi: 10.1111/j.1469-7793.2000.00415.x. PubMed PMID: WOS:000086905000011.

53. Smyrnias I, Mair W, Harzheim D, Walker SA, Roderick HL, Bootman MD. Comparison of the T-tubule system in adult rat ventricular and atrial myocytes, and its role in excitation-contraction coupling and inotropic stimulation. Cell Calcium. 2010;47(3):210-23. Doi: 10.1016/j.ceca.2009.10.001. PubMed PMID: WOS:000276430100002.

54. Tidball JG, Cederdahl JE, Bers DM. Quantitative-analysis of regional variability in the distribution of transverse tubules in rabbit myocardium. Cell and Tissue Research. 1991;264(2):293-8. Doi: 10.1007/bf00313966. PubMed PMID: WOS:A1991FJ45800011.

55. Kirk MM, Izu LT, Chen-Izu Y, McCulle SL, Wier WG, Balke CW, et al. Role of the transverse-axial tubule system in generating calcium sparks and calcium transients in rat atrial myocytes. Journal of Physiology-London. 2003;547(2):441-51. Doi: 10.1113/jphysiol.2002.034355. PubMed PMID: WOS:000183570500011.

56. Ayettey AS, Navaratnam V. T-tubule system in specialized and general myocardium of rat. Journal of Anatomy. 1978;127(SEP):125-40. PubMed PMID: WOS:A1978FR17700011.

57. Ayettey AS, Navaratnam V, Yates RD. Ultrastructure of the internodal myocardium in the rat. Journal of Anatomy. 1988;158:77-90. PubMed PMID: WOS:A1988N906900007.

58. Soeller C, Crossman D, Gilbert R, Cannell MB. Analysis of ryanodine receptor clusters in rat and human cardiac myocytes. Proceedings of the National Academy of Sciences of the United States of America. 2007;104(38):14958-63. Doi: 10.1073/pnas.0703016104. PubMed PMID: WOS:000249715100017.

59. Jayasinghe ID, Crossman DJ, Soeller C, Cannell MB. A new twist in cardiac muscle: dislocated and helicoid arrangements of myofibrillar z-disks in mammalian ventricular myocytes. Journal of Molecular and Cellular Cardiology. 2010;48(5):964-71. Doi: 10.1016/j.yjmcc.2009.12.012. PubMed PMID: WOS:000276982800020.

60. Mangoni ME, Couette B, Bourinet E, Platzer J, Reimer D, Striessnig J, et al. Functional role of L-type $Ca_V1.3$ Ca^{2+} channels in cardiac pacemaker activity. Proceedings of the National Academy of Sciences of the United States of America. 2003;100(9):5543-8. Doi: 10.1073/pnas.0935295100. PubMed PMID: WOS:000182612600103.

61. Crespo LM, Grantham CJ, Cannell MB. Kinetics, stoichiometry and role of the na-ca exchange mechanism in isolated cardiac myocytes. Nature. 1990;345(6276):618-21. Doi: 10.1038/345618a0. PubMed PMID: WOS:A1990DJ24300061.

62. Bridge JHB, Smolley JR, Spitzer KW. The relationship between charge movements associated with ica and ina-ca in cardiac myocytes. Science. 1990;248(4953):376-8. Doi: 10.1126/science.2158147. PubMed PMID: WOS:A1990CZ83700042.

63. Thomas MJ, Sjaastad I, Andersen K, Helm PJ, Wasserstrom JA, Sejersted OM, et al. Localization and function of the Na^+/Ca^{2+}-exchanger in normal and detubulated rat cardiomyocytes. Journal of Molecular and Cellular Cardiology. 2003;35(11):1325-37. Doi: 10.1016/j.yjmcc.2003.08.005. PubMed PMID: WOS:000186847400003.

64. Sobie EA, Cannell MB, Bridge JHB. Allosteric activation of Na^+/Ca^{2+} exchange by L-type Ca^{2+} current augments the trigger flux for SR Ca^{2+} release in ventricular myocytes. Biophysical Journal. 2008;94(7):54-56. Doi: 10.1529/biophysj.107.127878. PubMed PMID: WOS:000254076300004.

65. Lines GT, Sande JB, Louch WE, Mork HK, Grottum P, Sejersted OM. Contribution of the Na^+/Ca^{2+}exchanger to rapid Ca^{2+} release in cardiomyocytes. Biophysical Journal. 2006;91(3):779-92. Doi: 10.1529/biophysj.105.072447. PubMed PMID: WOS:000239086800003.

66. Viatchenko-Karpinski S, Terentyev D, Jenkins LA, Lutherer LO, Gyorke S. Synergistic interactions between Ca^{2+} entries through L-type Ca^{2+} channels and Na^{+}/Ca^{2+} exchanger in normal and failing rat heart. Journal of Physiology-London. 2005;567(2):493-504. Doi: 10.1113/jphysiol.2005.091280. PubMed PMID: WOS:000231914100013.

67. Dibb KM, Graham HK, Venetucci LA, Eisner DA, Trafford AW. Analysis of cellular calcium fluxes in cardiac muscle to understand calcium homeostasis in the heart. Cell Calcium. 2007;42(4-5):503-12. Doi: 10.1016/j.ceca.2007.04.002. PubMed PMID: WOS:000249746200016.

68. Carl SL, Felix K, Caswell AH, Brandt NR, Brunschwig JP, Meissner G, et al. Immunolocalization of triadin, dhp receptors, and ryanodine receptors in adult and developing skeletal-muscle of rats. Muscle & Nerve. 1995;18(11):1232-43. Doi: 10.1002/mus.880181104. PubMed PMID: WOS:A1995RZ44300002.

69. Forbes MS, Vanniel EE. Membrane systems of guinea-pig myocardium – ultrastructure and morphometric studies. Anatomical Record. 1988;222(4):362-79. Doi: 10.1002/ar.1092220409. PubMed PMID: WOS:A1988R639500008.

70. McFarland TP, Milstein ML, Cala SE. Rough endoplasmic reticulum to junctional sarcoplasmic reticulum trafficking of calsequestrin in adult cardiomyocytes. Journal of Molecular and Cellular Cardiology. 2010;49(4):556-64. Doi: 10.1016/j.yjmcc.2010.05.012. PubMed PMID: WOS:000281875900003.

71. Jewett PH, Leonard SD, Sommer JR. Chicken cardiac-muscle – its elusive extended junctional sarcoplasmic reticulum and sarcoplasmic reticulum fenestrations. Journal of Cell Biology. 1973;56(2):595-600. Doi: 10.1083/jcb.56.2.595. PubMed PMID: WOS:A1973O715300025.

72. Dolber PC, Beyer EC, Junker JL, Spach MS. Distribution of gap-junctions in dog and rat ventricle studied with a double-label technique. Journal of Molecular and Cellular Cardiology. 1992;24(12):1443-57. Doi: 10.1016/0022-2828(92)91085-j. PubMed PMID: WOS:A1992KG87900006.

73. Glacy SD. Pattern and time course of rhodamine-actin incorporation in cardiac myocytes. Journal of Cell Biology. 1983;96(4):1164-7. Doi: 10.1083/jcb.96.4.1164. PubMed PMID: WOS:A1983QH96000026.

Primary Antibody	Raised in	Expression pattern	Concentration	Supplier Catalog #
α-actinin	Ms	Striated	1:50	Abcam (ab9465)
Dystrophin	Rbt	Cell membrane	1:50	Abcam (ab15277)
NCX1	Ms IgM	Cell membrane	1:50	Thermo Fisher Scientific (MA3-926)
RyR2	Ms	Intracellular striations	1:50	Thermo Fisher Scientific (MA3-916)
SERCA2a	Ms	Cell membrane and striated	1:50	Thermo Fisher Scientific (MA3-933)
Phalloidin	Fluorescent dye, 565	Intracellular striations	1:100	Thermo Fisher Scientific (R415)
Wheat germ agglutinin (WGA)	Fluorescent dye, 488	Cell membrane and extracellular space and striations in ventricular cells	1:100	Thermo Fisher Scientific (W11261)

Table 1. Primary antibodies details used in human SN preparations and rat/mouse isolated single cells immunofluorescent experiments.

Secondary Antibody	Fluorochrome	Colour of emission	Wavelength absorbed/emitted (nm)	Supplier Catalog #
Anti-Rbt IgG	FITC	Green	495/519	Millipore (AP132F)
Anti-Rbt IgG	Cy3	Red	555/565	Millipore (AP132C)
Anti-Ms IgG	FITC	Green	495/519	Millipore (AP124F)
Anti-Ms IgG	Cy3	Red	555/565	Millipore (AP124C)
Anti-Ms IgM	FITC	Green	495/519	Sigma (SLBG5659)

Table 2. Summary of the secondary antibodies. The secondary antibodies were primed to the appropriate primary antibodies (described in Table 1), according to the species they have been raised to. They were diluted to concentration 1:100 in 1%BSA. Incubation period with secondary antibodies was 2 hours at room temperature.

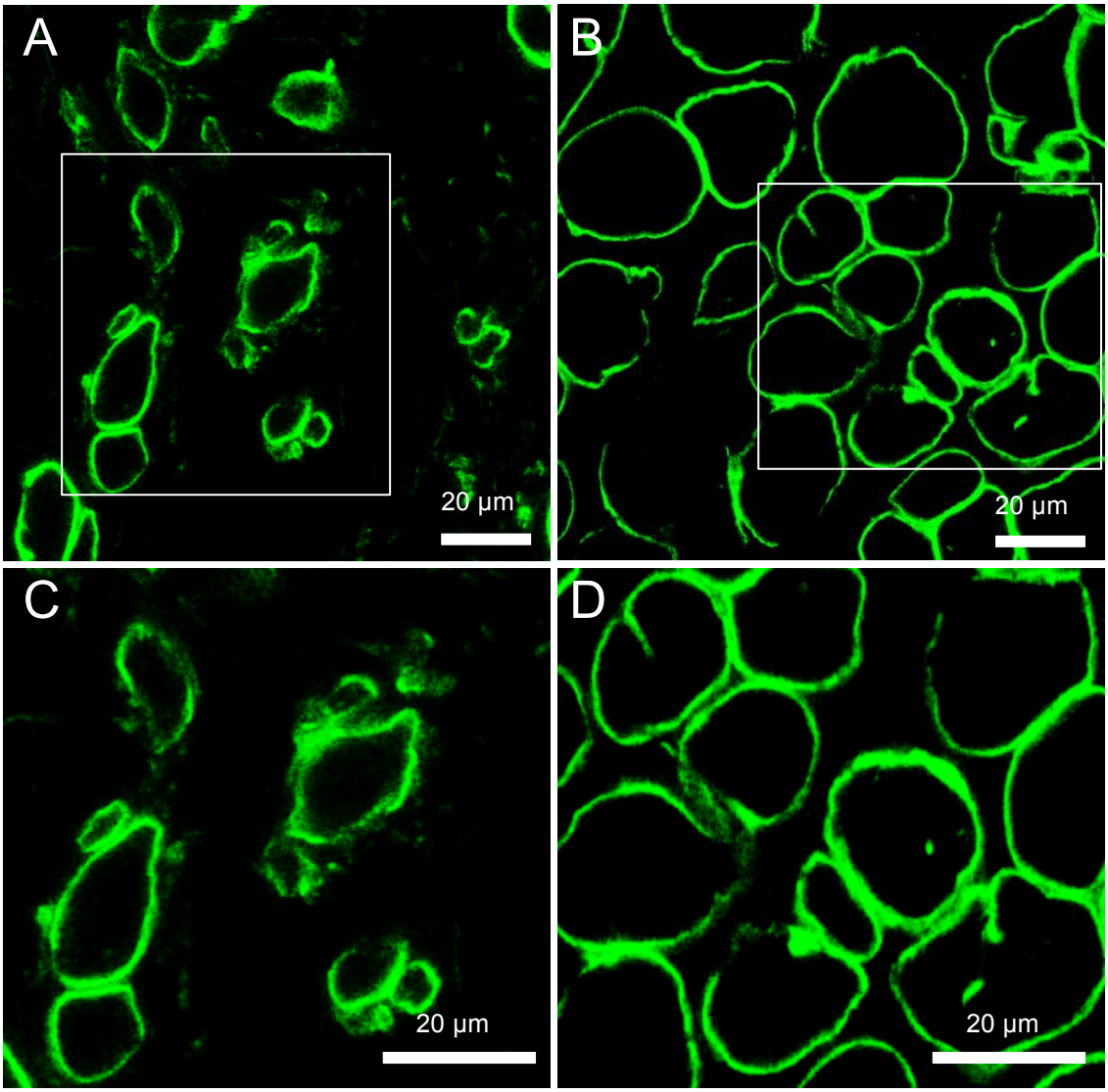

Figure 1. Expression of dystrophin in human SN and RA. A and B show low power images of dystrophin immunolabelling (green signal) of SN and RA, respectively. White boxes in A and B denote magnified regions in panel C and D, respectively (n=6).

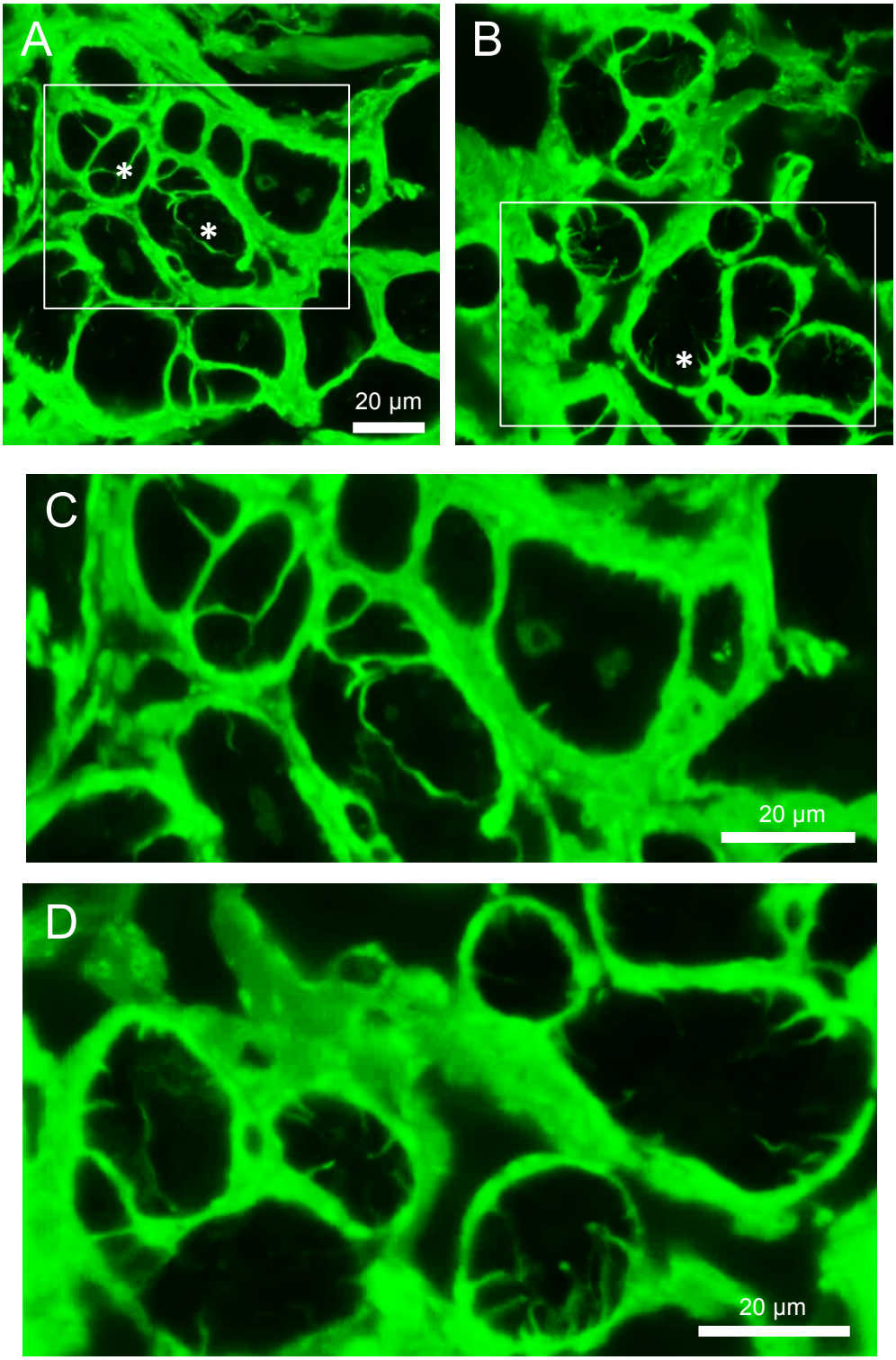

Figure 2. WGA staining of cell membrane and t-tubular invaginations in human SN. A and B show low power images of WGA staining (green signal) of SN. White boxes in A and B denote magnified regions in panel C and D, respectively. White asterisks denote t-tubular invaginations (n=6).

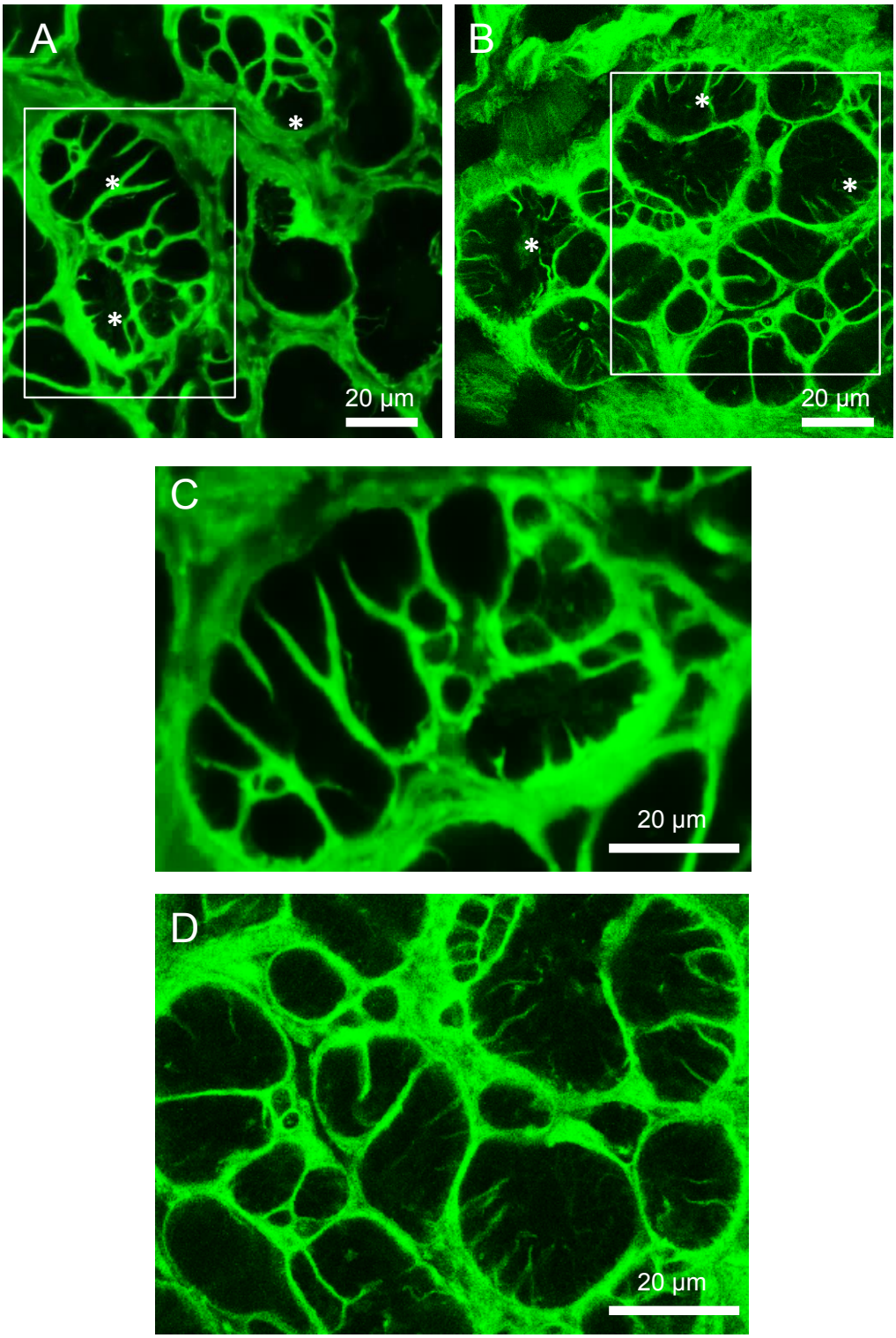

Figure 3. WGA staining of cell membrane and t-tubular invaginations in human RA. A and B show low power images of WGA staining (green signal) of RA. White boxes in A and B denote magnified regions in panel C and D, respectively. White asterisks denote t-tubular invaginations (n=6).

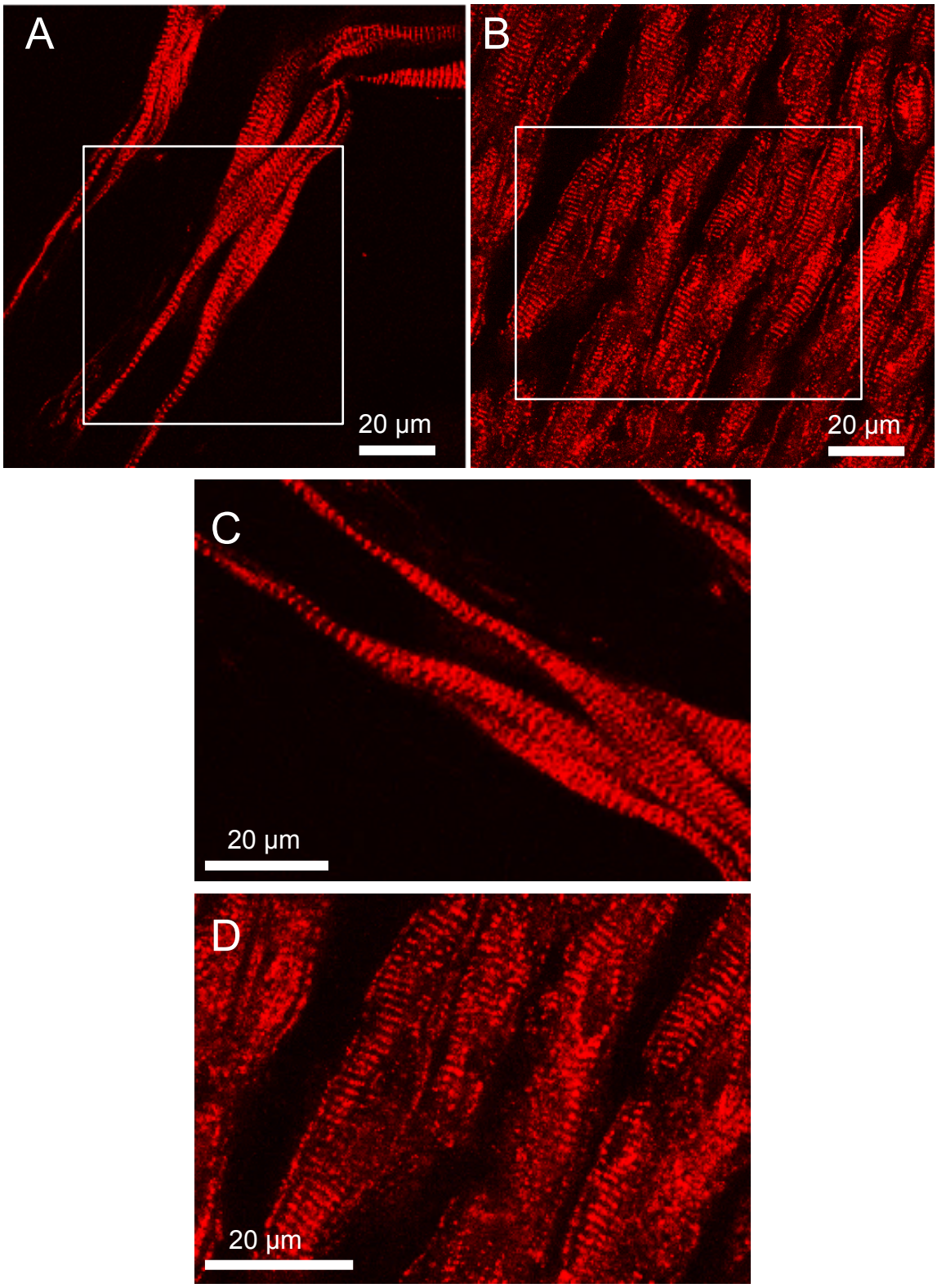

Figure 4. Expression of RyR2 in human SN and RA. A and B show low power images of RyR2 immunolabelling (green signal) of SN and RA, respectively. White boxes in A and B denote magnified regions in panel C and D, respectively (n=6).

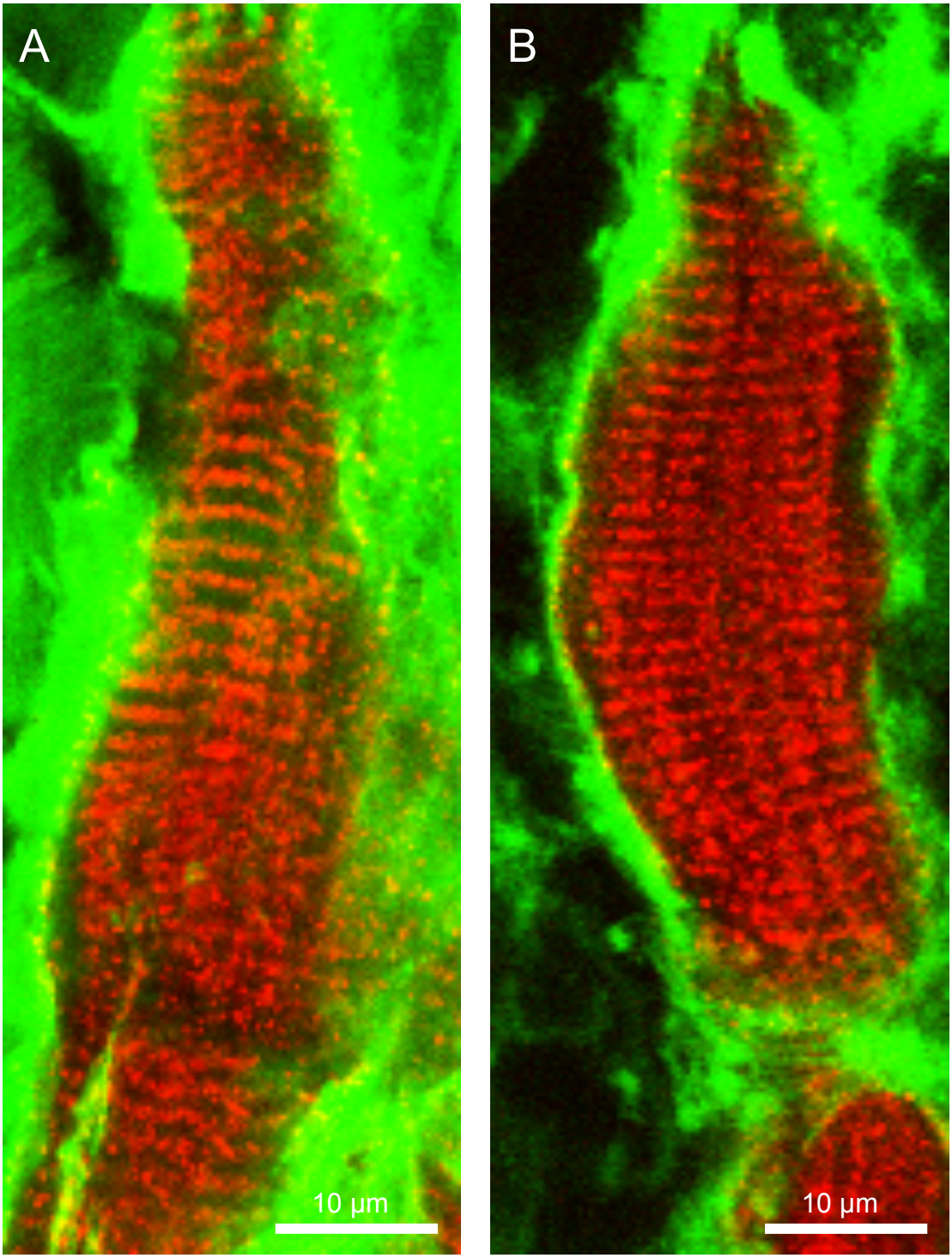

Figure 5. WGA and RyR2 staining in human SN and RA. A and B show high magnification images of WGA (green signal) and RyR2 (red signal) staining of SN and RA, respectively (n=6).

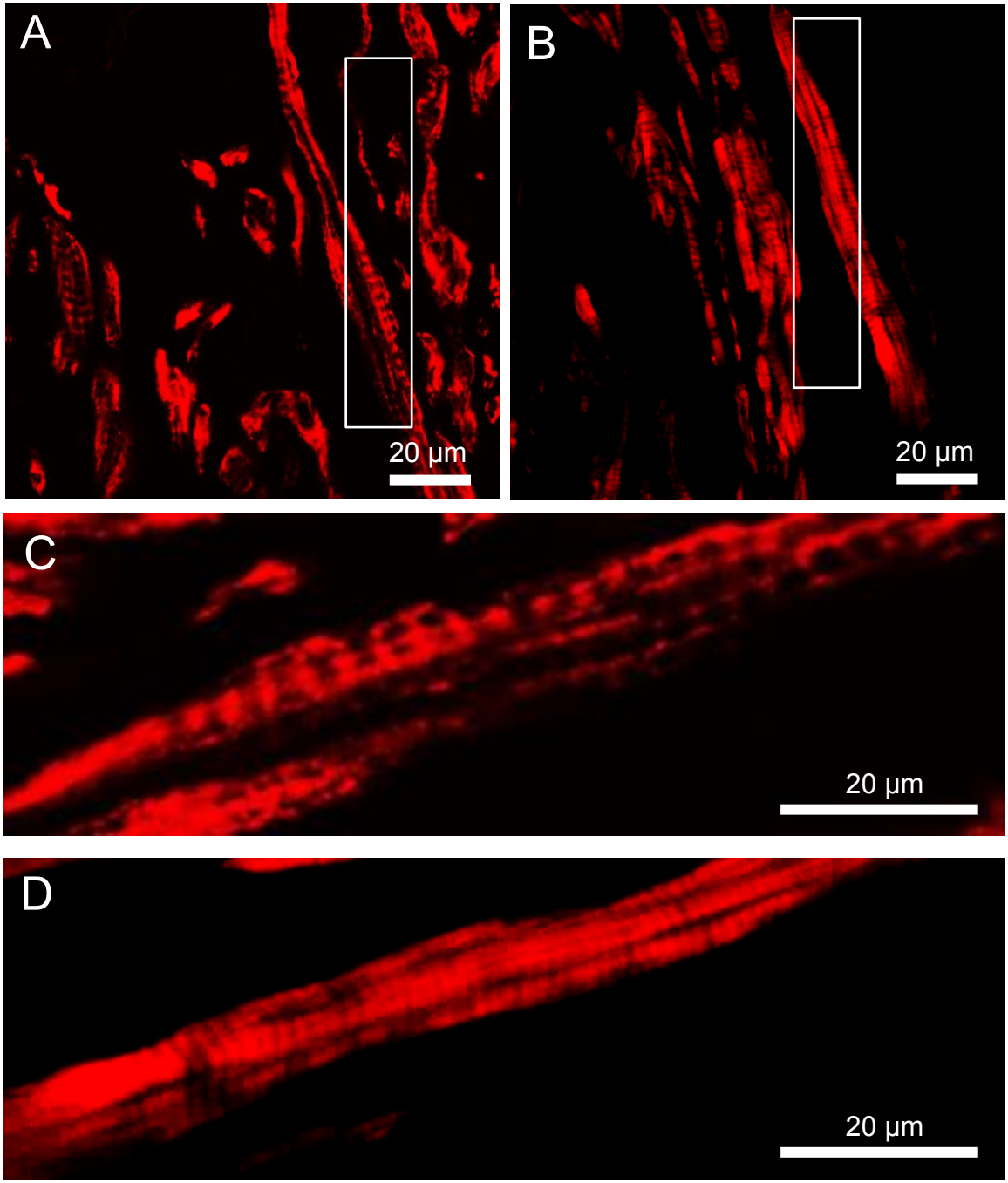

Figure 6. Expression of SERCA2a in human SN and RA. A and B show low power images of SERCA2a (red signal) immunolabelling of SN and RA, respectively. White boxes in A and B denote magnified regions in panel C and D, respectively (n=6).

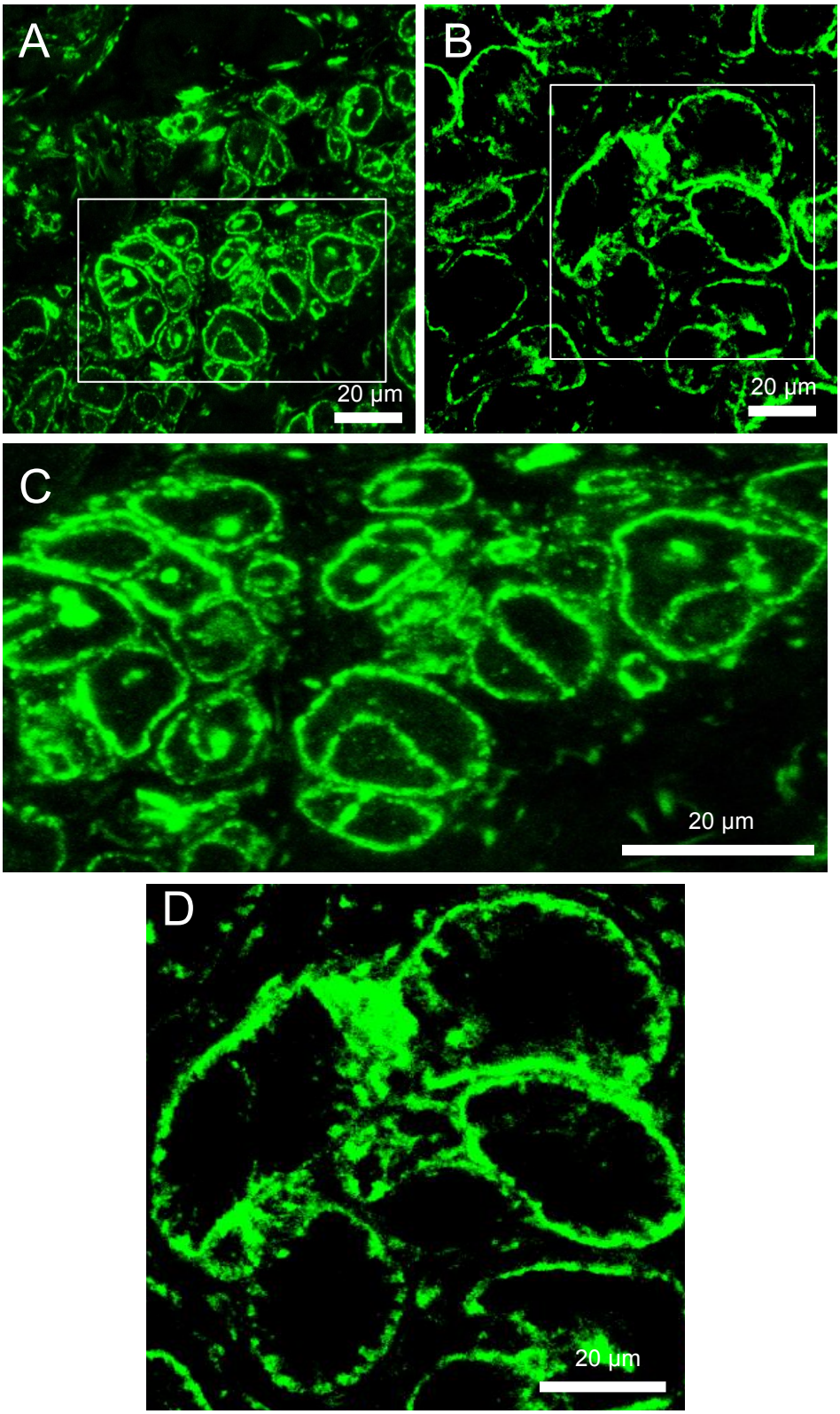

Figure 7. Expression of NCX1 in human SN and RA. A and B show low power images of NCX1 (green signal) immunolabelling of SN and RA, respectively. White boxes in A and B denote magnified regions in panel C and D, respectively (n=6).

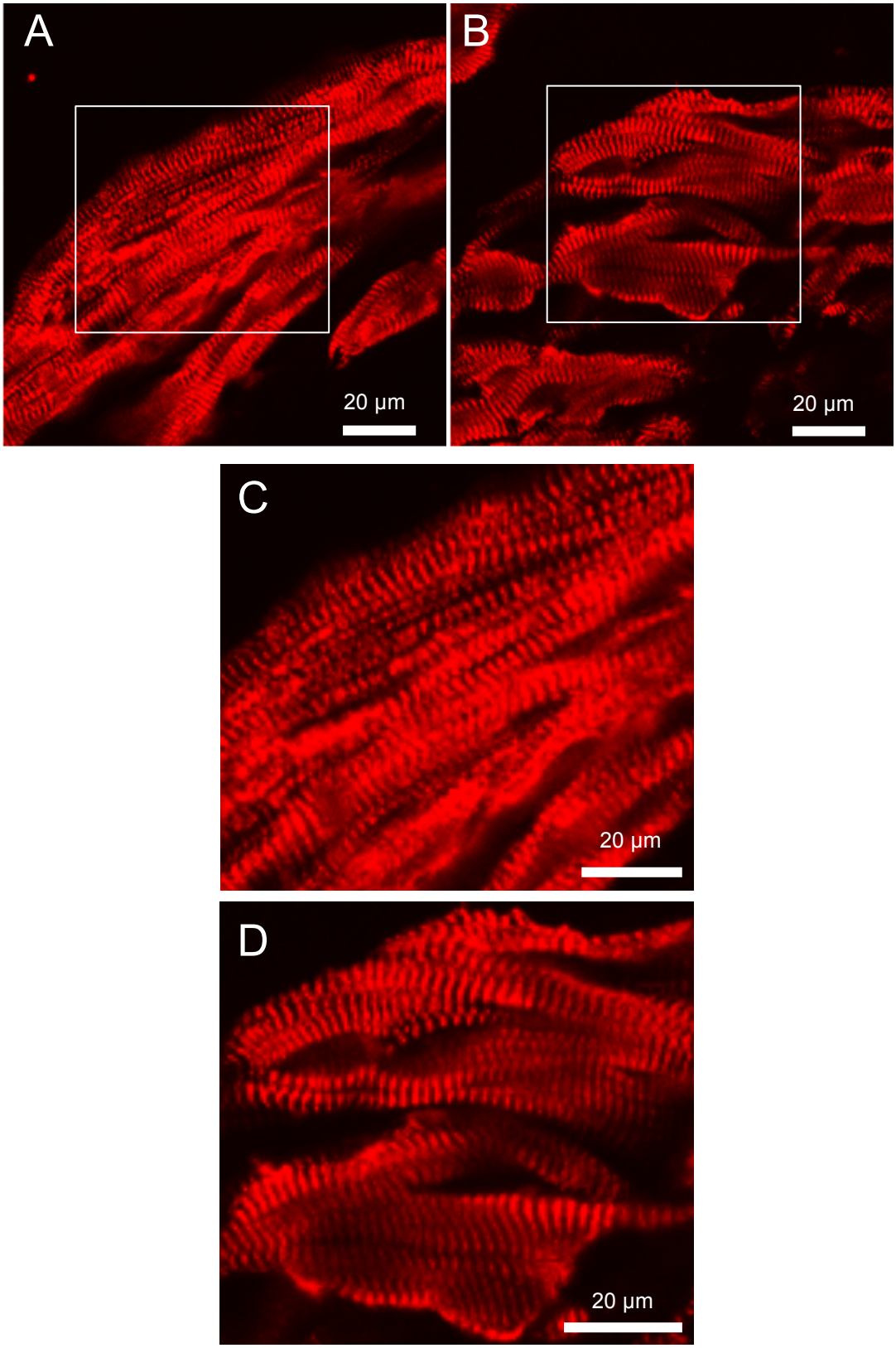

Figure 8. Expression of α-actinin in human SN and RA. A and B show low power images of α-actinin (red signal) immunolabelling of SN and RA, respectively. White boxes in A and B denote magnified regions in panel C and D, respectively (n=6).

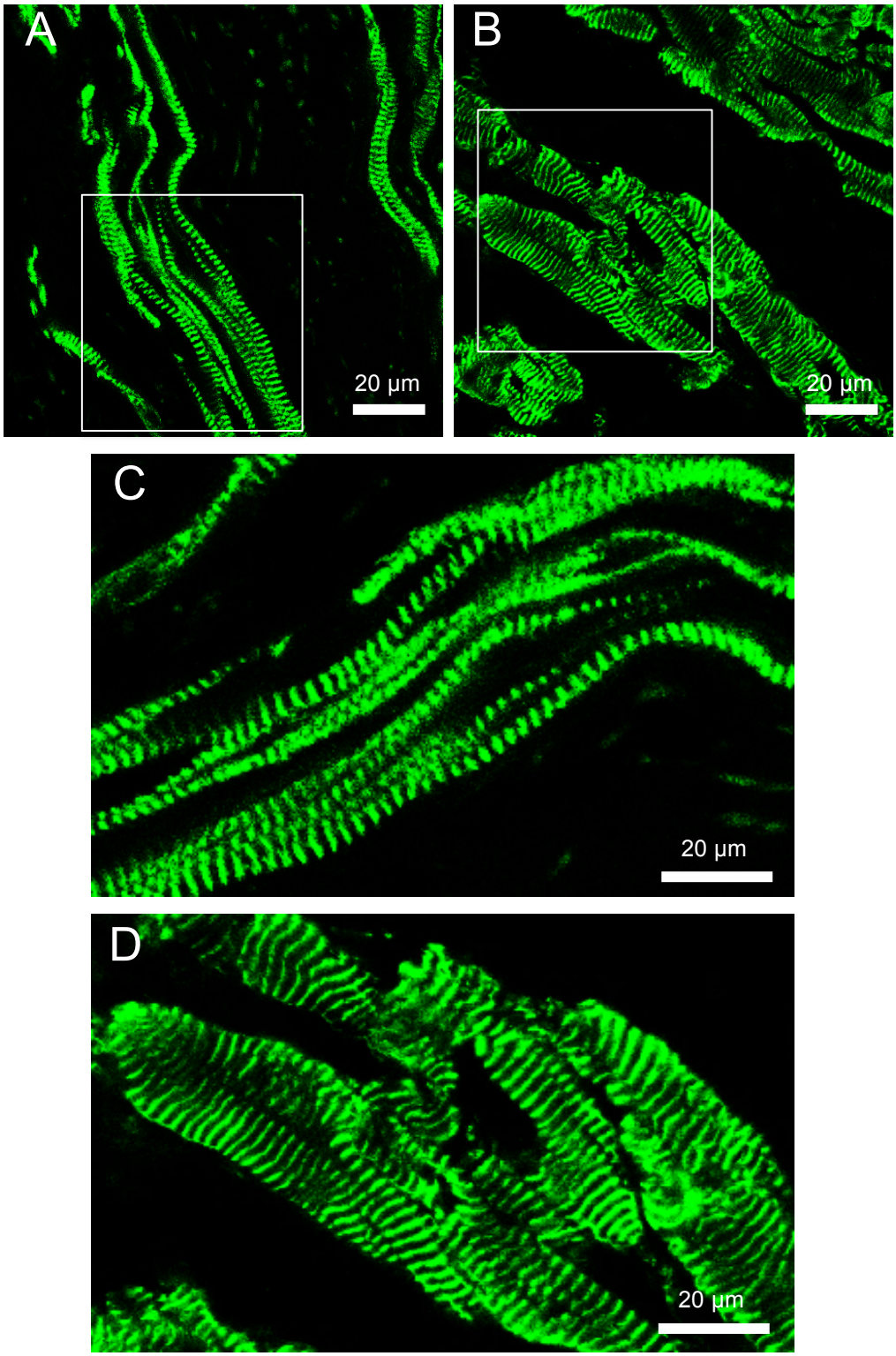

Figure 9. Expression of α-actinin in human SN and RA. A and B show low power images of α-actinin (green signal) immunolabelling of SN and RA, respectively. White boxes in A and B denote magnified regions in panel C and D, respectively (n=6).

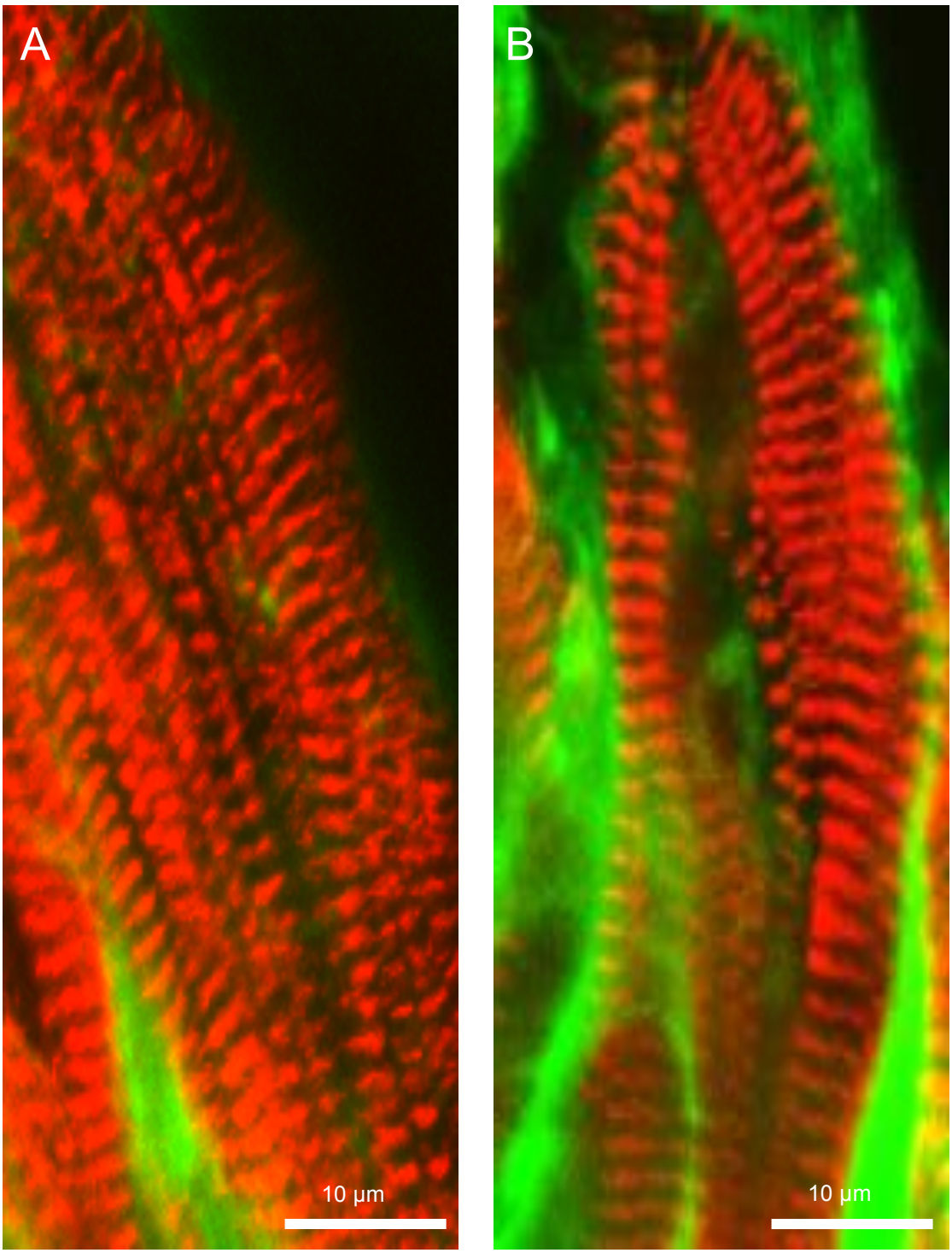

Figure 10. WGA and α-actinin staining in human SN and RA. A and B show high magnification images of α-actinin (red signal) immunolabelling and WGA (green signal) staining of SN and RA, respectively (n=6).

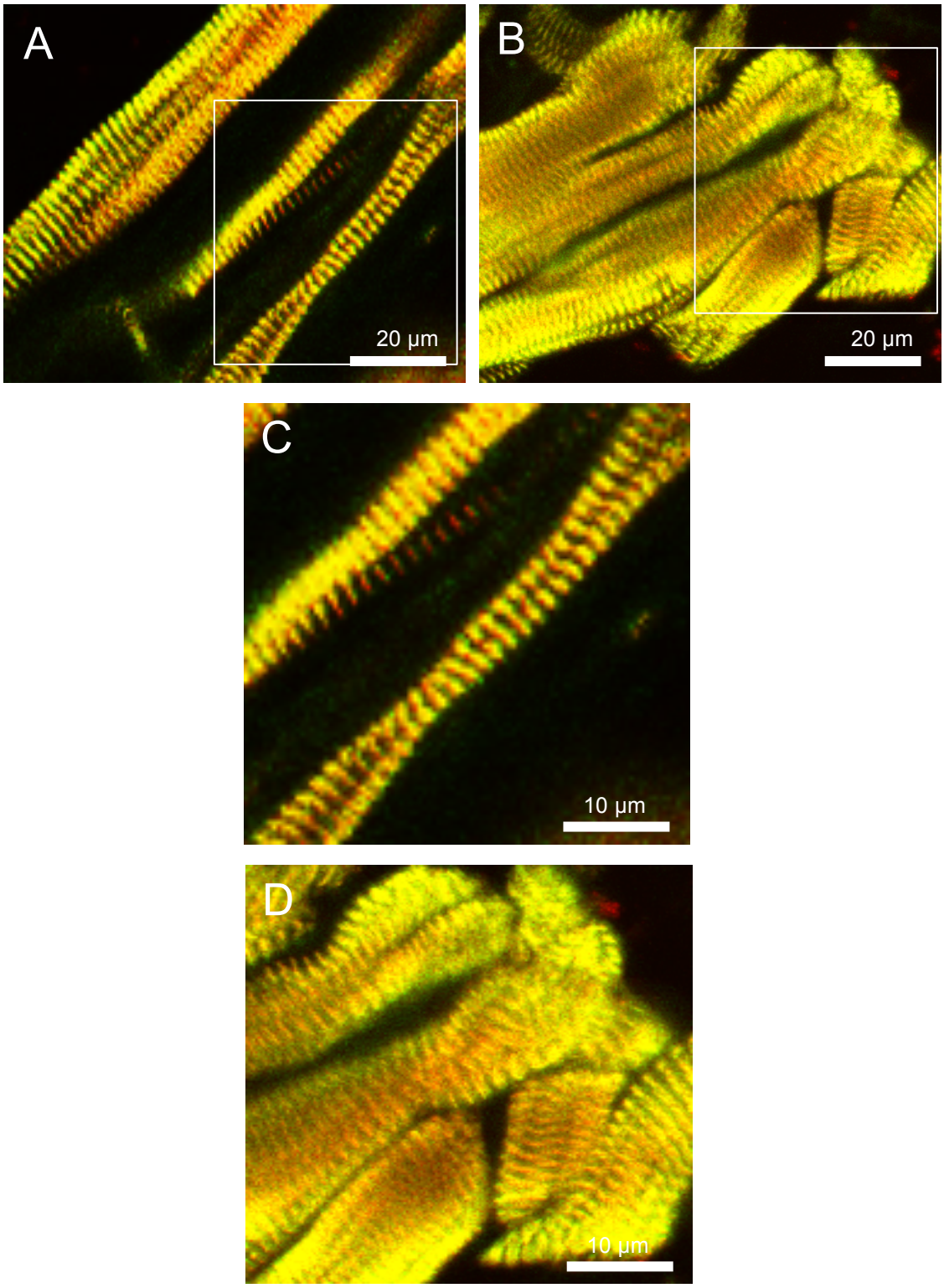

Figure 11. Expression of RyR2 and α-actinin in human SN and RA. A and B show low power images of double labelling with antibodies for α-actinin (red signal) and RyR2 (green signal) of SN and RA, respectively. White boxes in A and B denote magnified regions in panel C and D, respectively (n=6).

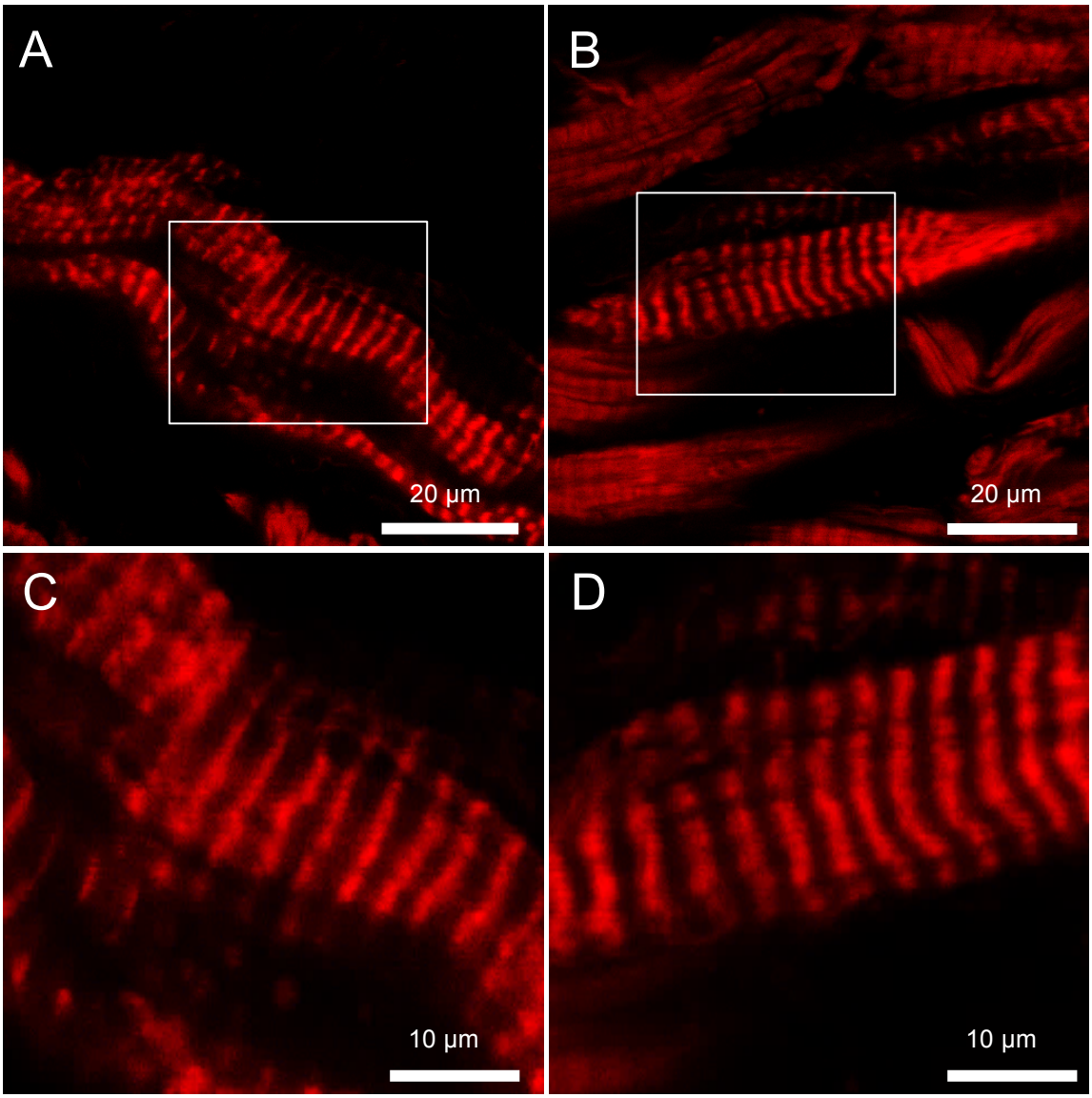

Figure 12. Phalloidin staining of sarcomeric actin in human SN and RA. A and B show low power images of phalloidin staining (red signal) of SN and RA, respectively. White boxes in A and B denote magnified regions in panel C and D, respectively (n=6).

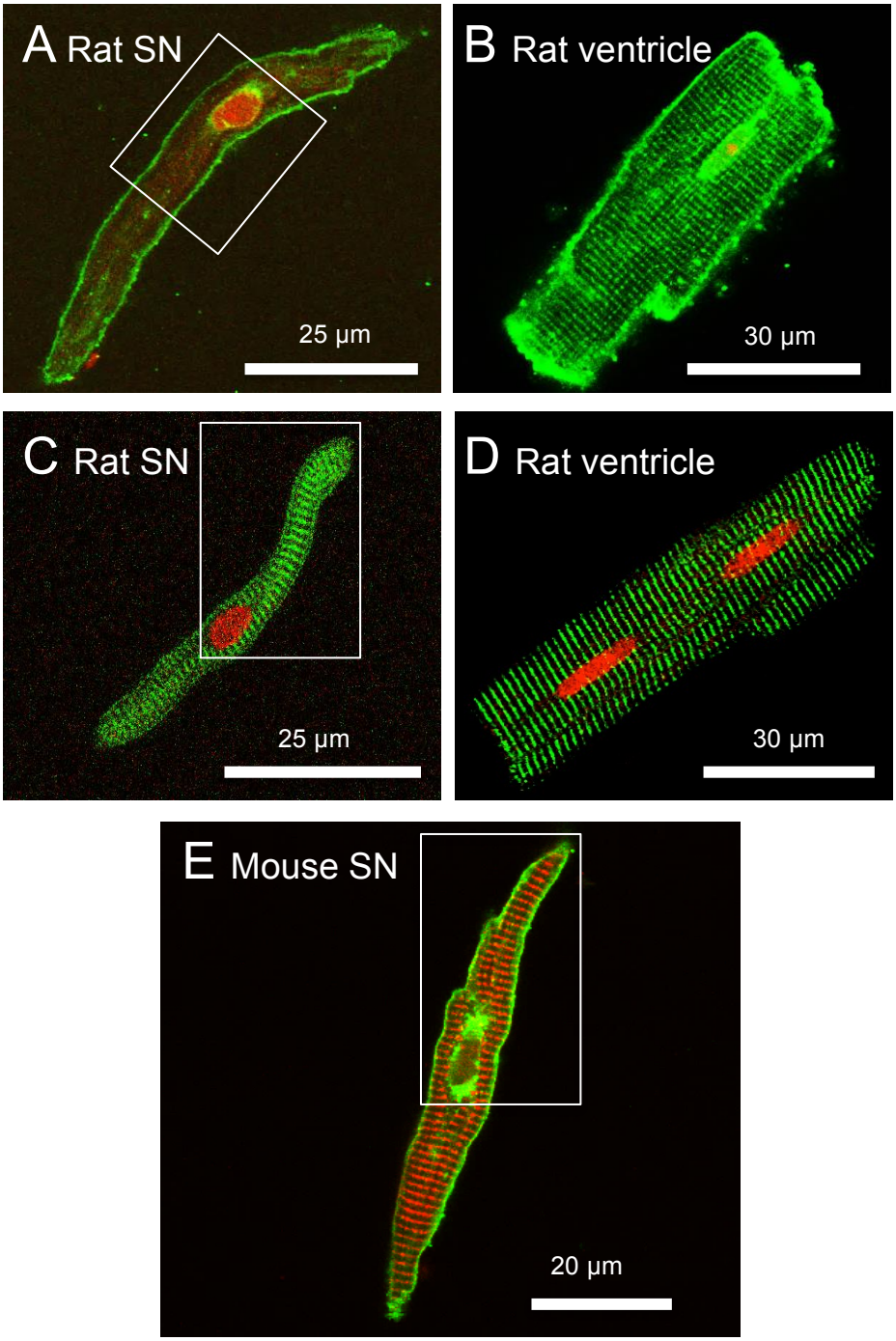

Figure 13. A and B WGA staining (green signal) cell membrane and t-tubular invaginations in single SN and ventricular rat myocytes, respectively. White box in A denotes magnified region in Figure 14 A. C and D RyR2 immunolabelling (green signal) of single SN and ventricular rat myocytes, respectively. White box in C denotes magnified region in Figure 14 B. E WGA (green signal) and α-actinin (red signal) staining of mouse SN myocytes. White box in E denotes magnified region in Figure 14 C. Cell nuclei were stained with propidium iodide (red signal).

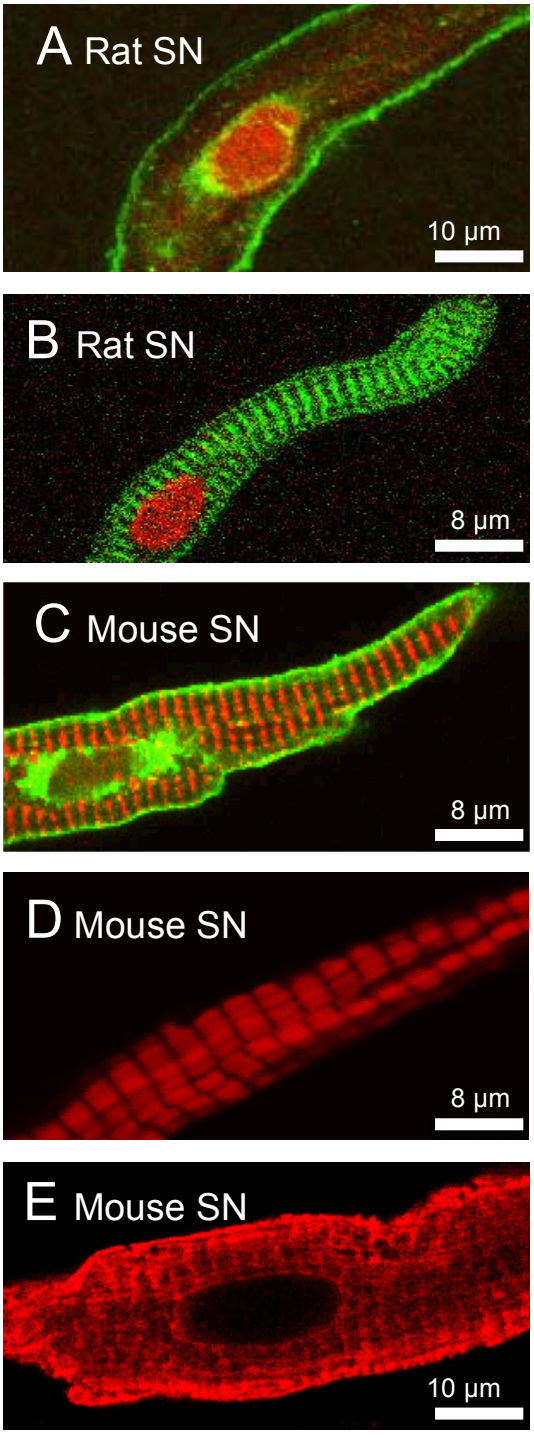

Figure 14. High magnification images of rat SN single myocytes stained for WGA (green signal) and RyR2 (green signal) expression in panel A and B, respectively. High magnification images of mouse SN single myocytes stained with WGA (green signal) and α-actinin (red signal) immunolabelling. Myocyte's nuclei from panels A, B, and C were stained red with propidium iodide. D. Mouse SN single myocytes stained with phalloidin (sarcomeric actin marker, red signal). E. Expression of SERCA2a (red signal) in mouse SN single myocytes.

Chapter 6

6 Identification of key transcription factors in the human sinus node versus right atrium

6.1 Introduction

It has been calculated that the heart produces ~2.4 billion beats during the human lifespan, after the discovery of the SN (Keith and Flack, 1907). Well-coordinated impulse initiation and propagation are its essential properties, as perturbations often result in brady/tachycardias, heart failure, or sudden cardiac death (Sumiyoshi et al., 2005). For these reasons, the molecular makeup of the cardiac conduction system and its concurrent function are tightly orchestrated by a gene regulatory network, which dictates the cardiac cell fate in the heart by forming distinct nodal or myocardial regions (Christoffels et al., 2006; Groot et al., 2007; Snarr et al., 2007; Xie et al., 2012). The cardiac impulse is generated in the SN, which is characterised by HCN4-dependent automaticity and slow conduction properties (Difrancesco and Tortora, 1991), driven by expression of low conductance gap junction genes GJD3 (Cx30.2) and GJA7 (Cx45), and low levels of SCN5A ($Na_V1.5$) (Chandler et al., 2009; Kanter et al., 1992; Kreuzberg et al., 2006). In contrast, the working myocardium, such as the RA, exhibits faster impulse conduction, which is essential for rapid synchronised contraction, produced by high conductance gap junctions GJA5 (Cx40) and GJA1 (Cx43) and higher levels of SCN5A ($Na_V1.5$) expression (Chandler et al., 2009; Kanter et al., 1992).

The cardiac conduction system and working myocardium are developed simultaneously during embryogenesis (Paff et al., 1968). Lineage studies suggest that the nodal tissue is

derived from cardiomyocyte precursor cells (Cheng et al., 1999; Gourdie et al., 1995), implying that a unique molecular mechanism is involved in the regional differentiation of the atrial myocytes into nodal cells. It has been suggested that this process occurs by repression of atrial myocytes differentiation and enhanced expression of nodal genes.

The SN formation is a complex and highly regulated process by gene networks that control its development, cell proliferation, and survival during embryogenesis and adulthood. MicroRNAs, as well as transcription factors (TFs), play a major role in these processes. TFs are regulatory molecules that control the transcription of DNA to mRNA, by having a direct contact with specific DNA sequences they are targeting (Latchman, 1997). TFs, unlike microRNAs that only negatively regulate mRNA translation, could have a turn on or turn off effect on their target genes, and depending on their availability in the cells, they maintain a varying gene expression during the cell fate determination (Latchman, 1997). A specific feature of TFs is that their sequence contains at least one binding site, which attaches to a DNA sequence in a close relation to the target gene they regulate (Mitchell and Tjian, 1989; Ptashne and Gann, 1997). The transcription factor gene network in the SN is divided into two major branches – T-box (Tbx) factors – Tbx1, Tbx3, Tbx5, and Tbx18, and the homeodomain factors – Shox2, Nkx2-5, and Isl1 (Greulich et al., 2011; Harvey et al., 2002; He et al., 2011). Shox (short stature homeobox) genes are a family of transcription factors regulating cell fate, cell cycle, and growth. Developing hearts of human embryos express Shox2 mRNA (Blaschke et al., 1998; Clement-Jones et al., 2000; Rao et al., 1997). Shox2 was found to be essential in mouse SN development as Shox2 knockout mice lacked Tbx3 and HCN4, major SN markers. Moreover, the SN region exhibited ectopic expression of Cx40 and Nkx2-5, essential working myocardium markers, indicating loss of nodal cell-like properties in the SN (Espinoza-Lewis et al., 2009). Tbx

family members have unique regulatory roles in cardiac development (Hoogaars et al., 2007a). Human Tbx3 mutations have been reported to cause Ulnar-Mammary syndrome, where ventricular septal defects, right ventricular hypertrophy, and pulmonary stenosis have been reported (Bamshad et al., 1997; Meneghini et al., 2006). Tbx3 was found to have a major role in the cardiac conduction system development (Hoogaars et al., 2004), and more specifically the generation, maturation, and functional maintenance of the SN (Hoogaars et al., 2007b). Previous studies report Tbx3-negative atrial and Tbx3-positive SN precursors cells, suggesting this transcription factor is essential for SN specialisation (Hoogaars et al., 2004). Tbx3 alongside Tbx18 were shown to regulate gene expression programmes, which result in regionalisation of the gene expression during SN formation (Wiese et al., 2009). The main role of Tbx5 in the cardiac conduction system has been focused in the atrioventricular node, atrioventricular bundle, and bundle branches (Moskowitz et al., 2004). Moreover, Tbx5 works in collaboration with Nkx2-5 in the formation of the ventricular conduction system (Moskowitz et al., 2007). Nkx2-5 in turn is reported to work in concert with other molecules for the formation of the atrioventricular node. Patients with heterozygous mutations for Nkx2-5 exhibit pronounced atrioventricular block as well as atrioventricular node and His bundle degeneration (Benson et al., 1999; Pashmforoush et al., 2004; Sarkozy et al., 2005). Our current study is focused on the expression profile of these transcription factors and their functional role in the SN. We hypothesise that TFs, as well as microRNAs, form regulatory feedback loops taking part in the control of SN function, during both embryogenesis and adulthood.

6.2 Methods

6.2.1 Next generation sequencing

Next generation sequencing (NGS) was performed on RNA samples collected from frozen SN preparations. SN samples were collected from the area around the SN artery and RA samples from the pectinate muscles remote from the SN region. Samples were collected from three human specimens (Table 6.1) in accordance with the protocol described by Chandler et al., Figure 1 (Chandler et al., 2011). NGS was performed in the Genomic Technologies Core Facility, University of Manchester. Quality, quantity, and integrity of the samples were measured by 2200 TapeStation (Agilent Technologies) to ensure their suitability for the experiment. Subsequently, the data were input into TruSeq® Stranded mRNA assay (Illumina, Inc.) libraries in order to produce more stable, single-stranded cDNA as follows:

Total RNA at concentration of 0.1-4 μg was purified to polyadenylated mRNA via magnetic separation technology, which works through hybridisation of covalent interactions of oligo $d(T)_{25}$ to poly (A) regions present in most eukaryotic mRNA. The mRNA sequences were fragmented into parts via divalent cations at higher temperature and random primers were used to reverse transcribe the mRNA fragments into single-stranded cDNA. DNA polymerase and RNase H mediated the synthesis of the second cDNA strand produced from RNA oligonucleotides, originating from the 5' end of the mRNA. The final cDNA library was generated by an addition of a single 'A' base, binding of adapters to the fragments and purification and enrichment via a PCR reaction. The cDNA libraries were incorporated into a multiplex system using the adapters; they were then pooled and clustered using cBlot instrument (Illumina). Optical flow-cells containing

the mRNA samples were then paired-end sequenced and mRNA was quantified through repeating 76 cycles twice, using an Illumina HiSeq4000 instrument. Ian Donaldson, a bioinformatition from the Genomic Technologies Core Facility, University of Manchester, used Bcl2fastq software (2.17.1.14) to generate an mRNA expression database for each individual SN vs. RA as individual values and calculate fold change expression between the two distinct anatomical regions. He also plotted the 1) principal component analysis (Figure 6.1) in order to confirm the SN and RA samples are showing consistent mRNA expression results and 2) volcano plot (Figure 6.2) indicating the significantly more and less expressed mRNAs from the two distinct heart regions.

Specimen number	Age	Gender	Cause of death	RNA quantity (ng/μl) SN/RA
1	19	Male	Suicide	114.11/389.00
2	21	Male	Suicide	35.3/59.66
3	54	Male	Intracranial haemorrhage	45.35/91.77

Table 6.1. Specimen information. Total RNA was extracted from SN and RA region of each specimen. SN samples were taken around the SN artery and RA samples were taken from the pectinate muscles.

6.2.2 Transcription factors and transcription regulators bioinformatics

Identification of the transcription factors and transcription regulators, which were significantly more expressed (log2 fold change>1), or significantly less expressed (log2 fold change<-1) in the SN was performed using Ingenuity Pathways Analysis (IPA; Ingenuity systems, Qiagen) web-based software. The IPA knowledge base contains information about experimentally validated molecules, origin and function of which can be

found in the published scientific literature. In order to narrow down the list of 2, 595 significantly more/less expressed molecules in the SN vs. RA, we used a transcription regulators target filter for molecules observed in the human only and the information, which was input in the software, contained gene name of the mRNA of interest, fold change of expression in the SN vs. RA, and p values. We focused on ISL1, Shox2, Nkx2-5, Tbx1, Tbx3, Tbx5, and Tbx18 because these were well known and described in the literature TFs involved in SN and working myocardium development and maintenance. Future experiments would focus on the rest of the TFs noted in our results, but as I had limited time available, I focused our work to what has been already known for this types of tissue and to confirm it.

6.3 Results

Our study sought to profile the expression of important transcription factors involved in the regulation of the pacemaking activity of the SN as well as the function of the RA. We mapped transcription factors in 3 human SN and their corresponding 3 RA. In order to verify the reliability of our mRNA samples, we produced principal component analysis (Figure 6.1) that confirmed two distinct mRNA profiles – SN and RA. This is a comparable analysis of the samples and it groups them into two distinct groups according to the overall mRNA expression.

Next generation sequencing data looked into the expression of 3060 most abundant mRNAs in 3 human SN vs. 3 RA. Volcano plot (Figure 6.2) summarises the results showing that 1238 mRNAs were significantly more in the SN (log2 fold change>1, $p<0.05$), and 1357 were significantly less in the RA compared to the SN (log2 fold

change<1, p<0.05). The expression of 465 mRNAs were not significantly different between the two distinct regions (log2 fold change is between -1 and 1).

Correlation comparison looked into the variability of transcription factors expression between SN and RA samples (Figure 6.3). This method was used to confirm if the three different samples show similar expression of the most significant transcription factors, and if there is any variability between them according to their results. Green to black colour indicated that the correlation between SN and their relative RA samples is relatively low (>0.85, Figure 6.3), whereas the correlation between SN samples only, and RA samples only - was significantly high (<0.85, Figure 6.3), indicated by dark to bright red colour. These results confirmed that samples correlate according to their transcription factor expression, meaning they express similar levels of transcription factors cDNA and are thus consistent.

In order to further narrow down the list of potential functional SN and RA regulators, IPA software was used to look into the expression of transcription regulators, and identified 68 transcription regulators significantly more expressed in the SN, compared to 60 transcription regulators significantly less expressed in the SN compared to the RA (transcriptional regulators gene name, SN and RA mean ± SEM values, log2 fold change and p values can be found in Table 6.2 and Table 6.3). The expression of these most abundant transcriptional regulators is plotted on Figure 6.4 and represents the relative expression of the transcriptional regulators in the SN and RA, respectively, as fold change in the SN vs. RA. This variable list of transcriptional regulators was further narrowed down and focused on the transcription factors that play roles in the formation and regulation of the SN and the RA such as Isl1 (which was upregulated by more than 12 times log2 fold change compared to the RA, and is the most highly expressed mRNA of all

3060 mRNAs in the SN), Tbx1, Shox2, Tbx3, and Tbx18, which were found to be upregulated in the SN; and Tbx5 and Nkx2-5, which were significantly less in the SN (Figure 6.5), respectively. The differential expression of these transcription factors, which are already reported in the literature to have a role in the phenotypical development of their respective regions, suggests that they continue to have a role in the SN and RA during adulthood. Furthermore, these data imply that these transcription factors may be involved in the complex regulation of ion channels, calcium-handling proteins, and connexins expression, which gives a unique functional character of the two distinct heart regions.

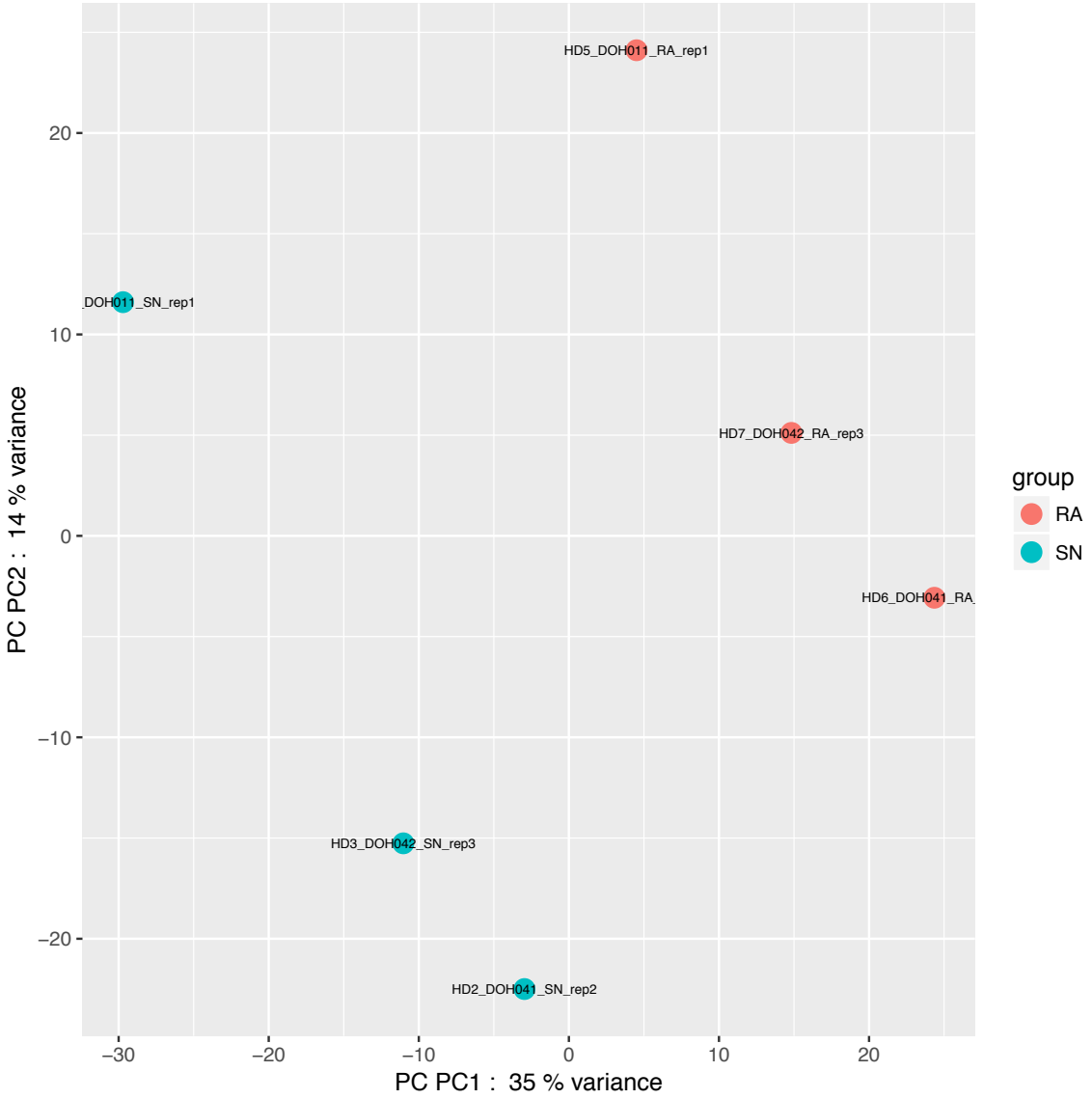

Figure 6.1. Principal component analysis profiling of mRNA samples harvested from 3 human SN and 3 RA. The graph is used to visualise the relatedness between the two different populations.

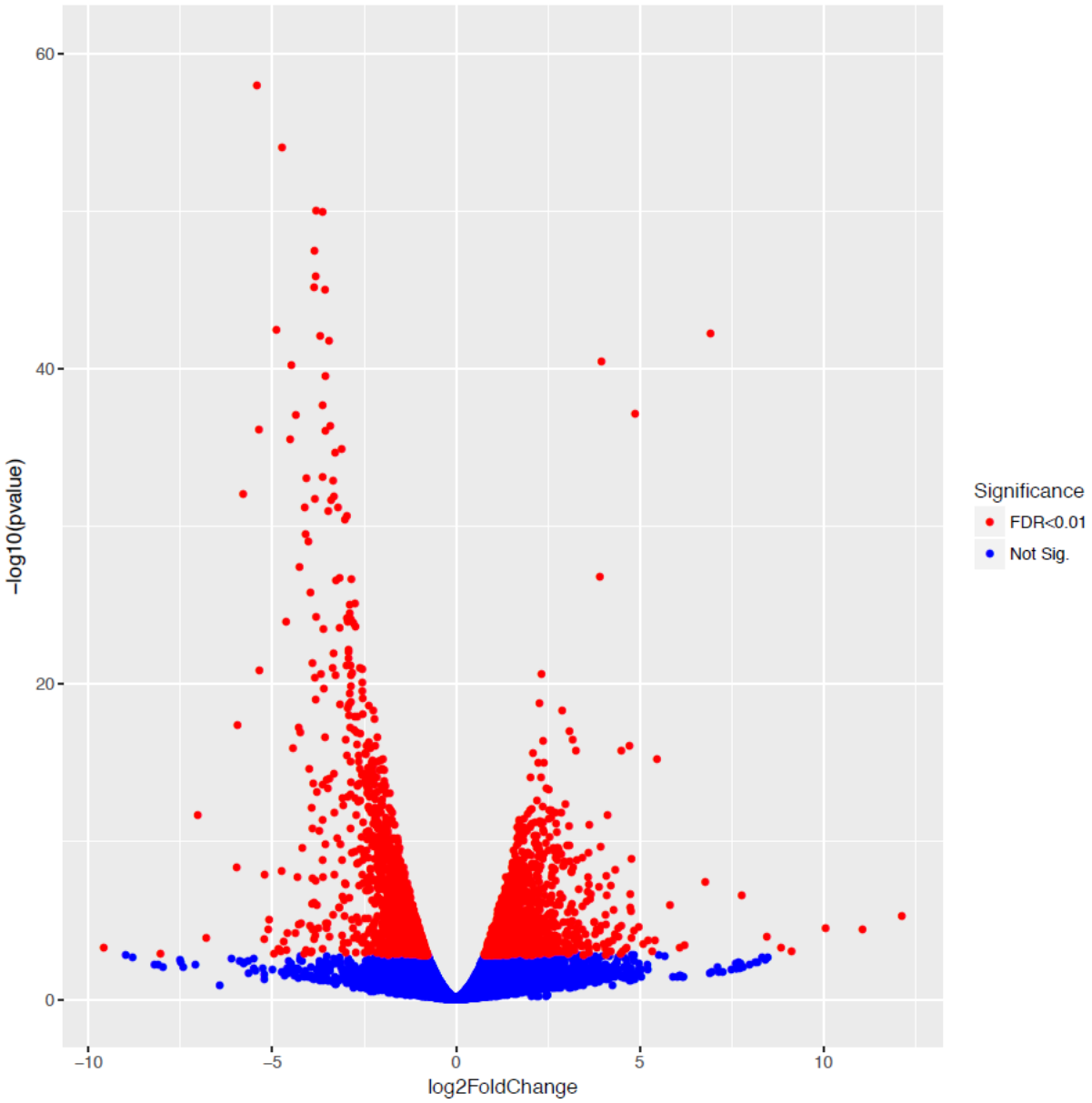

Figure 6.2. NGS mRNA data. Log2Fold Change≥0 indicates mRNAs more expressed in the SN, whereas log2Fold Change≤0 indicates mRNAs less expressed in the SN compared to the RA; significance is depicted by red colour for significantly more/less expressed, or blue non-significantly more/less expressed mRNAs. Bcl2fastq software (2.17.1.14) was used to analyse and statistically assess the data, n=3.

Transcription regulator ID	SN mean	SN SEM	RA mean	RA SEM	Log fold change	P value
ISL1	208.879	83.062	0	0	12.14	5.18E-06
VENTX	98.187	15.838	10.922	3.75	3.294	1.47E-09
PHOX2B	74.57	23.194	10.887	6.165	3.131	1.55E-06
HOXB4	221.93	24.513	37.187	24.114	3.091	1.76E-10
SOX2	153.772	53.947	21.604	6.022	2.776	2.52E-10
DLX2	48.099	20.607	8.451	4.757	2.738	0.000231
HOXC4	107.812	34.363	15.536	3.518	2.723	3.04E-08
HOXB3	440.507	40.289	76.885	29.006	2.722	1.43E-12
MYCN	61.499	5.433	10.308	4.002	2.689	1.55E-05
BATF	61.748	22.495	11.799	6.641	2.674	2.61E-05
CEBPA	282.356	65.316	52.355	24.256	2.653	2.39E-10
HOXA3	122.178	35.992	18.937	3.932	2.61	2.42E-07
BCL11B	39.23	22.307	8.633	6.676	2.608	0.000748
HDAC10	38.406	10.63	6.879	1.777	2.465	0.000572
DLX1	108.905	48.375	20.363	11.822	2.433	1.18E-05
HOXA5	61.832	13.331	12.492	4.679	2.387	4.97E-05
HOXB2	776.382	153.16	166.1	53.351	2.319	8.9E-15
TBX1	131.445	67.297	36.094	25.787	2.261	0.000238
SHOX2	1039.71	260.04	223.735	78.368	2.25	2.91E-10
FOXD3	385.436	175.537	84.572	47.553	2.199	1.56E-08
RUNX3	97.062	41.225	25.676	14.122	2.041	2.07E-05
RUNX2	101.047	16.069	25.667	3.726	1.959	3.48E-05
VAV1	107.197	57.514	24.553	11.685	1.912	0.000403
HOXD8	85.567	7.471	26.22	9.035	1.852	0.000404
TBX3	1972.733	469.804	543.995	115.281	1.845	2.01E-08
RUNX1	412.141	61.976	112.9	13.806	1.841	5.98E-08
SPI1	381.48	186.713	119.83	69.676	1.799	1.38E-08
MSC	1603.09	546.664	490.11	191.398	1.798	1.68E-11
DTX1	249	39.096	74.937	20.187	1.793	3.08E-07
IKZF1	189.948	118.644	46.666	22.659	1.792	5.2E-06
PRDM16	456.732	25.624	137.165	9.657	1.727	1.6E-08
KCNIP3	389.946	148.584	138.006	68.334	1.607	2.59E-07
GLI1	183.878	38.227	57.936	7.13	1.607	0.000102
LZTS1	234.963	59.31	76.747	13.548	1.572	2.03E-05
MLXIPL	234.667	80.361	79.937	22.441	1.522	4.09E-05
TGFB1I1	2466.217	284.716	872.904	75.898	1.477	4.59E-08
PYCARD	301.691	77.164	101.776	6.302	1.475	1.29E-05
TWIST1	377.545	84.672	143.105	42.079	1.47	5.24E-06
HLX	782.153	165.116	306.64	117.08	1.468	4.32E-07
HEY2	457.506	13.418	165.326	11.391	1.463	5.52E-07
TBX2	1749.702	175.142	658.368	122.01	1.434	4.49E-06

Transcription regulator ID	SN mean	SN SEM	RA mean	RA SEM	Log fold change	P value
MAF	1475.905	276.728	548.679	102.208	1.418	2.9E-08
SOX10	2026.732	753.631	662.197	179.093	1.394	3.14E-06
CIITA	398.745	111.455	149.505	36.256	1.381	3.76E-06
IER2	5491.416	1798.91	2118.285	678.573	1.361	1.72E-08
TBX18	1190.75	86.23333	470.92	64.5568	1.345	2.47E-06
NFKBIZ	870.258	184.484	329.93	38.444	1.338	8.14E-05
HIC1	1362.142	353.431	521.178	112.365	1.323	6.68E-07
NLRC5	341.15	66.534	136.747	23.483	1.303	3.12E-05
GLI2	347.127	75.203	137.196	19.863	1.283	0.000438
LMO2	687.174	86.682	319.748	115.363	1.28	0.000666
IRF7	493.157	124.674	213.957	75.26	1.256	3.26E-05
KLF2	6750.78	1240.935	2732.485	295.238	1.253	6.74E-07
HR	419.256	156.295	151.074	40.595	1.249	0.000433
SOX9	3348.057	108.482	1507.809	373.24	1.231	3.93E-05
NUPR1	5710.273	179.142	2548.803	440.63	1.199	1.16E-05
BACH2	226.331	59.842	97.96	20.395	1.13	0.00141
ATF5	540.281	69.534	247.84	41.619	1.127	0.000122
MEOX1	1350.634	629.078	662	360.592	1.108	2.59E-05
SOX13	1369.973	110.721	631.294	47.328	1.104	1.76E-05
SOX17	584.337	39.839	290.279	85.723	1.101	0.000309
LBH	2394.91	443.351	1091.937	135.245	1.093	0.000535
AKNA	677.906	142.21	319.611	57.408	1.055	0.000102
CERS5	896.236	87.785	433.37	61.242	1.054	8.91E-05
LYL1	379.379	41.071	181.422	9.254	1.038	0.00088
SMARCD2	1516.491	365.786	742.922	193.867	1.03	4.21E-05
TSC22D3	9758.316	3669.472	4380.536	1004.956	1.03	0.000242
SREBF1	4927.952	1336.04	2308.654	325.077	1.001	0.000109

Table 6.2. Significantly higher expressed transcription regulators in the SN. The table includes mRNA gene names, relative expression in the SN compared to the RA ± SEM, log fold change $\Delta Ct_{(Target)}$-$\Delta Ct_{(Housekeeper)}$ and p values, calculated via Bcl2fastq software (2.17.1.14), n=3.

Transcription regulator ID	SN mean	SN SEM	RA mean	RA SEM	Log fold change	P value
MYT1	3.126	2.298	32.681	10.734	-3.899	3.42E-05
ASB15	123.674	37.790	1739.861	474.424	-3.848	3.507E-48
ASB5	16.300	7.161	133.294	23.129	-3.233	6.354E-11
HAND1	6.15	1.766	56.44	19.813	-3.029	5.26E-06
SALL1	9.075	3.795	67.701	33.401	-2.798	2.916E-05
HOPX	194.455	62.767	1157.648	446.288	-2.549	3.02E-20
TBX20	400.478	52.818	2094.381	304.501	-2.392	2.129E-15
VGLL2	32.552	29.600	60.589	25.769	-2.293	7.169E-04
NKX2-5	1116.112	308.341	5549.073	1761.584	-2.287	1.249E-12
MLIP	1407.866	431.711	6203.713	1222.175	-2.268	7.430E-16
STAT4	140.858	42.809	581.692	74.953	-2.153	9.570E-10
PROX1	514.407	198.737	1897.360	415.061	-2.021	1.408E-10
HSF2	422.250	19.749	1691.197	128.986	-2.009	2.603E-15
CASKIN1	98.435	21.743	370.275	36.706	-1.973	5.828E-08
SMYD1	1604.484	589.106	5358.148	819.541	-1.960	1.098E-07
PPP1R13L	859.854	207.086	3018.562	350.626	-1.900	4.578E-12
DCAF6	2723.082	396.688	9437.394	312.369	-1.836	9.185E-12
TBX5	2894.793	967.928	9297.928	1916.888	-1.825	2.394E-08
PPARGC1A	858.408	314.360	2627.464	651.225	-1.814	3.428E-06
CERS6	1222.011	380.239	3551.558	784.415	-1.665	1.281E-08
NOCT	43.806	0.646	159.363	65.339	-1.663	1.393E-04
ACTN2	21634.431	7833.845	59256.856	5474.155	-1.662	8.432E-06
ASB4	23.684	6.879	70.022	13.042	-1.645	1.224E-03
KCTD1	401.470	33.964	1268.950	310.905	-1.602	4.689E-08
MITF	598.513	213.906	1802.958	727.443	-1.578	2.191E-08
MEF2A	2578.413	233.194	7634.998	757.997	-1.577	9.992E-11
CAND2	590.303	136.063	1630.819	216.947	-1.539	1.044E-08
GTF2I	466.899	108.962	1313.898	292.866	-1.514	8.863E-09
ZBTB20	158.281	30.758	626.103	388.802	-1.494	6.158E-05
KANK1	2571.452	526.933	6727.928	204.166	-1.458	5.888E-08
GRIP1	68.755	20.714	197.073	92.005	-1.422	6.054E-04
HLF	737.032	112.679	1921.831	194.315	-1.416	1.972E-08
KAT2B	1121.328	73.391	3010.476	471.115	-1.408	5.433E-07
NFE2L1	10964.520	1829.637	28663.931	4334.959	-1.400	1.864E-08
NCOA4	3405.760	431.596	8749.216	571.405	-1.389	1.010E-08
COPS5	794.737	79.793	1980.436	268.256	-1.315	2.910E-06
PBX3	1224.393	47.244	3027.975	201.759	-1.314	1.912E-07
SFMBT1	138.972	33.019	327.697	65.700	-1.285	2.215E-04
CHCHD3	1259.526	186.752	2966.429	190.626	-1.273	7.311E-06
ZNF189	453.549	22.899	1185.676	426.572	-1.228	9.397E-05
YAF2	766.448	115.140	1719.524	37.999	-1.211	1.065E-05

Transcription regulator ID	SN mean	SN SEM	RA mean	RA SEM	Log fold change	P value
HIVEP2	538.440	57.714	1286.742	295.821	-1.201	3.879E-04
YBX3	6104.641	277.970	13980.831	1611.231	-1.191	1.167E-06
CBX4	602.128	129.064	1333.066	241.324	-1.186	4.406E-05
TEAD1	2063.731	110.694	4656.889	513.296	-1.174	3.338E-06
FHL2	4488.626	1459.722	12576.092	7584.572	-1.173	1.026E-03
TRIM24	400.102	64.223	875.524	95.024	-1.160	2.382E-05
GTF3A	2393.535	216.862	5320.791	640.947	-1.153	2.201E-05
RFX2	352.593	55.933	918.063	340.632	-1.133	9.973E-04
BRCA1	126.173	10.455	282.040	60.510	-1.120	5.047E-04
SATB1	493.157	124.674	213.957	75.26	1.256	3.26E-05
HDAC9	258.074	32.224	549.930	51.861	-1.112	6.608E-05
TCEA3	828.140	135.026	1736.017	182.424	-1.098	8.004E-05
FEM1A	1145.289	200.935	2378.667	319.940	-1.088	9.824E-05
MKL2	956.58	331.959	2660.534	1659.107	-1.075	0.000449
HMGA1	420.776	54.922	856.277	41.092	-1.058	0.000238
ASB8	637.596	50.060	1291.190	48.396	-1.037	5.749E-05
MLX	969.099	65.291	1959.077	140.850	-1.026	3.449E-05
NCOA2	835.154	95.142	1727.3	381.213	-1.018	0.000197
NPAS2	736.022	124.618	1503.172	308.439	-1.017	0.00094

Table 6.3. Significantly lower expressed transcription regulators in the SN. The table includes mRNA gene names, relative expression in the SN compared to the RA ± SEM, log fold change ($\Delta Ct_{(Target)}$-$\Delta Ct_{(Housekeeper)}$) and p values, calculated via Bcl2fastq software (2.17.1.14), n=3.

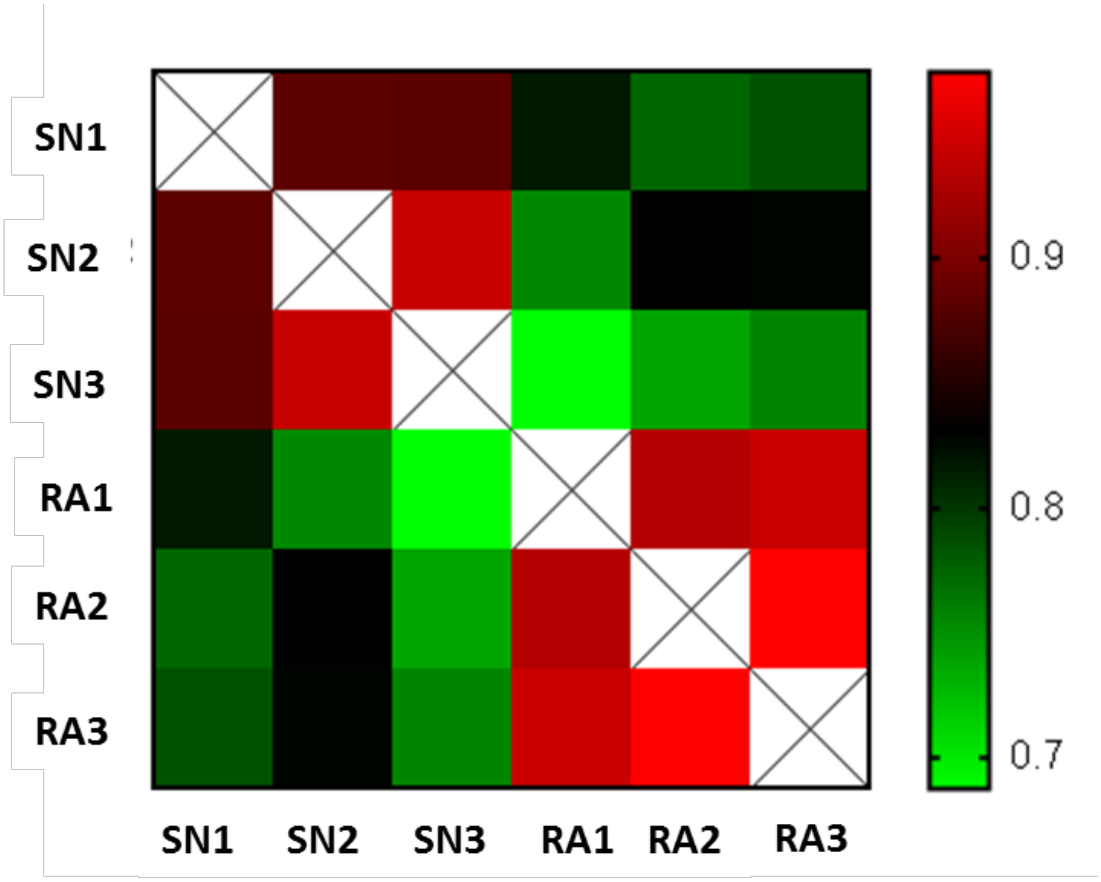

Figure 6.3. SN and RA samples correlation. SN1 and RA1 samples were extracted from specimen 1, SN2 and RA2 from specimen 2 and so on. The correlation was performed on the significantly lower or higher transcription factors cDNA expression in the SN and the RA samples. Perfect correlation is considered as 1 (bright red), and the lower the number the lower the correlation (bright green). Individual sample values were taken from NGS data. Analysis was performed through correlation analysis in GraphPad Prism 7.0 software.

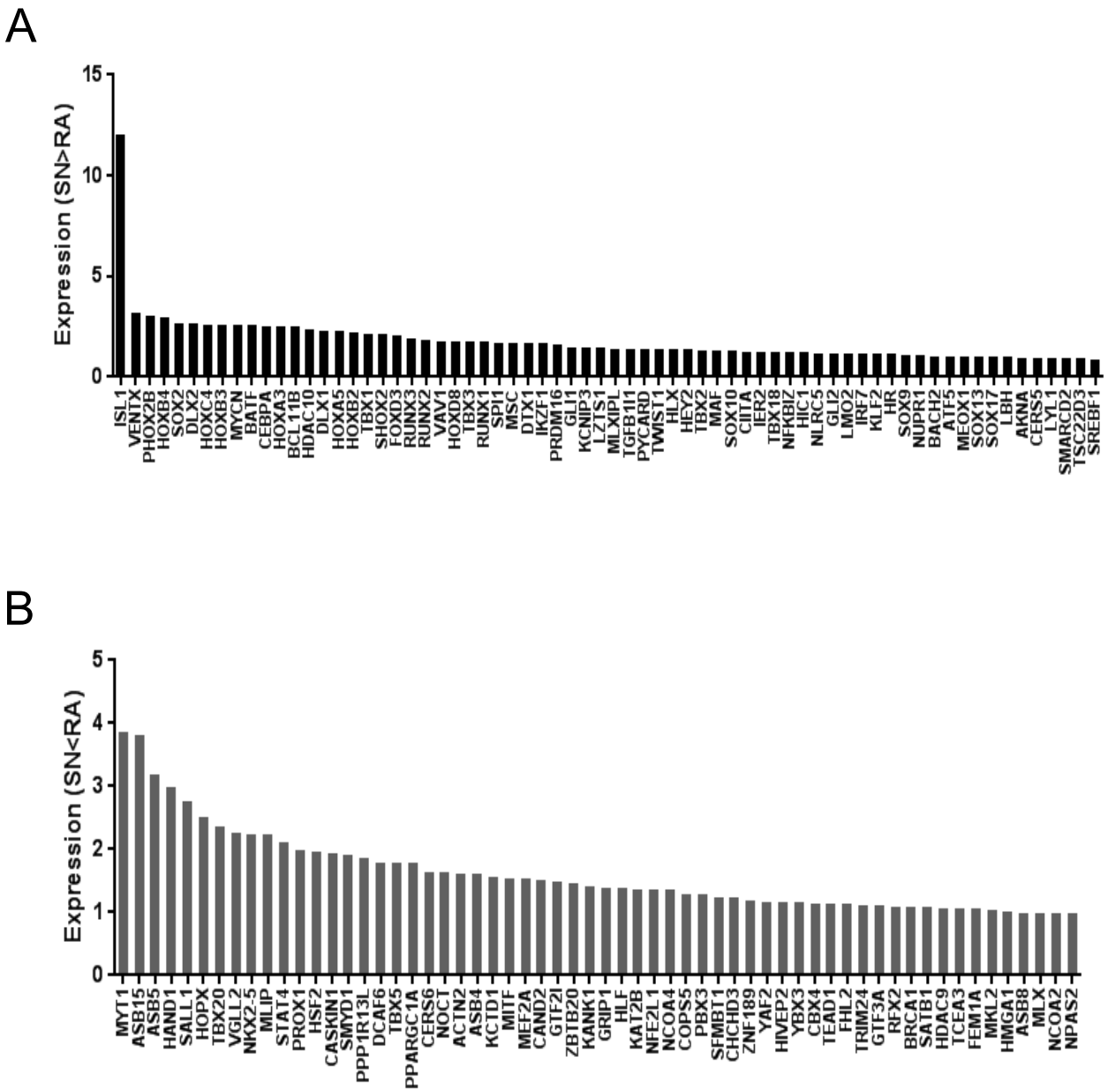

Figure 6.4. Significantly more (A) or less (B) expressed mRNAs in the SN compared to the RA. NGS analysis discovered 68 transcription regulators were significantly more expressed and 60 were significantly less expressed in the SN. Data was analysed via Bcl2fastq software (2.17.1.14), n=3. Plots were created via GraphPad Prism 7.0.

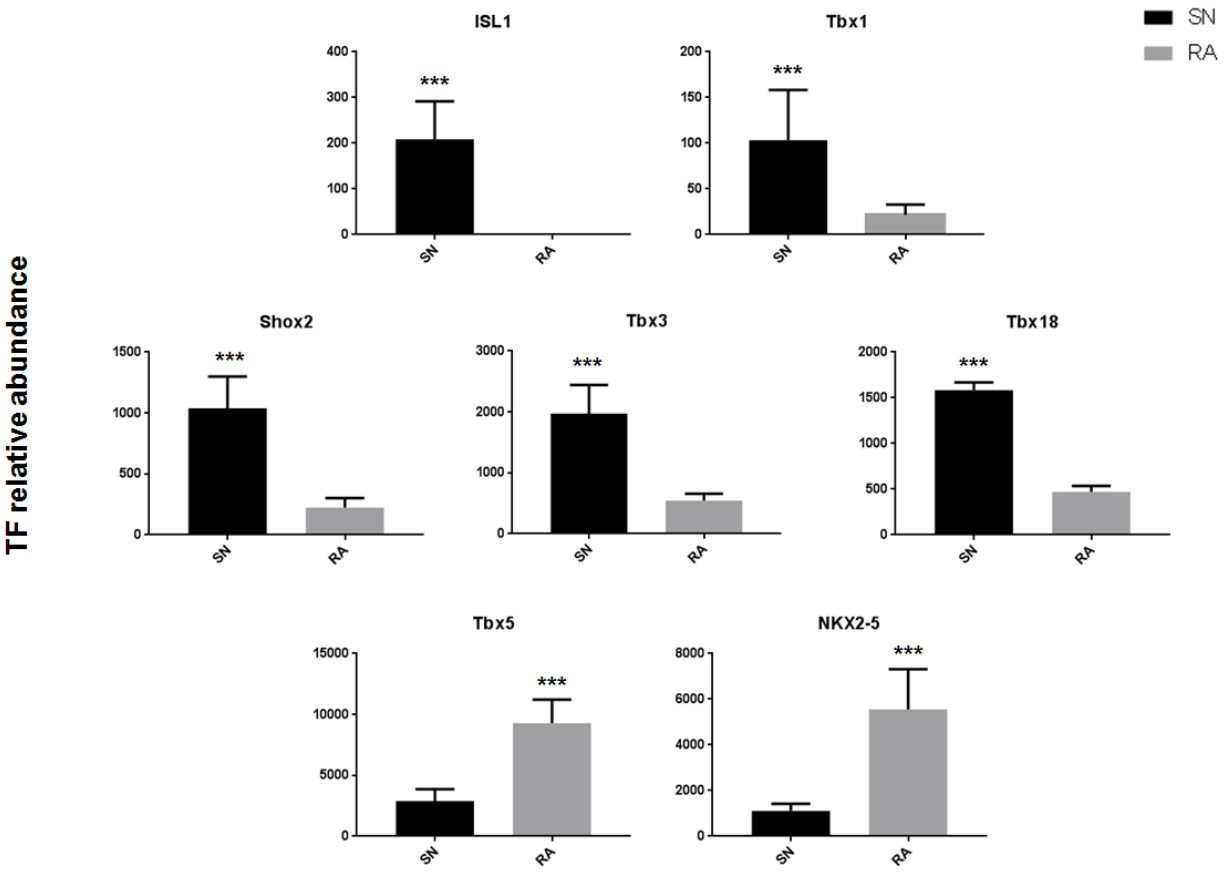

Figure 6.5. Significantly more or less expressed transcription factors (TFs) in the SN compared to the RA. Data is presented as relative abundance of transcription factors' (TF) mRNA against housekeeper gene ± SEM, analysed via Bcl2fastq software (2.17.1.14), n=3. Plots were created via GraphPad Prism 7.0.

6.4 Discussion

Isl1 is the most abundantly expressed transcription factor in the SN compared to the RA, suggesting that it plays a leading role in SN regulation. Similarly to what we show, Isl1 expression was reported to be maintained in the SN during adulthood (Sun et al., 2007; Vedantham et al., 2015). Deletion of Isl1 in zebrafish induced bradycardia accompanied with irregular heartbeat and pauses (de Pater et al., 2009; Tessadori et al., 2012). Liang et al. produced an Isl1 mutant mouse with a deletion of the gene specifically in the SN region, which led to sinus arrhythmia, reduced SN cell differentiation, and proliferation during embryogenesis and embryonic lethality. In situ hybridisation revealed significantly reduced expression of genes critical for SN function genes such as HCN4, Shox2, and Tbx3 (Liang et al., 2015). These data suggest that Isl1 is a requirement for proliferation and survival of SN cells, and it directly affects the expression of a number of genes that are critical for the pacemaker activity in the mouse and human heart.

Tbx1, Tbx3, Tbx18, and Shox2 are also significantly higher expressed in the human SN. Similarly to Isl1, Shox2 was reported to be crucial for SN development, and deficiency of the gene caused reduced SN cells proliferation and differentiation, and bradycardia, resulting in embryonic lethality (Blaschke et al., 2007), which implies that SN formation fails in the absence of Shox2. Shox2 was found to have an indirect positive effect on the expression of major pacemaker genes Tbx3 and HCN4 by negatively regulating Nkx2-5 (a repressor of Tbx3 and HCN4 gene expression) (Blaschke et al., 2007; Espinoza-Lewis et al., 2009). It was also shown to indirectly repress the expression of major working myocardium genes GJA1 (Cx43) and GJA5 (Cx40) through Nkx2-5 inhibition (Blaschke et al., 2007; Espinoza-Lewis et al., 2009). HCN4-restricted Isl1 knockout mice were reported to exhibit significant downregulation of Tbx3, HCN4, HCN1, and CACNA1G

($Ca_V3.1$) genes, and upregulation of the working myocardium genes GJA1 (Cx43), GJA5 (Cx40), and SCN5A ($Na_V1.5$) (Vedantham et al., 2015). Downregulation of Nkx2-5 gene expression has been shown to attenuate the morphological and functional defects in Shox2 knockout mice (Ye et al., 2015). This suggests that these transcription factors work in an antagonistic manner and imbalanced expression of either leads to heart defects, which can be rescued by supressing the expression of the other dominating transcription factor. Shox2 has been also suggested to positively reinforce Isl1 expression through direct and indirect mechanisms via Nkx2-5 transcriptional repression (Hoffmann et al., 2013; Ye et al., 2015). These findings indicate that Shox2 plays an essential role in SN formation by transcriptional reinforcement of Isl1, direct Nkx2-5 transcriptional repression, or Nkx2-5-dependent GJA1 (Cx43), and GJA5 (Cx40) regulation, while reinforcing nodal genes Tbx3, HCN4, HCN1, and CACNA1G ($Ca_V3.1$) expression. The working myocardium, including the RA, lacks Shox2 expression, resulting in significantly higher levels of Nkx2-5, which we suggest in turn activates working myocardium genes GJA1 (Cx43), GJA5 (Cx40), and SCN5A ($Na_V1.5$) and represses ectopic expression of pacemaker genes Tbx3, HCN4, HCN1, and CACNA1G ($Ca_V3.1$).

Similarly to our results, Tbx3 has been shown to be highly expressed in the SN, where it represses the working myocardium gene programme directly by repressing GJA1 (Cx43), GJA5 (Cx40) and ANP (atrial natriuretic peptide) (Mommersteeg et al., 2007). A recent study has reported that Tbx3 is a dosage-dependent regulator of the SN, as graded decrease in Tbx3 is associated with bradycardia, reduced SN size, and ectopic upregulation of the aforementioned myocardium-specific genes (Frank et al., 2012). The role of Tbx3 in the adult heart was implied by reports that arrhythmias was induced by Tbx3 knockdown in an adult mouse model, suggesting Tbx3 is a requirement for cardiac conduction system

homoeostasis (Frank et al., 2012). Overexpression of Tbx3 in the working myocardium results in upregulation of nodal genes (HCN4, GJD2 (Cx30.2), and CACNA1G ($Ca_V3.1$)), and ectopic pacemaker formation leading to arrhythmias in mice (Hoogaars et al., 2007b). An upstream regulator of Tbx3, Baf250a, together with Tbx3 itself, and the histone Deacetylase 3 (HDAC3) act in a coordinated fashion to maintain low Nkx2-5 levels in the SN (Wu et al., 2014). Tbx3 is a major nodal transcription factor, which positively regulates pacemaker ion channels, inhibits the expression of typical myocardium gap junctions, and synergistically together with other transcription factors negatively regulates the expression of major myocardium transcription factors such as Nkx2-5.

Tbx18, unlike Tbx3, which is found in other types of nodal tissue types too (Hoogaars et al., 2007b; Horsthuis et al., 2009), is specifically expressed in SN precursor cells. Its distinct expression is demonstrated by Christoffels et al., 2006, where the gene is essential for the morphological formation of the SN 'head' structure (Aanhaanen et al., 2010; Mommersteeg et al., 2010). These funding have been further substantiated by research in Tbx18 knockout models, characterised by loss of the SN 'head' structure, while the 'tail' structure was shown to be preserved. Ectopic expression of Tbx18 in ventricular myocytes was shown to convert them into pacemaker-like cells (Cho et al., 2012; Christoffels et al., 2006). Similarly to Shox2 and Tbx3, Tbx18 was shown to induce a negative feedback loop upon Nkx2-5 (Christoffels et al., 2006). It was also reported that Tbx18 induces transcriptional repression of GJA1 (Cx43), without affecting GJA5 (Cx40) and GJC1 (Cx45) (Kapoor et al., 2011), suggesting it is working in a coordinated fashion with Tbx3 in the transcriptional reinforcement of nodal genes, and repression of working myocardium genes, although its mechanism of action is still unclear.

Tbx1 has been related to malformations in the morphogenesis of the cardiac outflow tract and is shown to cause congenital heart defects similar to the ones observed in the DiGeorge syndrome (Baldini, 2004; Xu et al., 2004; Zhang et al., 2006). Tissue specific Tbx1 knockout mice were produced to show the function of Tbx1 in the cardiac outflow tract, reporting that the transcription factor is involved in nodal cell proliferation in the secondary heart field during embryogenesis, from which SN originates. It was also shown that Tbx1 is required in Nkx2-5-expressing cells for the formation of the aorto-pulmonary septum (Xu et al., 2004), suggesting they are working in parallel.

Tbx5 and Nkx2-5 were ~2 times less expressed in the human SN compared to the RA. Tbx5, interestingly, has a dual function in both nodal and working myocardium development, and thus its function varies depending on the tissue context. Mice lacking Tbx5 gene were reported to exhibit a decrease in cell differentiation in the inflow tract, with spontaneous and sustained atrial fibrillation due to spontaneous depolarisation (Bruneau et al., 2001). Tbx5 was also found to reinforce the expression of Shox2 and Tbx3 in the SN (Puskaric et al., 2010). Moreover, Tbx5 haploinsufficiency in mice led to Shox2 and Tbx3 translational repression in the inflow tract and subsequent sinus node dysfunction (Basson et al., 1999). In the working myocardium, however, Tbx5 acts as transcriptional promoter of Pitx2, and both transcription factors synergistically repress SCN5A ($Na_V1.5$), GJA1 (Cx45) and RyR2 in the atria. In addition, dose-dependent Tbx5 reduction in this region causes myocardial automaticity and atrial fibrillation susceptibility (Nadadur et al., 2016). These results suggest that Tbx5 has an important function in the working myocardium as well as the SN, which is possibly dependent on complex transcription factors feedback loops that are essential to sustain regular heart rhythm, and alterations in these complex loops can lead to atrial fibrillation susceptibility.

Nkx2-5 is a major cardiac development transcription factor the absence of which causes embryonic lethality (Terada et al., 2011). Nkx2-5 is an important promoter of the fast conduction gene programme in the working myocardium due to reinforcement of GJA1 (Cx43), GJA5 (Cx40), and SCN5A ($Na_V1.5$) genes through Tbx3 inhibition (Espinoza-Lewis et al., 2009; Ye et al., 2015), and further inhibition of nodal genes such as HCN4, HCN1, and CACNA1G ($Ca_V3.1$) as previously mentioned. Its regional function depends on its expression levels compared to Tbx3 and Tbx5, which in dose-dependent manner would produce a negative feedback loop and inhibition of Nkx2-5 expression. Although Tbx5 and Nkx2-5 act antagonistically in the SN and the working myocardium, interestingly, they work in a synergistic manner in the atrioventricular node formation, where they enhance GJA5 (Cx40) expression, important for fast conduction (Bruneau et al., 2001; Jay et al., 2004). We could conclude that Tbx5 and Nkx2-5 function varies depending on their regional expression; however, their widespread expression in the embryonic heart does not imply that their expression is a sole requirement for the cardiac conduction system development, and their function appears to be more important in the working myocardium.

Human lineage studies report association between congenital cardiac defects and Nkx2-5 and Tbx5 mutations (Schott et al., 1998). Research in Nkx2-5 deficient mice following these lineage studies confirmed existence of congenital cardiac defects phenotype (Jay et al., 2004). Tbx5 knockout mice were also shown to exhibit Hold-Oram syndrome phenotype (Bruneau et al., 2001). These studies suggest that Nkx2-5 and Tbx5 are not only involved in cardiac morphogenesis during embryonic stages of development, but are also essential during adulthood.

In addition to transcription factors, microRNAs also play a role in the cardiac conduction system gene regulatory network by fine-tuning gene expression through posttranscriptional silencing. In contrast with transcription factors, which can positively or negatively regulate their target genes, microRNAs are only supressing the translation of their target mRNAs. Several microRNAs have been already shown in the scientific literature to take part in cardiac conduction system development or in response to athletic training. miR-1 has been reported to be a HCN4 mRNA inhibitor (Fu et al., 2011). Muscle-specific miR-1-2 knockout mice exhibited profound electrical conduction deviations in the heart that resulted in reduced heart rate, shortened PR intervals, and prolonged QRS interval as well as abnormal cardiac morphogenesis and dysregulated cell cycle (Zhao et al., 2007). miR-1 was also found to be negatively regulated by the major developmental heart transcription factor Nkx2-5 in two cell lines. Nkx2-5 transfected HL-1 cells, derived from atrial cardiomyocytes, and primary cardiomyocytes were shown to express reduced miR-1 levels. Mutation at Nkx2-5 binding site for miR-1 abolished their interaction, confirming miR-1 is directly supressed by Nkx2-5 (Qian et al., 2011).

Athletic training-induced sinus bradycardia in mice was found to be a result of HCN4 downregulation and decrease in I_f, together with upregulation of miR-1 and NRSF (transcriptional inhibitor of HCN4 (Kuratomi et al., 2007)), suggesting a potential explanation for bradycardia as adaptation to exercise training in athletes (D'Souza et al., 2014) . Further experiments in athletically trained mice showed that Nkx2-5 upregulation in the heart reinforces the expression of miR-423-5p, which in turn represses HCN4 expression and I_f in the heart (D'Souza et al., 2017). Inhibition of miR-423-5p with anti-miR-423-5p antagomiR rescued HCN4 levels and I_f and abolished the training-induced bradycardia (D'Souza et al., 2017). These data imply that the cardiac conduction system

transcription regulatory network is a major coordinator of cardiac morphology and function in both health and disease.

Chapter 7

7 The effect of miR-133a-3p on beating rate and HCN4 expression in cardiac-derived iPSCs

7.1 Introduction

Takahashi and Yamanaka (2006) were the first to discover that somatic cells can be reprogrammed to generate induced pluripotent stem cells (iPSCs). This was achieved by introducing four retrovirally-transduced transcription factors (OCT4, SOX2, KLF4, and cMYC) in mouse dermal fibroblasts. Soon after this discovery human iPSCs (hiPSCs) were generated by either using the same transcription factors (Takahashi et al., 2007) or a slightly different combination of OCT4, SOX2, LIN28, and NANOG transcription factors (Yu et al., 2007). HiPSC derived cardiomyocytes (HiPSC-CMs) were then induced from foetal and new-born tissue samples (Zhang et al., 2009). qPCR analysis and/or immunohistochemistry demonstrated that hiPSCs express a number of cardiac-specific transcription factors such as Nkx2-5, GATA-4, and myocyte enhancer factor 2C (MEF2C) in addition to structural sarcomeric proteins such as α-actinin, cardiac troponin I and T, sarcomere myosin heavy chain (MHC), atrial and ventricular myosin light chains (MLC2a and MLC2v), and atrial natriuretic factor (ANF) (Kehat et al., 2001; Tanaka et al., 2009; Xu et al., 2002; Yokoo et al., 2009; Zhang et al., 2009). It was shown that the expression of these molecules is typical for differentiated hiPSCs only in comparison to undifferentiated cells where their expression was significantly lower (Gupta et al., 2010).

In order to further characterise the molecular nature of hiPSC-CMs and to confirm their similarities with true human cardiomyocytes, qPCR analysis of the cardiac ion channels

transcripts was performed, demonstrating expression of 1) $Na_V1.5$ (SCN5A), responsible for I_{Na}, which underlies myocytes excitability and defines conduction velocity; 2) $Ca_V1.2$ (CACNA1C) and $Ca_V1.3$ (CACNA1D), responsible for $I_{Ca,L,}$ involved in the cardiac excitation-contraction mechanism; 3) KCNH2 (hERG) and KCNQ1, components of $I_{K,r}$ and $I_{K,s}$, which cause action potential repolarisation after excitation; 4) HCN4, the most significantly expressed hyperpolarisation-activated cyclic nucleotide-gated potassium channel isoform in the SN, responsible for I_f and the cardiac automaticity; 5) Kir2.1, conducting $I_{K,ur}$, and 6) $K_V4.3$, conducting I_{to} (Tanaka et al., 2009; Yokoo et al., 2009; Zwi et al., 2009).

Functional experiments using patch clamp to measure the action potential in spontaneously contracting single cells, isolated from hiPSC embryoid bodies demonstrated that a majority (70-74%) of action potentials had ventricular-like features and a smaller number had atrial- and nodal-like action potentials. The nodal-like action potentials were characterised by more positive maximum diastolic potential, slower action potential upstroke, and a distinct depolarisation phase 4, compared to the ventricular-like action potentials (Fatima et al., 2011; Itzhaki et al., 2011; Ma et al., 2011; Moretti et al., 2010).

A few studies look into ionic currents in hiPSCs. HiPSCs Na^+ current kinetic properties were observed to be consistent with those of mature native human ventricular cardiomyocytes I_{Na} (Davis et al., 2012; Ma et al., 2011), where it causes action potential depolarisation. In terms of Ca^{2+} currents, as already mentioned, there are two major ones that regulate the mammalian contractility – L-type Ca^{2+} current, conducted by mainly $Ca_V1.2$ and $Ca_V1.3$, and T-type Ca^{2+} current, conducted by $Ca_V3.1$ (Nerbonne and Kass, 2005). Ma et al., 2011 reported a clear presence of $I_{Ca,L}$, but absence of $I_{Ca,T}$, which is present in the cardiac conduction system and facilitates the pacemaker depolarisation after

I_f activation (Ono and Iijima, 2010). $I_{Ca,T}$ is also absent in mature human ventricular cardiomyocytes, suggesting that the nodal-like hiPSCs are potentially immature ventricular-like myocytes. $I_{K,r}$ and $I_{K,s}$ were reported to be present in hiPSCs (Itzhaki et al., 2011; Ma et al., 2011; Moretti et al., 2010), but $I_{K,ur}$, important for repolarisation of the action potential in the working myocardium during phase 3 (Nerbonne and Kass, 2005), was absent. $I_{K,1}$, the inward rectifier current, which is an important contributor to the resting membrane potential in atrial and ventricular myocytes (Dhamoon and Jalife, 2005), and the transient outward current, $I_{to,}$ were found to be also present in hiPSCs (Ma et al., 2011; Moretti et al., 2010). Ma et al., 2011 also demonstrated presence of I_f current in hiPSCs (Ma et al., 2011), which might have a role in the spontaneous activity in these cells. Synnergren et al., suggested that the high I_f current density in hiPSCs compared to human atrial and ventricular myocytes could be explained by the fact that hiPSCs express higher levels of HCN1, HCN2, and HCN4 as compared to human mature cardiomyocytes (Synnergren et al., 2012).

The discovery that adult somatic cells could be reprogrammed and induced into iPSCs gives the opportunity of creating unique patient- and disease-specific hiPSC lines, which could be further turned into embryonic stem cells. In turn, this gives the possibility to create and study genetically diverse human model systems, allowing the investigation of disease mechanisms.

We showed that miR-133a-3p is highly expressed in human RA vs. SN (Chapter 3), and it has been further reported to bind to and inhibit the expression of HCN2 and HCN4 (Xiao et al., 2012). In collaboration with Dr. Vadim Fedorov and Dr. Ning Li, The Ohio State University, we confirmed that miR-133a-3p is significantly more expressed in human healthy RA compared to SN tissue (Figure 7.1). Moreover, we found that miR-133a-3p

expression is upregulated in heart failure SN compared to healthy. These findings set the basis of the hypothesis that miR-133a-3p has in important physiological and pathophysiological role in the heart and it potentially supresses HCN4 expression in the working myocardium, however, during heart failure it affects HCN4 in the SN.

miR-133 was identified as the most abundant microRNA in the working myocardium and it is muscle-specific (McCarthy and Esser, 2007). miR-133 and miR-1 were initially reported to take part in muscle hypertrophy and growth (McCarthy and Esser, 2007). miR-133 involvement in human cardiac hypertrophy was also demonstrated (Care et al., 2007b). In contrast, transverse aortic constriction (TAC)-induced hypertrophy in mice caused downregulation of miR-133 expression. It was suggested that miR-133 targeted NFATc4 and calcineurin as well as Rac and Cdc4, which are signalling molecules and transcription factors, involved in cardiac hypertrophy (Care et al., 2007b; Dong et al., 2010).

A few other groups reported a more complex role of miR-133 in cardiac hypertrophy. miR-133a knockout in a mouse model was found to be embryonically lethal due to cardiac defects (Liu et al., 2008a). It was noticed that miR-133-overexpressing mice that underwent TAC had significantly lower levels of myocardial fibrosis and improved ventricular function, without the side effect of cardiac hypertrophy (Matkovich et al., 2010). Duisters et al., demonstrated that there is a reverse relationship between miR-133 and calcineurin expression in cardiac hypertrophy, where calcineurin expression and activity was increased in contrast with miR-133 (Duisters et al., 2009). In a conclusion, miR-133 plays an essential role in cardiac development and hypertrophy; however, its overexpression could be cardioprotective in certain pathophysiological processes.

miR-133a together with miR-1 are important regulators of pluripotent stem cells differentiation (Hwang et al., 2015). Recent studies looking to induce mature cells into

cardiac-like pluripotent stem cells used microRNA cocktails including miR-133a, miR-1, miR-122, miR-208, and miR-499 (Jayawardena et al., 2012; Liu et al., 2008a; Nam et al., 2013; Zhao et al., 2005). These data imply that microRNAs play an essential role in hiPSCs differentiation and maintenance. Due to (1) the role of miR-133 described above, (2) the fact that we observed it to be more expressed in healthy human RA vs. SN (Chapter 3), and (3) the prediction we made in Chapter 3 that it inhibits HCN4 expression, we endeavored to further study miR-133a-3p effect on hiPSCs. We hypothesised that forced overexpression of the miR-133a-3p will induce reduction of the spontaneous beating rate of these cells, as it will potentially target HCN4 expression, reduce it, and thus inhibit the action potential frequency, and its subsequent beating rate.

7.2 Methods

7.2.1 iPSCs plating, maintenance, and differentiation

The cardiac cells differentiation of hiPSCs was performed by Dr. Anna Liakhovitskaia, University of Manchester, according to the protocol produced by Burridge et al., 2016. Cells were seeded at low-density concentration of 1:400, they were grown for four days, by the time they became 65-85% confluent, and were either passaged or differentiated (Burridge et al., 2014). HiPSCs were differentiated towards cardiomyocytes lineage as a monolayer. Contracting cells were observed after day 8 from the beginning of the differentiation, and transfections were performed between days 10 to day 17 after beginning of differentiation (Table 7.1).

7.2.2 miR-133a-3p transfection of hiPSCs

Transfection mixture contained 2 ml CDM3 cardiomyocytes maintenance media (Burridge et al., 2014), 1.5 µl lipofectamine RNAiMAX (Life Technologies), 2 µl miR-133a-3p (final concentration 1 nm/µl), and/or 2 µl Cy3-tagged pre-miR scrambled negative control (Ambion, final concentration 1 nm/µl), and/or graphene oxide (GO; final concentration 10 nm/µl; kindly provided by Prof. Kostas Kostarelos and Dr. Irene De Lazaro Del Rey, University of Manchester). Cells were then incubated at 37°C/5%CO_2. The culture medium CDM3 comprised of RPMI 1640, rice-derived recombinant human albumin, and L-ascorbic acid 2-phosphate as previously described by Burridge et al., 2014. Total incubation time was 6 hours. Videos and bright field images (Epiphan Capture Tool (DVI2USB 3.0)) and fluorescent images (EVOS digital inverted microscope (Life Technologies)) were taken immediately before transfection (Time point 1, TP1), 2 hours after transfection (Time point 2, TP2), 4 hours after transfection (Time point 3, TP3), and 6 hours after transfection (Time point 4, TP4). The spontaneous beating rate per minute was calculated for each well by counting manually the contractions produced by the cell monolayer. Data was plotted as a timeline for time point 0 to 6, where time point 0 shows the beating rate before transfection, and then beating rate was counted at 2, 4, and 6 hours after transfection via GraphPad Prism 7.0 and analysed using One-way ANOVA, considering significance when $p<0.05$.

7.2.3 Human SN and RA total RNA collection and quantitive PCR

Total RNA was collected from SN and RA samples that were isolated from 3 human non-heart failure, healthy hearts and 5 heart failure hearts. The samples were then reverse transcribed, preamplified and qPCR for microRNA-133a-3p was carried out for heart

failure and non-heart failure hearts by Dr. Ning Li, Dr. Vadim Federov's lab, The Ohio State University, Cardiac Transplant team and Lifeline of Ohio. Total RNA was isolated using mirVana miRNA Isolation Kit (Life Technologies, AM1560) according to the manufacterer's instructions . Quality and quantity of the mRNA was assessed via NanoDrop ND-1000 spectrophotometer (NanoDrop Technologies, Wilmington, DE, USA).

Reverse transcription of the total RNA was performed using TaqMan microRNA Reverse Transcription Kit (Thermo Fisher Scientific, 4366596) according to the manufacterer's instructions. The product from the RT reaction was amplified using TaqMan Small RNA Assay and TaqMan Universal PCR Master Mix (Thermo Fisher Scientific, 4324018). Primer assays were purchased from Thermo Fisher Scientific (has-miR-133a-3p, assay ID-002246 and control U6, assay ID-001973). qPCR reation was performed using BIO-RAD CFX Connect real-time system (Bio-Rad Laboratories). Samples were run in duplicates. The reaction conditions started with denaturation at 95°C, followed by 40 cycles of 95°C for 15 seconds and 60°C for 1 minute. U6 was used as an endogenous control and miR-133a-3p was normalised to its expression. Data were calculated as $2^{-\Delta Ct,}$ where ΔCt is $\Delta Ct_{miR\text{-}133a\text{-}3p}$-$\Delta Ct_{U6}$. Statistical analysis was performed using student's t-test to analyse the effect of heart failure and non-heart failure (control) on miR-133a-3p expression in human SN and RA. Data was considered as statistically significant when $p<0.05$.

7.2.4 iPSCs total RNA isolation

After the end of the experiment, cells were washed three times with phosphate-buffered saline (Sigma-Aldrich), and dissociated from their wells using TrypLE Express (Thermo Fusher Scientific) via incubation for 5 minutes at 37°C. The process was stopped by

addition of DMEM/F12 (Sigma-Aldrich) and cells were centrifuged at 300 rpm for 5 minutes. The samples were then resuspended into 350 µl RLT buffer ((Qiagen RNeasy Micro Kit for mRNA cDNA, Qiagen) containing 10 µl β-mercaptoethanol), flash frozen in liquid nitrogen and kept at -80°C. Total RNA was then isolated using Qiagen Rneasy Micro Kit for mRNA cDNA, Qiagen according to manufactere's instructions. RNA quality and quantity was determined using a NanoDrop ND-1000 spectrophotometer (NanoDrop Technologies, Wilmington, DE, USA). Cell treatment, mRNA concentration, and quality of the samples is described in Table 7.1.

Sample	Treatment	Concentration [ng/µl]	260/280	260/230
1	miR-133a-3p	268.2	1.97	1.41
2		56.2	1.73	0.69
3		103	2.06	1.48
4		505.6	2.02	1.95
5		122.8	1.59	0.76
1	CTR	218.2	2.11	0.71
2		132	1.82	1.10
3		116.8	2.02	1.43
4		120.2	2.08	0.19
5		57.5	1.87	1.24
6		172.1	2.07	2.08
1	Scrambled miR	136	2.0	0.89
2		114.7	2.07	0.41
3		194	1.95	1.55
4		77	2.02	0.48

Table 7.1. iPSCs samples, RNA quantity and RNA quality. Total RNA was extracted via Qiagen RNeasy Micro Kit for mRNA cDNA, Qiagen. RNA properties were measured using NanoDrop Technologies, Wilmington, DE, USA. 260/280 and 260/230 are ratios of absorbance at these wavelengths (nm), they assess the purity of the RNA , and ratio of ~2.0 is accepted as pure RNA, with no contamination of ethanl or genomic DNA.

7.2.5 iPSCs qPCR for miR-133a-3p and miR-486-3p expression

Total RNA was converted to microRNA cDNA using qScript microRNA cDNA Synthesis kit (Quanta BioScience) according to manufacterer's protocol. Primers were purchased from Exiqon (miR-133a-3p, 204788 and miR-486-3p, 204107). qPCR was performed using ABI Prism 7900 HT Sequence Detection System (Applied Biosystems/Life Technologies Corporation, Carlsbad, CA, USA). The reaction mixture consisted of 1 µl cDNA, 1 µl primer assay, 5 µl SYBR Green Master Mix (Applied Biosystems), and DNase-free water. Samples were run in triplicates. The reaction conditions started with denaturation at 95°C for 10 minutes, followed by amplification and quantification step produced by 40 cycles of 95°C for 10 seconds and 60°C for 1 minute. The melt curve conditions were defined by 95°C for 15 seconds, 60°C for 15 seconds, and 95°C for 15 seconds. MicroRNA expression levels were calculated by the ΔCt method and normalised to the expression of RNU1A1 (Qiagen, YP00203909).

7.2.6 iPSCs qPCR for HCN4 expression

Total RNA was converted into mRNA cDNA using RNeasy Micro Kit for mRNA cDNA (Qiagen) according to manufacterer's protocol. HCN4 primer was purchased from Qiagen (QT00191387). The reaction conditions were as follows: 50°C for 2 minutes, 95°C for 10 minutes, 40 cycles of 95°C for 15 seconds, 60°C for 1 minute. The melt curve conditions were the same as the ones for microRNA qPCR. mRNA expression levels were calculated according to the ΔCt method and normalised to the expression of 18S or GAPDH (Qiagen, QT0102448075).

7.2.7 Statistical analysis

miR-133a-3p relative expression in human SN vs. RA in heart failure (n=3) and non-heart failure (n=5) was analysed through two-way ANOVA method. miR-133a-3p and miR-486-3p cDNA relative expression in hiPSCs was compared via student's t-test, n=6. One-way ANOVA measured the mean beating rate of hiPSCs treated with miR-133a-3p (n=11), CTR (n=4), or Cy3-tagged scrambled miR (n=9). Two-way ANOVA was used to analyse HCN4 mRNA relative expression in hiPSCs treated miR-133a-3p, and CTR, as well as miR-133a-3p and HCN4 mRNA relative expression in miR-133a-3p-treated hiPSCs, n=5. All analysis was performed with GraphPad Prism 7.0, data were considered significant when $p \leq 0.05$.

7.3 Results

Similarly to what we showed in Chapter 3, Figure 3.6, Dr. Ning Li's qPCR analysis of healthy, non-heart failure human hearts confirmed higher expression of miR-133a-3p in the RA compared to SN. Human heart failure SNs, however, were expressing significantly higher levels of miR-133a-3p compared to the healthy SNs (Figure 7.1). The expression of miR-133a-3p in heart failure RA remained unchanged, and no significant difference of the microRNA was observed between the nodal tissue and the working myocardium of the RA in disease. These preliminary data implied that miR-133a-3p is playing an important role in the human healthy RA, whereas heart failure leads to an increase of its expression in the nodal tissue. Since these results also confirmed what we have already observed in healthy human hearts (significantly higher expression of miR-133a-3p in the human RA compared to SN), we decided to further test if miR-133a-3p plays an important role in cardiac function.

In relation to our data about the role of miR-486-3p in the human heart (Chapter 3 and 4), we looked into the expression of miR-486-3p in CTR-treated hiPSCs (Figure 7.2 A). miR-486-3p was found to be expressed in hiPSCs, however, its expression was significantly lower than that of miR-133a-3p (Figure 7.2 A). Figure 7.2 B and C show that $\Delta Ct_{miR\text{-}133a\text{-}3p}$ is 22 cycles, whereas $\Delta Ct_{miR\text{-}486\text{-}3p} \sim 27$ cycles. Lower miR-486-3p ΔCt value corresponded to lower RNA concentration in hiPSCs in comparison with miR-133a-3p. These data show significantly high basal level of miR-133a-3p in hiPSCs, suggesting it plays a regulatory role in hiPSCs.

The next step of our study was to look at miR-133a-3p effect on hiPSCs, as this cell line is the closest system to the human heart, which we can use for functional experiments. Unfortunately, SN isolated rat or mouse cells were not an appropriate model to study miR-133a-3p effect on HCN4 expression and function, as we found no binding sites of human miR-133a-3p to mouse/rat HCN4 mRNA sequences. Table 7.2, however, shows 3 predicted binding sites of miR-133a-3p and 5 predicted binding sites of miR-486-3p to human HCN4 (predictions were performed in RNU22 website). For this reason, hiPSCs were the most logical model choice. Figures 7.3 and 7.4 show bright field images of the hiPSCs in different treatment conditions. Control (CTR) cells were treated with either lipofectamine, or lipofectamine and graphene oxide (GO), in order to assess if the transfection agents have any effect on the cells alone. Figure 7.3 B and 7.4 B show cells transfected with scrambled Cy3 dye-tagged microRNA and either lipofectamine, or lipofectamine and GO. Figure 7.3 C and 7.4 C show cells transfected with miR-133a-3p with lipofectamine or lipofectamine and GO.

Treatment with lipofectamine vs. lipofectamine and GO was performed in order to discover, which is a better transfection reagent for hiPSCs and to assess if lipofectamine

and GO are potentially toxic to the cells. Cells remained viable and with unchanged beating rate after 6 hours of transfection, suggesting no toxicity was produced by lipofectamine or GO.

miR-133a-3p was not fluorescently tagged, thus the success of the transfection could only be assessed by visual interpretation of the scrambled miR (Cy3 dye-tagged) distribution. HiPSCs transfection with scrambled miR or scrambled miR and GO showed no fluorescence higher than background (Figure 7.5 A, C and E), suggesting that GO could not produce a satisfactory level of transfection on its own. Scrambled miR with lipofectamine or lipofectamine and GO (Figure 7.5 B, D and F), however, produced red fluorescent signal potentially from the inside of the cells, indicating successful transfection of the cells with the fluorescently-tagged control reagent.

No significant difference of the beating rate of miR-133a-3p, CTR, or scrambled miR transfected hiPSCs over 6 hours was observed (Figure 7.6 A). However, a trend towards downregulation of the beating rate in miR-133a-3p-treated cells compared to CTR and scrambled miR-treated cells after 4 hours of transfection could be noticed (Figure 7.6 A). Further analysis of the total average beating rate over the whole 6 hour time period revealed that the scrambled miR-treated cells exhibited significantly higher average beating rate compared to CTR- and miR-133a-3p-treated hiPSCs (Figure 7.6 B). The values used to plot Figure 7.6 B are described in detail in Table 7.3.

Following the functional beating rate experiments, total hiPSCs RNA was collected and qPCR for miR-133a-3p and HCN4 was performed. HCN4 expression was found to be significantly higher in CTR cells, compared to miR-133a-3p-treated cells, indicating HCN4 expression has been inhibited by miR-133a-3p (Figure 7.7 A). Figure 7.7 B shows CTR-treated cells' ΔCt_{HCN4} value is 25, whereas miR-133a-3p-treated cells' ΔCt_{HCN4} value

is 29. These data confirmed that miR-133a-3p-treated cells expressed significantly lower HCN4 RNA concentrations compared to CTR-treated ones and demonstrated that there is a negative correlation between the expression of the miR-133a-3p and HCN4.

Further comparison of miR-133a-3p and HCN4 ΔCt values from miR-133a-3p-treated cells showed miR-133a-3p expression was significantly higher compared to HCN4 expression (Figure 7.7 C), confirming the negative correlation between miR-133a-3p and HCN4 expression.

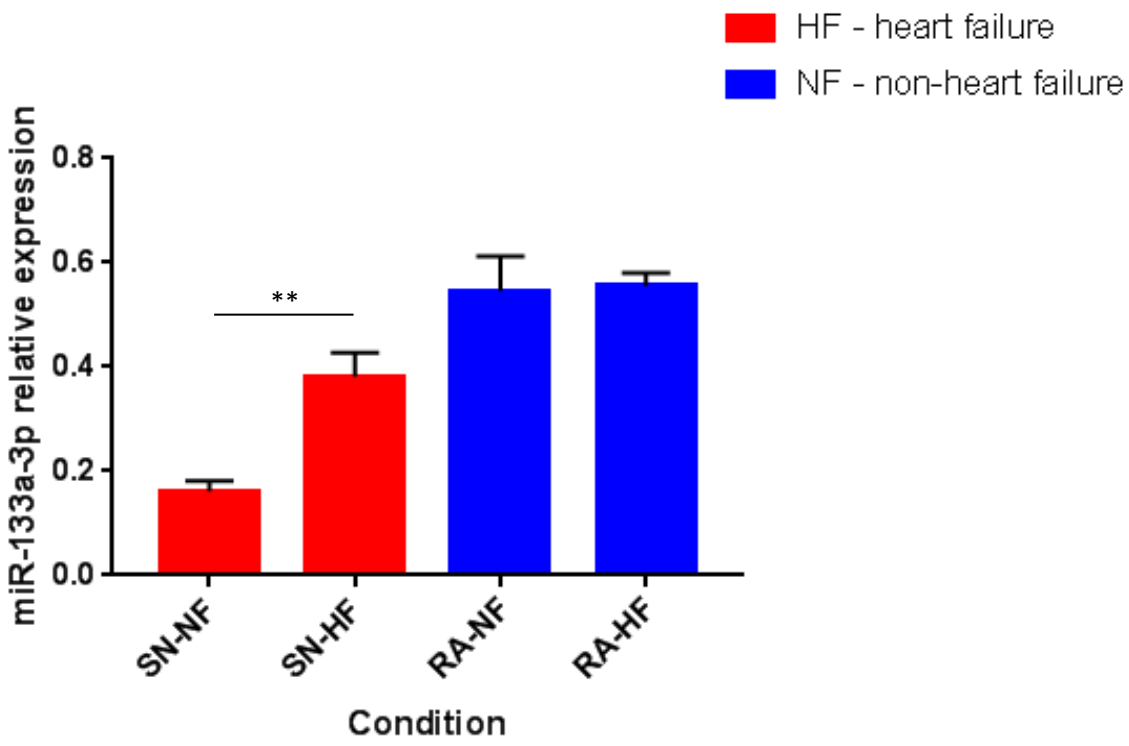

Figure 7.1. miR-133a-3p relative expression in human SN vs. RA in heart failure (red) and non-heart failure (blue). Data was determined by using qPCR analysis. Average threshold values were obtained using CFX Maestro Software (Bio-Rad Laboratories). U6 endogenous control was used to normalise miR-133a-3p across each sample. Two-way ANOVA was used to statistically analyse the data, and statistical significance was considered as $p \leq 0.05$. Bar represent mean ± SEM. Non-heart failure hearts n=3, heart failure hearts n=5.

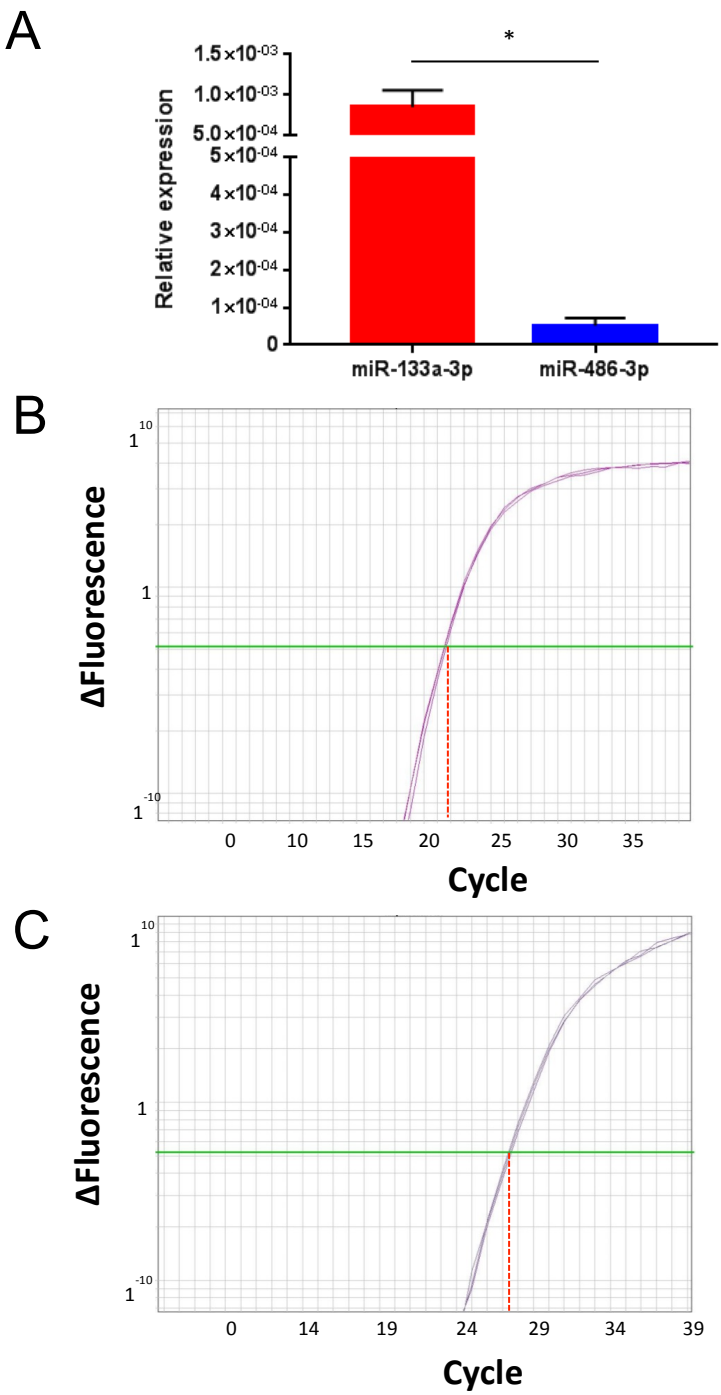

Figure 7.2. miR-133a-3p and miR-486-3p cDNA relative expression from CTR-treated hiPSCs. A. Average threshold values were obtained using RQ Manager 1.2.1. RNU1A1 endogenous control was used to normalise the results. Student's t-test was used to statistically analyse the data, and statistical significance was considered as p≤0.05. Bar represents mean ± SEM, n= 6. B. miR-133-3p and C. miR-486-3p amplification curves, where triplicate of representative samples were shown; red lines represent calculation of the threshold cycle (Ct) value.

miR name and sequence	Leftmost position of predicted target site	Heteroduplex
has-miR-133a-3p 53- UUUGGUCCCCUUCAACCAGCUG - 74	293	GGGCTGGGCAGGGGTGGGAGTGGC : |||| | :: | |||| : : : GTCGACC-AACTTC-CCCTGGTTT
	466	ACCTTGGGAGAAAAGGGCCAGG : ||| ||| || | |: : GTCGACCAACTTCCCCTGGTTT
	1673	GGAATGGT-GGGTGGGATGGAG |||| | :: |||| : : | : GTCGACCAACTTCCCCTGGTTT
has-miR-486-3p 46- CGGGGCAGCUCAGUACAGGAU - 66	393	AACTTGGAGCTCCACTCTGCCCCC | : || : || | || || || TAGGAC ATGA CTCGACGGGGC
	413	CCCCAGAAAGGGGCTGCCCTG | | | : | || || || : | TAGGACATGACTCGACGGGGC
	940	CTTCTGTTTATTGAGTCTGCTCTG || || | || | ||| | : |: | TAGGACA TGACTC GACGGGGC
	1617	GGTGGGTG-GGAGCCAGGCCTTG | |: || || | | | : : | TAGGACATGACTCG ACGGGGC
	1927	AGCCAAGGTCAGGGGTCTGCCCCT || | | | : | || ||| || TAGG ACATGACTC GACGGGGC

Table 7.2. miR-133a-3p and miR-486-3p binding sites to the HCN4 3'UTR. MicroRNA sequences were obtained from miRBase website. 3'UTR sequence of HCN4 was confirmed in genome.ucsc.edu. MicroRNA matching with HCN4 3'UTR sequences was performed in RNU22 website.

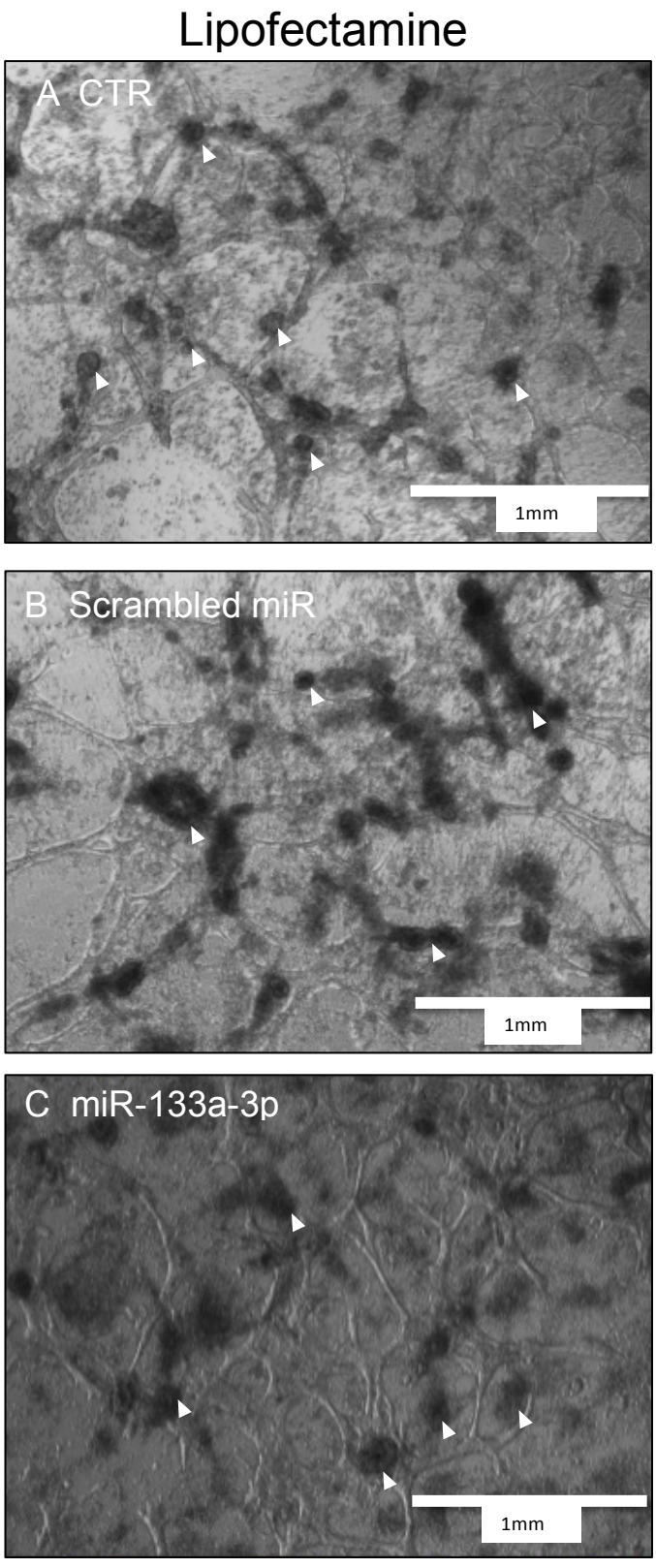

Figure 7.3. Human induced pluripotent stem cells (hiPSCs) transfection with lipofectamine. A. CTR, control only; B. Scrambled miR, Cy3-tagged; C. miR-133a-3p. Bright field images were taken through Epiphan Capture Tool (DVI2USB 3.0). Dark spots appointed with white arrows are nuclei.

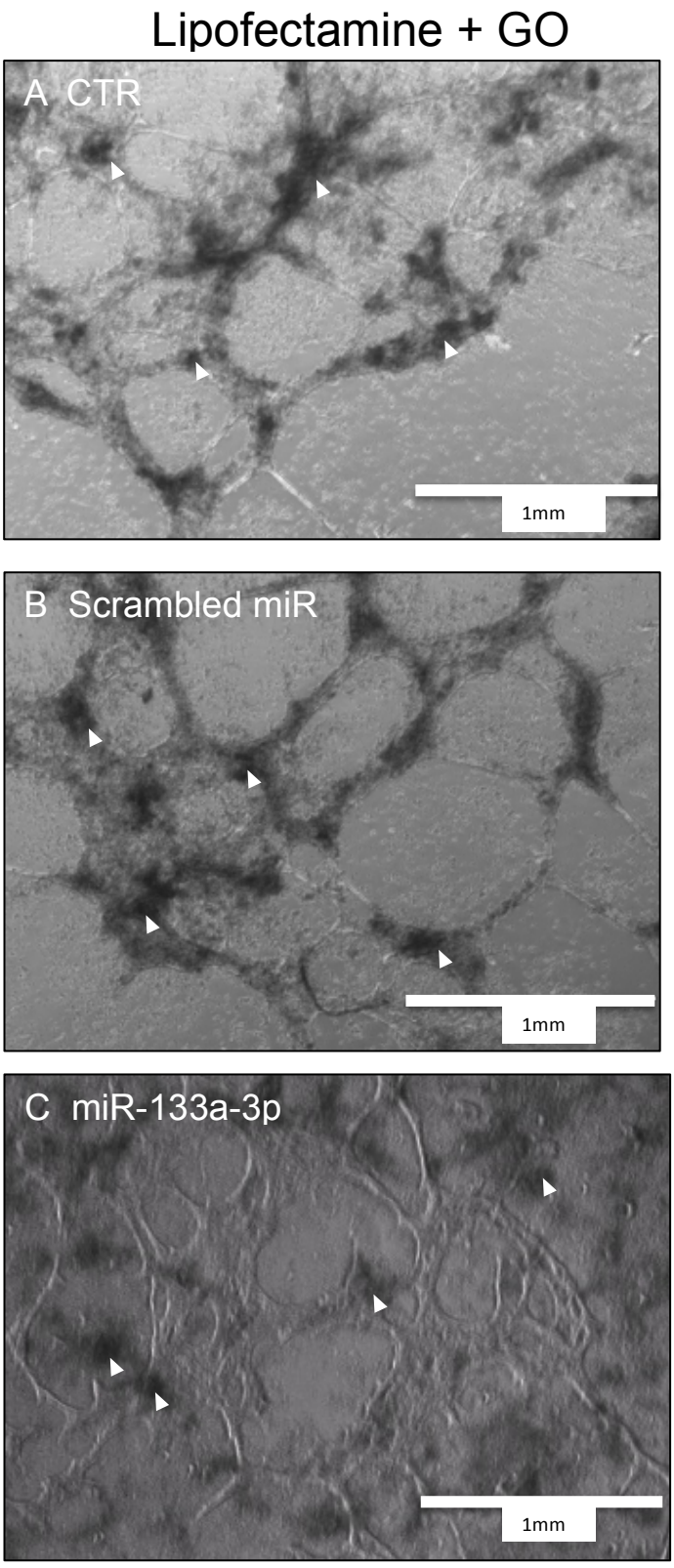

Figure 7.4. Human induced pluripotent stem cells (hiPSCs) transfection with lipofectamine and graphene oxide (GO). A. CTR, control only; B. Scrambled miR, Cy3-ltagged; C. miR-133a-3p. Bright field images were taken through Epiphan Capture Tool (DVI2USB 3.0). Dark spots appointed with white arrows are nuclei.

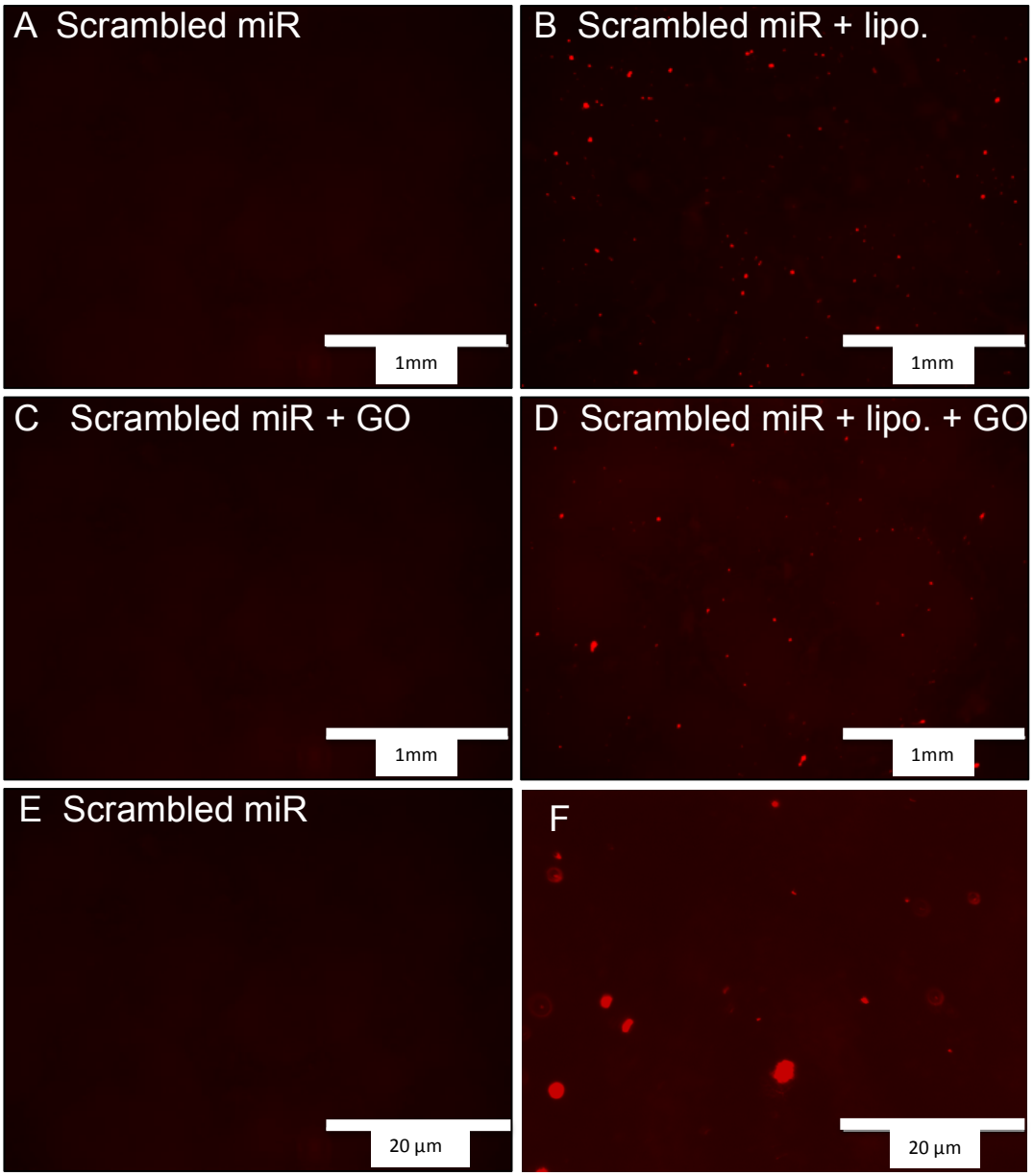

Figure 7.5. Human induced pluripotent stem cells (hiPSCs) transfection with lipofectamine and/or graphene oxide (GO). Fluorescent images were taken by EVOS digital inverted microscope (Life Technologies) 6 hours after transfection. Bright red spots in panel B, D and F. represent hiPSCs transfected with Cy3-tagged scrambled miR.

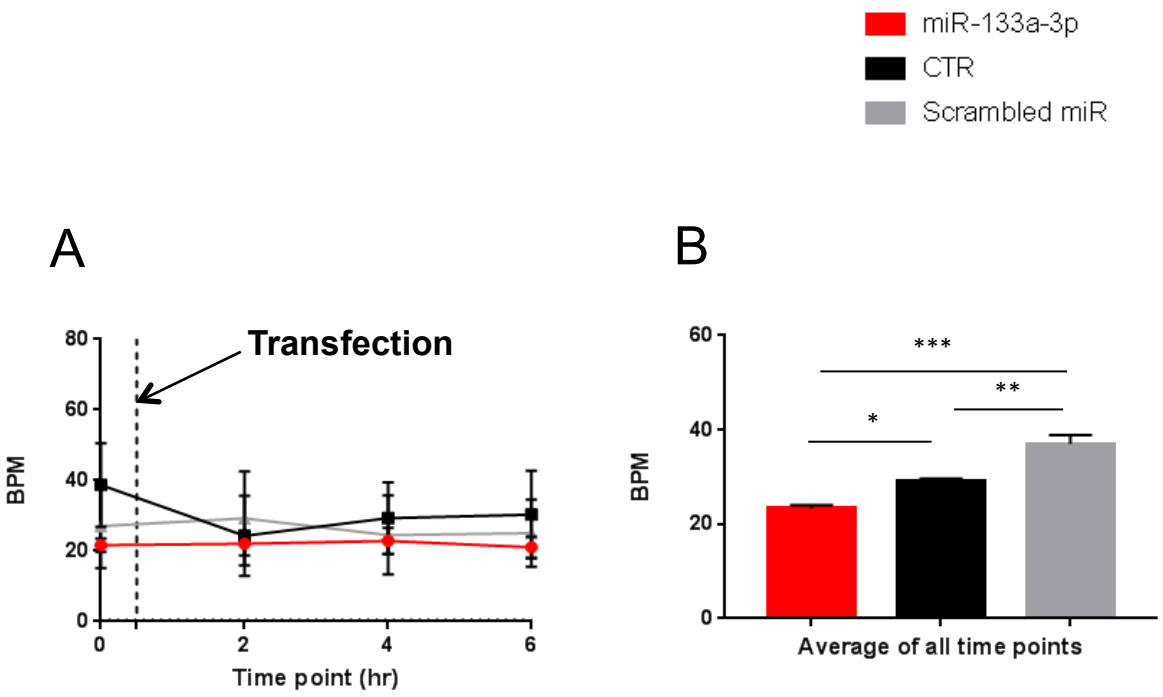

Figure 7.6. HiPSCs transfection with miR-133a-3p, CTR, Cy3-tagged scrambled miR and lipofectamine or lipofectamine and GO. A. Mean beating rate before transfection (time point 0) and after 2, 4 and 6 hours after transfection respectively. B. Comparison of mean beating rate of the different treatments at all time points. Data represented as mean ± SEM. Statistical analysis performed via one-way ANOVA, GraphPad Prism 6.0; * $p<0.05$, ** $p<0.005$, *** $p<0.0005$.

Treatment	BPM Mean±SEM Time point 0	BPM Mean±SEM Time point 2	BPM Mean±SEM Time point 4	BPM Mean±SEM Time point 6	BPM Mean±SEM (Average of all Time points)
miR-133a-3p (n=11)	23.3 ± 3	22.4 ± 2.9	23.4 ± 3.1	24.3 ± 4.5	23.3 ± 1.4
CTR (n=4)	40.3 ± 8.6	32.3 ± 11.3	35.8 ± 9.6	39.8 ± 12.9	29.1 ± 0.5
Scrambled miR (n=9)	27 ± 9.9	29.6 ± 10.2	26.7 ± 10.6	33 ± 11.2	37 ± 1.9

Table 7.3. Mean ± SEM beating rate of hiPSCs over time points 0, 2, 4 and 6, respectively, and their average beating rate over all time points. Statistical analysis performed via one-way ANOVA, GraphPad Prism 7.0.

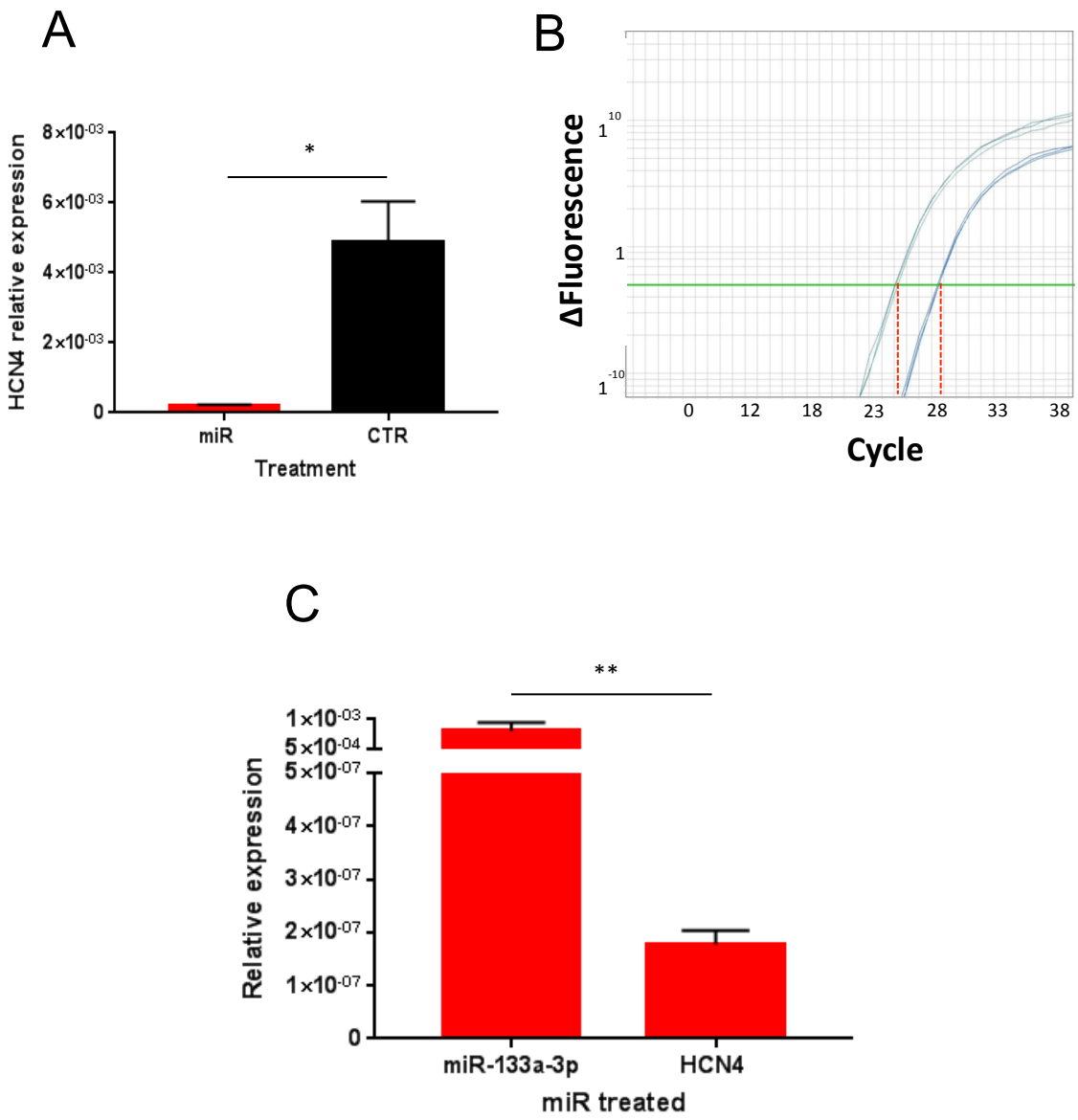

Figure 7.7. A. HCN4 relative expression in hiPSCs treated miR-133a-3p (red), and CTR (black). B. HCN4 amplification curve, where triplicate of representative samples were shown; red lines represent calculation of the threshold cycle (Ct) value. C. miR-133a-3p and HCN4 relative expression in miR-133a-3p-treated hiPSCs. Average threshold values were obtained using RQ Manager 1.2.1. RNU1A1 endogenous control was used to normalise miR-133a-3p and GAPDH was used for HCN4 normalisation. Two-way ANOVA was used to statistically analyse the data, and statistical significance was considered as $p \leq 0.05$. Bars represent mean ± SEM. miR n = 5, CTR n= 6.

7.4 Discussion

Currently, an emerging body of work focuses on cardiac- and nodal-like hiPSCs cells as a potential therapeutic method regarding the improvement of the cardiac function in disease. Nodal-like hiPSCs are of specific interest as a source material for the creation of biological pacemakers as an alternative to electronic devices. The discussion in this sections aims to summarise the functional and molecular results we have produced while examining the effect of miR-133a-3p on hiPSCs cells, its expression, and the expression of miR-486-3p, as major microRNAs predicted to target HCN4 expression. Moreover, the discussion will indicate the major limitations that have been encountered during the experiments.

We found that miR-133a-3p is more abundantly expressed in human RA compared to SN in 3 healthy, non-heart failure hearts. However, its levels are significantly upregulated in heart failure SN. miR-133a-3p was chosen to be functionally assessed in hiPSCs as we initially observed (Chapter 3) its expression is lower in SN vs. RA, suggesting it plays a specific role in the RA where its expression is higher. As it was already discussed in Chapter 3, miR-133a-3p was predicted to target HCN4 expression in the human RA, where it prevents the initiation of pacemaking activity. Moreover, human miR-133a-3p was predicted to have a high chance of binding to the 3'UTR region of human HCN4 (Table 7.2). Its overexpression in the SN during disease, however, indicates involvement in the pathological processes during heart failure possibly through direct targeting of HCN4 and changing the molecular environment in the SN. This hypothesis is based on our discovery that miR-133a-3p is predicted to bind to HCN4 transcript, and that a recently published paper reported HCN4 downregulation in human heart failure SN (Li et al., 2015).

A substantial amount of scientific data provides information about miR-133a as a major regulator during cardiac development. miR-133a stands out in the literature as a muscle-specific microRNA and it has been previously reported to be expressed in adult cardiac and skeletal muscle tissue, where it plays a role in myogenesis (Chen et al., 2006; Horak et al., 2016; Zhao et al., 2005). miR-133a is also associated with processes involved in heart development (Koutsoulidou et al., 2011; Weber et al., 2015). Matkovich et al., showed that overexpression of miR-133a-3p during cardiac development, on the other hand, inhibits the proliferation of cardiomyocytes and prolongs action potential QT intervals in mouse ventricular myocytes by reducing the transient outward K^+ current I_{to} (Matkovich et al., 2010). Further analysis revealed a decrease of K_V4 (KCNIP2) channel mRNA levels, responsible for I_{to} current (Matkovich et al., 2010). Interestingly, miR-133a was not predicted to bind to KCNIP2 mRNA, suggesting the prediction softwares used to match microRNAs with their mRNA targets are not always perfectly reliable sources of information. Double knockout mice for both mature forms of miR-133a (miR-133a-3p and miR-133a-5p) exhibited increased cardiomyocytes proliferation and apoptosis, resulting in deformations in the ventricular septum (Liu et al., 2008a).

Hypertrophic and failing hearts were reported to exhibit downregulation of miR-133a levels, suggesting that decrease of the microRNA levels could lead to cardiac pathologies. Furthermore, overexpression of miR-133a was found to reverse the pathological phenotypes observed initially (Care et al., 2007b; Sayed et al., 2007; van Rooij et al., 2006). A rat model of left ventricular hypertrophy was reported to express significant upregulation of HCN2 and HCN4 levels, accompanied with downregulation of miR-1 and miR-133a. Forced overexpression of miR-1 and miR-133a prevented HCN2 and HCN4 upregulation in hypertrophied cardiomyocytes, suggesting a possible mechanism for the

electrical remodelling in hypertrophic hearts (Luo et al., 2008). These data further imply that miR-133a-3p could have a role in the working myocardium, where it targets and inhibits HCN2 and HCN4 expression, and prevents the initiation and propagation of pacemaking currents. Upregulation of miR-133a-3p in heart failure SN that we observed, however, is potentially playing role in the pathophysiology of SN dysfunction.

Since we suggested that miR-133a-3p plays a role in regulation of the human heart by potentially inhibiting HCN4 expression in the RA, we decided to proceed with functional experiments and assess if it targets HCN4 expression in hiPSCs. We showed that CTR hiPSC express a significant amount of miR-133a-3p, which indicated that the microRNA is still present in the cells after maturation and potentially performs a regulatory role there. miR-133a-3p transfection of hiPSCs showed a trend towards decrease of the beating rate after 4 hours, despite the fact that no significance was observed. qPCR analysis of the expression of miR-133a-3p in hiPSCs was performed in order to confirm the success of the transfection procedure, showing upregulation of the microRNA in the transfected cells in comparison with HCN4 expression, which was downregulated. Moreover, CTR-treated cells expressed significantly higher levels of HCN4 in comparison with miR-133a-3p-treated cells. Results indicated that HCN4 expression inhibition in hiPSCs could be explained by the forced expression of miR-133a-3p, which in turn targets and inhibits it.

qPCR results show that miR-133a-3p, miR-486-3p, and HCN4 mRNAs are expressed in hiPSCs, suggesting that the cultured cells contain a variety of cardiac cells including nodal-like cells that beat spontaneously and synchronously due to HCN4 presence. The coordinated manner of contraction also indicated electrically communicative tissue, potentially due to connexins expression. A study by Haraguchi et al., also reported expression of HCN4 in hiPSCs as well as MLC-2a and MLC-2v (myosin light chain 2

genes, expressed in the working myocardium) suggesting that the culture system maintains a potential to differentiate into several different types of cardiomyocytes, including pacemaker cells, which produce electrical signal (Haraguchi et al., 2015). HiPSC-CMs were also found to express RyR2, SERCA2a, and NKX1 as well as Cx43, $Ca_V1.3$, and hERG (Hwang et al., 2015). A recent lineage study looked into the role of miR-1 and miR-133a in pluripotent stem cell differentiation, reporting that both are upregulated during this cell fate stage (Izarra et al., 2017). Interestingly, forced overexpression of miR-1 was enhancing cell differentiation, while miR-133a-3p opposed and inhibited it, concluding both microRNAs play role in mesodermal and cardiac fate of pluripotent stem cells (Izarra et al., 2017).

microRNAs, as well as transcription factors, play a major role in the development, maturation, and specification of the various cardiac tissue types. It has been observed that external overexpression of these solely, or in combination leads to differentiation of various cardiac tissue types and in many cases their expression persists in adult tissue, suggesting they are not only important during development, but also play key roles in the maintenance of the specific molecular environment, and changes could lead to pathologies. Cell fate change from somatic to hiPSCs has been largely achieved through forced exogenous overexpression of lineage specific transcription factors. Such an example is the reprogramming of mouse fibroblasts into embryonic stem cells-like through transduction with 4 transcription factors – OCT4, SOX2, KLF4, and cMYC (Takahashi et al., 2007). Shortly after that similar reprograming was done with human somatic cells and introduction of OCT4, SOX2, LIN28, and NANOG transcription factors (Yu et al., 2007). Zhang et al., generated functional cardiomyocytes using these same transcription factors from foetal and new-born tissue samples (Zhang et al., 2009). The group reported action

potential recordings from ventricular, atrial, and nodal-like cells. 72% of the hiPSCs were ventricular-like cells, and the nodal-like cells were comprising about 10-20% of the cellular population (Zhang et al., 2009). Ma et al., conducted a similar study and looked into the morphology of hiPSCs derived from human fibroblasts (Ma et al., 2011). A mix of ventricular, atrial and nodal-like cells was reported, where nodal-like cells accounted for 22% of the cell culture, and I_f was measured from individual cells (Ma et al., 2011). In a very recent study, pluripotent stem cells derived from human keratinocytes were introduced into dogs' hearts. Their hearts were extracted 13 weeks later and histological and electrophysiological studies determined that the hiPSCs introduced lost their pluripotency markers, appeared to be positive for cardiac-specific markers, and exhibited I_f-dependent automaticity, suggesting they have made first steps in the creation of a biological pacemaker (Chauveau et al., 2017). They have observed, however, differences in the rate and rhythm of hiPSCs, leaving room for further improvement (Chauveau et al., 2017).

Another popular method of cell fate reprogramming included the overexpression of transcription factors Gata4, Tbx5, and Mef2c (Chen et al., 2012; Hirai et al., 2013; Ieda et al., 2010; Inagawa et al., 2012; Wang et al., 2015). Variability between the induced cells were significant and the similarities with mature cardiomyocytes were marginal in terms of their molecular and electrophysiological phenotype (Chen et al., 2012). Another recent study looked into the role of transcription factor Tbx18 in mouse adipose-derived stem cells. Transduction with Tbx18-containing adenovirus resulted in pacemaker-like cells that were expressing typical pacemaker cell genes such as Tbx3, sarcomeric α-actinin, and HCN4, where their mRNA and protein levels were increased (Sun et al., 2018).

miR-1 and miR-133a were added to the transcription factors cocktails (Nam et al., 2013; Zhao et al., 2015), or used solely (Jayawardena et al., 2014; Jayawardena et al., 2012) to switch adult cells into hiPSCs. miR-1 was found to interact with SRF, Mef2c, MyoD, and Nkx2-5 in a regulatory feedback loop as it either inhibits, or enhances their expression (Liu et al., 2007; Qian et al., 2011; Zhao et al., 2005). In combination with other microRNAs such as miR-122, miR-208, and miR-499 it was shown to switch 28% of cardiac fibroblasts to cardiomyocyte-like cells (Jayawardena et al., 2014; Jayawardena et al., 2012). A very recent study reported a protocol for culturing nodal-like pluripotent stem cells, which maintained high expression of SN hallmark genes such as HCN4, Tbx3, and Tbx18 in contrast with Nkx2-5 and Tbx5, which were less expressed; furthermore, they were responsive to adrenergic and cholinergic stimulation, and were able to pace rat ventricular myocytes (Schweizer et al., 2017). These data imply that any future studies concerning the SN and the cardiac conduction system should be performed into these newly developed specific cells for a more precise and effective experimentation.

Overall, the current knowledge about nodal-like hiPSC-CMs molecular and electrophysiological properties is limited. The results suggest that hiPSCs express various nodal cell-like markers, transcription factors, microRNAs, specific proteins, and ionic currents including I_f. Transcription factors and microRNAs decide not only the cell fate during tissue development, but potentially form feedback loops of regulation that affects the molecular background of the adult cells. Despite the large amount of published data concerning the SN formation, the genetic pathway behind that has been partly revealed and more information on microRNAs and transcription factors interactions is needed. HiPSCs cardiac-like cells appear to be inhomogeneous with prevalent ventricular-like cells. It still remains to be determined whether the nodal-like hiPSC-CMs in these cell preparations are

of a true nodal lineage, or they are simply immature automated ventricular-like cells that exhibit pacemaker activity.

Our study compared two different transfection agents in hiPSCs – GO and lipofectamine, finding out that cardiac hiPSCs were successfully transfected with lipofectamine, but no transfection was achieved with GO. We also observed that cells incubated with GO are viable after 6 hours of transfection. Since hiPSCs and tissue engineering have become an attractive new field of biomedicine research, biocompatible scaffold materials and graphene have also increased their popularity, as graphene has been shown to stimulate cell proliferation and accelerate cell differentiation in species like Chinese hamster ovary cells (Mthunzi et al., 2014). In contrast with our results, graphene oxide polyethyleneimine was found to produce high transfection efficiency compared to polyethyleneimine (another transfection agent) alone in HeLa cells; similarly to us, they showed low cytotoxicity (Feng et al., 2011). A more recent study looked into the transfection efficiency of graphene oxide polyethyleneimine, showing that the transfection agent is successfully loading mRNA in adult adipose tissue-derived fibroblasts and resulted in generation of hiPSCs (Choi et al., 2016), without the need of repetitive daily transfections, which are usually required in hiPSCs generation protocols. In a conclusion, we observed no GO cytotoxicity, however, its transfection efficacy in cardiac hiPSCs was not as effective as it has been previously reported in the literature.

7.4.1 Limitations and future directions

Although the data looks promising and gives an interesting insight into the molecular background of hiPSCs, it also raises questions that could be potentially explained by the multiple limitations, which have been encountered during the experiments themselves. With respect to the transfection of the hiPSCs with miR-133a-3p, the major limitation that

prevented us to confirm the successful entry of the microRNAs inside the cells was the fact that miR-133a-3p was not fluorescently tagged, unlike the Cy3-tagged scrambled miR. We could observe a red fluorescent signal from the hiPSCs transfected with scrambled miR and lipofectamine or lipofectamine and GO (Figure 7.5 B, D and F). No signal was observed from the cells transfected with scrambled miR and GO only (Figure 7.5 A, C and E), suggesting GO could not successfully introduce the Cy3-tagged scrambled miR to the intracellular space. miR-133a-3p tagging was contraindicated as literature reports that dye-tagging of small molecules such as microRNAs, which are about 20 nucleotides long, prevents a successful transfection, and also leads to non-specific interactions, as it prevents the microRNA sequence to bind to its target mRNAs (Lu et al., 2016).

The most significant limitation of this study was the baseline spontaneous activity beating rate variability that was observed in every cell culture and every cell passage. We used hiPSCs from 4 different passages. Every next passage of cells had faster beating rate, possibly, due to better differentiation properties. The cells were frozen and kept at -80°C. After thawing, they need to be passaged at least 4 to 5 times before transfection experiments. Relying on other group's help due to lack of experience in hiPSCs, however, we started transfection protocols from passage 1, so with every new passage of cells, their baseline beating rate increased too. The plan of the experiment had to be changed dependng on the cells too, as not all of them would produce spontanous activity, so they had to be excluded from the experiment. Moreover, cell passage 1, which had lowest beating rate, was used for transfection with miR-133a-3p and lipofectamine or lipofectamine and GO only. Cell passage 2, which had higher baseline beating rate than passage 2, was used for miR-133a-3p and lipofectamine or lipofectamine and GO, or CTR treatements only. Passage 3, which had higher beating rate than cell passage 2, was used

for scrambled miR treatments only. And passage 4, which again had a higher beating rate than passage 3, was used for CTR or scrambled miR transfections only. The lack of controls at every transfection experiments, and the difference between the beating rate through passages, which varied between 12 to 55 beats per minute made the analysis and the interpratation of the data significantly challenging. Furthermore, the n number of transfections for the day was determined depending on the number of wells containing spontanously beating hiPSCs, which resulted into different n numbers for the different treatments. The information about the treatments, n numbers, average beating rate per time point and total average of beating rate per treatment could be found in Table 7.3 as well as the plot summarising the average beating rate per treatment (Figure 7.6). As we can see, the average beating rate for scrambled miR-treated cells is significantly higher than both miR-133a-3p- and CTR-treated cells. CTR-treated cells beating rate is also significantly higher than the beating rate of miR-133a-3p-treated cells. These results could be both because miR-133a-3p has an inhibitory effect on HCN4, which results in a decrease of the beating rate of the hiPSCs, or also because scrambled miR-treated cells were from passages 3 and 4, which were better differentiated with higher baseline beating rates, whereas miR-133a-3p-treated cells were from passage 1 and 2, which were possibly less differentiated after thawing, and their baseline beating rates were lower than these of CTR- and scramled miR-treated cells.

Although all cells were differentiated accoring to the protocol mentioned in the methods section, their molecular features might have been different as their functional features were different too. In the future, we will need to use preferably cell culture with nodal-like cells only, and the protocol to generate them has already been described by Schweizer et al., (Schweizer et al., 2017). The lower beating rate might have been an indication of low

abundancies of nodal-like cells as well as slower differentiation and lower expression of transcription factors, microRNAs, and mRNAs too. The average beating rates we observed (Tavle 7.3) are two-three times less compared to the beating rate of hiPSCs clusters generated by Schweizer et al., which produced robust beating rates of 70-90 beats per minute (Schweizer et al., 2017).

In the future, it would be recommended that these experiment are repeated with cells that have been passaged at least 4 times prior to experiments, and controls are produced for every different passage after transfection so that appropriate comparisons could be produced.

In summary, this study showed that miR-133a-3p potentially plays in an important role in cardiac health and disease, and it is a potential therapeutic target. It could be also used in addition with a variety of transcription factors in the creation of a biological pacamaker through pluripotent stem cells molecular regulaion. Cardiac hiPSCs were shown to express HCN4, miR-133a-3p, and miR-486-3p, suggesting that they have the potential to differentiate into mature cardiac cells, which could be used for either modelling of cardiac pathologies, or even as a therapeutic agent. Since we have looked into the transcription factors expression profile in the human SN and RA, it would be interesting to investigate the transcription profile of cardiac hiPSCs in the future, which will further enhance our knowledge about the gene regulatory machinery in these cells, and the potential interaction between microRNAs and transcription factors that control them.

Chapter 8

8 Summary, limitations, and future directions

8.1 Chapter 3 - Identification of key small non-coding microRNAs controlling the pacemaker mechanisms in the human sinus node

MicroRNAs have been found to be major regulators of the cardiac function (Kim, 2013; Luo et al., 2008; Xiao et al., 2012), however, little is known about their role in modulating the expression of key genes involved in the SN pacemaking mechanism – the membrane-voltage clock and Ca^{2+} clock. For this reason the aim of this study was to map the expression of key microRNAs in the healthy human SN in comparison with RA.

To characterise the human SN and RA tissue that we used in the study, we performed histological, immunohistochemical, and western blot experiments. The results of the histological characterisation confirmed the SN region by the presence of small, sparse cells embedded into a substantial network of connective tissue. In contrast the RA was characterised by well-organised cardiomyocytes embedded in less connective tissue and exceeding the size of the myocytes present in the SN. Histology confirmed the location of the SN on the epicardial surface of the right posterior wall of the RA as previously demonstrated (Chandler et al., 2011; Chandler et al., 2009; James et al., 1995). The significant amounts of connective tissue in human SN have been previously described (Alings et al., 1995), so connective tissue has been used as a marker of SN and it could distinguish it from the surrounding RA.

Cell size differences were further confirmed by performing immunolabelling for caveolin3, which demonstrated RA myocytes exhibit significantly larger diameter in comparison with SN myocytes (Figure 3.1 B, C and D). Similar SN and RA myocytes dimensions were described previously (Chandler et al., 2011; Lowe et al., 1988).

Immunohistochemical experiments compared the protein expression of the major pacemaking channel HCN4, responsible for I_f, L-type ($Ca_V1.3$) and T-type ($Ca_V3.1$) Ca^{2+} channels, responsible for $I_{Ca,L}$ and $I_{Ca,T}$, respectively, as well as Cx43, a large conductance connexin absent from the SN (Figure 3.2). As previously reported, HCN4, $Ca_V1.3$, and $Ca_V3.1$ immunolabelling was highly abundant in the SN compared to the RA where only background fluorescence was exhibited (Chandler et al., 2009). In contrast, Cx43 fluorescence levels were higher in the human RA compared to the SN. Furthermore, immunoblotting analysis showed that Cx43 involved in electrical coupling between cells, $Na_V1.5$, responsible for the conduction of I_{Na}, NCX1, important for Ca^{2+} extrusion after diastolic depolarisation, and SERCA2a, responsible for Ca^{2+} recycling in the SR protein levels were significantly lower in the human SN compared to the RA (Figure 3.3). The expression of membrane clock and Ca^{2+} clock proteins was in agreement with previous studies we have performed on human SN vs. RA samples (Chandler et al., 2009).

We also studied the protein expression of transcription factors critical for the SN formation - Tbx18. Immunoblotting results demonstrated that Tbx18 at protein level is significantly more expressed in the human SN compared to the RA (Figure 3.3), suggesting it has a key role in the homeostasis of the cardiac conduction system during adulthood, and not only during embryogenesis. Tbx18 was shown to regulate gene expression programmes that result in regionalisation of the developing SN and its corresponding gene profile (Wiese et al., 2009). It was also reported to produce a negative effect upon Nkx2-5 expression

(Christoffels et al., 2006). Tbx18 induces transcriptional repression of GJA1 (Cx43), without affecting GJA5 (Cx40) and GJC1 (Cx45) (Kapoor et al., 2011), suggesting it is working through transcriptional reinforcement of nodal genes, and repression of working myocardium genes. It was shown for the first time in our study that Tbx18, which is functionally regulating the adult human heart, is significantly upregulated in the SN compared to the RA working myocardium.

The most significant result that we reported in Chapter 3 was the expression of 48 microRNAs that were less expressed in the human SN (Figure 3.4 A) vs. 18 microRNA that were significantly more expressed in the human SN (Figure 3.4 B). In order to focus our work on the microRNAs that are potentially regulating the pacemaking activity of the SN, we predicted 15 microRNAs target ion channels, connexins, and Ca^{2+}-handling proteins (Figure 3.5 and 3.6) involved in the regulation of the membrane-voltage and Ca^{2+} clocks using Ingenuity Pathway Analysis software and target mRNA predicted by Chandler et al., 2009. miR-10b-5p was found to target Cx40; miR-153 was predicted to target $Ca_V1.2$, RyR2, and $Na_V1.5$; miR-198 - $Ca_V1.2$, RyR2, and ERG; miR-204 - $Ca_V1.2$; miR-215 - $K_V1.4$; miR-512-5p - Cx43; and miR-1225-3p – $Na_V1.5$ (Table 3.1). MicroRNAs that were significantly less expressed in the SN such as miR-1-3p was found to target Tbx3, HCN1, and HCN4; miR-30c-5p - $Ca_V1.3$, HCN1, and HCN4; miR-133a-3p – HCN4; miR-371-3p - $Ca_V1.3$ and Cx45; miR-422a – Tbx3; miR-429 – Tbx18; miR-486-3p - $Ca_V1.3$, $Ca_V3.1$, HCN1, and HCN4; and miR-938 - $Ca_V1.3$ (Table 3.1).

The study encountered limitations posed by small number of human samples due to limited availability. As it can be observed in Table S1 (Supplement file) there was significant variability in specimen age, gender, source, and cause of death, which predisposes the results to further variability. None of the causes of death, however, were related to a

disease that could affect the heart. Moreover, we observed that the prediction interactions and number of binding sites of microRNAs and their target mRNAs made by Ingenuity Pathway Analysis, TargetScan Human, and TarBase softwares are not always correct. For example, Tbx18 was predicted to have one binding site for miR-429, however, when we performed luciferase assay for Tbx18 expression in miR-429-transfected H9C2 cells, we discovered no downregulation of Tbx18 luciferase signal, leading to the conclusion that miR-429 does not bind to and inhibit Tbx18 mRNA (Chapter 4).

Further progression of this study could potentially involve functional validation of the binding of predicted microRNAs to their target genes using luciferase reporter gene assay followed by qPCR for the expression of microRNA and mRNA levels. In order to use a more appropriate human related *in vitro* model, we could potentially use hiPSCs nodal-derived cells. This could be transfected with microRNAs and target mRNAs of interest to observe changes of their beating rate and subsequent qPCR, immunolabelling/blotting for changes in target genes and protein levels could be performed. Moreover, a combination of microRNAs such as miR-486-3p and miR-429 could be injected in order to induce more pronounced effect.

8.2 Chapter 4 - miR-486-3p regulates pacemaker activity in the human heart via the funny, HCN4, channel

Chapter 4 is a continuation of the work in Chapter 3 and it focuses on miR-1-3p, miR-30c-5p, miR-133a-3p, miR-371-3p, miR-429, miR-486-3p, and miR-153-3p involvement in the regulation of key functional molecules in the SN vs. RA (Chapter 4, Table 4.1). The major aims of the study were to 1) determine if these key 7 microRNAs have binding sites for their predicted targets and if they are conserved in human and rat (Table 4.1 and 4.2), and

2) if the microRNAs have any functional effect on *ex vivo* rat SN preparations and the predicted target expression levels.

The main finding of the study was that miR-486-3p and miR-429 significantly reduced the beating rate of the rat SN. qPCR analysis of miR-486-3p and HCN4 levels revealed significant upregulation of miR-486-3p after injection in *ex vivo* rat SN preparations, while HCN4 mRNA levels were significantly downregulated. In order to identify if HCN4 protein levels were also affected by miR-486-3p overexpression, we performed immunolabelling experiment that demonstrated significant reduction of HCN4 protein levels in miR-486-3p-injected rat SN preparations compared to control. To confirm miR-486-3p binds to the HCN4 3'UTR, we performed a luciferase reporter gene assay. HCN4 luciferase activity was inhibited by miR-486-3p, confirming miR-486-3p binds to HCN4 3'UTR and causes its post-transcriptional repression.

qPCR analysis, as well as luciferase report gene assay for Tbx18, however, showed no changes of Tbx18 mRNA levels and no binding of miR-429 to Tbx18 3'UTR. These data imply that the predictions for binding sites of microRNAs and their target mRNAs made by Ingenuity Pathway Analysis, TargetScan Human, and TarBase softwares are not always correct. For this reason, a luciferase reporter gene assay should be carried out before functional validation of the effect of the microRNA in order to confirm if the microRNA in question binds to its predicted target first. These data need to be then further confirmed with qPCR for the mRNA levels of expression of the target gene. Furthermore, H9C2 cells that we used for luciferase reporter gene assays are not an ideal model as they are rat-derived cardiomyocytes. A better *in vitro* model would be human nodal-derived iPSCs that could be also used for experiments involving anti-miRs. A previous study by our group reported that anti-miR for miR-423-5p, which was found to be upregulated in bradycardiac

SN and to inhibit HCN4 levels, rescued HCN4 levels as well as I_f in an athletically trained mouse SN model (D'Souza et al., 2017). Anti-miR oligonucleotides are synthetically designed molecules used to neutralise microRNA function by blocking their effect (Lennox and Behlke, 2011).

Before functionally validating microRNAs effect on target mRNAs in rat SN preparations, it would be important to confirm if the binding sites of the target mRNAs are conserved amongst species, as for example, miR-133a-3p was predicted to bind to human HCN4, but rat HCN4 does not express the same binding sites (Chapter 4, Table 4.2), leading to no effect on the rat SN preparation beating rate. Another potential way to approach this issue would be to use human nodal-derived iPSCs as a more appropriate model since hiPSCs potentially express endogenous levels of key pacemaking molecules such as HCN4 (Chapter 7).

8.3 Chapter 5 - Do human heart pacemaker cell have t-tubules?

Larger mammal species such as sheep, pig, and human were reported to express t-tubules in their atrial myocytes (Caldwell et al., 2014; Dibb et al., 2009; Lenaerts et al., 2009; Richards et al., 2011). However, nothing was known about the presence of t-tubules in the human SN yet, therefore the aim of the current study was to determine the t-tubular organisation in the human SN and the surrounding RA mainly by examining Ca^{2+} clock proteins.

The main finding of our study was that there are sparse t-tubules in some human SN myocytes, visualised with WGA staining (Chapter 5, Figure 5.2). WGA, however, was found to accumulate non-specifically in the connective tissue surrounding the SN and RA myocytes, and it was also staining the nucleus membrane of the cardiomyocytes. For these

reasons, it will be useful to repeat the experiment with another t-tubular marker i.e. specific antibody to t-tubular proteins ideally could be used, as that would omit non-specific binding. Another widely used marker of the t-tubules is di-4-ANEPPS/di-8-ANEPPS, a lipophilic membrane marker, which stains the cell membrane and its invaginations. Di-4-ANEPPS has been previously used in the characterisation of ventricular and atrial tissue from rat, ferret, and sheep in health and heart failure (Caldwell et al., 2014; Dibb et al., 2009). A very recent study on cardiac tissue grown from hiPSCs determined the cell structure and the presence of t-tubular network by using both WGA and di-8-ANEPPS as t-tubular markers (Ronaldson-Bouchard et al., 2018). They also observed similar accumulation of WGA staining in the connective tissue at the extracellular space around the cardiomyocytes (Ronaldson-Bouchard et al., 2018).

Our current study also confirmed striated expression pattern of RyR2 and SERCA2a in both SN and RA (Chapter 5, Figure 5.6 and 5.7) as previously described (Lyashkov et al., 2007; Musa et al., 2002).

We also reported colocalisation of the RyR2 intracellular striated expression pattern with α-actinin (marker of the Z-lines, (Chapter 5, Figure 5.11)). Neither, however, were colocalised with WGA (t-tubular marker, (Chapter 5, Figure 5.5 and 5.10)), suggesting their striated expression pattern and the RyR2 clustering around the Z-lines allows more efficient Ca^{2+} signalling and closer proximity to the junctional and corbular SR network. Important limitation is that both figure 5.5 and 5.10 do not show t-tubular organisation with WGA in either tissue types, which does not allow us to conclude with certainty if RyR2 and α-actinin colocalise with the t-tubular network. Single labelling WGA images, however, show sparse t-tubules in the SN and well organised such in the RA.

Future work would require double labelling experiments on human SN vs. ventricular tissue, as a control, for RyR2 and SERCA2a as well as RyR2 and α-actinin, and t-tubular labelling.

More single and double labelling experiments could be performed with antibodies raised against dystrophin, NCX1, and a t-tubular marker as they showed some invaginations in the cell membrane of atrial cells (Chapter 5, Figure 5.1, 5.3 and 5.7). Thus, it would be interesting to further study their collocalisation and potential relationships.

Since we are interested in the relationship between RyR2 organisation in the cardiomyocytes and the Ca^{2+}-handling proteins important for efficient Ca^{2+} homeostasis in the cells, it would be important to study phospholamban and calsequestrin expression in human SN and RA. Previous data reported that RyR2 forms complexes with calsequestrin, where it sequesters Ca^{2+} in the SR and increases RyR2 opening probability (Gyorke et al., 2004; Zhang et al., 1997). Phospholamban in turn regulates SERCA2a by inhibiting its activity (Briston et al., 2011; Periasamy et al., 2008).

8.4 Chapter 6 - Identification of key transcription factors in the human sinus node versus right atrium

The current study focused on mapping the expression profile of transcription factors in adult human SN vs. RA. We identified 68 transcriptional regulators significantly more expressed in the SN, and 60 that were significantly less expressed in the SN compared to the RA (Chapter 6, Table 6.2 and 6.3). This variable list of transcriptional regulators was further narrowed down to the transcription factors that play roles in the formation and regulation of the SN and the RA, respectively, such as Isl1, Tbx1, Shox2, Tbx3, and

Tbx18, which were upregulated in the SN; and Tbx5 and Nkx2-5 that were downregulated in the SN compared to the RA (Chapter 6, Table 6.5).

Previous literature has reported the role of Isl1, Tbx3, Tbx5, and Nkx2-5 in the cardiac conduction system and the working myocardium during cardiac development as well as maturation and functional maintenance (Bruneau et al., 2001; Frank et al., 2012; Jay et al., 2004; Sun et al., 2007; Vedantham et al., 2015). Other transcription factors like Tbx1 and Tbx18 were found to be important in nodal cell proliferation during embryogenesis (Christoffels et al., 2006; Xu et al., 2004; Zhang et al., 2006), but their function in the adult heart is not known yet. For this reason, the expression of Tbx1 and Tbx18 in the adult human SN needs to be confirmed not only by NGS analysis, but through individual qPCR for each gene too, as NGS is a more sensitive, but not as specific approach for studying mRNA expression.

MicroRNAs such as miR-1 and miR-133 were previously found to play various roles in the heart in both physiological and pathological context (Care et al., 2007b; Luo et al., 2008; Zhao et al., 2007). Our current study reported miR-486-3p targets HCN4. Moreover, a previous study by our group reported that upregulation of Nkx2-5 results in increased miR-423-5p expression and subsequent downregulation of HCN4 and inhibition of I_f (D'Souza et al., 2017). In our current study we also predicted that some microRNAs target cardiac conduction specific transcription factors. All of these interactions suggest transcription factors can control microRNA expression and vice versa, which is another interesting field to be studied.

Further progression of this work would require validation of transcription factor targets with luciferase reporter gene assay and qPCR analysis. Similarly to what we already

discussed, an ideal cell culture model for transcription factors targets would be nodal-derived iPSCs or cultured rat nodal tissue as previously described (Morris et al., 2013).

8.5 Chapter 7 - The effect of miR-133a-3p on beating rate and HCN4 in cardiac-derived iPSCs

Our previous data reported miR-133a-3p is significantly more expressed in the healthy, human SN compared to RA, and we also predicted miR-133a-3p is targeting HCN4 (Chapter 7, Figure 7.1). We hypothesised that overexpression of miR-133a will induce reduction of the spontaneous beating rate of hiPSCs derived cardiomyocytes, as it will potentially target endogenous HCN4 expression, reduce it and thus inhibit the action potential frequency, and the subsequent beating rate.

Our data, however, demonstrated no change in the beating rate of iPSCs after 24-hour transfection period (Figure 7.6). Trend towards reduction of the beating rate was noticed at the last few hours, suggesting that longer incubation time or higher miR-133a-3p concentration might produce a significant effect.

The comparison between lipofectamine and GO as transfection systems proved lipofectamine is much more efficient as transfection reagent, while no transfection was observed with GO (Figure 7.5). GO, however, did not seem to be toxic as cells were viable at the end of the experiments, and their beating rate remained unchanged.

Despite the fact that no functional change of the beating rate of miR-133a-3p transfected iPSCs was observed, there was significant downregulation of HCN4 mRNA compared to control (Figure 7.7 A), suggesting miR-133a-3p induces HCN4 post-transcriptional repression.

Further experimental work would require the use of nodal-derived iPSCs. The cells used have not been characterised, and they potentially contain higher abundance of ventricular and atrial-like cells, but few nodal-like cells. This cellular heterogeneity could explain why the beating rate was not affected by the miR-133a-3p forced overexpression. Further characterisation of the morphology and molecular background of the iPSCs could be performed using immunolabelling against HCN4 and other SN cells markers, and qPCR for the expression of important membrane-voltage and Ca^{2+} clock proteins.

Another potentially more efficient approach that could be taken in microRNA transfections of either tissue preparations or cell lines could involve microRNA gene incorporation into adenoviral vectors. This method could overcome the limitations related to low transfection efficiency, and could produce better and more reliable functional results.

A possible method to further study microRNA mediated effects on iPSCs derived cardiomyocytes beating rate would be anti-miR transfections. As already described by D'Souza et al., HCN4 expression, as well as I_f, was rescued in an athletically trained mouse model (D'Souza et al., 2017). Similarly, it would be interesting to observe if anti-miR-133a-3p would reverse the effect of miR-133a-3p on iPSCs and increase endogenous HCN4 levels.

8.6 Final remarks

Our current study looked into the expression of major pacemaking microRNAs and TFs as important regulators of both the differentiation and modulation of SN and working myocardium function. From our functional studies we can conclude that miR-486-3p is a potential regulator of RA function through inhibition of the major pacemaking channel HCN4. miR-429 also exhibits important RA function through the inhibition of pacemaking

activity, but its targets remain unknown as it was found it does not bind to and inhibit Tbx18 expression. Our group previously looked into the function of miR-1 and miR-423-5p in athletically trained mice where it found that overexpression of the working myocardium TF Nkx2-5 in the SN stimulates miR-1, miR-423-5p, as well as miR-486-3p, which were found to target and thus downregulate HCN4 (D'Souza et al., 2017). These data suggest that alterations in the regulatory machinery of the SN during pathogenesis lead to abnormal AP resulting in bradycardia in this specific case. Our hiPSCs did not have their function affected by miR-133a-3p overexpression (potentially due to variabilities in the cell batches), but showed downregulation of HCN4 expression. Furthermore, we predict that Isl1, Tbx1, Tbx3, Tbx18, and Shox2 significantly higher expression in the mature human SN would stimulate the expression of miRs- 10b-5p, 153-3p, 198, 204-5p, 215-5p, 1225-5p (Figure 8.1), which in turn are predicted to major working myocardium specific proteins and TFs such as Cx40, Cx43, $Na_V1.5$, $Ca_V1.2$, $K_V1.4$, RyR2, and Nkx2-5 (Figure 8.1), and thus not only take part in SN differentiation, but also normal function during development and adulthood.

The dual function of the TFs allows both repression/stimulation of major pacemaking proteins through direct or indirect (through microRNAs) interactions. Similarly, TFs could affect the expression of other TFs either directly or through microRNAs interactions. These complex mechanisms provide a wide field for research that could be used in the regulation of the heart rhythm in the mature heart through fine-tuning of the levels of expression of target molecules.

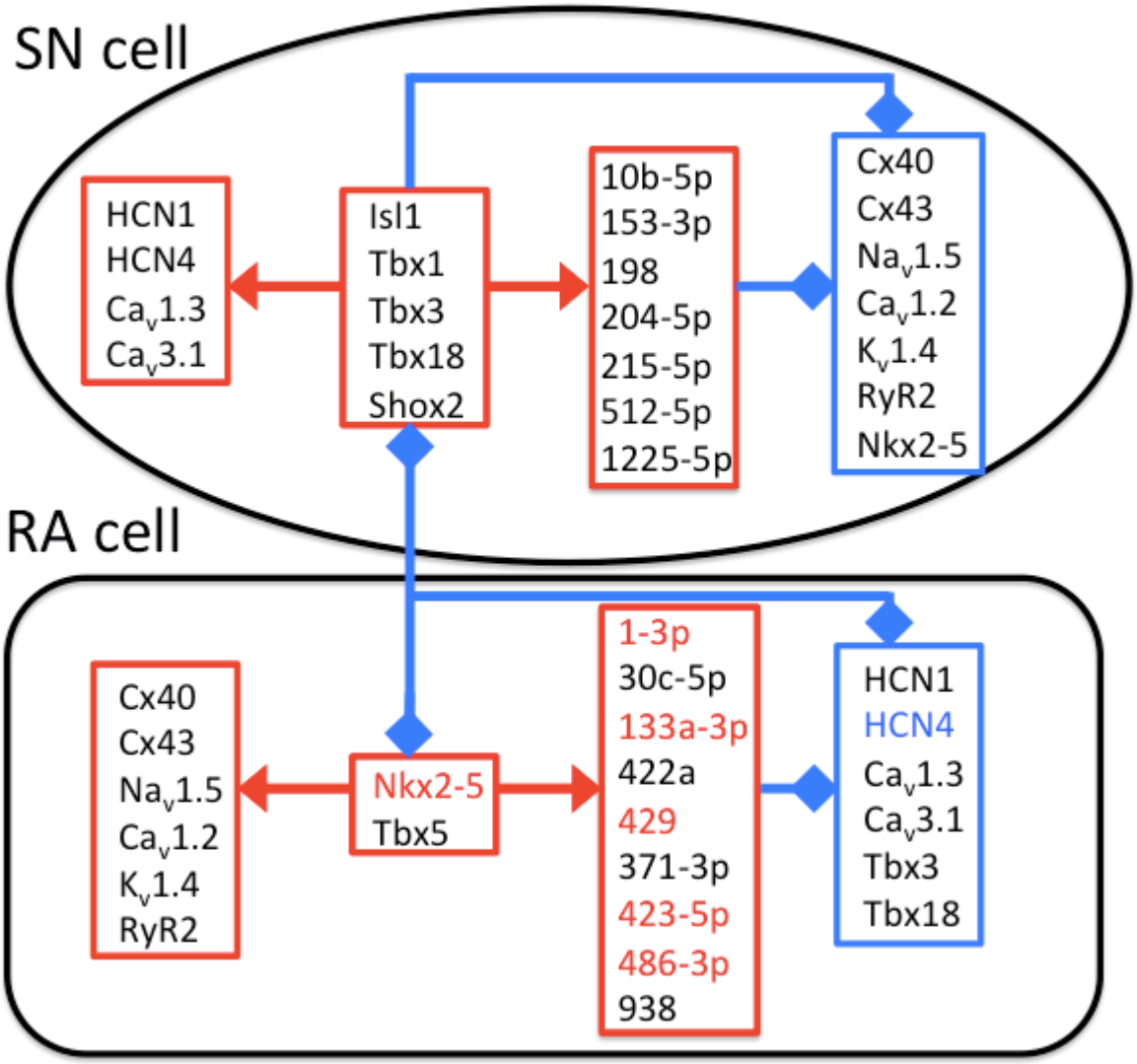

Figure 8.1. Transcription factors and microRNAs in the regulation of major pacemaking channels in the SN and RA. Higher expression is indicated in red, while lower expression – blue. Enhanced expression of Isl1, Tbx1, Tbx3, Tbx18, and Shox2 controls SN differentiation from the RA, and inhibits the RA development gene programme through inhibition of myocardium specific TFs, and stimulation of microRNAs inhibiting working myocardium specific molecules. Similar mechanisms are proposed for RA development and control too. Thus positive and negative feedback mechanisms are formed.

References

Aanhaanen, W. T. J., M. T. M. Mommersteeg, J. Norden, V. Wakker, C. de Gier-de Vries, R. H. Anderson, A. Kispert, A. F. M. Moorman, and V. M. Christoffels, 2010, Developmental origin, growth, and three-dimensional architecture of the atrioventricular conduction axis of the mouse heart: Circulation Research, v. 107, p. 728-U98.

Alings, A. M. W., R. F. Abbas, and L. N. Bouman, 1995, Age-related changes in structure and relative collagen content of the human and feline sinoatrial node - A comparative study: European Heart Journal, v. 16, p. 1655-1667.

Alings, A. M. W., R. F. Abbas, B. Dejonge, and L. N. Bouman, 1990, Structure and function of the simian sinoatrial node (macaca-fascicularis): Journal of Molecular and Cellular Cardiology, v. 22, p. 1453-1466.

Alings, A. M. W., and L. N. Bouman, 1993, Electrophysiology of the aging rabbit and cat sinoatrial node - a comparative-study: European Heart Journal, v. 14, p. 1278-1288.

Andelfinger, G., A. R. Tapper, R. C. Welch, C. G. Vanoye, A. L. George, and D. W. Benson, 2002, KCNJ2 mutation results in Andersen syndrome with gender specific cardiac and skeletal muscle phenotype: Circulation, v. 106, p. 60-60.

Anyukhovsky, E. P., E. A. Sosunov, P. Chandra, T. S. Rosen, P. A. Boyden, P. Danilo, and M. R. Rosen, 2005, Age-associated changes in electrophysiologic remodeling: a potential contributor to initiation of atrial fibrillation: Cardiovascular Research, v. 66, p. 353-363.

Arya, M., I. S. Shergill, M. Williamson, L. Gommersall, N. Arya, and H. R. H. Patel, 2005, Basic principles of real-time quantitative PCR: Expert Review of Molecular Diagnostics, v. 5, p. 209-219.

Atkinson, A. J., S. Logantha, G. Hao, J. Yanni, O. Fedorenko, A. Sinha, S. H. Gilbert, A. P. Benson, D. L. Buckley, R. H. Anderson, M. R. Boyett, and H. Dobrzynski, 2013, Functional, anatomical, and molecular investigation of the cardiac conduction system and arrhythmogenic atrioventricular ring tissue in the rat heart: Journal of the American Heart Association, v. 2.

Aurora, A. B., A. I. Mahmoud, X. Luo, B. A. Johnson, E. van Rooij, S. Matsuzaki, K. M. Humphries, J. A. Hill, R. Bassel-Duby, H. A. Sadek, and E. N. Olson, 2012, MicroRNA-214 protects the mouse heart from ischemic injury by controlling Ca^{2+} overload and cell death: Journal of Clinical Investigation, v. 122, p. 1222-1232.

Azene, E. M., T. Xue, and R. A. Li, 2003, Molecular basis of the effect of potassium on heterologously expressed pacemaker (HCN) channels: Journal of Physiology-London, v. 547, p. 349-356.

Baddour, L. M., A. E. Epstein, C. C. Erickson, B. P. Knight, M. E. Levison, P. B. Lockhart, F. A. Masoudi, E. J. Okum, W. R. Wilson, L. B. Beerman, A. F. Bolger, N. A. M. Estes, M. Gewitz, J. W. Newburger, E. B. Schron, K. A. Taubert, Y. Council Cardiovasc Dis, A. Council Cardiovasc Surg, N. Council Cardiovasc, C. Council Clinical, and Q. Interdisciplinary Council, 2010, Update on cardiovascular implantable electronic device infections and their management a scientific statement from the american heart association: Circulation, v. 121, p. 458-477.

Baker, K., K. S. Warren, G. Yellen, and M. C. Fishman, 1997, Defective "pacemaker" current I_f in a zebrafish mutant with a slow heart rate: Proceedings of the National Academy of Sciences of the United States of America, v. 94, p. 4554-4559.

Bakker, M. L., G. J. J. Boink, B. J. Boukens, A. O. Verkerk, M. van den Boogaard, A. D. den Haan, W. M. H. Hoogaars, H. P. Buermans, J. M. T. de Bakker, J. Seppen, H. L. Tan, A. F. M. Moorman, P. A. C. t Hoen, and V. M. Christoffels, 2012, T-box transcription factor TBX3 reprogrammes mature cardiac myocytes into pacemaker-like cells: Cardiovascular Research, v. 94, p. 439-449.

Baldini, A., 2004, DiGeorge syndrome: an update: Current Opinion in Cardiology, v. 19, p. 201-204.

Bamshad, M., R. C. Lin, D. J. Law, W. S. Watkins, P. A. Krakowiak, M. E. Moore, P. Franceschini, R. Lala, L. B. Holmes, T. C. Gebuhr, B. G. Bruneau, A. Schinzel, J. G. Seidman, C. E. Seidman, and L. B. Jorde, 1997, Mutations in human TBX3 alter limb, apocrine and genital development in ulnar-mammary syndrome: Nature Genetics, v. 16, p. 311-315.

Bao, H. Q., Y. Z. Pan, Y. Ping, N. G. Sahoo, T. F. Wu, L. Li, J. Li, and L. H. Gan, 2011, Chitosan-functionalized graphene oxide as a nanocarrier for drug and gene delivery: Small, v. 7, p. 1569-1578.

Bartel, D. P., 2009, MicroRNAs: target recognition and regulatory functions: Cell, v. 136, p. 215-233.

Baruscotti, M., A. Bucchi, C. Viscomi, G. Mandelli, G. Consalez, T. Gnecchi-Rusconi, N. Montano, K. R. Casali, S. Micheloni, A. Barbuti, and D. DiFrancesco, 2011, Deep bradycardia and heart block caused by inducible cardiac-specific knockout of the pacemaker channel gene HCN4: Proceedings of the National Academy of Sciences of the United States of America, v. 108, p. 1705-1710.

Baruscotti, M., and D. DiFrancesco, 2004, Pacemaker channels: cardiac engineering: from Genes and Cells to Structure and Function, v. 1015, p. 111-121.

Baruscotti, M., D. DiFrancesco, and R. B. Robinson, 1996, A TTX-sensitive inward sodium current contributes to spontaneous activity in newborn rabbit sinoatrial node cells: Journal of Physiology-London, v. 492, p. 21-30.

Baruscotti, M., R. Westenbroek, W. A. Catterall, D. DiFrancesco, and R. B. Robinson, 1997, The newborn rabbit sino-atrial node expresses a neuronal type I-like Na^+ channel: Journal of Physiology-London, v. 498, p. 641-648.

Basson, C. T., T. S. Huang, R. C. Lin, D. R. Bachinsky, S. Weremowicz, A. Vaglio, R. Bruzzone, R. Quadrelli, M. Lerone, G. Romeo, M. Silengo, A. Pereira, J. Krieger, S. F. Mesquita, M. Kamisago, C. C. Morton, M. E. M. Pierpont, C. W. Muller, J. G. Seidman, and C. E. Seidman, 1999, Different TBX5 interactions in heart and limb defined by Holt-Oram syndrome mutations: Proceedings of the National Academy of Sciences of the United States of America, v. 96, p. 2919-2924.

Benditt, D. G., C. C. Gornick, D. Dunbar, A. Almquist, and S. Poolschneider, 1987, Indications for electrophysiologic testing in the diagnosis and assessment of sinus node dysfunction: Circulation, v. 75, p. 93-99.

Benson, D. W., G. M. Silberbach, A. Kavanaugh-McHugh, C. Cottrill, Y. Z. Zhang, S. Riggs, O. Smalls, M. C. Johnson, M. S. Watson, J. G. Seidman, C. E. Seidman, J. Plowden, and J. D. Kugler, 1999, Mutations in the cardiac transcription factor NKX2.5 affect diverse cardiac developmental pathways: Journal of Clinical Investigation, v. 104, p. 1567-1573.

Biffi, M., M. Bertini, D. Saporito, M. Ziacchi, C. Martignani, I. Diemberger, and G. Boriani, 2010, Actual pacemaker longevity: the benefit of stimulation by automatic capture verification: pace-pacing and clinical electrophysiology, v. 33, p. 873-881.

Blaschke, R. J., N. D. Hahurij, S. Kuijper, S. Just, L. J. Wisse, K. Deissler, T. Maxelon, K. Anastassiadis, J. Spitzer, S. E. Hardt, H. Scholer, H. Feitsma, W. Rottbauer, M. Blum, F. Meijlink, G. Rappold, and A. Groot, 2007, Targeted mutation reveals essential functions of the homeodomain transcription factor Shox2 in sinoatrial and pacemaking development: Circulation, v. 115, p. 1830-1838.

Blaschke, R. J., A. P. Monaghan, S. Schiller, B. Schechinger, E. Rao, H. Padilla-Nash, T. Ried, and G. A. Rappold, 1998, SHOT, a SHOX-related homeobox gene, is implicated in craniofacial, brain, heart, and limb development: Proceedings of the National Academy of Sciences of the United States of America, v. 95, p. 2406-2411.

Bleeker, W. K., A. J. C. Mackaay, M. Massonpevet, L. N. Bouman, and A. E. Becker, 1980, Functional and morphological organization of the rabbit sinus node: Circulation Research, v. 46, p. 11-22.

Boettger, T., and T. Braun, 2012, A new level of complexity the role of microRNAs in cardiovascular development: Circulation Research, v. 110, p. 1000-1013.

Bogdanov, K. Y., T. M. Vinogradova, and E. G. Lakatta, 2001, Sinoatrial nodal cell ryanodine receptor and Na^{+}-Ca^{2+} exchanger - molecular partners in pacemaker regulation: Circulation Research, v. 88, p. 1254-1258.

Boineau, J. P., T. E. Canavan, R. B. Schuessler, M. E. Cain, P. B. Corr, and J. L. Cox, 1988, Demonstration of a widely distributed atrial pacemaker complex in the human-heART: Circulation, v. 77, p. 1221-1237.

Boink, G. J., M. L. Bakker, A. O. Verkerk, D. Bakker, J. M. de Bakker, J. Seppen, V. M. Christoffels, and H. L. Tan, 2008, Inducible TBX3 Overexpression as a tool for biopacemaker engineering: Circulation, v. 118, p. S340-S340.

Boyden, P. A., and B. F. Hoffman, 1981, The effects on atrial electrophysiology and structure of surgically induced right atrial enlargement in dogs: Circulation Research, v. 49, p. 1319-1331.

Boyett, M. R., A. D'Souza, H. G. Zhang, G. M. Morris, H. Dobrzynski, and O. Monfredi, 2013, Athlete's bradycardia may be a multifactorial mechanism Reply: Journal of Applied Physiology, v. 114, p. 1757-1757.

Boyett, M. R., H. Honjo, and I. Kodama, 2000, The sinoatrial node, a heterogeneous pacemaker structure: Cardiovascular Research, v. 47, p. 658-687.

Boyett, M. R., H. Honjo, M. Yamamoto, M. R. Nikmaram, R. Niwa, and I. Kodama, 1999, Downward gradient in action potential duration along conduction path in and around the sinoatrial node: American Journal of Physiology-Heart and Circulatory Physiology, v. 276, p. H686-H698.

Boyett, M. R., S. Inada, S. Yoo, J. Li, J. Liu, J. Tellez, I. D. Greener, H. Honjo, R. Billeter, M. Lei, H. Zhang, I. R. Efimov, and H. Dobrzynski, 2006, Connexins in the sinoatrial and atrioventricular nodes: Cardiovascular Gap Junctions, v. 42, p. 175-197.

Brette, F., and C. Orchard, 2003, T-tubule function in mammalian cardiac myocytes: Circulation Research, v. 92, p. 1182-1192.

Briston, S. J., J. L. Caldwell, M. A. Horn, J. D. Clarke, M. A. Richards, D. J. Greensmith, H. K. Graham, M. C. S. Hall, D. A. Eisner, K. M. Dibb, and A. W. Trafford, 2011, Impaired beta-adrenergic responsiveness accentuates dysfunctional excitation-contraction coupling in an ovine model of tachypacing-induced heart failure: Journal of Physiology-London, v. 589, p. 1367-1382.

Brummer, A., and J. Hausser, 2014, MicroRNA binding sites in the coding region of mRNAs: Extending the repertoire of post-transcriptional gene regulation: Bioessays, v. 36, p. 617-626.

Bruneau, B. G., G. Nemer, J. P. Schmitt, F. Charron, L. Robitaille, S. Caron, D. A. Conner, M. Gessler, M. Nemer, C. E. Seidman, and J. G. Seidman, 2001, A murine model of Holt-Oram syndrome defines roles of the T-box transcription factor Tbx5 in cardiogenesis and disease: Cell, v. 106, p. 709-721.

Bucchi, A., A. Barbuti, M. Baruscotti, and D. DiFrancesco, 2007, Heart rate reduction via selective 'funny' channel blockers: Current Opinion in Pharmacology, v. 7, p. 208-213.

Bucchi, A., A. N. Plotnikov, I. Shlapakova, P. Danilo, Y. Kryukova, J. H. Qu, Z. J. Lu, H. L. Liu, Z. M. Pan, I. Potapova, B. KenKnight, S. Girouard, I. S. Cohen, P. R. Brink, R. B. Robinson, and M. R. Rosen, 2006, Wild-type and mutant HCN channels in a tandem biological-electronic cardiac pacemaker: Circulation, v. 114, p. 992-999.

Burke, J. H., J. J. Goldberger, F. A. Ehlert, J. T. Kruse, M. A. Parker, and A. H. Kadish, 1996, Gender differences in heart rate before and after autonomic blockade: Evidence against an intrinsic gender effect: American Journal of Medicine, v. 100, p. 537-543.

Burridge, P. W., E. Matsa, P. Shukla, Z. C. Lin, J. M. Churko, A. D. Ebert, F. Lan, S. Diecke, B. Huber, N. M. Mordwinkin, J. R. Plews, O. J. Abilez, B. Cui, J. D. Gold, and J. C. Wu, 2014, Chemically defined generation of human cardiomyocytes: Nature Methods, v. 11, p. 855-860.

Caldwell, J. L., C. E. R. Smith, R. F. Taylor, A. Kitmitto, D. A. Eisner, K. M. Dibb, and A. W. Trafford, 2014, Dependence of cardiac transverse tubules on the BAR domain protein amphiphysin II (BIN-1): Circulation Research, v. 115, p. 986-U157.

Callis, T. E., K. Pandya, H. Y. Seok, R.-H. Tang, M. Tatsuguchi, Z.-P. Huang, J.-F. Chen, Z. Deng, B. Gunn, J. Shumate, M. S. Willis, C. H. Selzman, and D.-Z. Wang, 2009, MicroRNA-208a is a regulator of cardiac hypertrophy and conduction in mice: Journal of Clinical Investigation, v. 119, p. 2772-2786.

Care, A., D. Catalucci, F. Felicetti, D. Bonci, A. Addario, P. Gallo, M.-L. Bang, P. Segnalini, Y. Gu, N. D. Dalton, L. Elia, M. V. G. Latronico, M. Hoydal, C. Autore, M. A. Russo, G. W. Dorn, II, O. Ellingsen, P. Ruiz-Lozano, K. L. Peterson, C. M. Croce, C. Peschle, and G. Condorelli, 2007a, MicroRNA-133 controls cardiac hypertrophy: Nature Medicine, v. 13, p. 613-618.

Care, A., D. Catalucci, F. Felicetti, D. Bonci, A. Addario, P. Gallo, M. L. Bang, P. Segnalini, Y. S. Gu, N. D. Dalton, L. Elia, M. V. G. Latronico, M. Hoydal, C. Autore, M. A. Russo, G. W. Dorn, O. Ellingsen, P. Ruiz-Lozano, K. L. Peterson, C. M. Croce, C.

Peschle, and G. Condorelli, 2007b, MicroRNA-133 controls cardiac hypertrophy: Nature Medicine, v. 13, p. 613-618.

Chandler, N., O. V. Aslanidi, D. Buckley, S. Inada, S. Birchall, A. Atkinson, D. Kirk, O. Monfredi, P. Molenaar, R. Anderson, V. Sharma, D. Sigg, H. Zhang, M. Boyett, and H. Dobrzynski, 2011, Computer three-dimensional anatomical reconstruction of the human sinus node and a novel paranodal area: Anatomical Record-Advances in Integrative Anatomy and Evolutionary Biology, v. 294, p. 970-979.

Chandler, N. J., I. D. Greener, J. O. Tellez, S. Inada, H. Musa, P. Molenaar, D. DiFrancesco, M. Baruscotti, R. Longhi, R. H. Anderson, R. Billeter, V. Sharma, D. C. Sigg, M. R. Boyett, and H. Dobrzynski, 2009, Molecular architecture of the human sinus node insights into the function of the cardiac pacemaker: Circulation, v. 119, p. 1562-1575.

Chauveau, S., E. P. Anyukhovsky, M. Ben-Ari, S. Naor, Y. P. Jiang, P. Danilo, T. Rahim, S. Burke, X. L. Qiu, I. A. Potapova, S. V. Doronin, P. R. Brink, O. Binah, I. S. Cohen, and M. R. Rosen, 2017, Induced pluripotent stem cell-derived cardiomyocytes provide in vivo biological pacemaker function: Circulation-Arrhythmia and Electrophysiology, v. 10.

Chen, B. Y., Y. J. Wu, P. J. Mohler, M. E. Anderson, and L. S. Song, 2009, Local control of Ca^{2+}-induced Ca^{2+} release in mouse sinoatrial node cells: Journal of Molecular and Cellular Cardiology, v. 47, p. 706-715.

Chen, C. C., K. G. Lamping, D. W. Nuno, R. Barresi, S. J. Prouty, J. L. Lavoie, L. L. Cribbs, S. K. England, C. D. Sigmund, R. M. Weiss, R. A. Williamson, J. A. Hill, and K. P. Campbell, 2003, Abnormal coronary function in mice deficient in alpha(1H) T-type Ca^{2+} channels: Science, v. 302, p. 1416-1418.

Chen, C. Y., and R. J. Schwartz, 1996, Recruitment of the tinman homolog Nkx-2.5 by serum response factor activates cardiac alpha-actin gene transcription: Molecular and Cellular Biology, v. 16, p. 6372-6384.

Chen, J. F., E. M. Mandel, J. M. Thomson, Q. L. Wu, T. E. Callis, S. M. Hammond, F. L. Conlon, and D. Z. Wang, 2006, The role of microRNA-1 and microRNA-133 in skeletal muscle proliferation and differentiation: Nature Genetics, v. 38, p. 228-233.

Chen, J. X., M. Krane, M. A. Deutsch, L. Wang, M. Rav-Acha, S. Gregoire, M. C. Engels, K. Rajarajan, R. Karra, E. D. Abel, J. C. Wu, D. Milan, and S. M. Wu, 2012, Inefficient reprogramming of fibroblasts into cardiomyocytes using Gata4, Mef2c, and Tbx5: Circulation Research, v. 111, p. 50-55.

Cheng, G., W. H. Litchenberg, G. J. Cole, T. Mikawa, R. P. Thompson, and R. G. Gourdie, 1999, Development of the cardiac conduction system involves recruitment within a multipotent cardiomyogenic lineage: Development, v. 126, p. 5041-5049.

Cheng, H., M. R. Lederer, R. P. Xiao, A. M. Gomez, Y. Y. Zhou, B. Ziman, H. Spurgeon, E. G. Lakatta, and W. J. Lederer, 1996, Excitation-contraction coupling in heart: New insights from Ca^{2+} sparks: Cell Calcium, v. 20, p. 129-140.

Cheng, Y., N. Tan, J. Yang, X. Liu, X. Cao, P. He, X. Dong, S. Qin, and C. Zhang, 2010, A translational study of circulating cell-free microRNA-1 in acute myocardial infarction: Clinical Science, v. 119, p. 87-95.

Chiang, C. H., Y. Su, Z. Wen, N. Yoritomo, C. A. Ross, R. L. Margolis, H. Song, and G. I. Ming, 2011, Integration-free induced pluripotent stem cells derived from schizophrenia patients with a DISC1 mutation: Molecular Psychiatry, v. 16, p. 358-360.

Cho, H. C., N. Kapoor, W. B. Liang, and E. Marban, 2012, Transcription factor-driven conversion of quiescent cardiomyocytes to pacemaker cells: Circulation, v. 126.

Cho, H. C., and E. Marban, 2010, Biological therapies for cardiac arrhythmias can genes and cells replace drugs and devices?: Circulation Research, v. 106, p. 674-685.

Choi, H. Y., T. J. Lee, G. M. Yang, J. Oh, J. Won, J. Han, G. J. Jeong, J. Kim, J. H. Kim, B. S. Kim, and S. G. Cho, 2016, Efficient mRNA delivery with graphene oxide-polyethylenimine for generation of footprint-free human induced pluripotent stem cells: Journal of Controlled Release, v. 235, p. 222-235.

Choi, W., I. Lahiri, R. Seelaboyina, and Y. S. Kang, 2010, Synthesis of graphene and its applications: a review: Critical Reviews in Solid State and Materials Sciences, v. 35, p. 52-71.

Christoffels, V. M., M. T. M. Mommersteeg, M. O. Trowe, O. W. J. Prall, C. de Gier-de Vries, A. T. Soufan, M. Bussen, K. Schuster-Gossler, R. P. Harvey, A. F. M. Moorman, and A. Kispert, 2006, Formation of the venous pole of the heart from an Nkx2-5-negative precursor population requires Tbx18: Circulation Research, v. 98, p. 1555-1563.

Cingolani, E., J. I. Goldhaber, and E. Marban, 2018, Next-generation pacemakers: from small devices to biological pacemakers: Nature Reviews Cardiology, v. 15, p. 139-150.

Clement-Jones, M., S. Schiller, E. Rao, R. J. Blaschke, A. Zuniga, R. Zeller, S. C. Robson, G. Binder, I. Glass, T. Strachan, S. Lindsay, and G. A. Rappold, 2000, The short stature homeobox gene SHOX is involved in skeletal abnormalities in Turner syndrome: Human Molecular Genetics, v. 9, p. 695-702.

Cohen, I. S., P. R. Brink, R. B. Robinson, and M. R. Rosen, 2005, The why, what, how and when of biological pacemakers: Nature Clinical Practice Cardiovascular Medicine, v. 2, p. 374-375.

Compton, O. C., and S. T. Nguyen, 2010, Graphene oxide, highly reduced graphene oxide, and graphene: versatile building blocks for carbon-based materials: Small, v. 6, p. 711-723.

Condorelli, G., M. V. G. Latronico, and E. Cavarretta, 2014, microRNAs in cardiovascular diseases current knowledge and the road ahead: Journal of the American College of Cardiology, v. 63, p. 2177-2187.

Corsten, M. F., R. Dennert, S. Jochems, T. Kuznetsova, D. R. Wagner, J. Staessen, L. Hofstra, S. Heymans, and B. Schroen, 2010, Circulating microRNA-208b and miR-499 reflect myocardial damage in cardiovascular disease: European Heart Journal, v. 31, p. 75-75.

D'Souza, A., A. Bucchi, A. B. Johnsen, S. Logantha, O. Monfredi, J. Yanni, S. Prehar, G. Hart, E. Cartwright, U. Wisloff, H. Dobryznski, D. DiFrancesco, G. M. Morris, and M. R. Boyett, 2014, Exercise training reduces resting heart rate via downregulation of the funny channel HCN4: Nature Communications, v. 5.

D'Souza, A., C. M. Pearman, Y. W. Wang, S. Nakao, S. Logantha, C. Cox, H. Bennett, Y. Zhang, A. B. Johnsen, N. Linscheid, P. C. Poulsen, J. Elliott, J. Coulson, J. McPhee, A. Robertson, P. A. D. Martins, A. Kitmitto, U. Wisloff, E. J. Cartwright, O. Monfredi, A. Lundby, H. Dobrzynski, D. Oceandy, G. M. Morris, and M. R. Boyett, 2017, Targeting miR-423-5p reverses exercise training-induced HCN4 channel remodeling and sinus bradycardia: Circulation Research, v. 121, p. 1058-1067.

Davis, L. M., M. E. Rodefeld, K. Green, E. C. Beyer, and J. E. Saffitz, 1995, Gap junction protein phenotypes of the human heart and conduction systeM: Journal of Cardiovascular Electrophysiology, v. 6, p. 813-822.

Davis, R. P., S. Casini, C. W. van den Berg, M. Hoekstra, C. A. Remme, C. Dambrot, D. Salvatori, D. Ward-van Oostwaard, A. A. M. Wilde, C. R. Bezzina, A. O. Verkerk, C. Freund, and C. L. Mummery, 2012, Cardiomyocytes derived from pluripotent stem cells recapitulate electrophysiological characteristics of an overlap syndrome of cardiac sodium channel disease: Circulation, v. 125, p. 3079-89.

de Bakker, J. M. T., and A. Zaza, 2007, Special issue on biopacemaking: clinically attractive, scientifically a challenge: Medical & Biological Engineering & Computing, v. 45, p. 115-118.

de Pater, E., L. Clijsters, S. R. Marques, Y. F. Lin, Z. V. Garavito-Aguilar, D. Yelon, and J. Bakkers, 2009, Distinct phases of cardiomyocyte differentiation regulate growth of the zebrafish heart: Development, v. 136, p. 1633-1641.

Denyer, J. C., and H. F. Brown, 1990, Pacemaking in rabbit isolated sinoatrial node cells during Cs^+ block of the hyperpolarization-activated current I_f: Journal of Physiology-London, v. 429, p. 401-409.

Devaux, Y., M. Vausort, G. P. McCann, D. Kelly, O. Collignon, L. L. Ng, D. R. Wagner, and I. B. Squire, 2013, A Panel of 4 microRNAs facilitates the prediction of left ventricular contractility after acute myocardial infarction: Plos One, v. 8.

Dhamoon, A. S., and J. Jalife, 2005, The inward rectifier current I_{K1} controls cardiac excitability and is involved in arrhythmogenesis: Heart Rhythm, v. 2, p. 316-324.

Di Mauro, D., R. Gaeta, A. Arco, D. Milardi, S. Lentini, M. Runci, G. Rizzo, and L. Magaudda, 2009, Distribution of costameric proteins in normal human ventricular and atrial cardiac muscle: Folia Histochemica Et Cytobiologica, v. 47, p. 605-608.

Dibb, K. M., J. D. Clarke, M. A. Horn, M. A. Richards, H. K. Graham, D. A. Eisner, and A. W. Trafford, 2009, Characterization of an extensive transverse tubular network in sheep atrial myocytes and its depletion in heart Failure: Circulation-Heart Failure, v. 2, p. 482-489.

DiFrancesco, D., 2010, The role of the funny current in pacemaker activity: Circulation Research, v. 106, p. 434-446.

Difrancesco, D., and P. Tortora, 1991, Direct activation of cardiac-pacemaker channels by intracellular cyclic-AMP: Nature, v. 351, p. 145-147.

Djinovic-Carugo, K., P. Young, M. Gautel, and M. Saraste, 1999, Structure of the alpha-actinin rod: Molecular basis for cross-linking of actin filaments: Cell, v. 98, p. 537-546.

Dobrzynski, H., R. H. Anderson, A. Atkinson, Z. Borbas, A. D'Souza, J. F. Fraser, S. Inada, S. Logantha, O. Monfredi, G. M. Morris, A. F. M. Moorman, T. Nikolaidou, H. Schneider, V. Szuts, I. P. Temple, J. Yanni, and M. R. Boyett, 2013, Structure, function and clinical relevance of the cardiac conduction system, including the atrioventricular ring and outflow tract tissues: Pharmacology & Therapeutics, v. 139, p. 260-288.

Dobrzynski, H., M. R. Boyett, and R. H. Anderson, 2007, New insights into pacemaker activity - Promoting understanding of sick sinus syndrome: Circulation, v. 115, p. 1921-1932.

Dobrzynski, H., J. Li, J. Tellez, I. D. Greener, V. P. Nikolski, S. E. Wright, S. H. Parson, S. A. Jones, M. K. Lancaster, M. Yamamoto, H. Honjo, Y. Takagishi, I. Kodama, I. R. Efimov, R. Billeter, and M. R. Boyett, 2005, Computer three-dimensional reconstruction of the sinoatrial node: Circulation, v. 111, p. 846-854.

Dong, D. L., C. Chen, R. Huo, N. Wang, Z. Li, Y. J. Tu, J. T. Hu, X. Chu, W. Huang, and B. F. Yang, 2010, Reciprocal repression between microRNA-133 and calcineurin regulates cardiac hypertrophy a novel mechanism for progressive cardiac hypertrophy: Hypertension, v. 55, p. 946-U249.

Dorn, T., A. Goedel, J. T. Lam, J. Haas, Q. H. Tian, F. Herrmann, K. Bundschu, G. Dobreva, M. Schiemann, R. Dirschinger, Y. C. Guo, S. J. Kuhl, D. Sinnecker, P. Lipp, K. L. Laugwitz, M. Kuhl, and A. Moretti, 2015, Direct Nkx2-5 transcriptional repression of Isl1 controls cardiomyocyte subtype identity: Stem Cells, v. 33, p. 1113-1129.

Drouin, E., 1997, Electrophysiologic properties of the adult human sinus node: Journal of Cardiovascular Electrophysiology, v. 8, p. 254-258.

Duisters, R. F., A. J. Tijsen, B. Schroen, J. J. Leenders, V. Lentink, I. van der Made, V. Herias, R. E. van Leeuwen, M. W. Schellings, P. Barenbrug, J. G. Maessen, S. Heymans, Y. M. Pinto, and E. E. Creemers, 2009, miR-133 and miR-30 regulate connective tissue growth factor implications for a role of microRNAs in myocardial matrix remodeling: Circulation Research, v. 104, p. 170-U61.

Durocher, D., F. Charron, R. J. Schwartz, R. Warren, and M. Nemer, 1997, The cardiac transcription factors Nkx2-5 and GATA-4 are mutual cofactors: Embo Journal, v. 16, p. 5687-5696.

Edelberg, J. M., W. C. Aird, and R. D. Rosenberg, 1998, Enhancement of murine cardiac chronotropy by the molecular transfer of the human beta2 adrenergic receptor cDNA: Journal of Clinical Investigation, v. 101, p. 337-343.

Edelberg, J. M., D. T. Huang, M. E. Josephson, and R. D. Rosenberg, 2001, Molecular enhancement of porcine cardiac chronotropy: Heart, v. 86, p. 559-562.

Ehler, E., V. M. Fowler, and J. C. Perriard, 2004, Myofibrillogenesis in the developing chicken heart: Role of actin isoforms and of the pointed end actin capping protein tropomodulin during thin filament assembly: Developmental Dynamics, v. 229, p. 745-755.

Er, F., R. Larbig, A. Ludwig, M. Biel, F. Hofmann, D. J. Beuckelmann, and U. C. Hoppe, 2003, Dominant-negative suppression of HCN channels markedly reduces the pacemaker current I_f and undermines spontaneous beating of neonatal cardiomyocytes: Circulation, v. 107, p. 485-489.

Espinoza-Lewis, R. A., L. Yu, F. L. He, H. B. Liu, R. H. Tang, J. L. Shi, X. X. Sun, J. F. Martin, D. Z. Wang, J. Yang, and Y. P. Chen, 2009, Shox2 is essential for the differentiation of cardiac pacemaker cells by repressing Nkx2-5: Developmental Biology, v. 327, p. 376-385.

Evans, R., and D. B. Shaw, 1977, Pathological-studies in sinoatrial disorder (sick sinus syndrome): British Heart Journal, v. 39, p. 778-786.

Fatima, A., G. Xu, K. Shao, S. Papadopoulos, M. Lehmann, J. J. Arnaiz-Cot, A. O. Rosa, F. Nguemo, M. Matzkies, S. Dittmann, S. L. Stone, M. Linke, U. Zechner, V. Beyer, H. C.

Hennies, S. Rosenkranz, B. Klauke, A. S. Parwani, W. Haverkamp, G. Pfitzer, M. Farr, L. Cleemann, M. Morad, H. Milting, J. Hescheler, and T. Saric, 2011, In vitro modeling of ryanodine receptor 2 dysfunction using human induced pluripotent stem cells: cellular physiology and biochemistry, v. 28, p. 579-592.

Fedorov, V. V., A. V. Glukhov, R. Chang, G. Kostecki, H. Aferol, W. J. Hucker, J. P. Wuskell, L. M. Loew, R. B. Schuessler, N. Moazami, and I. R. Efimov, 2010, Optical mapping of the isolated coronary-perfused human sinus node: Journal of the American College of Cardiology, v. 56, p. 1386-1394.

Fedorov, V. V., W. J. Hucker, H. Dobrzynski, L. V. Rosenshtraukh, and I. R. Efimov, 2006, Postganglionic nerve stimulation induces temporal inhibition of excitability in rabbit sinoatrial node: American Journal of Physiology-Heart and Circulatory Physiology, v. 291, p. H612-H623.

Feng, L. Z., S. A. Zhang, and Z. A. Liu, 2011, Graphene based gene transfection: Nanoscale, v. 3, p. 1252-1257.

Fischer, M., J. Kamp, L. G. C. Riesgo, I. Robertson-Steel, J. Overton, A. Ziemann, T. Krafft, and E. E. D. Grp, 2011, Comparing emergency medical service systems-A project of the European Emergency Data (EED) Project: Resuscitation, v. 82, p. 285-293.

Flack, M., 1910, An investigation of the sino-auricular node of the mammalian heart: Journal of Physiology-London, v. 41, p. 64-77.

Fortescue, E. B., C. I. Berul, F. Cecchin, E. P. Walsh, J. K. Triedman, and M. E. Alexander, 2004, Patient, procedural, and hardware factors associated with pacemaker lead failures in pediatrics and congenital heart disease: Heart Rhythm, v. 1, p. 150-159.

Frank, D. U., K. L. Carter, K. R. Thomas, R. M. Burr, M. L. Bakker, W. A. Coetzee, M. Tristani-Firouzi, M. J. Bamshad, V. M. Christoffels, and A. M. Moon, 2012, Lethal arrhythmias in Tbx3-deficient mice reveal extreme dosage sensitivity of cardiac conduction system function and homeostasis: Proceedings of the National Academy of Sciences of the United States of America, v. 109, p. E154-E163.

Frank, J. S., G. Mottino, F. Chen, V. Peri, P. Holland, and B. S. Tuana, 1994, Subcellular-distribution of dystrophin in isolated adult and neonatal cardiac myocytes: American Journal of Physiology-Cell Physiology, v. 267, p. C1707-C1716.

Fu, J. D., S. N. Rushing, D. K. Lieu, C. W. Chan, C. W. Kong, L. Geng, K. D. Wilson, N. Chiamvimonvat, K. R. Boheler, J. C. Wu, G. Keller, R. J. Hajjar, and R. A. Li, 2011, Distinct Roles of MicroRNA-1 and miR-499 in ventricular specification and functional maturation of human embryonic stem cell-derived cardiomyocytes: Plos One, v. 6.

Gaskell, W. H., 1883, On the innervation of the heart, with especial reference to the heart of the tortoise: The Journal of physiology, v. 4, p. 43-230.14.

Gauss, R., R. Seifert, and U. B. Kaupp, 1998, Molecular identification of a hyperpolarization-activated channel in sea urchin sperm: Nature, v. 393, p. 583-587.

Gautel, M., and K. Djinovic-Carugo, 2016, The sarcomeric cytoskeleton: from molecules to motion: Journal of Experimental Biology, v. 219, p. 135-145.

Girmatsion, Z., P. Biliczki, A. Bonauer, G. Wimmer-Greinecker, M. Scherer, A. Moritz, A. Bukowska, A. Goette, S. Nattel, S. H. Hohnloser, and J. R. Ehrlich, 2009, Changes in microRNA-1 expression and I_{K1} up-regulation in human atrial fibrillation: Heart Rhythm, v. 6, p. 1802-1809.

Gitlin, L., S. Karelsky, and R. Andino, 2002, Short interfering RNA confers intracellular antiviral immunity in human cells: Nature, v. 418, p. 430-434.

Glass, C., and D. K. Singla, 2011, MicroRNA-1 transfected embryonic stem cells enhance cardiac myocyte differentiation and inhibit apoptosis by modulating the PTEN/Akt pathway in the infarcted heart: American Journal of Physiology-Heart and Circulatory Physiology, v. 301, p. H2038-H2049.

Goldoni, D., J. M. Yarham, M. K. McGahon, A. O'Connor, J. Guduric-Fuchs, K. Edgar, D. M. McDonald, D. A. Simpson, and A. Collins, 2012, A novel dual-fluorescence strategy for functionally validating microRNA targets in 3 ' untranslated regions: regulation of the inward rectifier potassium channel $K_{ir}2.1$ by miR-212: Biochemical Journal, v. 448, p. 103-113.

Gomes, J. A., and S. L. Winters, 1987, The origins of the sinus node pacemaker complex in man - demonstration of dominant and subsidiary foci: Journal of the American College of Cardiology, v. 9, p. 45-52.

Gourdie, R. G., T. Mima, R. P. Thompson, and T. Mikawa, 1995, Terminal diversification of the myocyte lineage generates purkinje-fibers of the cardiac conduction system: Development, v. 121, p. 1423-1431.

Grant, A. O., M. P. Carboni, V. Neplioueva, C. F. Starmer, M. Memmi, C. Napolitano, and S. Priori, 2002, Long QT syndrome, Brugada syndrome, and conduction system disease are linked to a single sodium channel mutation: Journal of Clinical Investigation, v. 110, p. 1201-1209.

Greiser, M., W. J. Lederer, and U. Schotten, 2011, Alterations of atrial Ca^{2+} handling as cause and consequence of atrial fibrillation: Cardiovascular Research, v. 89, p. 722-733.

Greulich, F., C. Rudat, and A. Kispert, 2011, Mechanisms of T-box gene function in the developing heart: Cardiovascular Research, v. 91, p. 212-222.

Griffiths-Jones, S., R. J. Grocock, S. van Dongen, A. Bateman, and A. J. Enright, 2006, miRBase: microRNA sequences, targets and gene nomenclature: Nucleic Acids Research, v. 34, p. D140-D144.

Groot, A., E. A. F. Mahtab, N. D. Hahurij, L. J. Wisse, M. C. Deruiter, M. Wijffels, and R. E. Poelmann, 2007, Nkx2.5-negative myocardium of the posterior heart field and its correlation with podoplanin expression in cells from the developing cardiac pacemaking and conduction system: Anatomical Record-Advances in Integrative Anatomy and Evolutionary Biology, v. 290, p. 115-122.

Guo, J., T. Z. Wang, T. H. Yang, J. M. Xu, W. T. Li, M. D. Fridman, J. T. Fisher, and S. T. Zhang, 2011, Interaction between the cardiac rapidly I_{Kr} and slowly I_{Ks} activating delayed rectifier potassium channels revealed by low K^+-induced hERG endocytic degradation: Journal of Biological Chemistry, v. 286, p. 34664-34674.

Gupta, M. K., D. J. Illich, A. Gaarz, M. Matzkies, F. Nguemo, K. Pfannkuche, H. Liang, S. Classen, M. Reppel, J. L. Schultze, J. Hescheler, and T. Saric, 2010, Global transcriptional profiles of beating clusters derived from human induced pluripotent stem cells and embryonic stem cells are highly similar: Bmc Developmental Biology, v. 10.

Gyorke, I., N. Hester, L. R. Jones, and S. Gyorke, 2004, The role of calsequestrin, triadin, and junctin in conferring cardiac ryanodine receptor responsiveness to luminal calcium: Biophysical Journal, v. 86, p. 2121-2128.

Haga, K., A. C. Kruse, H. Asada, T. Yurugi-Kobayashi, M. Shiroishi, C. Zhang, W. I. Weis, T. Okada, B. K. Kobilka, T. Haga, and T. Kobayashi, 2012, Structure of the human M2 muscarinic acetylcholine receptor bound to an antagonist: Nature, v. 482, p. 547-U147.

Hagiwara, N., H. Irisawa, and M. Kameyama, 1988, Contribution of 2 types of calcium currents to the pacemaker potentials of rabbit sino-atrial node cells: Journal of Physiology-London, v. 395, p. 233-253.

Hao, X. J., Y. M. Zhang, X. Z. Zhang, M. Nirmalan, L. Davies, D. Konstantinou, F. Yin, H. Dobrzynski, X. Wang, A. Grace, H. G. Zhang, M. Boyett, C. L. H. Huang, and M. Lei, 2011, TGF-beta1-mediated fibrosis and ion channel remodeling are key mechanisms in producing the sinus node dysfunction associated with SCN5A deficiency and aging: Circulation-Arrhythmia and Electrophysiology, v. 4, p. 397-U231.

Haqqani, H. M., and J. M. Kalman, 2007, Aging and sinoatrial node dysfunction - Musings on the not-so-funny side: Circulation, v. 115, p. 1178-1179.

Haraguchi, Y., K. Matsuura, T. Shimizu, M. Yamato, and T. Okano, 2015, Simple suspension culture system of human iPS cells maintaining their pluripotency for cardiac cell sheet engineering: Journal of Tissue Engineering and Regenerative Medicine, v. 9, p. 1363-1375.

Harvey, R. P., D. Lai, D. Elliott, C. Biben, M. Solloway, O. Prall, F. Stennard, A. Schindeler, N. Groves, L. Lavulo, C. Hyun, T. Yeoh, M. Costa, M. Furtado, and E. Kirk, 2002, Homeodomain factor Nkx2-5 in heart development and disease: Cold Spring Harbor Symposia on Quantitative Biology, v. 67, p. 107-114.

He, A. B., S. W. Kong, Q. Ma, and W. T. Pu, 2011, Co-occupancy by multiple cardiac transcription factors identifies transcriptional enhancers active in heart: Proceedings of the National Academy of Sciences of the United States of America, v. 108, p. 5632-5637.

Heinz, G., C. Kratochwill, P. Buxbaum, G. Kreiner, G. Laufer, H. Gossinger, and A. Laczkovics, 1992, Long-term intrinsic pacemaker function in patients paced for sinus node deficiency after cardiac transplantation: Pace-Pacing and Clinical Electrophysiology, v. 15, p. 2061-2067.

Heinzel, F. R., V. Bito, L. Biesmans, M. Wu, E. Detre, F. von Wegner, P. Claus, S. Dymarkowski, F. Maes, J. Bogaert, F. Rademakers, J. D'Hooge, and K. Sipido, 2008, Remodeling of T-tubules and reduced synchrony of Ca^{2+} release in myocytes from chronically ischemic myocardium: Circulation Research, v. 102, p. 338-346.

Herrmann, S., J. Stieber, G. Stockl, F. Hofmann, and A. Ludwig, 2007, HCN4 provides a 'depolarization reserve' and is not required for heart rate acceleration in mice: Embo Journal, v. 26, p. 4423-4432.

Hibino, H., A. Inanobe, K. Furutani, S. Murakami, I. Findlay, and Y. Kurachi, 2010, Inwardly rectifying potassium channels: their structure, function, and physiological roles: Physiological Reviews, v. 90, p. 291-366.

Hirai, H., N. Katoku-Kikyo, S. A. Keirstead, and N. Kikyo, 2013, Accelerated direct reprogramming of fibroblasts into cardiomyocyte-like cells with the MyoD transactivation domain: Cardiovascular Research, v. 100, p. 105-113.

Hiroi, Y., S. Kudoh, K. Monzen, Y. Ikeda, Y. Yazaki, R. Nagai, and I. Komuro, 2001, Tbx5 associates with Nkx2-5 and synergistically promotes cardiomyocyte differentiation: Nature Genetics, v. 28, p. 276-280.

Hoffmann, S., I. M. Berger, A. Glaser, C. Bacon, L. Li, N. Gretz, H. Steinbeisser, W. Rottbauer, S. Just, and G. Rappold, 2013, Islet1 is a direct transcriptional target of the homeodomain transcription factor Shox2 and rescues the Shox2-mediated bradycardia: Basic Research in Cardiology, v. 108.

Hong, T. T., J. W. Smyth, D. C. Gao, K. Y. Chu, J. M. Vogan, T. S. Fong, B. C. Jensen, H. M. Colecraft, and R. M. Shaw, 2010, BIN1 Localizes the L-Type calcium channel to cardiac t-tubules: Plos Biology, v. 8.

Hoogaars, W. M. H., P. Barnett, A. F. M. Moorman, and V. M. Christoffels, 2007a, T-box factors determine cardiac design: Cellular and Molecular Life Sciences, v. 64, p. 646-660.

Hoogaars, W. M. H., A. Engel, J. F. Brons, A. O. Verkerk, F. J. de Lange, L. Y. E. Wong, M. L. Bakker, D. E. Clout, V. Wakker, P. Barnett, J. H. Ravesloot, A. F. M. Moorman, E. E. Verheijck, and V. M. Christoffels, 2007b, Tbx3 controls the sinoatrial node gene program and imposes pacemaker function on the atria: Genes & Development, v. 21, p. 1098-1112.

Hoogaars, W. M. H., A. Tessari, A. F. M. Moorman, P. A. J. de Boer, J. Hagoort, A. T. Soufan, M. Campione, and V. M. Christoffels, 2004, The transcriptional repressor Tbx3 delineates the developing central conduction system of the heart: Cardiovascular Research, v. 62, p. 489-499.

Horak, M., J. Novak, and J. Bienertova-Vasku, 2016, Muscle-specific microRNAs in skeletal muscle development: Developmental Biology, v. 410, p. 1-13.

Horsthuis, T., H. P. J. Buermans, J. F. Brons, A. O. Verkerk, M. L. Bakker, V. Wakker, D. E. W. Clout, A. F. M. Moorman, P. A. C. t Hoen, and V. M. Christoffels, 2009, Gene expression profiling of the forming atrioventricular node using a novel Tbx3-based node-specific transgenic reporter: Circulation Research, v. 105, p. 61-U175.

Hu, Y. F., J. F. Dawkins, H. C. Cho, E. Marban, and E. Cingolani, 2014, Biological pacemaker created by minimally invasive somatic reprogramming in pigs with complete heart block: Science Translational Medicine, v. 6.

Huang, X., P. Yang, Y. Du, J. B. Zhang, and A. Q. Ma, 2007, Age-related down-regulation of HCN channels in rat sinoatrial node: Basic Research in Cardiology, v. 102, p. 429-435.

Hund, T. J., and P. J. Mohler, 2008, Ankyrin-based targeting pathway regulates human sinoatrial node automaticity: Channels, v. 2, p. 404-406.

Huser, J., L. A. Blatter, and S. L. Lipsius, 2000, Intracellular Ca^{2+} release contributes to automaticity in cat atrial pacemaker cells: Journal of Physiology-London, v. 524, p. 415-422.

Huser, J., S. L. Lipsius, and L. A. Blatter, 1996, Calcium gradients during excitation-contraction coupling in cat atrial myocytes: Journal of Physiology-London, v. 494, p. 641-651.

Hwang, H. S., D. O. Kryshtal, T. K. Feaster, V. Sanchez-Freire, J. H. Zhang, T. J. Kamp, C. C. Hong, J. C. Wu, and B. C. Knollmann, 2015, Comparable calcium handling of human iPSC-derived cardiomyocytes generated by multiple laboratories: Journal of Molecular and Cellular Cardiology, v. 85, p. 79-88.

Ieda, M., J. D. Fu, P. Delgado-Olguin, V. Vedantham, Y. Hayashi, B. G. Bruneau, and D. Srivastava, 2010, Direct reprogramming of fibroblasts into functional cardiomyocytes by defined factors: Cell, v. 142, p. 375-386.

Inagawa, K., K. Miyamoto, H. Yamakawa, N. Muraoka, T. Sadahiro, T. Umei, R. Wada, Y. Katsumata, R. Kaneda, K. Nakade, C. Kurihara, Y. Obata, K. Miyake, K. Fukuda, and M. Ieda, 2012, Induction of cardiomyocyte-like cells in infarct hearts by gene transfer of Gata4, Mef2c, and Tbx5: Circulation Research, v. 111, p. 1147-1156.

Ionta, V., W. B. Liang, E. H. Kim, R. Rafie, A. Giacomello, E. Marban, and H. C. Cho, 2015, SHOX2 overexpression favors differentiation of embryonic stem cells into cardiac pacemaker cells, Improving Biological Pacing Ability: Stem Cell Reports, v. 4, p. 129-142.

Irisawa, H., H. F. Brown, and W. Giles, 1993, Cardiac pacemaking in the sinoatrial node: Physiological Reviews, v. 73, p. 197-227.

Irving, T., Y. M. Wu, T. Bekyarova, G. P. Farman, N. Fukuda, and H. Granzier, 2011, Thick-filament strain and interfilament spacing in passive muscle: effect of titin-based passive tension: Biophysical Journal, v. 100, p. 1499-1508.

Itzhaki, I., S. Rapoport, I. Huber, I. Mizrahi, L. Zwi-Dantsis, G. Arbel, J. Schiller, and L. Gepstein, 2011, Calcium handling in human induced pluripotent stem cell derived cardiomyocytes: Plos One, v. 6.

Ivey, K. N., A. Muth, J. Arnold, F. W. King, R. F. Yeh, J. E. Fish, E. C. Hsiao, R. J. Schwartz, B. R. Conklin, H. S. Bernstein, and D. Srivastava, 2008, MicroRNA regulation of cell lineages in mouse and human embryonic stem cells: Cell Stem Cell, v. 2, p. 219-229.

Izarra, A., I. Moscoso, S. Canon, C. Carreiro, D. Fondevila, J. Martin-Caballero, V. Blanca, I. Valiente, A. Diez-Juan, and A. Bernad, 2017, miRNA-1 and miRNA-133a are involved in early commitment of pluripotent stem cells and demonstrate antagonistic roles in the regulation of cardiac differentiation: Journal of Tissue Engineering and Regenerative Medicine, v. 11, p. 787-799.

James, T. N., 1961, Anatomy of human sinus node: Anatomical Record, v. 141, p. 109-&.

James, T. N., K. Kawamura, F. L. Meijler, S. Yamamoto, F. Terasaki, and T. Hayashi, 1995, Anatomy of the sinus node, av node, and his-bundle of the heart of the sperm whale

(physeter macrocephalus), with a note on the absence of an os cordis: Anatomical Record, v. 242, p. 355-373.

James, T. N., L. Sherf, G. Fine, and A. R. Morales, 1966, Comparative ultrastructure of sinus node in man and dog: Circulation, v. 34, p. 139-145.

Jay, P. Y., B. S. Harris, C. T. Maguire, A. Buerger, H. Wakimoto, M. Tanaka, S. Kupershmidt, D. M. Roden, T. M. Schultheiss, T. X. O'Brien, R. G. Gourdie, C. I. Berul, and S. Izumo, 2004, Nkx2-5 mutation causes anatomic hypoplasia of the cardiac conduction system: Journal of Clinical Investigation, v. 113, p. 1130-1137.

Jayawardena, T., M. Mirotsou, and V. J. Dzau, 2014, Direct reprogramming of cardiac fibroblasts to cardiomyocytes using microRNAs: stem cell transcriptional networks: Methods and Protocols, v. 1150, p. 263-272.

Jayawardena, T. M., B. Egemnazarov, E. A. Finch, L. N. Zhang, J. A. Payne, K. Pandya, Z. P. Zhang, P. Rosenberg, M. Mirotsou, and V. J. Dzau, 2012, MicroRNA-mediated in vitro and in vivo direct reprogramming of cardiac fibroblasts to cardiomyocytes: Circulation Research, v. 110, p. 1465-1478.

Jones, S. A., M. K. Lancaster, and M. R. Boyett, 2004, Ageing-related changes of connexins and conduction within the sinoatrial node: Journal of Physiology-London, v. 560, p. 429-437.

Joung, B., P. S. Chen, and S. F. Lin, 2011, The role of the calcium and the voltage clocks in sinoatrial node dysfunction: Yonsei Medical Journal, v. 52, p. 211-219.

Joyner, R. W., R. Kumar, D. A. Golod, R. Wilders, H. J. Jongsma, E. E. Verheijck, L. Bouman, W. N. Goolsby, and A. C. G. Van Ginneken, 1998, Electrical interactions between a rabbit atrial cell and a nodal cell model: American Journal of Physiology-Heart and Circulatory Physiology, v. 274, p. H2152-H2162.

Joyner, R. W., and F. J. L. Vancapelle, 1986, Propagation through electrically coupled cells - how a small sa nodedrives a large atrium: Biophysical Journal, v. 50, p. 1157-1164.

Ju, Y. K., Y. Chu, H. Chaulet, D. Lai, O. L. Gervasio, R. M. Graham, M. B. Cannell, and D. G. Allen, 2007, Store-operated Ca^{2+} influx and expression of TRPC genes in mouse sinoatrial node: Circulation Research, v. 100, p. 1605-1614.

Juopperi, T. A., W. R. Kim, C. H. Chiang, H. M. Yu, R. L. Margolis, C. A. Ross, G. L. Ming, and H. J. Song, 2012, Astrocytes generated from patient induced pluripotent stem cells recapitulate features of Huntington's disease patient cells: Molecular Brain, v. 5.

Kalman, J. M., R. J. Lee, W. G. Fisher, M. C. Chin, P. Ursell, C. A. Stillson, M. D. Lesh, and M. M. Scheinman, 1995, Radiofrequency catheter modification of sinus pacemaker function guided by intracardiac echocardiography: Circulation, v. 92, p. 3070-3081.

Kanter, H. L., J. E. Saffitz, and E. C. Beyer, 1992, Cardiac myocytes express multiple gap junction proteins: Circulation Research, v. 70, p. 438-444.

Kapoor, N., G. Galang, E. Marban, and H. C. Cho, 2011, Transcriptional suppression of connexin43 by TBX18 undermines cell-cell electrical coupling in postnatal cardiomyocytes: Journal of Biological Chemistry, v. 286, p. 14073-14079.

Kapoor, N., W. B. Liang, E. Marban, and H. C. Cho, 2013, Direct conversion of quiescent cardiomyocytes to pacemaker cells by expression of Tbx18: Nature Biotechnology, v. 31, p. 54-69.

Kasahara, H., T. Ueyama, H. Wakimoto, M. K. Liu, C. T. Maguire, K. L. Converso, P. M. Kang, W. J. Manning, J. Lawitts, D. L. Paul, C. I. Berul, and S. Izumo, 2003, Nkx2.5 homeoprotein regulates expression of gap junction protein connexin43 and sarcomere organization in postnatal cardiomyocytes: Journal of Molecular and Cellular Cardiology, v. 35, p. 243-256.

Kehat, I., D. Kenyagin-Karsenti, M. Snir, H. Segev, M. Amit, A. Gepstein, E. Livne, O. Binah, J. Itskovitz-Eldor, and L. Gepstein, 2001, Human embryonic stem cells can differentiate into myocytes with structural and functional properties of cardiomyocytes: Journal of Clinical Investigation, v. 108, p. 407-414.

Kehat, I., L. Khimovich, O. Caspi, A. Gepstein, R. Shofti, G. Arbel, I. Huber, J. Satin, J. Itskovitz-Eldor, and L. Gepstein, 2004, Electromechanical integration of cardiomyocytes derived from human embryonic stem cells: Nature Biotechnology, v. 22, p. 1282-1289.

Keith, A., 1942, The sino-auricular node - a historical note: British Heart Journal, v. 4, p. 77-79.

Keith, A., and M. Flack, 1907, The form and nature of the muscular connections between the primary divisions of the vertebrate heart: Journal of Anatomy and Physiology, v. 41, p. 172-189.

Kim, G. H., 2013, MicroRNA regulation of cardiac conduction and arrhythmias: Translational Research, v. 161, p. 381-392.

Kim, H., R. Namgung, K. Singha, I. K. Oh, and W. J. Kim, 2011, Graphene oxide-polyethylenimine nanoconstruct as a gene delivery vector and bioimaging Tool: Bioconjugate Chemistry, v. 22, p. 2558-2567.

Kirchhof, C., F. I. M. Bonke, M. A. Allessie, and W. Lammers, 1987, The influence of the atrial myocardium on impulse formation in the rabbit sinus node: Pflugers Archiv-European Journal of Physiology, v. 410, p. 198-203.

Klietsch, R., J. M. Ervasti, W. Arnold, K. P. Campbell, and A. O. Jorgensen, 1993, Dystrophin-glycoprotein complex and laminin colocalize to the sarcolemma and transverse tubules of cardiac muscle: Circulation Research, v. 72, p. 349-360.

Kockskamper, J., K. A. Sheehan, D. J. Bare, S. L. Lipsius, G. A. Mignery, and L. A. Blatter, 2001, Activation and propagation of Ca^{2+} release during excitation-contraction coupling in atrial myocytes: Biophysical Journal, v. 81, p. 2590-2605.

Kodama, I., and M. R. Boyett, 1985, Regional differences in the electrical-activity of the rabbit sinus node: Pflugers Archiv-European Journal of Physiology, v. 404, p. 214-226.

Kodama, I., M. R. Nikmaram, M. R. Boyett, R. Suzuki, H. Honjo, and J. M. Owen, 1997, Regional differences in the role of the Ca^{2+} and Na^{+} currents in pacemaker activity in the sinoatrial node: American Journal of Physiology-Heart and Circulatory Physiology, v. 272, p. H2793-H2806.

Koutsoulidou, A., N. P. Mastroyiannopoulos, D. Furling, J. B. Uney, and L. A. Phylactou, 2011, Expression of miR-1, miR-133a, miR-133b and miR-206 increases during development of human skeletal muscle: Bmc Developmental Biology, v. 11.

Kreuzberg, M. M., G. S. Sohl, J. S. Kim, V. K. Verselis, K. Willecke, and F. F. Bukauskas, 2005, Functional properties of mouse connexin30.2 expressed in the conduction system of the heart: Circulation Research, v. 96, p. 1169-1177.

Kreuzberg, M. M., K. Willecke, and F. F. Bukauskas, 2006, Connexin-mediated cardiac impulse propagation: Connexin 30.2 slows atrioventricular conduction in mouse heart: Trends in Cardiovascular Medicine, v. 16, p. 266-272.

Kumarswamy, R., A. R. Lyon, I. Volkmann, A. M. Mills, J. Bretthauer, A. Pahuja, C. Geers-Knorr, T. Kraft, R. J. Hajjar, K. T. Macleod, S. E. Harding, and T. Thum, 2012, SERCA2a gene therapy restores microRNA-1 expression in heart failure via an Akt/FoxO3A-dependent pathway: European Heart Journal, v. 33, p. 1067-1075.

Kuratomi, S., A. Kuratomi, K. Kuwahara, T. M. Ishii, K. Nakao, Y. Saito, and M. Takano, 2007, NRSF regulates the developmental and hypertrophic changes of HCN4 transcription in rat cardiac myocytes: Biochemical and Biophysical Research Communications, v. 353, p. 67-73.

Lagos-Quintana, M., R. Rauhut, A. Yalcin, J. Meyer, W. Lendeckel, and T. Tuschl, 2002, Identification of tissue-specific microRNAs from mouse: Current Biology, v. 12, p. 735-739.

Lakatta, E. G., and D. DiFrancesco, 2009, What keeps us ticking: a funny current, a calcium clock, or both?: Journal of Molecular and Cellular Cardiology, v. 47, p. 157-170.

Landgraf, P., M. Rusu, R. Sheridan, A. Sewer, N. Iovino, A. Aravin, S. Pfeffer, A. Rice, A. O. Kamphorst, M. Landthaler, C. Lin, N. D. Socci, L. Hermida, V. Fulci, S. Chiaretti, R. Foa, J. Schliwka, U. Fuchs, A. Novosel, R. U. Muller, B. Schermer, U. Bissels, J. Inman, Q. Phan, M. C. Chien, D. B. Weir, R. Choksi, G. De Vita, D. Frezzetti, H. I. Trompeter, V. Hornung, G. Teng, G. Hartmann, M. Palkovits, R. Di Lauro, P. Wernet, G. Macino, C. E. Rogler, J. W. Nagle, J. Y. Ju, F. N. Papavasiliou, T. Benzing, P. Lichter, W. Tam, M. J. Brownstein, A. Bosio, A. Borkhardt, J. J. Russo, C. Sander, M. Zavolan, and T. Tuschl, 2007, A mammalian microRNA expression atlas based on small RNA library sequencing: Cell, v. 129, p. 1401-1414.

Lanet, E., E. Delannoy, R. Sormani, M. Floris, P. Brodersen, P. Crete, O. Voinnet, and C. Robaglia, 2009, Biochemical evidence for translational repression by arabidopsis microrNAs: Plant Cell, v. 21, p. 1762-1768.

Latchman, D. S., 1997, Transcription factors: An overview: International Journal of Biochemistry & Cell Biology, v. 29, p. 1305-1312.

Le Scouarnec, S., N. Bhasin, C. Vieyres, T. J. Hund, S. R. Cunha, O. Koval, C. Marionneau, B. Chen, Y. Wu, S. Demolombe, L.-S. Song, H. Le Marec, V. Probst, J.-J. Schott, M. E. Anderson, and P. J. Mohler, 2008, Dysfunction in ankyrin-B-dependent ion channel and transporter targeting causes human sinus node disease: Proceedings of the National Academy of Sciences of the United States of America, v. 105, p. 15617-15622.

Leenaars, M., and C. F. M. Hendriksen, 2005, Critical steps in the production of polyclonal and monoclonal antibodies evaluation and recommendations: Ilar Journal, v. 46, p. 269-279.

Lees-Miller, J. P., J. Q. Guo, J. R. Somers, D. E. Roach, R. S. Sheldon, D. E. Rancourt, and H. J. Duff, 2003, Selective knockout of mouse ERG1 B potassium channel eliminates I_{Kr} in adult ventricular myocytes and elicits episodes of abrupt sinus bradycardia: Molecular and Cellular Biology, v. 23, p. 1856-1862.

Lei, M., C. Goddard, J. Liu, A. L. Leoni, A. Royer, S. S. M. Fung, G. S. Xiao, A. Q. Ma, H. G. Zhang, F. Charpentier, J. I. Vandenberg, W. H. Colledge, A. A. Grace, and C. L. H. Huang, 2005, Sinus node dysfunction following targeted disruption of the murine cardiac sodium channel gene Scn5a: Journal of Physiology-London, v. 567, p. 387-400.

Lei, M., H. Honjo, I. Kodama, and M. R. Boyett, 2001, Heterogeneous expression of the delayed-rectifier K^+ currents $I_{K,r}$ and $I_{K,s}$ in rabbit sinoatrial node cells: Journal of Physiology-London, v. 535, p. 703-714.

Lei, M., S. A. Jones, J. Liu, M. K. Lancaster, S. S. M. Fung, H. Dobrzynski, P. Camelliti, S. K. G. Maier, D. Noble, and M. R. Boyett, 2004, Requirement of neuronal- and cardiac-type sodium channels for murine sinoatrial node pacemaking: Journal of Physiology-London, v. 559, p. 835-848.

Lenaerts, I., V. Bito, F. R. Heinzel, R. B. Driesen, P. Holemans, J. D'Hooge, H. Heidbuchel, K. R. Sipido, and R. Willems, 2009, Ultrastructural and functional remodeling of the coupling between Ca^{2+} influx and sarcoplasmic reticulum Ca^{2+} release in right atrial myocytes from experimental persistent atrial fibrillation: Circulation Research, v. 105, p. 876-U111.

Lennox, K. A., and M. A. Behlke, 2011, Chemical modification and design of anti-miRNA oligonucleotides: Gene Therapy, v. 18, p. 1111-1120.

Leuranguer, V., A. Monteil, E. Bourinet, G. Dayanithi, and J. Nargeot, 2000, T-type calcium currents in rat cardiomyocytes during postnatal development: contribution to hormone secretion: American Journal of Physiology-Heart and Circulatory Physiology, v. 279, p. H2540-H2548.

Lewis, B. P., C. B. Burge, and D. P. Bartel, 2005, Conserved seed pairing, often flanked by adenosines, indicates that thousands of human genes are microRNA targets: Cell, v. 120, p. 15-20.

Li, G. R., J. L. Feng, L. X. Yue, M. Carrier, and S. Nattel, 1996, Evidence for two components of delayed rectifier K^+ current in human ventricular myocytes: Circulation Research, v. 78, p. 689-696.

Li, N., T. A. Csepe, B. J. Hansen, H. Dobrzynski, R. S. D. Higgins, A. Kilic, P. J. Mohler, P. M. L. Janssen, M. R. Rosen, B. J. Biesiadecki, and V. V. Fedorov, 2015, Molecular mapping of sinoatrial node hcn channel expression in the human heart: Circulation-Arrhythmia and Electrophysiology, v. 8, p. 1219-1227.

Liang, X. Q., Q. Q. Zhang, P. Cattaneo, S. W. Zhuang, X. H. Gong, N. J. Spann, C. Z. Jiang, X. K. Cao, X. D. Zhao, X. L. Zhang, L. Bu, G. Wang, H. S. V. Chen, T. Zhuang, J. Van, P. Geng, L. N. Luo, I. Banerjee, Y. H. Chen, C. K. Glass, A. C. Zambon, J. Chen, Y. F. Sun, and S. M. Evans, 2015, Transcription factor ISL1 is essential for pacemaker development and function: Journal of Clinical Investigation, v. 125, p. 3256-3268.

Lin, X., C. A. David, J. B. Donnelly, M. Michaelides, N. S. Chandel, X. L. Huang, U. Warrior, F. Weinberg, K. V. Tormos, S. W. Fesik, and Y. Shen, 2008, A chemical genomics screen highlights the essential role of mitochondria in HIF-1 regulation: Proceedings of the National Academy of Sciences of the United States of America, v. 105, p. 174-179.

Lipman, N. S., L. R. Jackson, L. J. Trudel, and F. Weis-Garcia, 2005, Monoclonal versus polyclonal antibodies: Distinguishing characteristics, applications, and information resources: Ilar Journal, v. 46, p. 258-268.

Liu, N., S. Bezprozvannaya, A. H. Williams, X. X. Qi, J. A. Richardson, R. Bassel-Duby, and E. N. Olson, 2008a, microRNA-133a regulates cardiomyocyte proliferation and suppresses smooth muscle gene expression in the heart: Genes & Development, v. 22, p. 3242-3254.

Liu, N., A. H. Williams, Y. Kim, J. McAnally, S. Bezprozvannaya, L. B. Sutherland, J. A. Richardson, R. Bassel-Duby, and E. N. Olson, 2007, An intragenic MEF2-dependent enhancer directs muscle-specific expression of microRNAs 1 and 133: Proceedings of the National Academy of Sciences of the United States of America, v. 104, p. 20844-20849.

Liu, Z., J. T. Robinson, X. M. Sun, and H. J. Dai, 2008b, PEGylated nanographene oxide for delivery of water-insoluble cancer drugs: Journal of the American Chemical Society, v. 130, p. 10876-10886.

Louch, W. E., H. K. Mork, J. Sexton, T. A. Stromme, P. Laake, I. Sjaastad, and O. M. Sejersted, 2006, T-tubule disorganization and reduced synchrony of Ca^{2+} release in murine cardiomyocytes following myocardial infarction: Journal of Physiology-London, v. 574, p. 519-533.

Lowe, J. E., T. Hartwich, M. Takla, and J. Schaper, 1988, Ultrastructure of electrophysiologically identified human sinoatrial nodes: Basic Research in Cardiology, v. 83, p. 401-409.

Lu, T., Z. W. Lin, J. W. Ren, P. Yao, X. W. Wang, Z. Wang, and Q. Y. Zhang, 2016, The Non-Specific Binding of Fluorescent-Labeled MiRNAs on Cell Surface by Hydrophobic Interaction: Plos One, v. 11.

Lu, Y., Y. Zhang, N. Wang, Z. Pan, X. Gao, F. Zhang, Y. Zhang, H. Shan, X. Luo, Y. Bai, L. Sun, W. Song, C. Xu, Z. Wang, and B. Yang, 2010, MicroRNA-328 contributes to adverse electrical remodeling in atrial fibrillation: Circulation, v. 122, p. 2378-2387.

Ludwig, A., X. G. Zong, M. Jeglitsch, F. Hofmann, and M. Biel, 1998, A family of hyperpolarization-activated mammalian cation channels: Nature, v. 393, p. 587-591.

Ludwig, A., X. G. Zong, J. Stieber, R. Hullin, F. Hofmann, and M. Biel, 1999, Two pacemaker channels from human heart with profoundly different activation kinetics: Embo Journal, v. 18, p. 2323-2329.

Luna-Zurita, L., C. U. Stirnimann, S. Glatt, B. L. Kaynak, S. Thomas, F. Baudin, M. A. H. Samee, D. He, E. M. Small, M. Mileikovsky, A. Nagy, A. K. Holloway, K. S. Pollard, C.

W. Muller, and B. G. Bruneau, 2016, Complex interdependence regulates heterotypic transcription factor distribution and coordinates cardiogenesis: Cell, v. 164, p. 999-1014.

Luo, X., H. Lin, Z. Pan, J. Xiao, Y. Zhang, Y. Lu, B. Yang, and Z. Wang, 2008, Down-regulation of miR-1/miR-133 contributes to re-expression of pacemaker channel genes HCN2 and HCN4 in hypertrophic heart: Journal of Biological Chemistry, v. 283, p. 20045-20052.

Luther, P. K., 1991, 3-dimensional reconstruction of a simple z-band in fish muscle: Journal of Cell Biology, v. 113, p. 1043-1055.

Luther, P. K., J. S. Barry, and J. M. Squire, 2002, The three-dimensional structure of a vertebrate wide (slow muscle) Z-band: Lessons on Z-band assembly: Journal of Molecular Biology, v. 315, p. 9-20.

Lyashkov, A. E., M. Juhaszova, H. Dobrzynski, T. M. Vinogradova, V. A. Maltsev, O. Juhasz, H. A. Spurgeon, S. J. Sollott, and E. G. Lakatta, 2007, Calcium cycling protein density and functional importance to automaticity of isolated sinoatrial nodal cells are independent of cell size: Circulation Research, v. 100, p. 1723-1731.

Ma, J. Y., L. Guo, S. J. Fiene, B. D. Anson, J. A. Thomson, T. J. Kamp, K. L. Kolaja, B. J. Swanson, and C. T. January, 2011, High purity human-induced pluripotent stem cell-derived cardiomyocytes: electrophysiological properties of action potentials and ionic currents: American Journal of Physiology-Heart and Circulatory Physiology, v. 301, p. H2006-H2017.

Mackenzie, L., M. D. Bootman, M. J. Berridge, and P. Lipp, 2001, Predetermined recruitment of calcium release sites underlies excitation-contraction coupling in rat atrial myocytes: Journal of Physiology-London, v. 530, p. 417-429.

Mangoni, M. E., B. Couette, E. Bourinet, J. Platzer, D. Reimer, J. Striessnig, and J. Nargeot, 2003, Functional role of L-type $Ca_v1.3$ Ca^{2+} channels in cardiac pacemaker activity: Proceedings of the National Academy of Sciences of the United States of America, v. 100, p. 5543-5548.

Mangoni, M. E., and J. Nargeot, 2008, Genesis and regulation of the heart automaticity: Physiological Reviews, v. 88, p. 919-982.

Mangoni, M. E., A. Traboulsie, A. L. Leoni, B. Couette, L. Marger, K. Le Quang, E. Kupfer, A. Cohen-Solal, J. Vilar, H. S. Shin, D. Escande, F. Charpentier, J. Nargeot, and P. Lory, 2006, Bradycardia and slowing of the atrioventricular conduction in mice lacking $Ca_V3.1$/alpha(1G) T-type calcium channels: Circulation Research, v. 98, p. 1422-1430.

Marban, E., and E. Cingolani, 2015, Direct reprogramming bypassing stem cells for therapeutics: Jama-Journal of the American Medical Association, v. 314, p. 19-20.

Marionneau, C., B. Couette, J. Liu, H. Y. Li, M. E. Mangoni, J. Nargeot, M. Lei, D. Escande, and S. Demolombe, 2005, Specific pattern of ionic channel gene expression associated with pacemaker activity in the mouse heart: Journal of Physiology-London, v. 562, p. 223-234.

Martins, P., M. Bourajjaj, M. Gladka, M. Kortland, R. J. van Oort, Y. M. Pinto, J. D. Molkentin, and L. J. De Windt, 2008, Conditional Dicer gene deletion in the postnatal myocardium provokes spontaneous cardiac remodeling: Circulation, v. 118, p. 1567-1576.

Maruyama, K., S. Matsubara, R. Natori, Y. Nonomura, S. Kimura, K. Ohashi, F. Murakami, S. Handa, and G. Eguchi, 1977, Connectin, an elastic protein of muscle - characterization and function: Journal of Biochemistry, v. 82, p. 317-337.

Matkovich, S. J., W. Wang, Y. Z. Tu, W. H. Eschenbacher, L. E. Dorn, G. Condorelli, A. Diwan, J. M. Nerbonne, and G. W. Dorn, 2010, MicroRNA-133a protects against myocardial fibrosis and modulates electrical repolarization without affecting hypertrophy in pressure-overloaded adult hearts: Circulation Research, v. 106, p. 166-U340.

Matsuyama, T. A., S. Inoue, Y. Kobayashi, T. Sakai, T. Saito, T. Katagiri, and H. Ota, 2004, Anatomical diversity and age-related histological changes in the human right atrial posterolateral wall: Europace, v. 6, p. 307-315.

McCarthy, J. J., and K. A. Esser, 2007, MicroRNA-1 and microRNA-133a expression are decreased during skeletal muscle hypertrophy: Journal of Applied Physiology, v. 102, p. 306-313.

McElroy, W. D., and C. S. Rainwater, 1948, Spectral energy distribution of the light emitted by firefly extracts: Journal of Cellular and Comparative Physiology, v. 32, p. 421-425.

Medvedev, S. P., A. I. Shevchenko, and S. M. Zakian, 2010, Induced pluripotent stem cells: problems and advantages when applying them in regenerative medicine: Acta Naturae, v. 2, p. 18-27.

Meneghini, V., S. Odent, N. Platonova, A. Egeo, and G. R. Merlo, 2006, Novel TBX3 mutation data in families with Ulnar-Mammary syndrome indicate a genotype-phenotype relationship: mutations that do not disrupt the T-domain are associated with less severe limb defects: European Journal of Medical Genetics, v. 49, p. 151-158.

Miake, J., E. Marban, and H. B. Nuss, 2002, Gene therapy - biological pacemaker created by gene transfer: Nature, v. 419, p. 132-133.

Milanesi, R., 2006, Familial sinus bradycardia associated with a mutation in the cardiac pacemaker channel (vol 254, pg151, 2006): New England Journal of Medicine, v. 354, p. 2520-2520.

Mitchell, P. J., and R. Tjian, 1989, Transcriptional regulation in mammalian-cells by sequence-specific dna-binding proteins: Science, v. 245, p. 371-378.

Moe, G. K., J. B. Preston, and H. Burlington, 1956, Physiologic evidence for a dual a-v transmission system: Circulation Research, v. 4, p. 357-375.

Mommersteeg, M. T. M., J. N. Dominguez, C. Wiese, J. Norden, C. de Gier-de Vries, J. B. E. Burch, A. Kispert, N. A. Brown, A. F. M. Moorman, and V. M. Christoffels, 2010, The sinus venosus progenitors separate and diversify from the first and second heart fields early in development: Cardiovascular Research, v. 87, p. 92-101.

Mommersteeg, M. T. M., W. M. H. Hoogaars, O. W. J. Prall, C. de Gier-de Vries, C. Wiese, D. E. W. Clout, V. E. Papaioannou, N. A. Brown, R. P. Harvey, A. F. M. Moorman, and V. M. Christoffels, 2007, Molecular pathway for the localized formation of the sinoatrial node: Circulation Research, v. 100, p. 354-362.

Mond, H. G., and G. Freitag, 2014, The cardiac implantable electronic device power source: evolution and revolution: Pace-Pacing and Clinical Electrophysiology, v. 37, p. 1728-1745.

Mond, H. G., and A. Proclemer, 2011, The 11th world survey of cardiac pacing and implantable cardioverter-defibrillators: calendar year 2009-a world society of arrhythmia's project: Pace-Pacing and Clinical Electrophysiology, v. 34, p. 1013-1027.

Monfredi, O., V. A. Maltsev, and E. G. Lakatta, 2013, Modern concepts concerning the origin of the heartbeat: Physiology, v. 28, p. 74-92.

Monfredi, O. J., A. B. Johnsen, H. Dobrzynski, T. Lloyd, J. Yanni, G. M. Morris, U. Wisloff, and M. R. Boyett, 2011, Is athletic training-induced bradycardia caused by a downregulation of the Ca^{2+} clock pacemaker mechanism in the sinoatrial node?: European Heart Journal, v. 32, p. 996-996.

Moorman, A. F. M., and V. M. Christoffels, 2003, Cardiac chamber formation: Development, genes, and evolution: Physiological Reviews, v. 83, p. 1223-1267.

Moretti, A., M. Bellin, A. Welling, C. B. Jung, J. T. Lam, L. Bott-Fluegel, T. Dorn, A. Goedel, C. Hoehnke, F. Hofmann, M. Seyfarth, D. Sinnecker, A. Schoemig, and K.-L. Laugwitz, 2010, Patient-specific induced pluripotent stem-cell models for long-qt syndrome: New England Journal of Medicine, v. 363, p. 1397-1409.

Morris, G. M., A. D'Souza, H. Dobrzynski, M. Lei, M. Choudhury, R. Billeter, Y. Kryukova, R. B. Robinson, P. A. Kingston, and M. R. Boyett, 2013, Characterization of a right atrial subsidiary pacemaker and acceleration of the pacing rate by HCN over-expression: Cardiovascular Research, v. 100, p. 160-169.

Moskowitz, I. P. G., J. B. Kim, M. L. Moore, C. M. Wolf, M. A. Peterson, J. Shendure, M. A. Nobrega, Y. Yokota, C. Berul, S. Izumo, J. G. Seidman, and C. E. Seidman, 2007, A molecular pathway including Id2, Tbx5, and Nkx2-5 required for cardiac conduction system development: Cell, v. 129, p. 1365-1376.

Moskowitz, I. P. G., A. Pizard, V. V. Patel, B. G. Bruneau, J. B. Kim, S. Kupershmidt, D. Roden, C. I. Berul, C. E. Seidman, and J. G. Seidman, 2004, The T-box transcription factor Tbx5 is required for the patterning and maturation of the murine cardiac conduction system: Development, v. 131, p. 4107-4116.

Mthunzi, P., K. He, S. Ngcobo, T. Khanyile, and J. H. Warner, 2014, Graphene for improved femtosecond laser based pluripotent stem cell transfection: Journal of Biophotonics, v. 7, p. 351-362.

Musa, H., M. Lei, H. Honjo, S. A. Jones, H. Dobrzynski, M. K. Lancaster, Y. Takagishi, Z. Henderson, I. Kodama, and M. R. Boyett, 2002, Heterogeneous expression of Ca^{2+} handling proteins in rabbit sinoatrial node: Journal of Histochemistry & Cytochemistry, v. 50, p. 311-324.

Nadadur, R. D., M. T. Broman, B. Boukens, S. R. Mazurek, X. A. Yang, M. van den Boogaard, J. Bekeny, M. Gadek, T. Ward, M. Zhang, Y. Qiao, J. F. Martin, C. E. Seidman, J. Seidman, V. Christoffels, I. R. Efimov, E. M. McNally, C. R. Weber, and I. P. Moskowitz, 2016, Pitx2 modulates a Tbx5-dependent gene regulatory network to maintain atrial rhythm: Science Translational Medicine, v. 8.

Nam, Y. J., K. H. Song, X. Luo, E. Daniel, K. Lambeth, K. West, J. A. Hill, J. M. DiMaio, L. A. Baker, R. Bassel-Duby, and E. N. Olson, 2013, Reprogramming of human fibroblasts toward a cardiac fate: Proceedings of the National Academy of Sciences of the United States of America, v. 110, p. 5588-5593.

Nerbonne, J. M., and R. S. Kass, 2005, Molecular physiology of cardiac repolarization: Physiological Reviews, v. 85, p. 1205-1253.

Ohki, E. C., M. L. Tilkins, V. C. Ciccarone, and P. J. Price, 2001, Improving the transfection efficiency of post-mitotic neurons: Journal of Neuroscience Methods, v. 112, p. 95-99.

Ono, K., and T. Iijima, 2010, Cardiac T-type Ca^{2+} channels in the heart: Journal of Molecular and Cellular Cardiology, v. 48, p. 65-70.

Ono, K., and H. Ito, 1995, Role of rapidly activating delayed rectifier K^{+} current in sinoatrial node pacemaker activity: American Journal of Physiology-Heart and Circulatory Physiology, v. 269, p. H453-H462.

Opthof, T., B. Dejonge, H. J. Jongsma, and L. N. Bouman, 1987a, Functional-morphology of the mammalian sinuatrial node: European Heart Journal, v. 8, p. 1249-1259.

Opthof, T., B. Dejonge, H. J. Jongsma, and L. N. Bouman, 1987b, Functional-morphology of the pig sinoatrial node: Journal of Molecular and Cellular Cardiology, v. 19, p. 1221-1236.

Opthof, T., B. Dejonge, M. Massonpevet, H. J. Jongsma, and L. N. Bouman, 1986, Functional and morphological organization of the cat sinoatrial node: Journal of Molecular and Cellular Cardiology, v. 18, p. 1015-1031.

Paff, G. H., R. J. Boucek, and T. C. Harrell, 1968, Observations on development of electrocardiogram: Anatomical Record, v. 160, p. 575-586.

Pardo, J. V., J. D. Siliciano, and S. W. Craig, 1983, Vinculin is a component of an extensive network of myofibril-sarcolemma attachment regions in cardiac-muscle fibers: Journal of Cell Biology, v. 97, p. 1081-1088.

Park, S., and R. S. Ruoff, 2009, Chemical methods for the production of graphenes: Nature Nanotechnology, v. 4, p. 217-224.

Pashmforoush, M., J. T. Lu, H. Y. Chen, T. St Amand, R. Kondo, S. Pradervand, S. M. Evans, B. Clark, J. R. Feramisco, W. Giles, S. Y. Ho, D. W. Benson, M. Silberbach, W. N. Shou, and K. R. Chien, 2004, Nkx2-5 pathways and congenital heart disease: Loss of ventricular myocyte lineage progressive cardiomyopathy and complete heart block: Cell, v. 117, p. 373-386.

Perde, F. V., A. Atkinson, J. Yanni, D. Dermengiu, and H. Dobrzynski, 2016, Morphological characteristics of the sinus node on postmortem tissue: Folia Morphologica, v. 75, p. 216-223.

Periasamy, M., P. Bhupathy, and G. J. Babu, 2008, Regulation of sarcoplasmic reticulum Ca^{2+} ATPase pump expression and its relevance to cardiac muscle physiology and pathology: Cardiovascular Research, v. 77, p. 265-273.

Pillai, R. S., C. G. Artus, and W. Filipowicz, 2004, Tethering of human Ago proteins to mRNA mimics the miRNA-mediated repression of protein synthesis: Rna-a Publication of the Rna Society, v. 10, p. 1518-1525.

Pinali, C., H. Bennett, J. B. Davenport, A. W. Trafford, and A. Kitmitto, 2013, Three-dimensional reconstruction of cardiac sarcoplasmic reticulum reveals a continuous network linking transverse-tubules this organization is perturbed in heart failure: Circulation Research, v. 113, p. 1219-U98.

Plotnikov, A. N., I. Shlapakova, M. J. Szabolcs, P. Danilo, B. H. Lorell, I. A. Potapova, Z. J. Lu, A. B. Rosen, R. T. Mathias, P. R. Brink, R. B. Robinson, I. S. Cohen, and M. R. Rosen, 2007, Xenografted adult human mesenchymal stem cells provide a platform for sustained biological pacemaker function in canine heart: Circulation, v. 116, p. 706-713.

Plotnikov, A. N., E. A. Sosunov, J. H. Qu, I. N. Shlapakova, E. P. Anyukhovsky, L. L. Liu, M. J. Janse, P. R. Brink, I. S. Cohen, R. B. Robinson, P. Danilo, and M. R. Rosen, 2004, Biological pacemaker implanted in canine left bundle branch provides ventricular escape rhythms that have physiologically acceptable rates: Circulation, v. 109, p. 506-512.

Postma, A. V., I. Denjoy, J. Kamblock, M. Alders, J. M. Lupoglazoff, G. Vaksmann, L. Dubosq-Bidot, P. Sebillon, M. Mannens, P. Guicheney, and A. A. M. Wilde, 2005, Catecholaminergic polymorphic ventricular tachycardia: RYR2 mutations, bradycardia, and follow up of the patients: Journal of Medical Genetics, v. 42, p. 863-870.

Potapova, I., A. Plotnikov, Z. J. Lu, P. Danilo, V. Valiunas, J. H. Qu, S. Doronin, J. Zuckerman, I. N. Shlapakova, J. Y. Gao, Z. M. Pan, A. J. Herron, R. B. Robinson, P. R. Brink, M. R. Rosen, and I. S. Cohen, 2004, Human mesenchymal stem cells as a gene delivery system to create cardiac pacemakers: Circulation Research, v. 94, p. 952-959.

Protze, S. I., J. Liu, U. Nussinovitch, L. Ohana, P. H. Backx, L. Gepstein, and G. M. Keller, 2017, Sinoatrial node cardiomyocytes derived from human pluripotent cells function as a biological pacemaker: Nature Biotechnology, v. 35, p. 56-68.

Ptashne, M., and A. Gann, 1997, Transcriptional activation by recruitment: Nature, v. 386, p. 569-577.

Puskaric, S., S. Schmitteckert, A. D. Mori, A. Glaser, K. U. Schneider, B. G. Bruneau, R. J. Blaschke, H. Steinbeisser, and G. Rappold, 2010, Shox2 mediates Tbx5 activity by regulating Bmp4 in the pacemaker region of the developing heart: Human Molecular Genetics, v. 19, p. 4625-4633.

Qian, L., J. D. Wythe, J. D. Liu, J. Cartry, G. Vogler, B. Mohapatra, R. T. Otway, Y. Huang, I. N. King, M. Maillet, Y. Zheng, T. Crawley, O. Taghli-Lamallem, C. Semsarian, S. Dunwoodie, D. Winlaw, R. P. Harvey, D. Fatkin, J. A. Towbin, J. D. Molkentin, D. Srivastava, K. Ocorr, B. G. Bruneau, and R. Bodmer, 2011, Tinman/Nkx2-5 acts via miR-1 and upstream of Cdc42 to regulate heart function across species: Journal of Cell Biology, v. 193, p. 1181-1196.

Qu, J. H., A. N. Plotnikov, P. Danilo, I. Shlapakova, I. S. Cohen, R. B. Robinson, and M. R. Rosen, 2003, Expression and function of a biological pacemaker in canine heart: Circulation, v. 107, p. 1106-1109.

Ramanathan, C., P. Jia, R. Ghanem, K. Ryu, and Y. Rudy, 2006, Activation and repolarization of the normal human heart under complete physiological conditions:

Proceedings of the National Academy of Sciences of the United States of America, v. 103, p. 6309-6314.

Rao, E., B. Weiss, M. Fukami, A. Rump, B. Niesler, A. Mertz, K. Muroya, G. Binder, S. Kirsch, M. Winkelmann, G. Nordsiek, U. Heinrich, M. H. Breuning, M. B. Ranke, A. Rosenthal, T. Ogata, and G. A. Rappold, 1997, Pseudoautosomal deletions encompassing a novel homeobox gene cause growth failure in idiopathic short stature and Turner syndrome: Nature Genetics, v. 16, p. 54-63.

Richards, M. A., J. D. Clarke, P. Saravanan, N. Voigt, D. Dobrev, D. A. Eisner, A. W. Trafford, and K. M. Dibb, 2011, Transverse tubules are a common feature in large mammalian atrial myocytes including human: American Journal of Physiology-Heart and Circulatory Physiology, v. 301, p. H1996-H2005.

Rigg, L., B. M. Heath, Y. Cui, and D. A. Terrar, 2000, Localisation and functional significance of ryanodine receptors during beta-adrenoceptor stimulation in the guinea-pig sino-atrial node: Cardiovascular Research, v. 48, p. 254-264.

Rigg, L., and D. A. Terrar, 1996, Possible role of calcium release from the sarcoplasmic reticulum in pacemaking in guinea-pig sino-atrial node: Experimental Physiology, v. 81, p. 877-880.

Rivier, F., A. Robert, M. Royuela, G. Hugon, A. Bonet-Kerrache, and D. Mornet, 1999, Utrophin and dystrophin-associated glycoproteins in normal and dystrophin deficient cardiac muscle: Journal of Muscle Research and Cell Motility, v. 20, p. 305-314.

Robinson, R. B., 2003, Hyperpolarization-activated cation currents: From molecules to physiological function: Annual Review of Physiology, v. 65, p. 453-480.

Robinson, R. B., P. R. Brink, I. S. Cohen, and M. R. Rosen, 2006, I_f and the biological pacemaker: Pharmacological Research, v. 53, p. 407-415.

Romaine, S. P. R., M. Tomaszewski, G. Condorelli, and N. J. Samani, 2015, MicroRNAs in cardiovascular disease: an introduction for clinicians: Heart, v. 101, p. 921-928.

Romoren, K., B. J. Thu, N. C. Bols, and O. Evensen, 2004, Transfection efficiency and cytotoxicity of cationic liposomes in salmonid cell lines of hepatocyte and macrophage origin: Biochimica Et Biophysica Acta-Biomembranes, v. 1663, p. 127-134.

Ronaldson-Bouchard, K., S. P. Ma, K. Yeager, T. Chen, L. J. Song, D. Sirabella, K. Morikawa, D. Teles, M. Yazawa, and G. Vunjak-Novakovic, 2018, Advanced maturation of human cardiac tissue grown from pluripotent stem cells: Nature, v. 556, p. 239-247.

Rosen, M. R., P. R. Brink, I. S. Cohen, and R. B. Robinson, 2004, Genes, stem cells and biological pacemakers: Cardiovascular Research, v. 64, p. 12-23.

Rubenstein, D. S., L. M. Fox, J. A. McNulty, and S. L. Lipsius, 1987, Electrophysiology and ultrastructure of eustachian ridge from cat right atrium - a comparison with sa node: Journal of Molecular and Cellular Cardiology, v. 19, p. 965-976.

Rubenstein, J. J., C. L. Schulman, P. M. Yurchak, and R. W. Desanctis, 1972, Clinical spectrum of sick sinus syndrome: Circulation, v. 46, p. 5-18.

Saadane, N., L. Alpert, and L. E. Chalifour, 1999, Expression of immediate early genes, GATA-4, and Nkx-2.5 in adrenergic-induced cardiac hypertrophy and during regression in adult mice: British Journal of Pharmacology, v. 127, p. 1165-1176.

Saiki, R. K., D. H. Gelfand, S. Stoffel, S. J. Scharf, R. Higuchi, G. T. Horn, K. B. Mullis, and H. A. Erlich, 1988, Primer-directed enzymatic amplification of dna with a thermostable DNA-polymerase: Science, v. 239, p. 487-491.

Sanchez-Quintana, D., J. A. Cabrera, J. Farre, V. Climent, R. H. Anderson, and S. Y. Ho, 2005, Sinus node revisited in the era of electroanatomical mapping and catheter ablation: Heart, v. 91, p. 189-194.

Sano, T., and S. Yamagishi, 1965, Spread of excitation from sinus node: Circulation Research, v. 16, p. 423-435.

Sarkozy, A., E. Conti, C. Neri, R. D'Agostino, M. C. Digilio, G. Esposito, A. Toscano, B. Marino, A. Pizzuti, and B. Dallapiccola, 2005, Spectrum of atrial septal defects associated with mutations of NKX2.5 and GATA4 transcription factors: Journal of Medical Genetics, v. 42.

Sayed, D., C. Hong, I. Y. Chen, J. Lypowy, and M. Abdellatif, 2007, MicroRNAs play an essential role in the development of cardiac hypertrophy: Circulation Research, v. 100, p. 416-424.

Schott, J. J., D. W. Benson, C. T. Basson, W. Pease, G. M. Silberbach, J. P. Moak, B. J. Maron, C. E. Seidman, and J. G. Seidman, 1998, Congenital heart disease caused by mutations in the transcription factor NKX2-5: Science, v. 281, p. 108-111.

Schuessler, R. B., J. P. Boineau, and B. I. Bromberg, 1996, Origin of the sinus impulse: Journal of Cardiovascular Electrophysiology, v. 7, p. 263-274.

Schulze-Bahr, E., A. Neu, P. Friederich, U. B. Kaupp, G. Breithardt, O. Pongs, and D. Isbrandt, 2003, Pacemaker channel dysfunction in a patient with sinus node disease: Journal of Clinical Investigation, v. 111, p. 1537-1545.

Schweizer, P. A., F. F. Darche, N. D. Ullrich, P. Geschwill, B. Greber, R. Rivinius, C. Seyler, K. Muller-Decker, A. Draguhn, J. Utikal, M. Koenen, H. A. Katus, and D. Thomas,

2017, Subtype-specific differentiation of cardiac pacemaker cell clusters from human induced pluripotent stem cells: Stem Cell Research & Therapy, v. 8.

Scriven, D. R. L., P. Dan, and E. D. W. Moore, 2000, Distribution of proteins implicated in excitation-contraction coupling in rat ventricular myocytes: Biophysical Journal, v. 79, p. 2682-2691.

Severs, N. J., 1995, Cardiac-muscle cell-interaction - from microanatomy to the molecular make-up of the gap junction: Histology and Histopathology, v. 10, p. 481-501.

Severs, N. J., S. R. Coppen, E. Dupont, H. I. Yeh, Y. S. Ko, and T. Matsushita, 2004, Gap junction alterations in human cardiac disease: Cardiovascular Research, v. 62, p. 368-377.

Shi, W. M., R. Wymore, H. G. Yu, J. Y. Wu, R. T. Wymore, Z. M. Pan, R. B. Robinson, J. E. Dixon, D. McKinnon, and I. S. Cohen, 1999, Distribution and prevalence of hyperpolarization-activated cation channel (HCN) mRNA expression in cardiac tissues: Circulation Research, v. 85, p. E1-E6.

Shiojima, I., I. Komuro, T. Oka, Y. Hiroi, T. Mizuno, E. Takimoto, K. Monzen, R. Aikawa, H. Akazawa, T. Yamazaki, S. Kudoh, and Y. Yazaki, 1999, Context-dependent transcriptional cooperation mediated by cardiac transcription factors Csx/Nkx-2.5 and GATA-4: Journal of Biological Chemistry, v. 274, p. 8231-8239.

Snarr, B. S., E. E. Wirrig, A. L. Phelps, T. C. Trusk, and A. Wessels, 2007, A spatiotemporal evaluation of the contribution of the dorsal mesenchymal protrusion to cardiac development: Developmental Dynamics, v. 236, p. 1287-1294.

Soeller, C., and M. B. Cannell, 1999, Examination of the transverse tubular system in living cardiac rat myocytes by 2-photon microscopy and digital image-processing techniques: Circulation Research, v. 84, p. 266-275.

Song, K., J. Backs, J. McAnally, X. Qi, R. D. Gerard, J. A. Richardson, J. A. Hill, R. Bassel-Duby, and E. N. Olson, 2006, The transcriptional coactivator CAMTA2 stimulates cardiac growth by opposing class II histone deacetylases: Cell, v. 125, p. 453-466.

Stephenson, R. S., A. Atkinson, P. Kottas, F. Perde, F. Jafarzadeh, M. Bateman, P. A. Iaizzo, J. C. Zhao, H. G. Zhang, R. H. Anderson, J. C. Jarvis, and H. Dobrzynski, 2017, High resolution 3-Dimensional imaging of the human cardiac conduction system from microanatomy to mathematical modeling: Scientific Reports, v. 7.

Sumiyoshi, M., Y. Nakazato, T. Tokano, M. Yasuda, Y. Mineda, Y. Nakata, and H. Daida, 2005, Sinus node dysfunction concomitant with Brugada syndrome: Circulation Journal, v. 69, p. 946-950.

Sun, Y. F., X. Q. Liang, and S. M. Evans, 2008, Islet1 progenitors in developing and postnatal heart: Cardiovascular Development, v. 18, p. 153-165.

Sun, Y. F., X. Q. Liang, N. Najafi, M. Cass, L. Z. Lin, C. L. Cai, J. Chen, and S. M. Evans, 2007, Islet 1 is expressed in distinct cardiovascular lineages, including pacemaker and coronary vascular cells: Developmental Biology, v. 304, p. 286-296.

Takahashi, K., K. Tanabe, M. Ohnuki, M. Narita, T. Ichisaka, K. Tomoda, and S. Yamanaka, 2007, Induction of pluripotent stem cells from adult human fibroblasts by defined factors: Cell, v. 131, p. 861-872.

Tanaka, H., C. Komikado, I. Namekata, H. Nakamura, M. Suzuki, Y. Tsuneoka, K. Shigenobu, and A. Takahara, 2008, Species difference in the contribution of T-type calcium current to cardiac pacemaking as revealed by R(-)-efonidipine: Journal of Pharmacological Sciences, v. 107, p. 99-102.

Tanaka, T., S. Tohyama, M. Murata, F. Nomura, T. Kaneko, H. Chen, F. Hattori, T. Egashira, T. Seki, Y. Ohno, U. Koshimizu, S. Yuasa, S. Ogawa, S. Yamanaka, K. Yasuda, and K. Fukuda, 2009, In vitro pharmacologic testing using human induced pluripotent stem cell-derived cardiomyocytes: Biochemical and Biophysical Research Communications, v. 385, p. 497-502.

Tauriainen, S., M. Virta, W. Chang, and M. Karp, 1999, Measurement of firefly luciferase reporter gene activity from cells and lysates using Escherichia coli arsenite and mercury sensors: Analytical Biochemistry, v. 272, p. 191-198.

Tellez, J. O., H. Dobrzynski, I. D. Greener, G. M. Graham, E. Laing, H. Honjo, S. J. Hubbard, M. R. Boyett, and R. Billeter, 2006, Differential expression of ion channel transcripts in atrial muscle and sinoatrial node in rabbit: Circulation Research, v. 99, p. 1384-1393.

Tellez, J. O., M. Maczewski, J. Yanni, P. Sutyagin, U. Mackiewicz, A. Atkinson, S. Inada, A. Beresewicz, R. Billeter, H. Dobrzynski, and M. R. Boyett, 2011, Ageing-dependent remodelling of ion channel and Ca^{2+} clock genes underlying sino-atrial node pacemaking: Experimental Physiology, v. 96, p. 1163-1178.

Terada, R., S. Warren, J. T. Lu, K. R. Chien, A. Wessels, and H. Kasahara, 2011, Ablation of Nkx2-5 at mid-embryonic stage results in premature lethality and cardiac malformation: Cardiovascular Research, v. 91, p. 289-299.

Terentyev, D., A. E. Belevych, R. Terentyeva, M. M. Martin, G. E. Malana, D. E. Kuhn, M. Abdellatif, D. S. Feldman, T. S. Elton, and S. Gyorke, 2009, miR-1 overexpression enhances Ca^{2+} release and promotes cardiac arrhythmogenesis by targeting PP2A regulatory subunit B56 alpha and Causing CaMKII-dependent hyperphosphorylation of RyR2: Circulation Research, v. 104, p. 514-521.

Tessadori, F., J. H. van Weerd, S. B. Burkhard, A. O. Verkerk, E. de Pater, B. J. Boukens, A. Vink, V. M. Christoffels, and J. Bakkers, 2012, Identification and functional characterization of cardiac pacemaker cells in zebrafish: Plos One, v. 7.

Thery, C., B. Gosselin, J. Lekieffre, and H. Warembourg, 1977, Pathology of sinoatrial node - correlations with electrocardiographic findings in 111 patients: American Heart Journal, v. 93, p. 735-740.

Thompson, J. T., M. S. Rackley, and T. X. O'Brien, 1998, Upregulation of the cardiac homeobox gene Nkx2-5 (CSX) in feline right ventricular pressure overload: American Journal of Physiology-Heart and Circulatory Physiology, v. 274, p. H1569-H1573.

Thum, T., D. Catalucci, and J. Bauersachs, 2008, MicroRNAs: novel regulators in cardiac development and disease: Cardiovascular Research, v. 79, p. 562-570.

Thum, T., P. Galuppo, S. Kneitz, J. Fiedler, C. Wolf, L. Van Laake, C. L. Mummery, S. Engelhardt, G. Ertl, and J. Bauersachs, 2007, MicroRNAs in the human heart: a clue to fetal gene reprogramming in heart failure: European Heart Journal, v. 28, p. 786-786.

Toko, H., W. D. Zhu, E. Takimoto, I. Shiojima, Y. Hiroi, Y. Z. Zou, T. Oka, H. Akazawa, M. Mizukami, M. Sakamoto, F. Terasaki, Y. Kitaura, H. Takano, T. Nagai, R. Nagai, and I. Komuro, 2002, Csx/Nkx2-5 is required for homeostasis and survival of cardiac myocytes in the adult heart: Journal of Biological Chemistry, v. 277, p. 24735-24743.

Tokuyasu, K. T., 1989, Immunocytochemical studies of cardiac myofibrillogenesis in early chick-embryos .3. generation of fasciae adherentes and costameres: Journal of Cell Biology, v. 108, p. 43-53.

Tokuyasu, K. T., and P. A. Maher, 1987, Immunocytochemical studies of cardiac myofibrillogenesis in early chick-embryos .2. generation of alpha-actinin dots within titin spots at the time of the 1st myofibril formation: Journal of Cell Biology, v. 105, p. 2795-2801.

Toyama, J. J., M. R. Boyett, E. Watanabe, H. Honjo, T. Anno, and I. Kodama, 1995, Computer simulation of the electrotonic modulation of pacemaker activity in the sinoatrial node by atrial muscle: Journal of Electrocardiology, v. 28, p. 212-215.

Tristani-Firouzi, M., J. Chen, J. S. Mitcheson, and M. C. Sanguinetti, 2001, Molecular biology of K^+ channels and their role in cardiac arrhythmias: American Journal of Medicine, v. 110, p. 50-59.

Ueda, K., K. Nakamura, T. Hayashi, N. Inagaki, M. Takahashi, T. Arimura, H. Morita, Y. Higashiuesato, Y. Hirano, M. Yasunami, S. Takishita, A. Yamashina, T. Ohe, M. Sunamori, M. Hiraoka, and A. Kimura, 2004, Functional characterization of a trafficking-

defective HCN4 mutation, D553N, associated with cardiac arrhythmia: Journal of Biological Chemistry, v. 279, p. 27194-27198.

Urthaler, F., B. H. Neely, G. R. Hageman, and L. R. Smith, 1986, Differential sympathetic-parasympathetic interactions in sinus node and AV junction: American Journal of Physiology, v. 250, p. H43-H51.

van Rooij, E., W. S. Marshall, and E. N. Olson, 2008a, Toward microRNA-based therapeutics for heart disease the sense in antisense: Circulation Research, v. 103, p. 919-928.

van Rooij, E., L. B. Sutherland, N. Liu, A. H. Williams, J. McAnally, R. D. Gerard, J. A. Richardson, and E. N. Olson, 2006, A signature pattern of stress-responsive microRNAs that can evoke cardiac hypertrophy and heart failure: Proceedings of the National Academy of Sciences of the United States of America, v. 103, p. 18255-18260.

van Rooij, E., L. B. Sutherland, J. E. Thatcher, J. M. DiMaio, R. H. Naseem, W. S. Marshall, J. A. Hill, and E. N. Olson, 2008b, Dysregulation of microRNAs after myocardial infarction reveals a role of miR-29 in cardiac fibrosis: Proceedings of the National Academy of Sciences of the United States of America, v. 105, p. 13027-13032.

van Weerd, J. H., and V. M. Christoffels, 2016, The formation and function of the cardiac conduction system: Development, v. 143, p. 197-210.

Vankempen, M. J. A., C. Fromaget, D. Gros, A. F. M. Moorman, and W. H. Lamers, 1991, Spatial-distribution of connexin43, the major cardiac gap junction protein, in the developing and adult-rat heart: Circulation Research, v. 68, p. 1638-1651.

Veca, L. M., F. S. Lu, M. J. Meziani, L. Cao, P. Y. Zhang, G. Qi, L. W. Qu, M. Shrestha, and Y. P. Sun, 2009, Polymer functionalization and solubilization of carbon nanosheets: Chemical Communications, p. 2565-2567.

Vedantham, V., G. Galang, M. Evangelista, R. C. Deo, and D. Srivastava, 2015, RNA sequencing of mouse sinoatrial node reveals an upstream regulatory role for Islet-1 in cardiac pacemaker cells: Circulation Research, v. 116, p. 797-803.

Veenstra, R. D., 1996, Size and selectivity of gap junction channels formed from different connexins: Journal of Bioenergetics and Biomembranes, v. 28, p. 327-337.

Veenstra, R. D., H. Z. Wang, E. M. Westphale, and E. C. Beyer, 1992, Multiple connexins confer distinct regulatory and conductance properties of gap-junctions in developing heart: Circulation Research, v. 71, p. 1277-1283.

Verheijck, E. E., A. C. G. Van Ginneken, R. Wilders, and L. N. Bouman, 1999, Contribution of L-type Ca^{2+} current to electrical activity in sinoatrial nodal myocytes of

rabbits: American Journal of Physiology-Heart and Circulatory Physiology, v. 276, p. H1064-H1077.

Verheijck, E. E., A. C. G. Vanginneken, J. Bourier, and L. N. Bouman, 1995, Effects of delayed rectifier current blockade by E-4031 on impulse generation in single sinoatrial nodal myocytes of the rabbit: Circulation Research, v. 76, p. 607-615.

Verheijck, E. E., A. Wessels, A. C. G. van Ginneken, J. Bourier, M. W. M. Markman, J. L. M. Vermeulen, J. M. T. de Bakker, W. H. Lamers, T. Opthof, and L. N. Bouman, 1998, Distribution of atrial and nodal cells within the rabbit sinoatrial node - Models of sinoatrial transition: Circulation, v. 97, p. 1623-1631.

Verkerk, A. O., M. van Borren, R. J. G. Peters, E. Broekhuis, K. Y. Lam, R. Coronel, J. M. T. de Bakker, H. L. Tan, R. Wilders, and Ieee, 2007a, Single cells isolated from human sinoatrial node: Action potentials and numerical reconstruction of pacemaker current: 29th Annual International Conference of the IEEE-Engineering-in-Medicine-and-Biology-Society, p. 904-907.

Verkerk, A. O., R. Wilders, M. M. G. J. van Borren, R. J. G. Peters, E. Broekhuis, K. Lam, R. Coronel, J. M. T. de Bakker, and H. L. Tan, 2007b, Pacemaker current I_f in the human sinoatrial node: European Heart Journal, v. 28, p. 2472-2478.

Vigoreaux, J. O., 1994, The muscle z-band - lessons in stress management: Journal of Muscle Research and Cell Motility, v. 15, p. 237-255.

Vinogradova, T. M., V. A. Maltsev, K. Y. Bogdanov, A. E. Lyashkov, and E. G. Lakatta, 2005, Rhythmic Ca^{2+} oscillations drive sinoatrial nodal cell pacemaker function to make the heart tick: Communicative Cardiac Cell, v. 1047, p. 138-156.

Vozzi, C., E. Dupont, S. R. Coppen, H. I. Yeh, and N. J. Severs, 1999, Chamber-related differences in connexin expression in the human heart: Journal of Molecular and Cellular Cardiology, v. 31, p. 991-1003.

Wahid, F., A. Shehzad, T. Khan, and Y. Y. Kim, 2010, MicroRNAs: Synthesis, mechanism, function, and recent clinical trials: Biochimica Et Biophysica Acta-Molecular Cell Research, v. 1803, p. 1231-1243.

Wakili, R., Y. H. Yeh, X. A. Y. Qi, M. Greiser, D. Chartier, K. Nishida, A. Maguy, L. R. Villeneuve, P. Boknik, N. Voigt, J. Krysiak, S. Kaab, U. Ravens, W. A. Linke, G. J. M. Stienen, Y. F. Shi, J. C. Tardif, U. Schotten, D. Dobrev, and S. Nattel, 2010, Multiple potential molecular contributors to atrial hypocontractility caused by atrial tachycardia remodeling in dogs: Circulation-Arrhythmia and Electrophysiology, v. 3, p. 530-U172.

Wang, J., Y. Bai, N. Li, W. D. Ye, M. Zhang, S. B. Greene, Y. Tao, Y. P. Chen, X. H. T. Wehrens, and J. F. Martin, 2014a, Pitx2-microRNA pathway that delimits sinoatrial node

development and inhibits predisposition to atrial fibrillation: Proceedings of the National Academy of Sciences of the United States of America, v. 111, p. 9181-9186.

Wang, L., Z. Q. Liu, C. Y. Yin, H. Asfour, O. Chen, Y. Z. Li, N. Bursac, J. D. Liu, and L. Qian, 2015, Stoichiometry of Gata4, Mef2c, and Tbx5 influences the efficiency and quality of induced cardiac myocyte reprogramming: Circulation Research, v. 116, p. 237-U82.

Wang, R., H. Wen, Y. C. Xu, Q. L. Chen, Y. Luo, Y. Q. Lin, and A. G. Xu, 2014b, Circulating microRNAs as a novel class of diagnostic biomarkers in gastrointestinal tumors detection: A Meta-Analysis Based on 42 Articles: Plos One, v. 9.

Warren, K. S., K. Baker, and M. C. Fishman, 2001, The slow mo mutation reduces pacemaker current and heart rate in adult zebrafish: American Journal of Physiology-Heart and Circulatory Physiology, v. 281, p. H1711-H1719.

Weber, K., N. Rostert, S. Bauersachs, and G. Wess, 2015, Serum microRNA profiles in cats with hypertrophic cardiomyopathy: Molecular and Cellular Biochemistry, v. 402, p. 171-180.

Wen, P., D. Song, H. Ye, X. Wu, L. Jiang, B. Tang, Y. Zhou, L. Fang, H. Cao, W. He, Y. Yang, C. Dai, and J. Yang, 2014, Circulating mir-133a as a biomarker predicts cardiac hypertrophy in chronic hemodialysis patients: Plos One, v. 9.

Wiese, C., T. Grieskamp, R. Airik, M. T. M. Mommersteeg, A. Gardiwal, C. de Gier-de Vries, K. Schuster-Gossler, A. F. M. Moorman, A. Kispert, and V. M. Christoffels, 2009, Formation of the sinus node head and differentiation of sinus node myocardium are independently regulated by Tbx18 and Tbx3: Circulation Research, v. 104, p. 388-397.

Wilson, K. D., S. J. Hu, S. Venkatasubrahmanyam, J. D. Fu, N. Sun, O. J. Abilez, J. J. A. Baugh, F. J. Jia, Z. Ghosh, R. A. Li, A. J. Butte, and J. C. Wu, 2010, Dynamic MicroRNA expression programs during cardiac differentiation of human embryonic stem cells role for miR-499: Circulation-Cardiovascular Genetics, v. 3, p. 426-U97.

Wong, J., D. Baddeley, E. A. Bushong, Z. Y. Yu, M. H. Ellisman, M. Hoshijima, and C. Soeller, 2013, Nanoscale distribution of ryanodine receptors and caveolin-3 in mouse ventricular myocytes: dilation of t-tubules near junctions: Biophysical Journal, v. 104, p. L22-L24.

Woo, S. H., L. Cleemann, and M. Morad, 2002, Ca^{2+} current-gated focal and local Ca^{2+} release in rat atrial myocytes: evidence from rapid 2-D confocal imaging: Journal of Physiology-London, v. 543, p. 439-453.

Wu, L. P., J. S. Xie, T. Li, Z. H. Mai, L. Wang, X. P. Wang, and T. S. Chen, 2017, Gene delivery ability of polyethylenimine and polyethylene glycol dual-functionalized nanographene oxide in 11 different cell lines: Royal Society Open Science, v. 4.

Wu, M., S. W. Peng, J. L. Yang, Z. D. Tu, X. Q. Cai, C. L. Cai, Z. Wang, and Y. Zhao, 2014, Baf250a orchestrates an epigenetic pathway to repress the Nkx2.5-directed contractile cardiomyocyte program in the sinoatrial node: Cell Research, v. 24, p. 1201-1213.

Xiao, J., D. Liang, Y. Zhang, Y. Liu, H. Zhang, Y. Liu, L. Li, X. Liang, Y. Sun, and Y.-H. Chen, 2011, MicroRNA expression signature in atrial fibrillation with mitral stenosis: Physiological Genomics, v. 43, p. 655-664.

Xiao, J., B. Yang, H. Lin, Y. Lu, X. Luo, and Z. Wang, 2012, Novel approaches for gene-specific interference via manipulating actions of microRNAs: Examination on the pacemaker channel genes HCN2 and HCN4 (Retraction of 212, pg 285, 2007): Journal of Cellular Physiology, v. 227, p. 877-877.

Xie, L. L., A. D. Hoffmann, O. Burnicka-Turek, J. M. Friedland-Little, K. Zhang, and I. P. Moskowitz, 2012, Tbx5-hedgehog molecular networks are essential in the second heart field for atrial septation: Developmental Cell, v. 23, p. 280-291.

Xu, C. H., S. Police, N. Rao, and M. K. Carpenter, 2002, Characterization and enrichment of cardiomyocytes derived from human embryonic stem cells: Circulation Research, v. 91, p. 501-508.

Xu, H. S., M. Morishima, J. N. Wylie, R. J. Schwartz, B. G. Bruneau, E. A. Lindsay, and A. Baldini, 2004, Tbx1 has a dual role in the morphogenesis of the cardiac outflow tract: Development, v. 131, p. 3217-3227.

Xu, M., H.-D. Wu, R.-C. Li, H.-B. Zhang, M. Wang, J. Tao, X.-H. Feng, Y.-B. Guo, S.-F. Li, S.-T. Lai, P. Zhou, L.-L. Li, H.-Q. Yang, G.-Z. Luo, Y. Bai, J. J. Xi, W. Gao, Q.-D. Han, Y.-Y. Zhang, X.-J. Wang, X. Meng, and S.-Q. Wang, 2012, Mir-24 Regulates junctophilin-2 expression in cardiomyocytes: Circulation Research, v. 111, p. 837-841.

Xue, T., H. C. Cho, F. G. Akar, S. Y. Tsang, S. P. Jones, E. Marban, G. F. Tomaselli, and R. A. Li, 2005, Functional integration of electrically active cardiac derivatives from genetically engineered human embryonic stem cells with quiescent recipient ventricular cardiomyocytes - Insights into the development of cell-based pacemakers: Circulation, v. 111, p. 11-20.

Yamamoto, M., H. Dobrzynski, J. Tellez, R. Niwa, R. Billeter, H. Honjo, I. Kodama, and M. R. Boyett, 2006, Extended atrial conduction system characterised by the expression of the HCN4 channel and connexin45: Cardiovascular Research, v. 72, p. 271-281.

Yan, L., Y. N. Chang, L. N. Zhao, Z. J. Gu, X. X. Liu, G. Tian, L. J. Zhou, W. L. Ren, S. Jin, W. Y. Yin, H. Q. Chang, G. M. Xing, X. F. Gao, and Y. L. Zhao, 2013, The use of polyethylenimine-modified graphene oxide as a nanocarrier for transferring hydrophobic

nanocrystals into water to produce water-dispersible hybrids for use in drug delivery: Carbon, v. 57, p. 120-129.

Yang, B. F., H. X. Lin, J. N. Xiao, Y. J. Lu, X. B. Luo, B. X. Li, Y. Zhang, C. Q. Xu, Y. L. Bai, H. Z. Wang, G. H. Chen, and Z. G. Wang, 2007, The muscle-specific microRNA miR-1 regulates cardiac arrhythmogenic potential by targeting GJA1 and KCNJ2: Nature Medicine, v. 13, p. 486-491.

Yang, Z., C. Pascarel, D. S. Steele, K. Kornukai, F. Brette, and C. H. Orchard, 2002, Na^{+}-Ca^{2+} exchange activity is localized in the T-tubules of rat ventricular myocytes: Circulation Research, v. 91, p. 315-322.

Yanni, J., J. O. Tellez, M. Maczewski, U. Mackiewicz, A. Beresewicz, R. Billeter, H. Dobrzynski, and M. R. Boyett, 2011, Changes in ion channel gene expression underlying heart failure-induced sinoatrial node dysfunction: Circulation-Heart Failure, v. 4, p. 496-514.

Yanni, J., J. O. Tellez, P. V. Sutyagin, M. R. Boyett, and H. Dobrzynski, 2010, Structural remodelling of the sinoatrial node in obese old rats: Journal of Molecular and Cellular Cardiology, v. 48, p. 653-662.

Ye, W. D., J. Wang, Y. N. Song, D. K. Yu, C. Sun, C. Liu, F. D. Chen, Y. D. Zhang, F. Wang, R. P. Harvey, L. Schrader, J. F. Martin, and Y. P. Chen, 2015, A common Shox2-Nkx2-5 antagonistic mechanism primes the pacemaker cell fate in the pulmonary vein myocardium and sinoatrial node: Development, v. 142, p. 2521-2532.

Yeh, Y. H., B. Burstein, X. Y. Qi, M. Sakabe, D. Chartier, P. Comtois, Z. G. Wang, C. T. Kuo, and S. Nattel, 2009, Funny current downregulation and sinus node dysfunction associated with atrial tachyarrhythmia a molecular basis for tachycardia-bradycardia syndrome: Circulation, v. 119, p. 1576-U44.

Yokoo, N., S. Baba, S. Kaichi, A. Niwa, T. Mima, H. Doi, S. Yamanaka, T. Nakahata, and T. Heike, 2009, The effects of cardioactive drugs on cardiomyocytes derived from human induced pluripotent stem cells: Biochemical and Biophysical Research Communications, v. 387, p. 482-488.

Yoon, K. J., H. N. Nguyen, G. Ursini, F. Y. Zhang, N. S. Kim, Z. X. Wen, G. Makri, D. Nauen, J. H. Shin, Y. Park, R. Chung, E. Pekle, C. Zhang, M. Towe, S. Mohammed, Q. Hussaini, Y. Lee, D. Rujescu, D. St Clair, J. E. Kleinman, T. M. Hyde, G. Krauss, K. M. Christian, J. L. Rapoport, D. R. Weinberger, H. J. Song, and G. L. Ming, 2014, Modeling a genetic risk for schizophrenia in iPSCs and mice reveals neural stem cell deficits associated with adherens junctions and polarity: Cell Stem Cell, v. 15, p. 79-91.

Young, P., C. Ferguson, S. Banuelos, and M. Gautel, 1998, Molecular structure of the sarcomeric Z-disk: two types of titin interactions lead to an asymmetrical sorting of alpha-actinin: Embo Journal, v. 17, p. 1614-1624.

Yu, J. Y., S. L. DeRuiter, and D. L. Turner, 2002, RNA interference by expression of short-interfering RNAs and hairpin RNAs in mammalian cells: Proceedings of the National Academy of Sciences of the United States of America, v. 99, p. 6047-6052.

Yu, J. Y., M. A. Vodyanik, K. Smuga-Otto, J. Antosiewicz-Bourget, J. L. Frane, S. Tian, J. Nie, G. A. Jonsdottir, V. Ruotti, R. Stewart, Slukvin, II, and J. A. Thomson, 2007, Induced pluripotent stem cell lines derived from human somatic cells: Science, v. 318, p. 1917-1920.

Zhang, J. H., G. F. Wilson, A. G. Soerens, C. H. Koonce, J. Y. Yu, S. P. Palecek, J. A. Thomson, and T. J. Kamp, 2009, Functional cardiomyocytes derived from human induced pluripotent stem cells: circulation research, v. 104, p. E30-E41.

Zhang, L., J. Kelley, G. Schmeisser, Y. M. Kobayashi, and L. R. Jones, 1997, Complex formation between junction, triadin, calsequestrin, and the ryanodine receptor - Proteins of the cardiac junctional sarcoplasmic reticulum membrane: Journal of Biological Chemistry, v. 272, p. 23389-23397.

Zhang, Z., T. Huynh, and A. Baldini, 2006, Mesodermal expression of Tbx1 is necessary and sufficient for pharyngeal arch and cardiac outflow tract development: Development, v. 133, p. 3587-3595.

Zhao, Y., J. F. Ransom, A. Li, V. Vedantham, M. von Drehle, A. N. Muth, T. Tsuchihashi, M. T. McManus, R. J. Schwartz, and D. Srivastava, 2007, Dysregulation of cardiogenesis, cardiac conduction, and cell cycle in mice lacking miRNA-1-2: Cell, v. 129, p. 303-317.

Zhao, Y., E. Samal, and D. Srivastava, 2005, Serum response factor regulates a muscle-specific microRNA that targets Hand2 during cardiogenesis: Nature, v. 436, p. 214-220.

Zhao, Y. B., P. Londono, Y. Q. Cao, E. J. Sharpe, C. Proenza, R. O'Rourke, K. L. Jones, M. Y. Jeong, L. A. Walker, P. M. Buttrick, T. A. McKinsey, and K. H. Song, 2015, High-efficiency reprogramming of fibroblasts into cardiomyocytes requires suppression of pro-fibrotic signalling: Nature Communications, v. 6.

Zicha, S., M. Fernandez-Velasco, G. Lonardo, N. L'Heureux, and S. Nattel, 2005, Sinus node dysfunction and hyperpolarization-activated (HCN) channel subunit remodeling in a canine heart failure model: Cardiovascular Research, v. 66, p. 472-481.

Zipes, D. P., J. Jalife, G. Petrone, and P. Punjabi, 2015, Cardiac electrophysiology: from cell to bedside, 6th edition: Perfusion-UK, v. 30, p. 431-432.

Zou, G. M., W. Wu, J. J. Chen, and J. D. Rowley, 2003, Duplexes of 21-nucleotide RNAs mediate RNA interference in differentiated mouse ES cells: Biology of the Cell, v. 95, p. 365-371.

Zwi, L., O. Caspi, G. Arbel, I. Huber, A. Gepstein, I. H. Park, and L. Gepstein, 2009, Cardiomyocyte differentiation of human induced pluripotent stem cells: Circulation, v. 120, p. 1513-1523.